SAFETY AND TRANSPORT
MEASUREMENT SCIENCE AND
TECHNOLOGY

CLOSE-RTK 3: High-performance Real-Time GNSS Services

Jan Johansson, Martin Lidberg, Per Jarlemark, Kent Ohlsson, Johan Löfgren, Lotti Jivall, and Tong Ning

RISE Report 2019:101

CLOSE-RTK 3: High-performance Real-Time GNSS Services

Jan Johansson[1,2], Martin Lidberg[3], Per Jarlemark[1], Kent Ohlsson[3], Johan Löfgren[2], Lotti Jivall[3], Tong Ning[3]

[1]Rise Research Institutes of Sweden AB

[2]Chalmers University of Technology

[3]Lantmäteriet

RISE Research Institutes of Sweden AB

RISE Report 2019:101
ISBN:978-91-89049-32-1
Borås 2019

© RISE Research Institutes of Sweden

Executive summary

CLOSE RTK 3: High-Performance Real-time GNSS Services

This report presents the results from the third project of the CLOSE effort (Chalmers, Lantmäteriet, Onsala, RISE). The first project, CLOSE-RTK, investigated error sources in Network-RTK and simulated how to improve the performance. The results were used as a basis for the densification, improvement and development of SWEPOS (https://swepos.lantmateriet.se/) during the last decade. The second project investigated how the ionosphere effects the Network-RTK services.

When the SWEPOS network are densified, the measurement uncertainty in the services are reduced. Thus, there is a need to continuously work in order to minimize effects from all significant error sources. Based on indications and experience from some 25 years operation of SWEPOS, we have here focused on effects and error sources related to GNSS reference stations. Several new GNSS monuments are installed in the vicinity of the new Twin telescopes at the Onsala Space Observatory. Four good locations for permanent GNSS installations were equipped with steel-grid masts serving as monuments for permanent GNSS installations. In two of these, the installation has been untouched over a period extending over one year, while two have been used to experiment with different installations of antennas, radomes, masthead, and the environment of the receiving systems. The purpose of CLOSE-RTK III has been both to improve the knowledge of the station-dependent effects in SWEPOS, and to quantify such effects by analyzing the collected observational data. Thus, the first work package has had the ultimate goal to provide knowledge and recommendations when building a new GNSS station and choosing the equipment to be used. The first work package also addresses the issue of some specific station-dependent effects such as the monument stability as a function of air temperature and sun radiation. The most important and significant results from these tests relates to the effects of using different radomes and antennas. The influence of adding a tribrach between the antenna and the mast as well as adding a microwave-absorbing plate at the stations has been investigated in detail. Furthermore, this study has looked in to the problem with birds landing on the antennas in order to keep watch over the surrounding. A bird-detection algorithm has been developed within the project.

In second work package we investigate the necessity, and possibility, to develop methods for station-dependent calibration in addition to the antenna-specific calibrations used to today. Since the performance of positioning services, e.g. Network-RTK, is steadily improved the error sources related to the continuously operating reference stations may soon be limiting factors for further improvement of performance. Station dependent effects are thus important in high accuracy GNSS positioning. Electrical coupling between the antenna and its near-field environment changes the characteristics of the antenna from what has been determined in e.g. absolute robot or chamber calibration.

When using the presently available antenna models GNSS determination of the height difference between the SWEPOS pillar antennas and the surrounding reference antennas gave ~ 10 mm too low heights for the SWEPOS antennas. This error was derived from a comparison with conventional terrestrial surveys. The result varied significantly between days, and also between different processing strategies. PCO/PCV errors derived from GNSS phase differences showed clear elevation-angle signatures that may cause systematic differences in the estimated height component and atmospheric delay, respectively. Electromagnetic coupling between the antenna and a metal plate below the antennas is probably contributing to the systematic PCO/PCV errors found.

Starting already in 2008 and continued in this project we have developed methods and carried out in-situ station calibration of the core permanent reference stations in

SWEPOS. The station calibration intends to determine the electrical center of the GNSS antenna, as well as the PCV (phase center variations) when the antenna is installed at a SWEPOS station. The purpose of the calibration has been to examine the site-dependent effects on the height determination as well as to establish site-dependent PCVs as a complement to absolute calibrations of the antenna-radome pair.

Our results have implications on a number of practical applications. To be mentioned is determination of the "local tie" between the GNSS reference point and the one from other instrumentation at fundamental geodetic stations. Usually, the L1 observable are used while observing the local GNSS networks in order to get as precise results as possible. But when used in the IGS, the L3 (ionosphere-free) observable is used and also solving for troposphere delays. Thus, an error at the 1 cm level is easily introduced due to PCO/PCV errors.

Since there are also other concepts emerging for precise real-time positioning, besides the so far used VRS-concept, the potential of these new concepts (MAC and PPP) are investigated in work package three. Basically, the requirements from the infrastructure are invariant of the chosen concept if we aim for a certain level of performance. There is e.g. an ongoing development of real time methods for Precise Point Positioning (PPP) based on local or regional augmentation systems often referred to as PPP-RTK. The present development also included new satellite signals and systems, thus, make available a three-frequency technique. The report also provides a schematic plan how such a service, based on PPP-RTK or rather Network-RTK, could be provided in the region of the Baltic Sea.

Finally, the design of a high precision positioning service for the Baltic Sea are investigated. Motivation is that international vessel-traffic could be further optimized if the uncertainty of vertical component in the navigation could be improved. The performance in the "Baltic Sea navigation service" would benefit from installation of some few off-shore GNSS reference stations that would be possible to locate to relatively shallow waters!

Gothenburg,

January 2019.

CLOSE-RTK 3: High-Performance Real-time GNSS Services

1 Introduction

During 2008-2009 the project CLOSE-RTK was launched with the aim to study and possibly improve the performance of the SWEPOS RTK service. The initial project investigated the influence of all the major sources of error both under the current station and satellite constellation as well as under the assumed conditions of a future expansion of the satellite and ground segments. CLOSE-RTK also focused on improved performance of network RTK by developing algorithms for the network RTK software. The CLOSE-RTK II project 2010-2011 investigated how an increased ionospheric activity effected the RTK measurement and especially the SWEPOS Network-RTK service. Furthermore, software tools for real time monitoring of the Ionosphere was developed. (Emardson et al 2009, 2011)

The CLOSE-RTK projects I and II have resulted in a reduced uncertainty in the services. Thus, this has made other error sources more significant. Especially, there is an increased requirement to e.g. investigate and reduce the station dependent effects in SWEPOS. Furthermore, new methods and algorithms for real time GNSS high-precision service are continuously becoming available. Except Network RTK (NRTK) based on VRS (Virtual Reference Station) the other methods like PPP (Precise Point Position) and MAC (Master-Auxiliary Concept) are now available.

The Swedish permanent network of GNSS stations, SWEPOS, is under continuous quest for improvements. One area that is particularly important is how the stations with receivers, antennas, radomes, cables, antenna-splitter and pillars/masts are built and linked together. One obvious requirement is that the installations are mechanically stable and do not sway because of wind or temperature changes. Furthermore it has been found that electromagnetic influences from the environment may interfere with the reception of GNSS signals. Thus, minimizing these effects are essential for further improvement of the robustness and precision in GNSS-methods.

For this reason, the project CLOSE-RTK III, reported here, has been running during 2014-2017. CLOSE-RTK III focuses partly on the increased understanding of different methods for location-based services, VRS, MAC and PPP, and secondly to study the errors related to the reference stations for GNSS with the goal to minimize them.

CLOSE-RTK III has been conducted within three Work Packages (WP). The first WP has had the ultimate goal to provide knowledge and recommendations when building a new GNSS station and choosing the equipment to be used. WP 1 also addresses the issue of some specific station-dependent effects such as the monument stability as a function of air temperature and sun radiation. In WP 2 we investigate the necessity, and possibility, to develop methods for station-dependent calibration in addition to the antenna-specific calibrations used to today. Finally, in WP 3, we investigate the ongoing development of real time methods for Precise Point Positioning (PPP) based on local or regional augmentation systems often referred to as PPP-RTK. The present development also included new satellite signals and systems, thus, make available a three-frequency technique. WP 3 also provides a schematic plan how such a service, based on PPP-RTK or rather Network-RTK, could be provided in the region of the Baltic Sea.

This page intentionally left blank.

2 WP 1 – Building the ultimate GNSS station

2.1 Introduction

Within CLOSE-RTK III, a GNSS-based test network has been established at Onsala Space Observatory 40 km south of Gothenburg. The network is collocated with the Onsala VLBI (Very Long Baseline Interferometer) antennas and surrounding the area where a new twin telescope is being built. Six good locations for permanent GNSS installations has been identified, and four of these are now equipped with steel-grid masts serving as monuments for permanent GNSS installations. In two of these (OTT1 and OTT6), the installation has been untouched over a period extending over one year, while two (OTT2 and OTT4) has been used to experiment with different installations of antennas, radomes, masthead, and the environment of the receiving systems. The purpose of CLOSE-RTK III has been both to improve the knowledge of the station-dependent effects in SWEPOS, and to quantify these by analyzing the collected observational data.

Within CLOSE-RTK III a new type of radome, OSOS, has been developed and tested. Possible effects of the OSOS radome have been examined, as well as an investigation of the influence of the so called OSOD radome. The OSOD radome is the main radome used in the SWEPOS network. A number of antennas and the combination of antennas and radomes, has also been individually calibrated using a robot-system by GEO++ in Hannover, but also in the anechoic chamber in Bonn.

2.2 OTT processing

We have analyzed the phase data of OTT2 and OTT4 for 16 weeks in 2015 i.e. day number 56-168 of the year. During this period, the hardware configurations of the two antennas and masts were changed once a week, according to the descriptions found in Appendix B. The aim of this analysis was to be able to follow the changes in estimated 3-d coordinates, as well as phase pattern that result from the change in configuration.

The processing of the phase data was made by differentiating data to station OTT1, which had no changes during this time. We derived excess values of the coordinates east, north and vertical components of stations OTT2 and OTT4 when using values of the baseline vectors between OTT2 and OTT1 as well as between OTT4 and OTT1 such that L1 results for GPS have zero mean for the first week. Daily solutions of coordinates and clock errors for GPS and GLONASS L1 and L2 and the “ionosphere-free” combination L3 were made without estimation of atmospheric parameters (just small corrections accounting for the height differences between the antennas). In addition, L3 solutions including atmospheric parameter estimations, denounced L3T, were made.

Identical antenna models were used for both ends of the baselines, except for some weeks. In the latter case the antenna models used are given in the bottom right part of the summary graphs (OTT4 day 140 – day 168).

In this section, some examples of weekly results with different experimental setups are discussed, as well as summarizing tables and some general conclusions from the experiments. Appendix A contains weekly result graphs of the processing for all the experimental setups, which are described in detail in Appendix B.

2.2.1 OTT-analysis example

The results given in Appendix A and B might require some introduction. This section is intended to provide reading instructions for these results. The first example relates to the changes of equipment made at the station OTT4 during the first week of March 2015.

2.2.1.1 Change of the experimental setup at OTT4 2015-03-04

According to Appendix B some changes were made at station OTT4 on 2015-03-04 corresponding to day number 63. The insulating plastic plate with the thickness of 3 mm was removed from the experimental setup. During the remounting of the antenna it was however noticed that its orientation had changed with approximately 7 degrees from the previous setup.

From the plots in Appendix A it can be found that the jump in the North component is in the range of 0.1-0.2 mm for both GPS and GLONASS L1 and L2. The size of the jump is found by comparing the numbers found in the plot for "OTT4 Day number 056-063" with the corresponding averages found in the plot called "OTT4 Day number 063-070". One possible explanation for this significant change is the 7° change in orientation.

The jump in the vertical component for the same epoch is found to be 3.0 ± 0.2 mm that is in close agreement with the thickness of the plastic plate that was removed.

No significant difference between the mean phase residuals between the plots "OTT4 Day number 056-063" and "OTT4 Day number 063-070" can be seen. The 3 mm position change is as stated in close agreement with the thickness of the plastic plate and we find no indication of any additional changes that could arise from the removal of the plastic plate. Thus, the electrical insulation in itself does not seem to alter the antenna pattern.

2.2.1.2 Change of the experimental setup at OTT4 2015-03-11

On day 70 a tribrach with adapter was installed on OTT4, and the 3 mm plastic plate was put back. The height of the tribrach was originally measured with a caliper to 77.0 mm; it was later adjusted to 78.6 mm (the later measurement did include the full height of the tribrach including the lower black part which is in physical contact to the foundation). A total vertical change of 81.6 mm could therefore be expected. From Figure "OTT4 Day number 063-070" and "OTT4 Day number 070-077" a vertical change of 80.75 ± 0.15 mm was found in L1 and L2 (also counting the 70 mm offset intentionally removed from graph for clarity).

The expected value of the change was as stated 78.6+3=81.6 mm, which is almost 1 mm more than what is measured from GNSS L1 and L2. In addition, L3T has changed even more and the graphs showing the mean residuals as a function of elevation angle has changed significantly. Thus, the use of the tribrach and adapter seems to have a small but detectable influence on the antenna pattern.

A change in the north components of 0.75 ± 0.05 mm is also found from the L1 and L2 results of Figures "OTT4 Day number 063-070" and "OTT4 Day number 070-077". Even if this is a small horizontal change it is statistically significant. The explanation could possibly be a small tilt in the north-south direction of the plate on the monument top. A tilt of 0.43˚ of this plate could move a phase center 100mm$\cdot sin 0.43^{\circ}$=0.75mm away from the center of the plate, if the phase center is located 100 mm above the antenna bottom. The adjusted tribrach could thereafter have moved the phase centers to be located straight above the plate center.

2.2.2 OTT-analysis results and comments

We have gathered the main parts of the configurations and results from the analysis in Tables 2.1 and 2.2 for OTT2 and OTT4, respectively. The tables focus mainly on the estimated vertical displacements for L1 and L3T. More details on the results are found in Appendix A, and the configuration in Appendix B.

The values in the vertical offset columns are mean values from Appendix A adjusted for the known heights of possible tribrachs, plates and for OTT4 height difference between the alternative mast tops.

Table 2.1 The configurations at station OTT2 during 16 experiment weeks. The estimated vertical offsets are the L1 and L3T results from Appendix A compensated for the known offset due to possible acrylic plate(s) and tribrach heights. One 3 mm acrylic plate is considered as being default.

Day of Year	Mast top	Acrylic Plate (mm)	Tribrach Adapter (mm)	ECCOSORB	Antenna	Radome	Estimated vertical offset L1/L3T (mm)	Comment
056-063	P[1)]	3	-	-	J-951[2)]	OSOS	0.0/0.6	Start/default
063-070	P	3	-	-	J-951	-	-0.5/1.1	Radome removed => Small effect but different sign for L1 and L3t
070-077	P	3	-	-	J-951	OSOS	0.0/0.8	Radome back => default configuration
077-084	P	3	-	-	J-951	OSOS	0.0/0.8	Radome removed but put back => default configuration
084-091	P	3	-	1	J-951	OSOS	-1.2/0.3	Eccosorb added => Small effects on both L1 and L3t. Also visible in residual plots.
091-098	P	3	-	1+	J-951	OSOS	-1.0/0.1	Double Eccosorb thickness added => same effect as above. Residual plot similarly affected. Extra Eccosorb does not seem necessary
098-105	P	20	72.4	1	J-951	OSOS	-1.7/-2.9	Eccosorb, thick acrylic plate and tribrach installed => clear offsets in L1 and L3t. Still, residual plot fairly flat.
105-112	P	20+3	72.4	1	J-951	OSOS	-2.2/-0.5	Eccosorb, thick and thin acrylic plates and tribrach installed => different effects for L1 and L3t results. L2 more affected than L1. Residual plots affected.
112-119	P	20+3	72.4	2	J-951	OSOS	-2.1/-0.1	Double Eccosorb, thick and thin acrylic plates and tribrach installed => different effects for L1 and L3t results. L2 more affected than L1. Residual plots affected. As

								above extra Eccosorb is not necessary.
119-126	P	20+3	72.4	-	J-951	OSOS	-1.3/-1.4	Same as above but without Eccosorb => Tribrach and thick acrylic plate seems to seriously affect especially L3t. Also, the influence of the Eccosorb depend on tribrach and acrylic plate thickness.
126-133	P	3	-	-	J-946[3)]	OSOS	0.1/1.4	Default installation => fairly similar to the original results including flat residuals.
133-140	P	3	-	-	J-946	-	-0.6/0.6	Radome removed => Small effect with the same sign for L1 and L3t. L1 results same as for the change at day 63 above. Change of L3t results, however, different sign. No significant difference in residual plots.
140-147	P	3	-	-	J-946	OSOS	0.1/1.2	Results from the previous two weeks verified.
147-154	P	-	-	-	J-946	OSOS	0.3/0.5	Thin acryl plate removed => very small effect on L1. L3t results slightly influenced.
154-161	P	-	-	-	J-946	-	-0.4/0.4	Radome removed => L1 results confirm the small radome effect (0.7 mm). Again slightly different on L3t.
161-168	P	-	-	-	J-946	OSOS	0.3/1.1	Radome back => L1 results confirm the small radome effect (0.7 mm). Again slightly different on L3t.

[1)]Circular plate on cylindrical pipe
[2)]JAVRINGANT_DM 00951, A0090951
[3)]JAVRINGANT_DM 00946, A0090946

Table 2.2 The configurations at station OTT4 during 16 experiment weeks. The estimated vertical offsets are the L1 and L3T results from Appendix A compensated for the known offset due to possible acrylic plate(s), tribrachs, and alternative mast top heights. One 3 mm acrylic plate is considered as being default.

Day of Year	Mast top	Acrylic Plate (mm)	Tribrach Adapter (mm)	ECCOSORB	Antenna	Radome	Estimated vertical offset L1/L3T (mm)	Comment
056-063	P[1)]	3	-	-	J-821[3)]	OSOS	0.0/0.6	Start/default
063-070	P	-	-	-	J-821	OSOS	0.1/0.0	Insensitive to electric insulation, “plain geometry”
070-077	P	3	78.6	-	J-821	OSOS	-0.7/-3.5	Significant signatures in (L1,L2) residuals-> -2mm in L3T
077-084	P	-	78.6	-	J-821	OSOS	-0.6/-3.6	Insensitive to electric insulation, “plain geometry”
084-091	O[2)] -62.6	3	72.5	-	J-821	OSOD	-1.3/-3.5	
091-098	O -62.6	3	72.5	-	J-821	-	-1.2/-1.7	Small change when removing OSOD radome
098-105	O -62.6	3	72.5	-	J-821	OSOS	-0.7/-1.1	Significant change when adding OSOS radome
105-112	O -62.6	3	72.5	-	J-821	OSOD	-1.0/-2.4	
112-119	O -62.6	-	72.5	-	J-821	OSOD	-0.9/-2.6	Insensitive to electric insulation, “plain geometry”
119-126	O -62.6	-	72.5	-	J-821	OSOD (r 1/3)	-1.1/-2.7	East North Vertical insensitive to radome rotation (0.2mm level)
126-133	O -62.6	-	72.5	-	J-821	OSOD (r 2/3)	-0.9/-2.3	ENV insensitive
133-140	O -62.6	-	72.5	-	J-821	OSOD (r 3/3)	-1.0/-2.3	ENV insensitive
140-147	P	3	-	-	LEIAR[4)]	LEIT[5)]	0.5/-5.6	In general larger spread in daily vertical estimates for LEIAR
147-154	P	3	-	-	LEIAR	-	2.3/-4.7	Clear vertical effect of radome, significantly smaller spread without radome
154-161	P	3	-	-	LEIAR	LEIT	0.4/-6.2	Large spread
161-168	P	3	-	-	LEIAR	LEIT	0.2/-6.9	Large spread

[1)]Circular plate on cylindrical pipe
[2)]Cirkular plate on rectangular pipe with support legs for radome. Height difference -62.6 mm estimated from the GPS L1 data
[3)]JAVRINGANT_DM 00821, A0090821
[4)]LEIAR – LEIAR25.R3, S.No.: 10170020, P/N: 01018079
[5)]LEIT – LEIT-radome Art.No: 765734

Some conclusions regarding the equipment drawn from the experiments follow:

- **LEIAR25.R3 antenna**. The LEIAR25 antenna with the LEIT radome give significantly larger spread in the daily solutions than other configurations. The LEIAR25 antenna without the radome give standard deviations that are comparable to those for other antennas. The mean vertical offset also changes significantly when adding/removing the radome.
- **OSOS and OSOD radomes**. Adding/removing an OSOS radome change the (L1) vertical on a 0.5 mm level. Two different OSOS radomes were tested. Adding/removing OSOD resulted in smaller vertical changes.
- **Acrylic plates**. The electric isolation created by the acrylic plates does not change the coupling between the antenna and monument for the radio frequency signals. Adding a 3 mm or 20 mm plate just changed the vertical offset accordingly.
- **Tribrach**. The introduction of a 50-100 mm tribrach changes the phase pattern significantly. This is probably an effect of creating a separation between antenna and monument with a length that is a significant fraction of the signal wave-lengths, but the possibly different electromagnetic properties of the tribrach than the antenna and monument can also have an effect. When the tribrach has been installed, the additional separation created by a plate again change the pattern.
- **Eccosorb plates**. An Eccosorb plate change the "long wave" elevation phase pattern, and estimated vertical on a ~1mm level. Adding an extra plate does not change the phase pattern significantly (it is not clear whether or not it is helpful to further reduce the "rapid" elevation phase pattern created by e.g. ground reflections).

2.2.3 Long-term monitoring of specific installation

After 16 weeks of continuous installation changes at OTT2 and OTT4 the end setup on Day 168 has been kept for a long-term monitoring. Future changes will be made based on the findings in paragraph 2.2.1., 2.2.2. and Appendix A. Several of setups will be tested again but this time during longer periods of time.

Furthermore, the installations have during the winter 2016 been exposed to a variety of weather conditions with very warm, cold, wet and dry air. The antennas/radomes have occasionally been covered with snow, ice or raindrops as well as seagulls.

2.3 Temperature dependence of the truss mast

One of the main objectives of static GNSS is to maintain local, regional, and global reference frames and networks. In Sweden, Lantmäteriet (the Swedish Mapping, Cadastral and land registration Authority) operates the SWEPOS network since the early 1990's.

The original SWEPOS monuments consist of 3 m tall heated circular concrete pillars that are firmly connected to crystalline bedrock. The monuments were designed this high in order to guarantee full satellite visibility above 10 degrees of elevation, to prevent vandalism and disturbances due to people and animals, and to mitigate snow effects.

The original 21 SWEPOS sites are now also equipped with additional GNSS monuments for redundancy purposes. These 3.20 m high truss masts monuments with a triangular cross section were developed by Lantmäteriet and investigated both in a study (Lehner 2011) at the Onsala Space Observatory in 2010 and within the OTT test network 2015-2016.

2.3.1 Earlier study of the SWEPOS truss mast

Within a MSc-project in 2010 (Lehner, 2011) survey methods to continuously observe local movements of GNSS monuments were developed. Several different monument types were studied in search for both the horizontal and the vertical deformation.

Vertical displacements will in general follow thermal expansion of the mast material. The Lantmäteriet truss mast has, according to Lehner, a thermal expansion coefficient of approximately 7.5ppm/K, which can be considered small. Temperature variation of up to 40 K in this 3.2 m mast type will lead to variations of the vertical of the mast top of up to 1.0 mm.

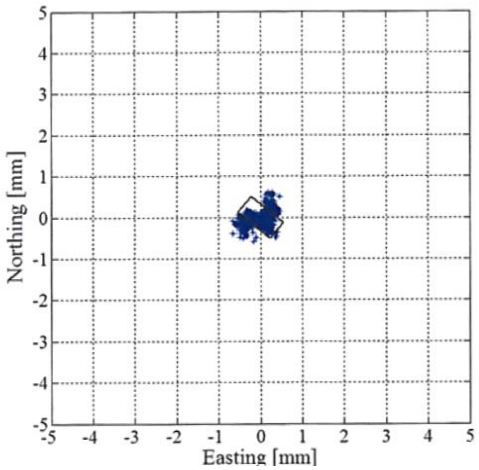

Figure 2.1 The horizontal motion of a Lantmäteriet truss mast top measured using terrestrial optical technique during June 24-28, 2010. From Lehner 2011.

Solar heating can cause horizontal variations in the mast top location. The study presented examples of several mm variations due to different expansion in parts of the masts that are solar lit and parts in shadow. This effect motivates the use of lighter monument constructions, such as truss masts, with its relatively high heat dissipation and reduced chance of differential heating; none of the legs are in complete shadow by the rest of the structure. In the study by Lehner the Lantmäteriet mast had horizontal

variations within ±1 mm for the mast top position, see Figure 2.1. It was also noted that the variations could be made smaller by shielding of monument, e.g., with a plastic pipe surrounding the steel grid mast.

2.3.2 Effects on OTT1 and OTT2

The OTT1 and OTT2 masts have been used for further investigations of the possible monument movement patterns due to changing solar and temperature interaction.
We used GNSS data from August 2015 and August 2016, two relatively sunny months, to measure the resulting motion of the OTT1 and OTT2 mast tops. As reference, we used the SWEPOS and IGS station ONSA, located approximately 500 meters away. Its monument is a 0.95 m high concrete structure, and its top is considered less affected by the weather conditions than the truss mast tops.

The estimated 3-dimensional displacements during August 2016 is shown in Figure 2,2. For the comparisons over 500 m baselines (OTT1-ONSA and OTT2-ONSA in the graph) the estimates are extra noisy due to unmodelled atmospheric effects, while for the comparisons OTT1-OTT2 the part of the motion that is common to the two masts is not seen in the displacements estimates. Hence the scatter in the OTT1-OTT2 baseline estimates is significantly smaller than in the others.

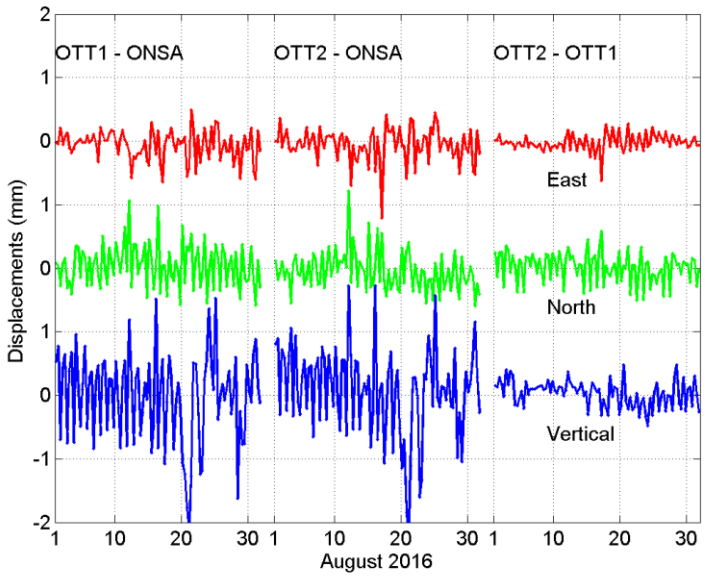

Figure 2.2 The estimated variations in the baselines between the antennas at OTT1, OTT2, and ONSA during August 2016. The displacements are averaged over 8 hours. The mean values have been set to zero for all curves.

We used open access weather data from a nearby station in the Swedish Meteorological and Hydrological Institute network to find correlations between mast motions and meteorological conditions. During the fall 2015 the truss mast at OTT2 was painted white in order to reduce its sensitivity to heating from solar radiation (see Figure 2.3). We therefore also looked for changes in the motion pattern of OTT2 between August 2015 and August 2016.

Figure 2.3 The OTT2 mast after being painted white in October 2015. The purpose is to reduce its sensitivity to heating from solar radiation.

The correlation between air temperature and baseline estimates, both horizontal and vertical components, was relatively small for all baselines. This is a consequence of the relatively small temperature variations during both months studied; the recorded temperatures stayed between 11.8 and 23.8˚C.

In order to study the influence of solar radiation we divided the GNSS data sets into 6 hour windows based on local standard time (one hour more than UTC) and studied the local times 3-9h, 9-15h, and 15-21h, when the sun was heating the masts from the east, south, and west, respectively. The variations with time of day were most pronounced on the baseline OTT1-OTT2, where the north components decreased around 12h local time (i.e. 9-15h), when the sun is in the south. The mean 3-dimensional displacements within a month for different local times are shown in Figure 2.4.

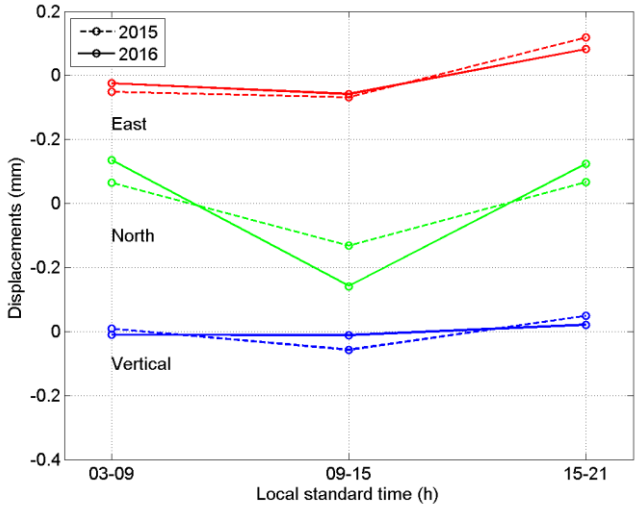

Figure 2.4 The monthly means of the displacements of OTT2 with respect to OTT1 for the three time windows during August 2015 and August 2016 respectively. The mean values have been set to zero for all curves.

A detailed investigation of the north component estimates of all baselines in the time periods 9-15h was then conducted. We compared the estimates with the data on the level of sun shine (in fraction of time with sun shine) for all days during the months studied. It was a priori thought that the greater decrease in the north components for 2016 seen in Figure 2.4 was a result of smaller variations of the painted OTT2, while the unpainted OTT1 bent to the north due to solar radiation heating from south. This a priori assumption

seems, however, not to be entirely correct. When plotting the north components at 9-15h for all baselines against the level of sun shine it became clear that OTT2 was relatively insensitive to the solar radiation, both before and after the painting. On the other hand, the north component of OTT1 had a significant dependence on the level of sun shine; and it is greater in August 2016 than it was in August 2015, see Figure 2.5. The reason for the difference in sensitivity between OTT1 and OTT2 requires further investigation.

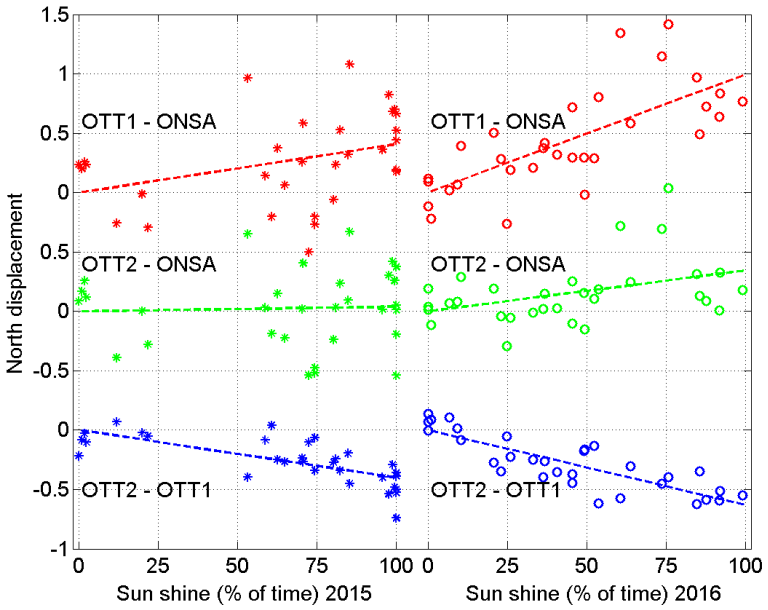

Figure 2.5 The daily estimates of the north components during 9-15h local standard time. The estimates are plotted against the fraction of time the area was sun lit. To each group of estimates a linear fit has been derived, which give an indication of the sensitivity to solar exposure. The data in each group has been adjusted zero for 0 % sun shine according to the fits.

2.4 Effect of birds sitting on antenna radomes

It was noticed that birds often visited station OTT6 at Onsala, Figure 2.6. We therefore used data from this station to assess the effect on the phase observables of such visits, and possible consequences on estimated coordinates in RTK.

Figure 2.6 A proud seagull on the station OTT6 5th June 2015.

2.4.1 Effects on phase observables

The time of two visits on the OTT6 antenna were recorded on day of year 156 and 162 by two colleagues, who also photographed the occasions. We used these observations as starting points and analyzed the baseline between OTT6 and OTT2 for a couple of hours around the recorded times. In Figure 2.7 we show the phase residuals for higher elevation satellites during two hours. Three visits lasting for several minutes are seen in the graphs. For comparison, we also present data from the baseline between OTT1 and OTT2, see Figure 2.8. No large phase deviations are seen for this baseline during the same time, indicating that the deviations in Figure 2.7 originate from OTT6. In Figure 2.9 we show one of the events in more detail.

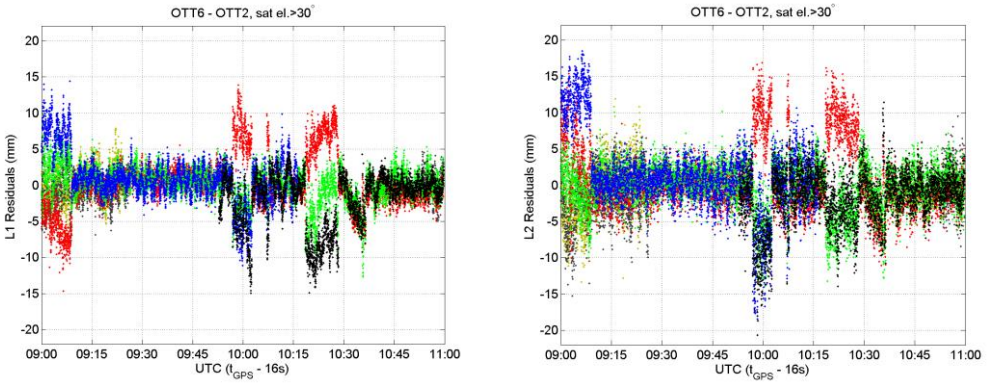

Figure 2.7 L1 (left) and L2 (right) residuals from processing the baseline OTT6 to OTT2 for 2 hours of data. Three presumed longer visits are seen. The time of the middle visit was noted while photographing the bird.

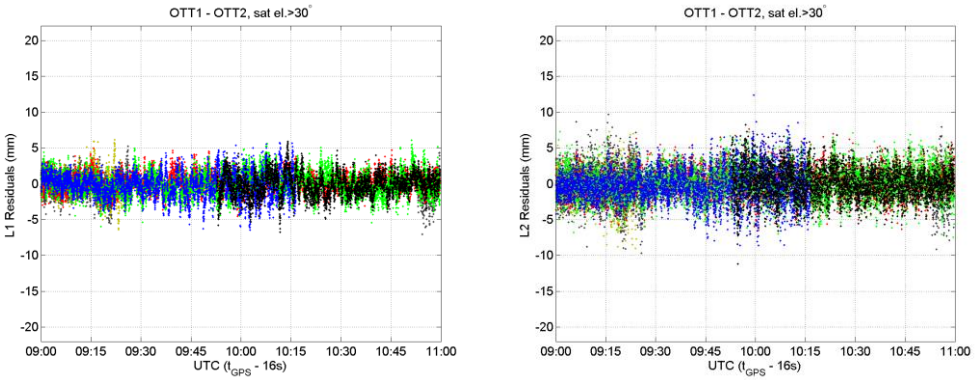

Figure 2.8 L1 (left) and L2 (right) residuals from processing the baseline OTT1 to OTT2 for 2 hours of data. No large deviations were seen on this baseline, indicating that neither OTT1 nor OTT2 had any visits during this time.

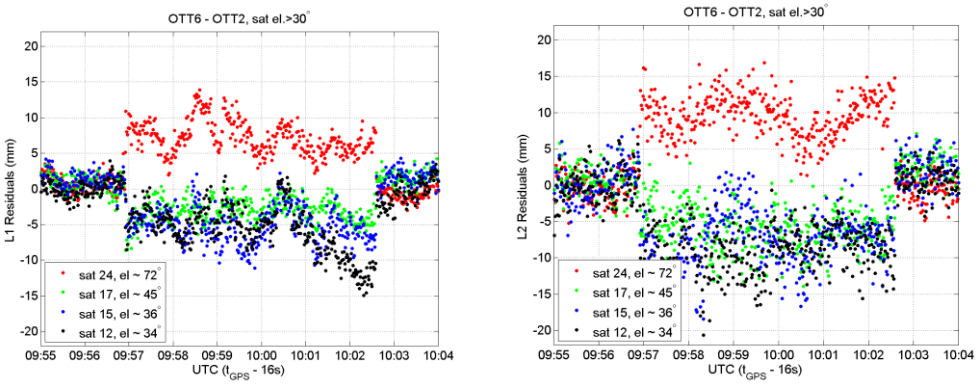

Figure 2.9 L1 (left) and L2 (right) residuals from processing the baseline OTT6 to OTT2. It should be noted that since a common receiver clock error is estimated, the residuals also for satellite observations not influence by the bird are affected by its presence.

2.4.2 Effects on estimated coordinates

From a total of eight identified visits lasting between 30 seconds and 10 minutes we estimated the position deviation of OTT6 as if it were an RTK rover with OTT2 as the

base station. The vertical component deviations were in general larger than the horizontal deviations. A positive vertical bias of 3 mm and an RMS value of 6 mm were found when solely using L1. When using L2 an 11 mm bias was found and the RMS value was 16 mm.

These results indicate that the visits of a bird on a base station in (network-) RTK occasionally could be large enough to be a major contributor to errors in rover coordinates, especially the vertical components.

2.4.3 The frequency of visits at different stations

In order to get a rapid check of expected visit of birds on station without doing a proper geodetic solution we formed L4 (geometry free linear combination) observables of the data from a couple of stations of interest. We studied OTT6 and, for comparison OTT1 at Onsala, as well as the relative nearby station Frölunda. It had been noticed by Lantmäteriet that the SWEPOS stations Trollhättan and Sollentuna were heavily visited. We therefore included them in the study, as well as their "neighbor" stations Väne-Åsaka and KTH.

We studied the change in time between samples in 1 second L4 data of the selected stations. For satellites with high elevation angles, say more than 45 degrees, the changes might be used as indications of bird visits at the stations, at least for occasion of low ionospheric activity. In order to sort out contributions from ionospheric variations or noise a threshold value can be used. We illustrate this in Figure 2.10.

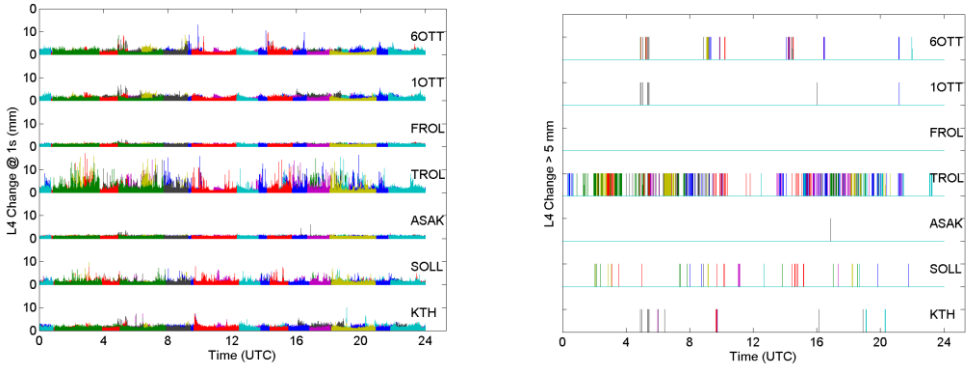

Figure 2.10 The left graph shows the change in L4 in 1 s for satellites with elevation angles greater than 45 degrees for the selected station. Most of the noticeable changes are believed to be due to birds on the radomes. Some changes around 5:00-5:30 AM are visible in several stations, and are likely to be due to ionospheric variations. In the right graph we show the binary results of either finding or not finding any changes greater than 5 minutes in the data of the left graph. Using this threshold value the stations of Trollhättan, Sollentuna and OTT6 seems to have most visiting birds.

In order to further study the consequences of visits at station Trollhättan we made a full geodetic PPP solution of data from this site for one full day, 5th June 2015. In the post-fit residuals, a large set of outliers at relatively high elevation angles was seen. In addition, the whole phase pattern has been distorted indicating many occasions of visits to this station. See Figure 2.11. As a comparison, we also show the results for station Väne-Åsaka in Figure 2.12.

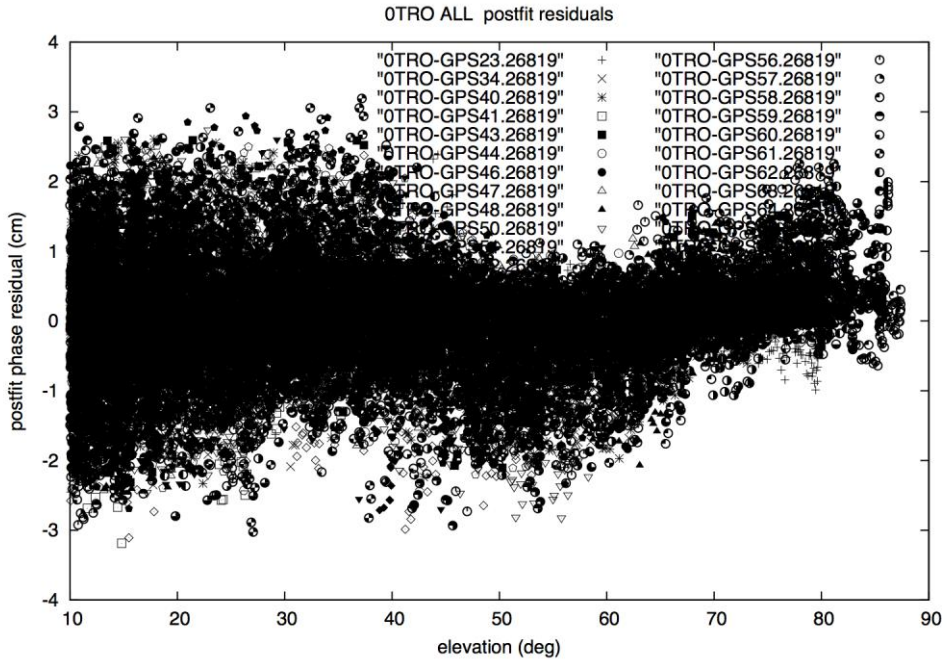

Figure 2.11. The post-fit residuals of one day of data from station Trollhättan. Sampling every 30 s has been used in the analysis.

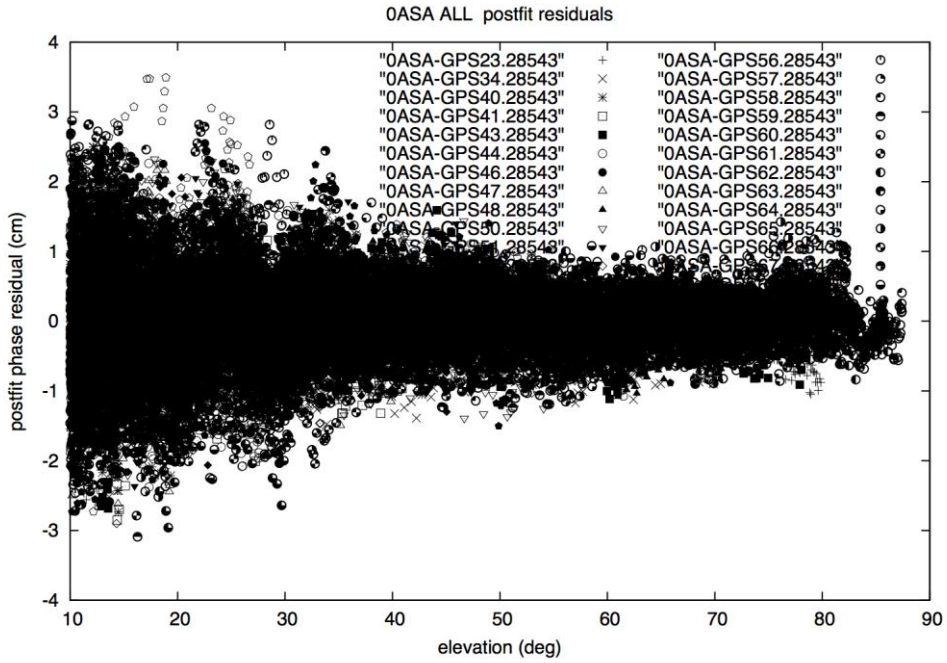

Figure 2.12. The post-fit residuals of one day of data from station Väne-Åsaka. Sampling every 30 s has been used in the analysis.

2.5 Building and testing the perfect site

Based on the findings in this chapter 2, we can conclude that there exist site dependent effects that have influence on GNSS positioning at a magnitude so it deserves further considerations. It is also described how different changes in the antenna installation influence the positioning qualitatively and quantitatively. We are however not in the position to give a complete detailed description on how to establish and test the "perfect GNSS site and installation". However, there are some aspects that may be considered.

There are several aspects influencing the performance of a GNSS reference station. These aspects can be related to the selection of the "site" on the one hand, and to the design of monument and choice of equipment and installation on the other hand.

Among the environmental requirements, we notice the free visibility of satellites around the horizon, possible disturbance/interference in the frequency bands, and the overall electromagnetic (EM) environment. There are also practical aspects that are important for a long lasting permanent GNSS station like protection against violence, easy access for maintenance personnel, good and stable access to data communication and power supply.

For long term stability of the monument, some pillar or truss-mast firmly connected to crystalline rock are usually good alternatives. To be considered are also the UNAVCO "deep drill" design (http://www.unavco.org/). Although some more "soft" ground with some vegetation around the monument may cause less multipath reflections compared to exposed bedrock, asphalt, or building roof tops, it may require extensive maintenance in cutting bushes and small trees.

The purpose of the monument is to support the receiving antenna with a stable foundation. For geophysical studies, the long-term stability is of outmost importance, while many recent applications (e.g. RTK reference stations or GNSS seismology) are also dependent on short term stability. The GNSS antenna should be able to receive the signal from the GNSS satellite as clean and un-disturbed as possible and if there are disturbances they should be possible to model numerically in the GNSS analysis. (The interaction between antenna and monument and its surrounding environment are discussed widely in this report and are not repeated or summarized here.)

The GNSS antenna is connected to the receiver through the antenna cable. Often there are antenna splitters, possibly with amplification, involved. These components are thus critical and important parts of the installation. The cable connectors and its assembling deserve some special attention. From the operation of SWEPOS, there are experiences that some combinations of antenna and receiver that seems to work well, while other combinations show problems in satellite tracking.

While evaluating an existing installation, or for verification of a newly installed stations, some criteria should be investigated. We do not have a complete list of criteria or "reasonable values" to present, but some ideas for further work.

To be examined are "signal strength" and "signal to noise ratio" (SNR), the amount of multi-path (MP), number of recorded epochs in relation to the theoretical possible, amount of cycle slips in recorded data files. For "signal strength" and SNR, it is usually OK to evaluate the values delivered by the receiver. Note that "reasonable level" of e.g. SNR differ considerable between receiver types. For checking MP, recorded epochs and satellites, cycle slips etc, the teqc-software have been widely used within the IGS. The recent G-Nut/Anibus software (http://www.pecny.cz/gop/index.php/gnss/sw/anubis) can handle also RINEX 3 files, and should be investigated. Also, software like RTK-lib

(http://www.rtklib.com/) and BNC (https://igs.bkg.bund.de/ntrip/download) deserves some consideration.

While evaluating a site, some modern receivers have options for built in spectrum analyzer, which is useful for checking for frequency interference.

Also processing the observations using traditional GNSS processing software like Bernese, GIPSY or GAMIT give a good indication of the quality of the data. To examine are phase residuals (if available), amount of solved ambiguities, noise in position time series, and agreement between solutions using different elevation cut off angle.

Preferably, a selection of criteria, and how to evaluate these, including indicative levels, should ideally be compiled into a complete concept.

3 WP 2 – Station calibration

3.1 Introduction

We use a method of in situ calibration of GNSS antennas on monuments, e.g. concrete pillars or steel grid masts, using visiting calibration antennas. The differential phase measurements between the visiting calibration antennas and the monument antennas are analyzed. The analysis method is practically insensitive to imperfections in the satellite orbit and clock models, as well as the atmospheric delay (both ionospheric and tropospheric). It has been described in "Station Calibration of the SWEPOS™ Network, Revised 2013-09-25" (Jarlemark et al 2012) see Appendix C. Parts of the station calibration have also been presented in Kempe et al (2010), and in Lidberg et al (2016). An earlier work on site-dependent effects are presented in Granström (2006).

The structure of the present analysis is given in Figure 3.1. The calibrations in Sections 3.3 and 3.4 have started with earlier established models for the monument antennas, where the antennas/antenna types have been calibrated "stand alone" without the monument (the models marked in yellow for Section 3.3, 3.4 and 3.5 in Figure 3.1). The measured phase differences between monument antenna and visiting calibration antennas were then used for estimating corrections of the original antenna model, called for by its mounting environment. This result in updated antenna + monument models (marked in green for Section 3.3, 3.4 and 3.5 in Figure 3.1). For the calibration of the steel grid mast antennas (see Section 3.4), we used the collocated pillar antennas, with their updated models as “visiting calibration antennas”.

Before a final analysis of the calibration measurements we assessed the models for the visiting calibration antennas (see Section 3.2), and discarded a set of models from the analysis.

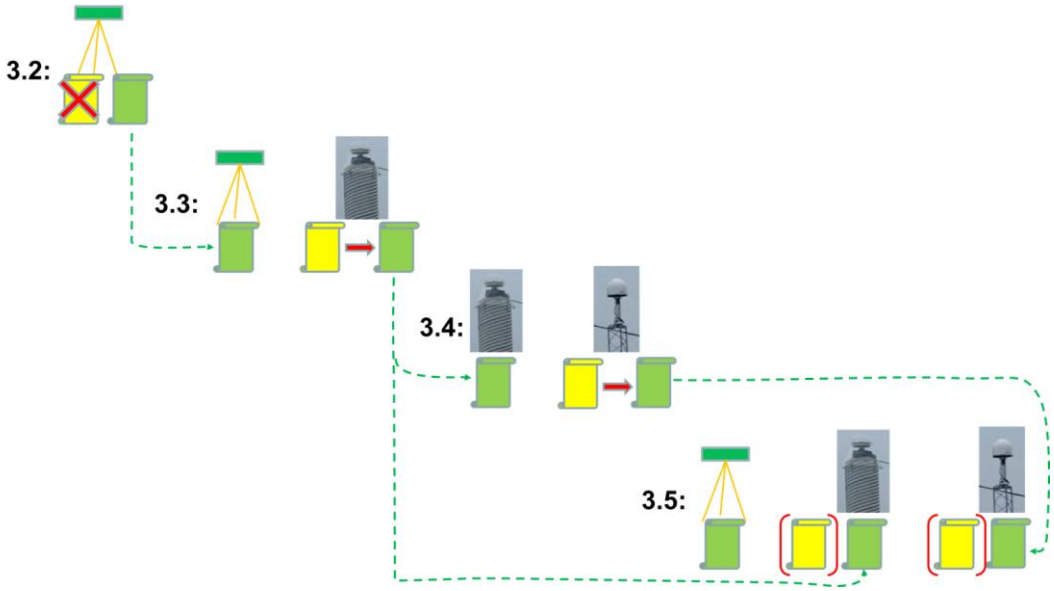

Figure 3.1 The structure of the station calibration work presented in this report. We first present an assessment of models for the visiting calibration antennas in Section 3.2. In Sections 3.3 and 3.4, we present calibrations of the pillar and steel-grid mast antennas. In Section 3.5, we present a revisit to six sites for a verification of the derived antenna + monument models.

In this study, we have focused on the use of the antennas for height determination, and therefore limited the investigation to elevation angle dependent phase effects, ignoring

trying to find azimuthal deviations. We have also limited the analysis to GPS, excluding GLONASS observations for the time being.

3.2 Calibration using visiting antennas

We use a set of markers, typically three, with leveling data to a physical point on the monument. The visiting calibration antennas are mounted on tripods, with reflection absorbing plates under each antenna. The antenna heights over the markers are determined to sub-mm using terrestrial methods.

Data are edited for outliers caused by a couple of different reasons. Since the height of the visiting antennas in general is less than the height of the monument antennas there are signals received by the visiting antennas that has passed in the vicinity of the monument, and signal diffraction can be observed. Nearby trees and other vegetation, as well as higher areas in the terrain can also lead to signal disturbances calling for data editing.

3.2.1 Quality of calibration models for visiting antennas

Several antennas used for site calibration were calibrated both by a group at the University of Bonn (Görres et al. 2006) and by GEO++ (Schmitz et al., 2008). It was noticed that the calibration results, given by two methods, often are fairly similar for L1, but differ significantly for L2. This illustrated in Figure 3.2. In the graph, the differences have arbitrarily been set to zero at 60˚.

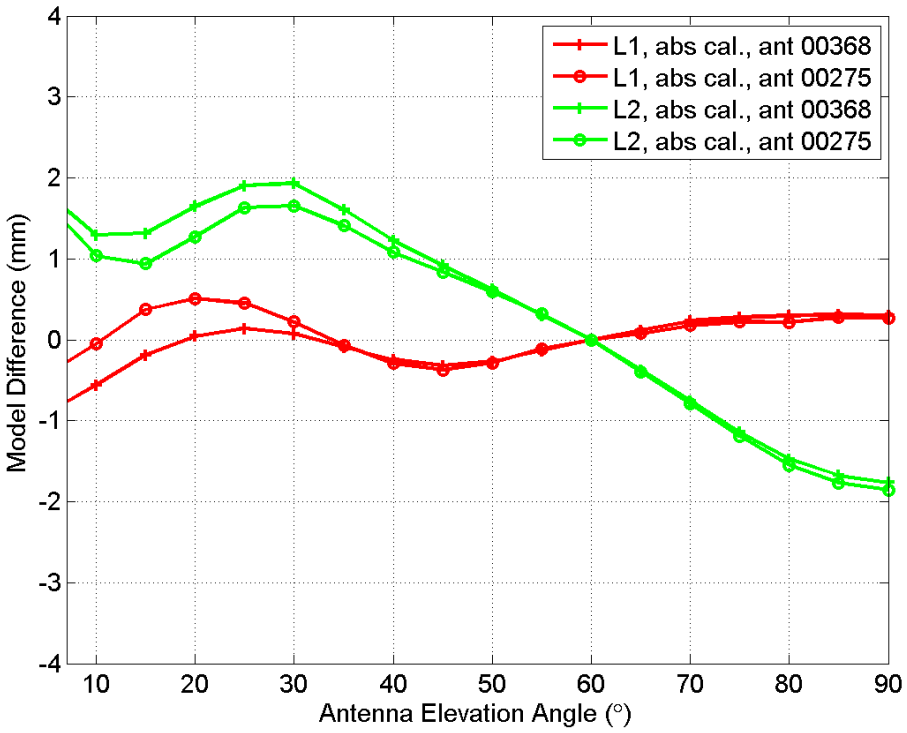

Figure 3.2 The difference in phase elevation signature between antenna models derived by the Bonn group and by GEO++. The phase signatures consist of combinations of azimuth independent PCVs and the vertical components of PCO scaled by -*sin*(*elevation*). The larger differences in L2 signatures are representative for the antennas calibrated by both facilities. In the graph, the differences have arbitrarily been set to zero at 60˚.

In order to determine the internal consistency of the calibration models from the two facilities, we conducted a test where data from two tilted antennas were analyzed. See Figure 3.3 for the experiment setup. The experiment lasted for approximately six days, doy 188-194, 2015.

Figure 3.3 The experiment setup at Onsala Space Observatory for determining the consistency of the calibration models from the two calibration facilities, the Bonn group and GEO++. The nearest northern antenna is tilted to west, 13˚, while the farther antenna is tilted to east, 14.5˚.

By the tilts we can make signals from the same satellite enter the two antennas at what appears as two different elevation angles. If there is an inconsistency in the antenna models for these two apparent elevation angles a possible bias in the residuals can appear in the data processing. We processed the data either as if the GEO++ model or as if the Bonn group model was applicable, separately. We then looked at the data residuals for the two processings and grouped them after apparent elevation angle, and averaged them. A clear pattern emerged, where the elevation patterns of the Bonn L2 residuals deviated from the other signals. This is seen in Figure 3.4.

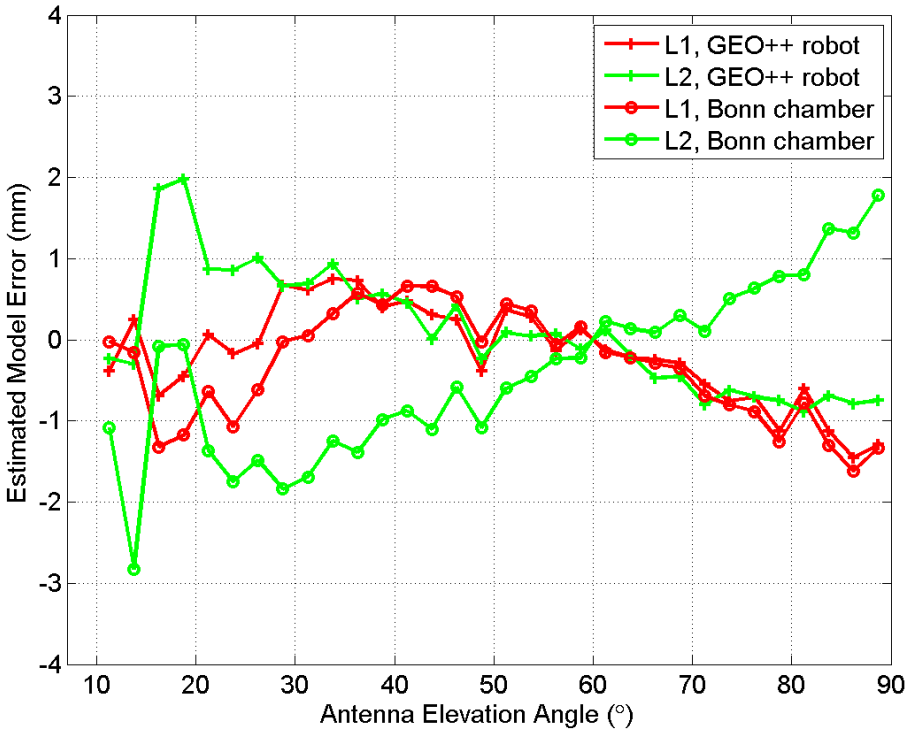

Figure 3.4 The estimated errors in the GEO++ and Bonn models of the two antennas tested in the configuration of tilted antennas. In the graph, the differences have arbitrarily been set to zero at 60˚.

When we combine the estimated L1 and L2 model errors to the corresponding L3 effect an even stronger signature appears for the Bonn models (see Figure 3.5). We simulated what the estimated L3 effect would lead to in L3T processing, i.e. coordinate estimation from L3 signal where also a tropospheric delay parameter is estimated. The results, seen in Figure 3.6, shows a minor effect on the vertical by the estimated GEO++ error, while a vertical effect of nearly 1 cm was seen for the Bonn model error. This level of difference between using GEO++ and Bonn models has also been found in L3T estimates of station height using the Bernese software. As a test of the consistency of the error estimation presented in Figure 3.4, we plotted the differences between the estimated model errors, and compared them to the *a priori* known model differences. See Figure 3.7. The estimate differences agreed fairly well with the signatures seen in the model differences.

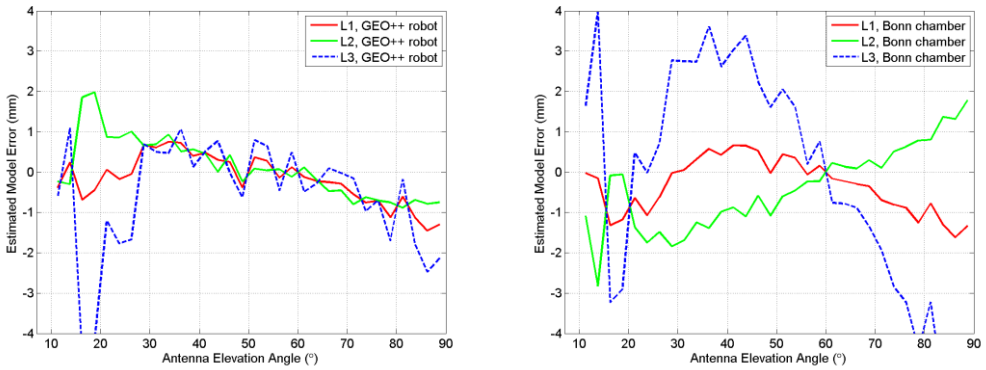

Figure 3.5 The estimated L1 and L2 model errors and the resulting L3 combination. The graph to the left shows the results for the GEO++ model, while the right graph shows the estimated Bonn model results.

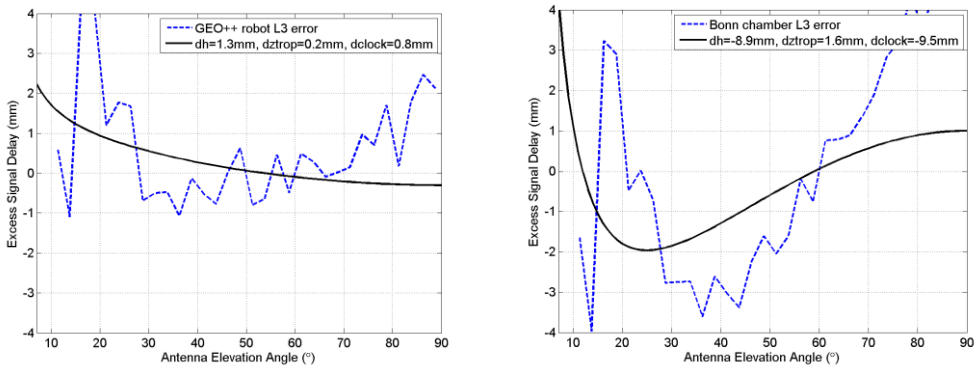

Figure 3.6 The L3 combination of the model errors and the resulting mean parameter values in simulated L3T solutions. The graph to the left shows the results for the GEO++ model, while the right graph shows the estimated Bonn model results.

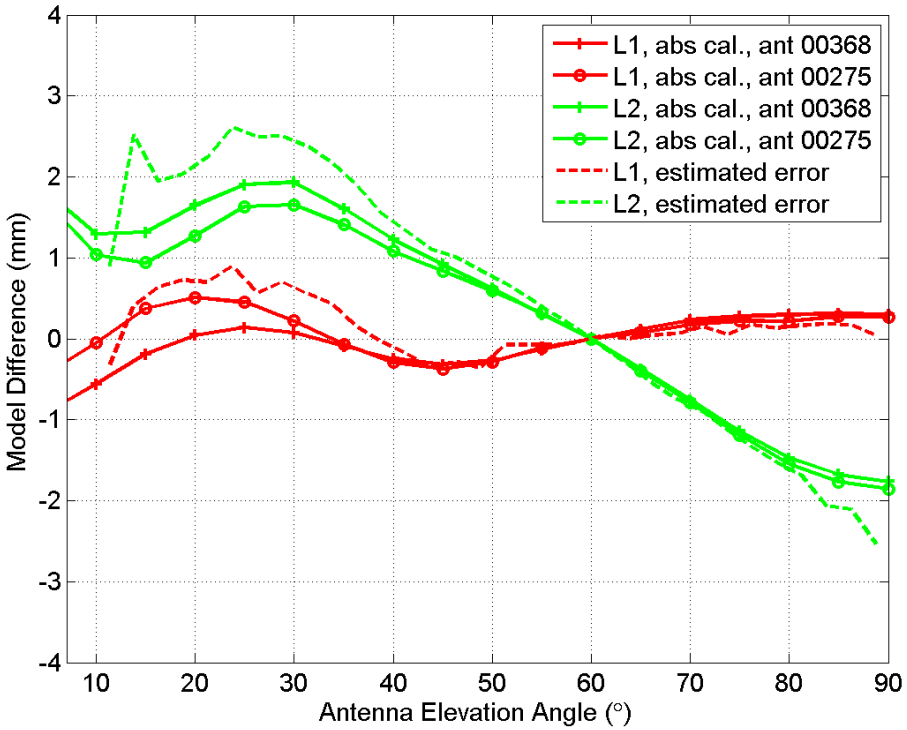

Figure 3.7 The difference between the estimated model errors, dashed lines, plotted together with the original model differences between the GEO++ and Bonn calibrations, solid lines. (Dashed lines in this graph is left minus right graph for L1 and L2 in figure 3.5; Solid lines are the same as in figure 3.2.)

The experiment with tilted antennas was repeated at SP, with two different setups involving antennas 368, 275, and 244. In the analysis the model error was estimated as piecewise linear functions in elevation angel with points every 5˚. The point at 60˚ was set to zero. In total 15 days were processed from the experiments at Onsala and SP. Figure 3.8 shows a compilation of the results from all 15 days. Based on these results we decided to use the GEO++ calibration models in the analysis that follows.

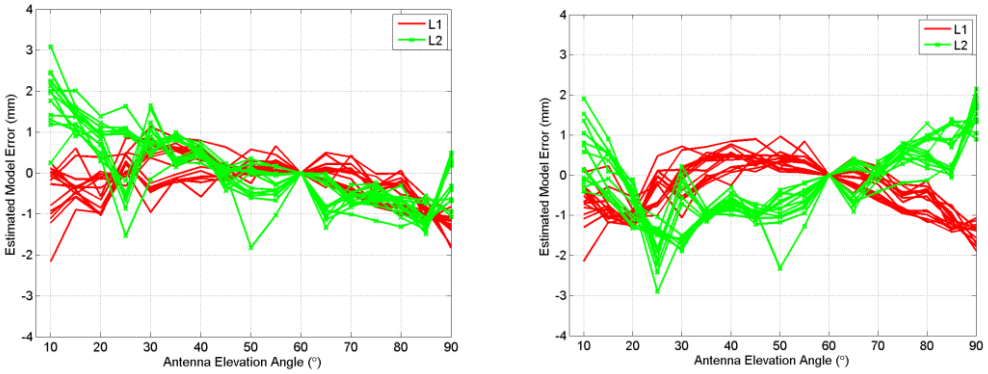

Figure 3.8 The estimated L1 and L2 model errors from daily estimates for the 15 experiment days at Onsala and SP. The graph to the left shows the results for the GEO++ model, while the right graph shows the estimated Bonn model results.

3.2.2 Influence of reflection absorbing plates

The antennas used as visiting antennas were themselves calibrated without any surrounding reflection absorbents, but when used in site visits a plate of the material Eccosorb (www.eccosorb.com) was mounted under the antenna. The reason for the plate is to reduce signal scatter from the ground to influence the site calibration, however the inclusion of an Eccosorb plate could also have changed the antenna phase pattern.

In order to find the possible phase pattern change we set up an experiment with three antennas with 0, 1 and 2 Eccosorb plates mounted under the choke rings, see Figure 3.9. The antennas were situated over markers with known height differences, and the measurements were carried out during approximately three days.

Figure 3.9 Three antennas with 0, 1 and 2 Eccosorb plates mounted under the choke rings.

The resulting mean residuals from processing different baseline combinations are shown in Figure 3.10. The "slow" elevation pattern in the upper graphs are likely to be connected with Eccosorb influence on the antenna pattern, while the more "rapid" variations at low elevation angles most likely are due to ground surface influence. Since the graphs indicate that there is no significant difference in the "slow" pattern between the use of one or two plates of Eccosorb we combined the results in the upper graphs of Figure 3.10 to form a graph of the difference between none and "any" plates of Eccosorb. The result is shown in Figure 3.11. In the figure, we have added fits to fourth order polynomials in an attempt to isolate the expected phase pattern changes due to the Eccosorb.

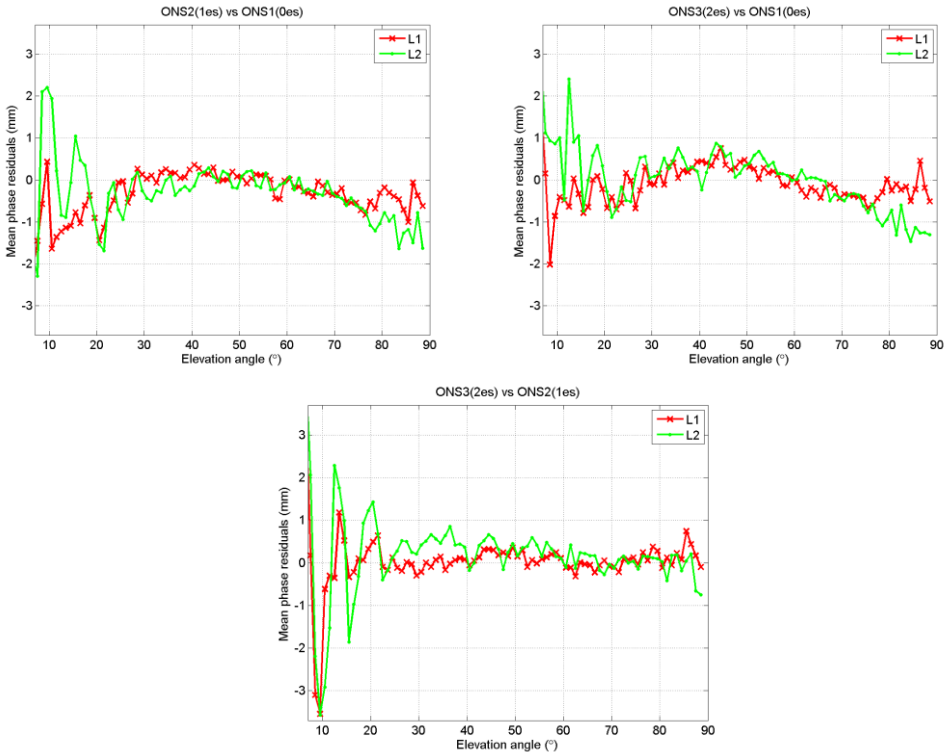

Figure 3.10 The mean residuals from the processing of data from antennas equipped with 0, 1, and 2 plates of Eccosorb. In the upper left graph 1 vs 0 plates are compared, while in the right graph it is 2 vs 0 plates. In the lower graph 2 vs 1 plates are compared.

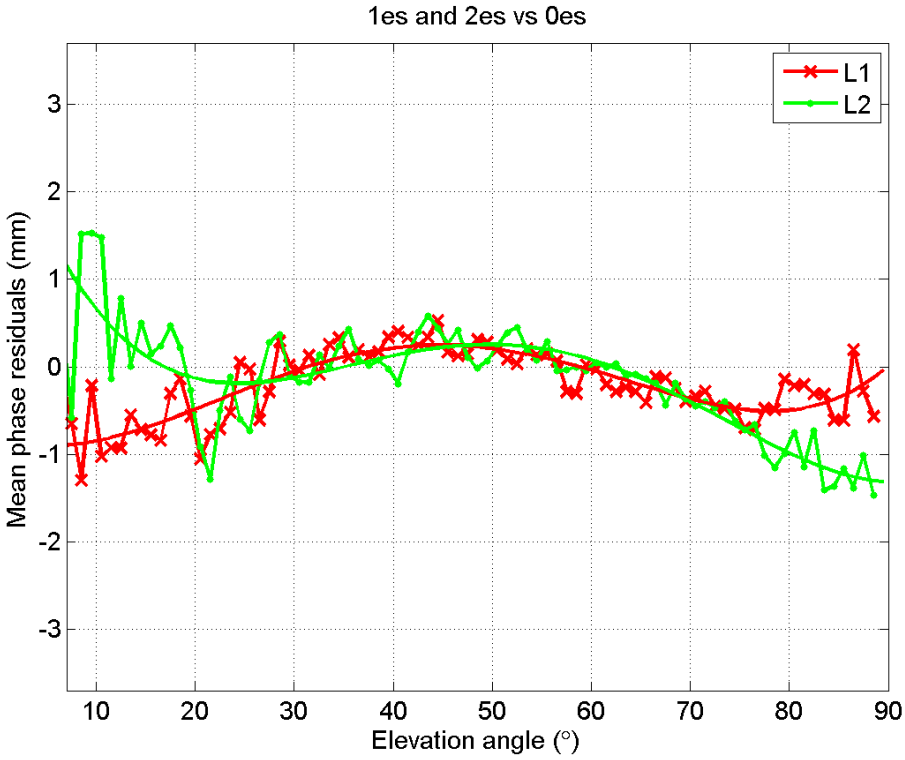

Figure 3.11 The mean residuals when using Eccosorb on one antenna (1 or 2 plates) and not using Eccosorb on the other antenna. The results are a combination of the results in the two upper graphs of Figure 3.10.

In Figure 3.12, we show the results of combining the L1 and L2 results of Figure 3.11 to L3. The smooth L3 fourth order polynomial curve was then used in a simulated L3T processing. A vertical offset of 2.7 mm was found. This is a preliminary indication of the size of influence of the Eccosorb on our visiting calibration antennas. Since the indicated size is relatively small, and uncertain we choose not to include the results in the following analysis.

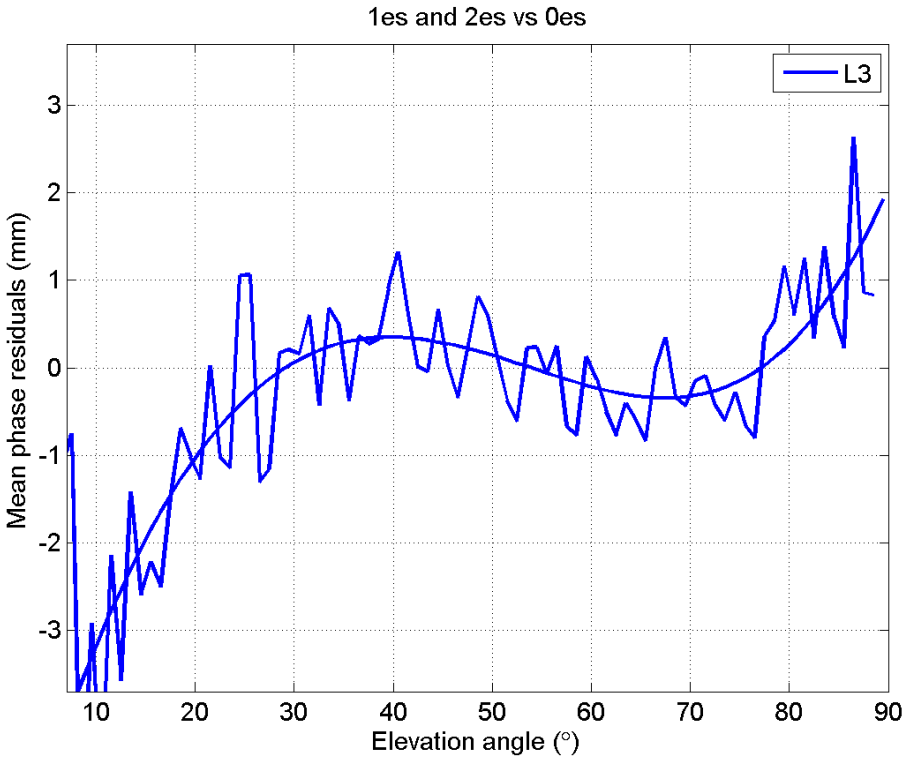

Figure 3.12 The mean residuals when using Eccosorb on one antenna and not using Eccosorb on the other antenna. It is a result of combining the L1 and L2 of Figure 3.11 to L3.

3.3 Station calibrations 2009-2013

3.3.1 Recapitulation of pillar calibration 2009-2010

The analysis of the pillar monument calibration was performed in 2013, and described in detail in "Station Calibration of the SWEPOS™ Network, Revised 2013-09-25", see appendix C. In this section, we recapitulate some results as they serve as background for the recent work.

In total nine SWEPOS pillar stations were calibrated by three visiting antennas using data from approximately 5 days per site. An elevation cut off angle of 12˚ was used in the estimations of the pillar antenna coordinates. For all sites, we used the antenna model presented as "AOAD/M_T, NONE" in the igs08.atx file. Some antennas had other type names, but their models in (i.e. the model available at the time of the measurements) igs08.atx were identical to the type used. Relatively strong elevation dependent deviations from the prescribed antenna PCV was found in the analysis. The deviation differed significantly between L1 and L2, but were on the other hand relatively similar in structure for all nine stations, see figure 3.13.

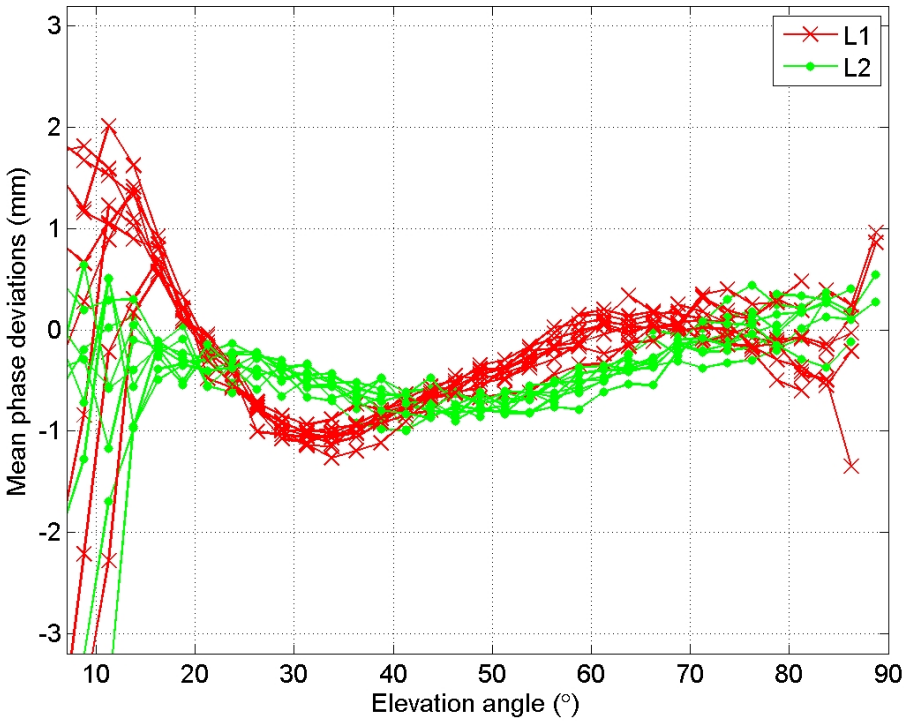

Figure 3.13 Phase deviation of the nine SWEPOS pillar stations investigated. The antenna model "AOAD/M_T, NONE" from the file igs08.atx was used in the analysis.

The deviations in the estimated L1 and L2 PCV become even greater when data are combined to L3. We simulated the effect of the deviations in L3T solutions (coordinate solutions using L3, where also tropospheric delay is estimated). It was found that the PCV deviations found, together with some minor vertical PCO deviations could be expected to give on the average 12 mm to low estimates of the vertical component of the stations. The standard deviation in the vertical offsets was 2.6 mm. See Table 3.1. The

vertical offset is in agreement with the typical vertical bias of ~10 mm presented by Kempe et al. (2010) using the same calibration measurements.

Table 3.1. Estimated vertical offsets and atmospheric delay difference when using L3 observables in L3T solutions and the original antenna model "AOAD/M_T, NONE"

Station	Vertical offset (mm)	Atmospheric delay offset (mm)
Östersund	-10.4	3.6
Sundsvall	-13.6	3.5
Leksand	-9.2	2.4
Karlstad	-7.0	2.4
Vänersborg	-13.6	3.5
Norrköping	-14.1	3.1
Jönköping	-15.7	4.0
Oskarshamn	-12.3	3.5
Hässleholm	-13.0	3.2
Mean	**-12.1**	**3.2**
Std	**2.6**	**0.5**

An updated antenna model file suited for the pillar station was constructed by adding the mean vertical PCO offsets and the mean PCV deviations to the original antenna model. The resulting L1 and L2 phase deviations when re-analyzing the data with the updated antenna model file is shown in Figure 3.14 and the resulting simulated L3T height deviation is found in Table 3.2.

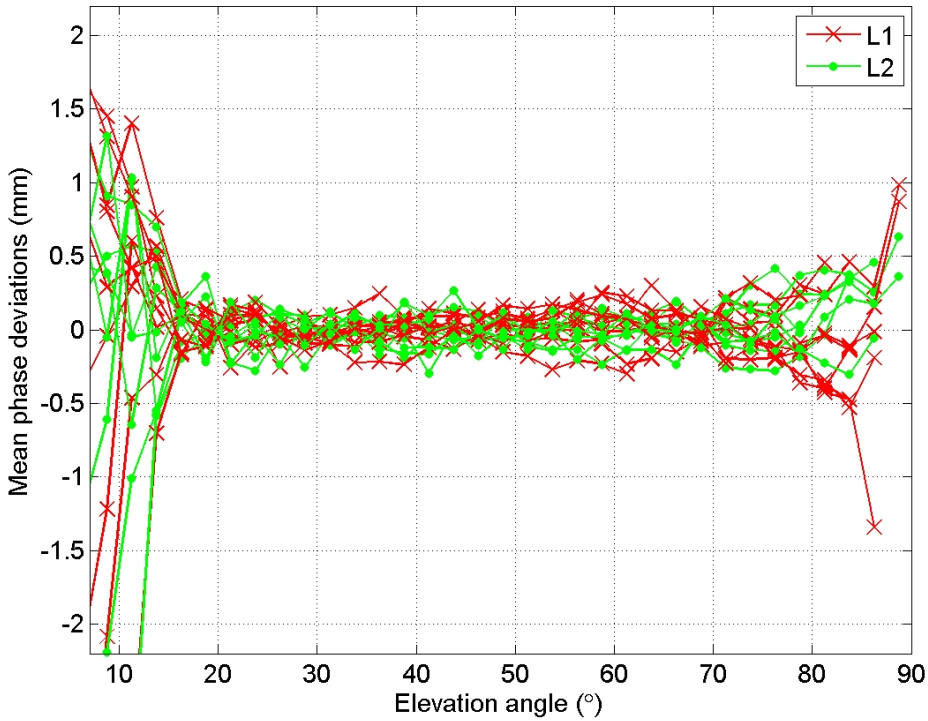

Figure 3.14 Phase deviation of the nine SWEPOS pillar stations investigated. The updated antenna model derived from the measurements was used in the analysis.

Table 3.2. Estimated vertical offsets and atmospheric delay difference when using L3 observables and solving for troposphere (L3T) and the updated PCO/PCV description file for pillar antennas.

Station	Vertical offset (mm)	Atmospheric delay offset (mm)
Östersund	2.4	0.1
Sundsvall	-1.4	0.2
Leksand	-1.4	-0.1
Karlstad	4.7	-0.8
Vänersborg	-2.1	0.4
Norrköping	-2.6	0.0
Jönköping	-4.2	0.8
Oskarshamn	-0.8	0.3
Hässleholm	-1.5	0.1
Mean	**-0.8**	**0.1**
Std	**2.6**	**0.4**

3.4 Mast calibration from 2013 data using co-located pillar antenna

In 2011 a second monument was installed at 19 of 21 fundamental stations. The purpose of the new monuments is to have modern installations able to track new satellite systems and signals, and they are equipped with modern antennas (LEIAR25.R3). To reduce the multipath effects that has been seen from the relatively wide pillar and the large metal plate, a steel grid mast was used for these new monuments. To keep the time series of the original 21 fundamental stations consistent, the antenna of these pillar stations will not be changed as long as they work properly. The antennas at these stations have a pre-amplifier open only for the GPS L1 and L2 frequencies and cannot track all new signals such as Galileo and GPS L5 properly.

We have calibrated 19 of the new steel grid mast stations using data from differentiating to the co-located pillar antennas. This is an easier way of calibration than the visiting antenna approach. It requires a set of leveling data between physical points on the two co-located monuments, instead of both leveling data and visiting antenna height measurements. On the other hand it is required that the antenna model of the reference monument antennas, in our case the SWEPOS concrete pillar antennas, are accurate. In this section, the analysis is based on using the updated concrete pillar monument antenna PCV+PCO model, described in Section 3.3, for the reference antennas. An elevation cut off angle of 10˚ was used.

All mast stations analyzed were equipped with Leiar25.R3 antennas and radomes that were individually calibrated by GEO++ before mounting. It was on beforehand noted that the individual models vertical L3 PCO could differ significantly from the type model. See figure 3.15 The standard deviation in the vertical for the PCO+PCV model was 5.4 mm for the Leiar25.R3 antennas, while it was only 1.3 mm for Javad D/M antennas investigated. It should be pointed out that the Javad antenna calibration did not include radomes. However, we do not think the radome effects only can explain the excess Leiar25.R3 spread.

Either the individual antenna + radome models or the type mean antenna type-specific model could be used as starting points for the derivation of new models for the mast antennas. However, a preliminary data analysis showed that the variations in the estimated L3 PCO:s for the antennas when using the individual models were about 50% greater than the variation when using the type model.

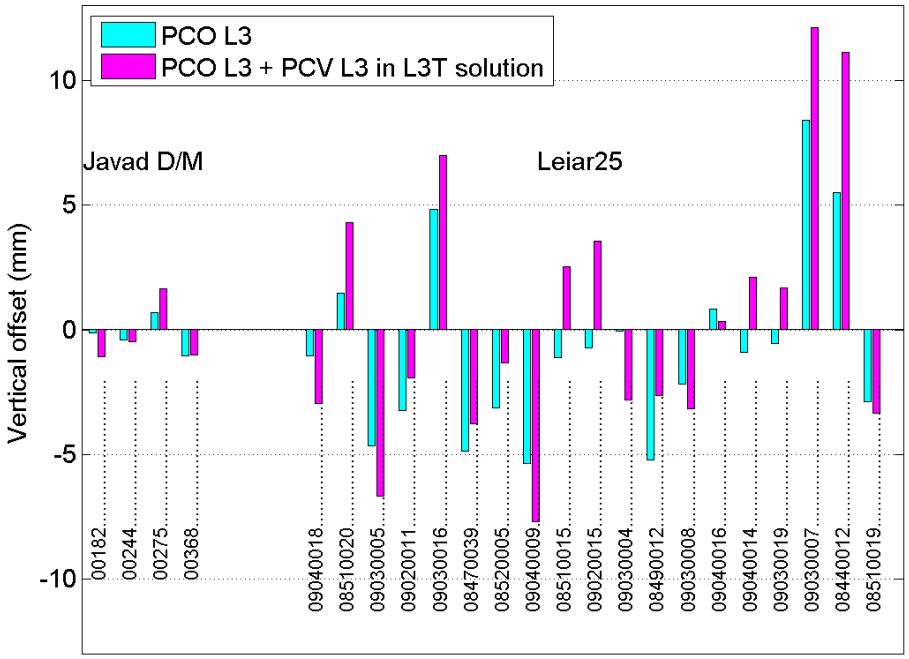

Figure 3.15 Deviations in individual antenna calibration models from type-specific models from GEO++. The cyan colored bars: the deviations of the vertical L3 PCO deviations. The magenta colored bars: the deviations when also (azimuth independent) PCVs were included in a simulated L3T solution, i.e. troposphere estimation included in the solution. The right group represents deviations from the LEIAR25.R3, LEIT model, while the left group represents deviations from the JNSCR_C146-22-1, NONE model. The Javad antenna calibration did not include radomes.

The conclusion that the type models have smaller variation than the individual models is of course very interesting, it implies that the calibrations of this type of antenna have larger variations than the antennas themselves! It should be mentioned that these antennas have been tested also at the antenna test field at Lantmäteriet earlier with different results (Figure 3.16). Unfortunately, these antenna test were only made without radome (they were carried out before it was decided which radome to use). PCO:s were estimated (when fixing the coordinates in the test field) and compared to PCO:s from Geo++ (type with and without LEIT and individual with LEIT). The average difference in height was approximately the same for all comparisons but the standard deviation was twice as large when comparing to the type values on L3 (3.1 mm compared to type values and 1.5 mm compared to individual values). The same data was also used for baseline processing by using the different antenna models from Geo++ (type with and without LEIT and individual with LEIT). In the comparison to known coordinates **the standard deviation** for the height differences is twice as large for the type models both when processing L3 (3.9/1.8) and L3T (7.0/3.6), but **the average difference** is slightly larger when using the individual models (2.5/2.2 and 17.3/15.9, respectively). The large differences for L3T depend most probably on the fact that we used antenna models for LEIT but the observations were carried out without radome, but strange is that the average height differenced is quite high, 15.5 mm, for L3T also when using the type model without radome.

Figure 3.16. The antenna test field on the roof of the Lantmäteriet building in Gävle.

We choose to use the type-specific model, "LEIAR25.R3, LEIT from the igs08.atx file as starting point for deriving updated antenna + monument models. Two weeks of data, doy 105-118 2013, were used in the mast station calibration. The results are compiled in the following four figures. Figure 3.17 shows estimated phase deviations from the antenna model PCV for L1 and L2. Significant signatures, to a large extent common to all sites, are found. The corresponding estimated offsets in the vertical PCOs are shown in Figure 3.18. In Figure 3.19, we show the mean phase deviations from PCV for L1 and L2, and a combination to L3 of the mean deviations, and in Figure 3.20 the vertical L3 PCOs.

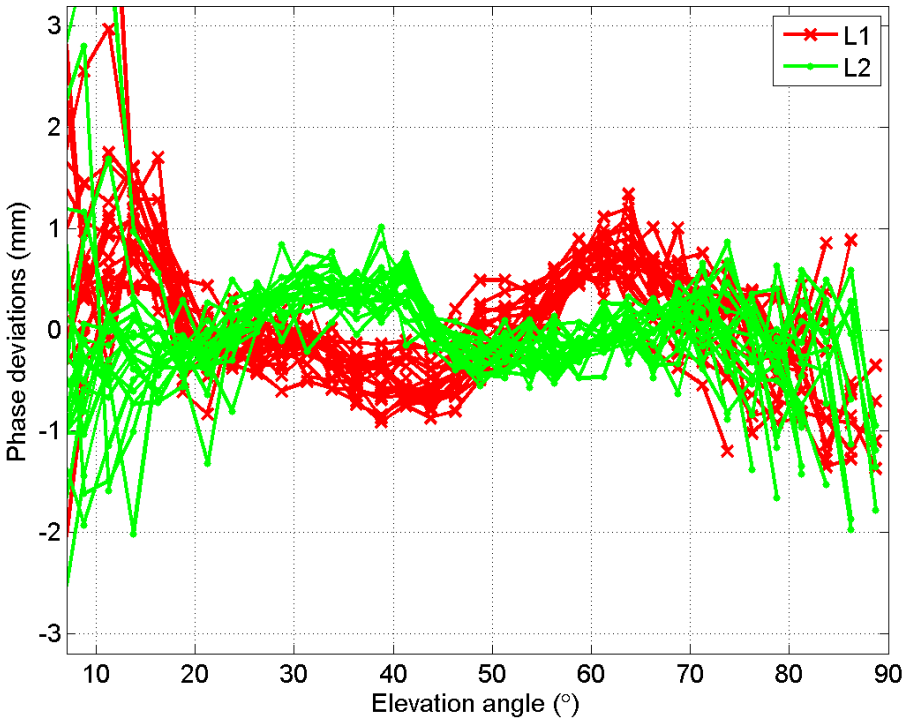

Figure 3.17 The estimated L1 and L2 phase deviations from the original model, "LEIAR25.R3, LEIT" for the 19 mast stations studied.

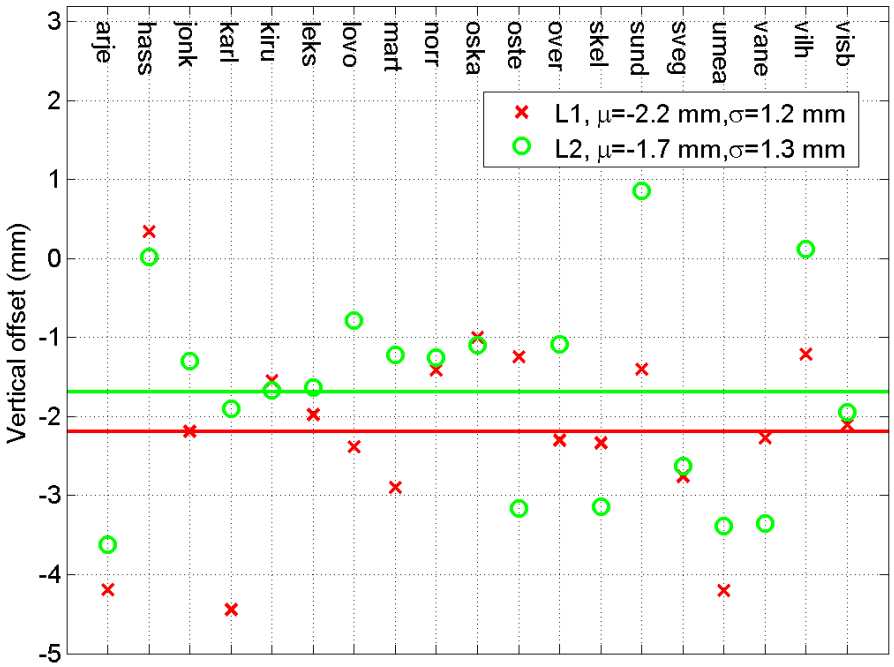

Figure 3.18 The estimated offsets for the modeled vertical components of PCO for the 19 mast stations. The mean values and standard deviations are given in the legends.

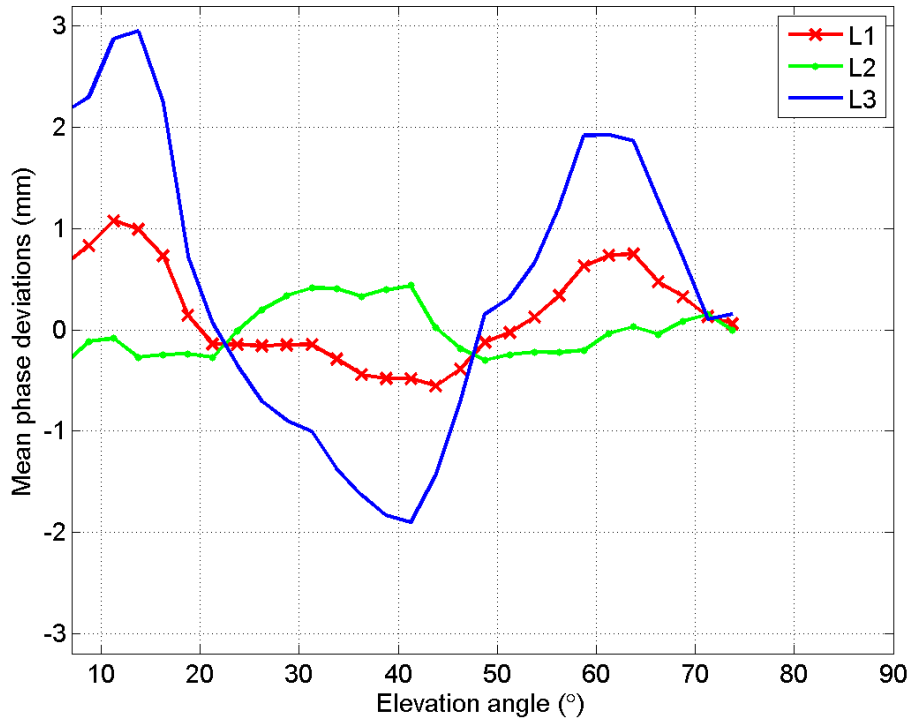

Figure 3.19 The mean of the estimated L1 and L2 phase deviations from the original model PCV, as well as the result when combining them to L3.

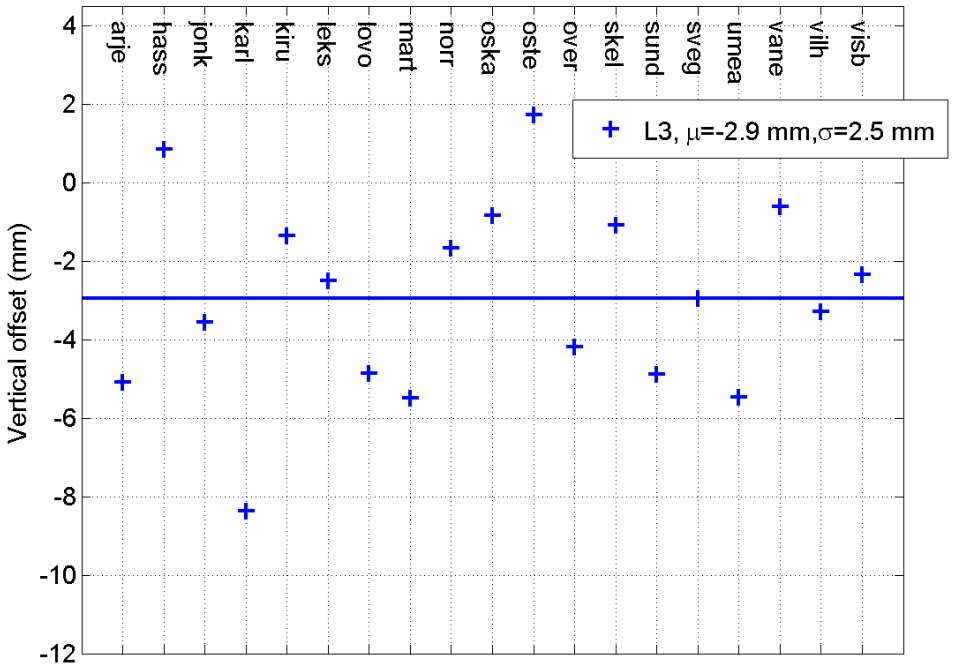

Figure 3.20 The L3 combination of the estimated L1 and L2 offsets for the modeled vertical components of PCO for the 19 mast stations. The mean value and standard deviation are given in the legends.

We simulated the effect of the data in L3T solutions. It was found that the strong PCV deviations found, together with the vertical PCO deviations could be expected to give on the average 11.5 mm to low estimates of the vertical component of the stations, i.e. of the same order as was found for the pillar stations earlier. See Table 3.3. The standard deviation in the vertical offsets was, however significantly larger, 5.0 mm for the mast stations, while it was 2.6 mm for the pillar stations.

We used the estimated mean L1 and L2 phase deviations, as well as the estimated mean vertical PCO offsets to create an updated general model for the mast antennas. Below in Table 3.4 we present the estimated vertical offset when using the updated model in L3T processing.

Table 3.3. Estimated vertical offsets when using L3 observables and the original PCO/PCV description model LEIAR25.R3, LEIT.

Station	Vertical offset (mm)
Arjeplog	-19.0
Hässleholm	-5.2
Jönköping	-11.0
Karlstad	-19.2
Kiruna	-9.0
Leksand	-10.3
Lovö	-17.4
Mårtsbo	-16.3
Norrköping	-7.4
Oskarshamn	-7.1
Östersund	-3.5
Överkalix	-13.9
Skellefteå	-12.6
Sundsvall	-15.5
Sveg	-12.6
Umeå	-17.6
Vänersborg	-4.4
Vilhelmina	-8.1
Visby	-11.5
Mean	**-11.5**
Std	**5.0**

Table 3.4. Estimated vertical offsets when using L3 observables and the updated PCO/PCV description file.

Station	Vertical offset (mm)
Arjeplog	-6.7
Hässleholm	5.5
Jönköping	-0.5
Karlstad	-8.4
Kiruna	3.8
Leksand	0.6
Lovö	-6.7
Mårtsbo	-5.1
Norrköping	3.1
Oskarshamn	3.5
Östersund	8.2
Överkalix	-1.6
Skellefteå	-0.6
Sundsvall	-4.2
Sveg	-1.4
Umeå	-6.0
Vänersborg	6.2
Vilhelmina	3.8
Visby	-1.1
Mean	**-0.4**
Std	**4.9**

The mean vertical offset is practically removed when using the updated antenna model, but the great spread between the stations remains. A component of the 4.9 mm standard deviation comes from the mismodeling of the reference pillar by the common pillar model used. In the pillar calibration the standard deviation was 2.6 mm and this should account for both the actual deviation between the pillar behavior, as well as the measurement errors in the calibration processing. Hence, we expect the deviation contribution from the pillar mismodeling to be smaller than 2.6 mm, and if we subtract the full value in quadrature 4.2 mm standard deviation remain as related to the mast model variations and measurement errors, i.e. still significantly larger than for the pillar station. A great spread in the day-to-day estimates of the vertical for this type of antenna and monument when equipped with LEIT radome was also presented in Section 2.2.

3.5 Verification of pillar and mast calibrations using 2015 data

We used the calibration visits to the stations in Hässleholm, Jönköping, Karlstad, Norrköping, Oskarshamn, and Vänersborg (see Figure 3.21) in October 2015 as means of verification of the results from the previous concrete pillar and steel grid mast calibrations. Three visiting antennas were placed over known markers and data were collected during approximately 6 days at each site. An elevation cut off angle of 12˚ was used. We noticed that disturbing vegetation had grown in the surroundings of the markers, and was often a larger problem than it was during the 2009-2010 calibration.

Figure 3.21. The SWEPOS site Vänersborg during a station calibration setup in November 2014. An Eccosorb plate is mounted directly below the choke-ring antenna. Note the typical SWEPOS concrete pillar and the recent steel-grid mast with the LEIAR25.R3 antenna and LEIT radome installed.

Below we present calculated vertical offsets of the monument antennas when using the new models derived in Section 3.3 and 3.4. For comparison, we also give the offsets when using the original models.

3.5.1 Concrete pillar stations

First, we present the analysis results for the original antenna model “AOAD/M_T, NONE” in Table 3.5. The L3T results agree fairly well with the results of Table 3.1.

Table 3.5. Estimated vertical offsets of the antennas on the concrete pillars when the model "AOAD/M_T, NONE" is used.

	L1	L2	L3	L3T
Hässleholm	-2.3	-0.5	-5.0	-10.1
Jönköping	-1.1	-0.1	-2.8	-11.2
Karlstad	0.7	1.2	-0.1	-6.8
Norrköping	-1.3	1.0	-4.8	-9.6
Oskarshamn	-1.9	-0.0	-4.7	-17.1
Vänersborg	-0.8	0.3	-2.5	-13.3
Mean	**-1.1**	**0.3**	**-3.3**	**-11.3**
Std	**1.0**	**0.6**	**1.9**	**3.5**

We analyzed the pillar stations data with the updated pillar antenna model, as described in Section 3.3. In addition, we also used this new general model together with the individual vertical L1 and L2 PCO values that were found in Section 3.3, forming partly individual models.

The L1 and L2 residuals, which are practically identical for the two processing models, are found in Figure 3.22. In Table 3.6, the corresponding vertical offsets for L1, L2, and L3 for the "pure" general model are found. We also included the results when the L3 combination was used in a simulated L3T solution. Fairly good agreements with the terrestrial measurements are found.

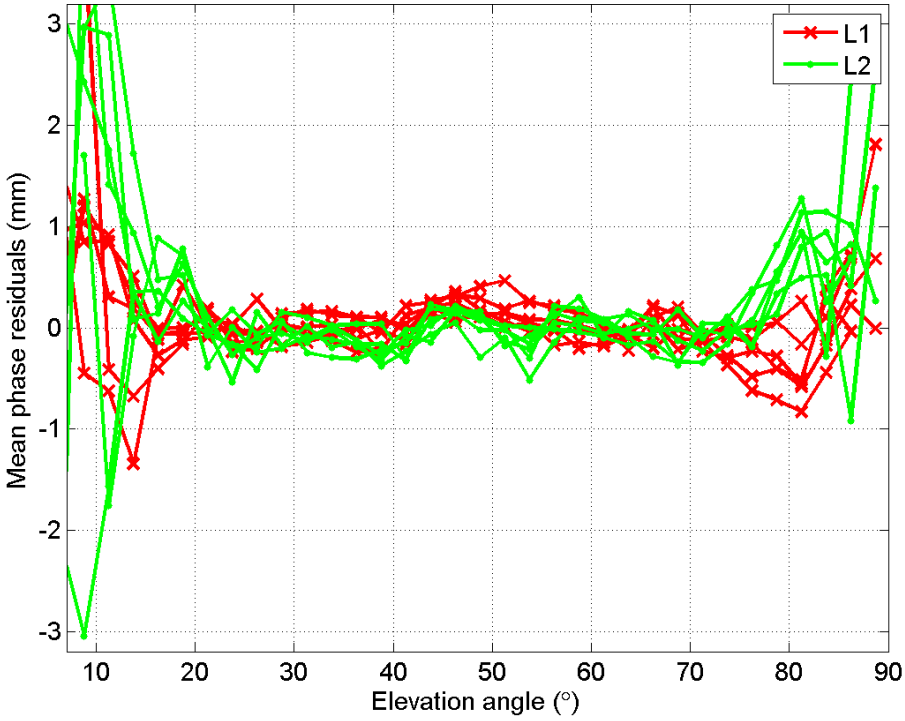

Figure 3.22. The L1 and L2 residuals when processing the 2015 pillar data with the updated antenna + monument model for the concrete pillar antennas.

Table 3.6. Estimated vertical offsets of the antennas on the concrete pillars when the general updated model from Section 3.3 is used.

	L1	L2	L3	L3T
Hässleholm	-2.3	-1.6	-3.3	3.2
Jönköping	-1.3	-1.2	-1.5	2.2
Karlstad	0.7	-0.1	1.7	6.8
Norrköping	-1.5	-0.2	-3.6	4.1
Oskarshamn	-2.0	-1.1	-3.3	-3.6
Vänersborg	-1.0	-0.9	-1.1	1.4
Mean	**-1.2**	**-0.9**	**-1.9**	**2.3**
Std	**1.0**	**0.6**	**2.0**	**3.5**

In table 3.7 we present the results for the case of individual models of the vertical PCO, but still the general PCV update (from the calibrations in 2009-2010, chapter 3.3.1). No improvement when compared to the general model used in Table 3.6 is found.

Table 3.7. Estimated vertical offsets of the antennas on the concrete pillars when the general updated model is used for PCV together with individual PCOs.

	L1	L2	L3	L3T
Hässleholm	-1.6	-2.0	-0.9	5.6
Jönköping	-0.7	-1.8	0.9	4.7
Karlstad	-0.4	-1.1	0.5	5.5
Norrköping	-1.2	-1.8	-0.4	7.3
Oskarshamn	-2.8	-2.9	-2.6	-2.9
Vänersborg	-0.7	-1.8	1.0	3.6
Mean	**-1.2**	**-1.9**	**-0.2**	**4.0**
Std	**0.9**	**0.6**	**1.4**	**3.6**

3.5.2 Steel-grid mast stations

First we present the analysis results for the original type-specific antenna model "LEIAR25.R3, LEIT" in Table 3.8. We also analyzed the data using individual calibration models for each mast antenna. The results from this analysis are given in Table 3.9. The L3T results of Table 3.8 agree fairly well with the results of Table 3.3. It is worth noting that the mean difference in L3T height offset of the individual models is "worse" than for the type-specific model (-16.1 vs -13.0 mm). This was also seen in the analysis of the data

from the test field at Lantmäteriet discussed in Section 3.4 (17.3 vs 15.9 mm, but with no radomes on the antennas).

Table 3.8. Estimated vertical offsets of the antennas on the steel-grid masts when the original model LEIAR25.R3, LEIT from igs08.atx is used

	L1	**L2**	**L3**	**L3T**
Hässleholm	-1.0	-0.7	-1.4	-4.8
Jönköping	-3.5	-1.4	-6.8	-18.8
Karlstad	-4.0	-1.1	-8.5	-19.3
Norrköping	-3.1	-1.2	-6.1	-15.5
Oskarshamn	-2.3	-1.1	-4.2	-15.9
Vänersborg	-2.5	-3.7	-0.6	-3.5
Mean	**-2.7**	**-1.5**	**-4.6**	**-13.0**
Std	**1.1**	**1.1**	**3.1**	**7.0**

Table 3.9. Estimated vertical offsets of the antennas on the steel-grid masts when the original model from GEO++ for antennas 08510020, 09030005, 09020011, 08510015, 09020015, and 09030007 are used

	L1	**L2**	**L3**	**L3T**
Hässleholm	-1.1	0.1	-3.0	-10.1
Jönköping	-1.2	-0.2	-2.6	-11.1
Karlstad	-3.1	-0.6	-7.1	-16.7
Norrköping	-2.3	-0.7	-4.9	-19.5
Oskarshamn	-1.4	0.7	-4.5	-20.6
Vänersborg	-3.7	-1.6	-6.8	-18.9
Mean	**-2.1**	**-0.4**	**-4.8**	**-16.1**
Std	**1.1**	**0.8**	**1.9**	**4.5**

The aim in Section 3.4 was to derive a general antenna + monument model for the steel grid masts. However, in the analysis of the October 2015 data we broadened the use of the Section 3.4 data. We used three different sets of models: 1) the updated general antenna model, 2) the updated general model for PCV together with individual vertical PCOs, and 3) individual vertical PCOs as well as individual PCVs estimated in the previous calibration. The results are given in Table 3.10, Table 3.11, and Table 3.12.

Table 3.10. Estimated vertical offsets when using the updated general PCO/PCV description file derived in Section 3.4.

	L1	**L2**	**L3**	**L3T**
Hässleholm	1.6	1.0	2.5	9.8
Jönköping	-1.1	0.3	-3.3	-4.6
Karlstad	-1.5	0.5	-4.6	-4.0
Norrköping	-0.7	0.5	-2.5	-1.4
Oskarshamn	0.1	0.6	-0.6	-1.7
Vänersborg	0.0	-1.9	3.0	10.6
Mean	**-0.3**	**0.1**	**-0.9**	**1.5**
Std	**1.1**	**1.0**	**3.1**	**6.9**

Table 3.11. Estimated vertical offsets when using the updated general PCV description, and individual PCOs.

	L1	**L2**	**L3**	**L3T**
Hässleholm	-1.0	-0.8	-1.3	6.0
Jönköping	-1.1	-0.1	-2.7	-4.0
Karlstad	0.8	0.7	0.8	1.5
Norrköping	-1.5	0.0	-3.8	-2.7
Oskarshamn	-1.1	0.0	-2.8	-3.8
Vänersborg	0.1	-0.3	0.6	8.3
Mean	**-0.6**	**-0.1**	**-1.5**	**0.9**
Std	**0.9**	**0.5**	**1.9**	**5.3**

Table 3.12. Estimated vertical offsets when using the individual PCOs as well as individual PCVs.

	L1	**L2**	**L3**	**L3T**
Hässleholm	-0.7	-0.8	-0.7	4.8
Jönköping	-1.2	-0.2	-2.6	-3.3
Karlstad	0.9	0.7	1.1	4.2
Norrköping	-1.3	0.0	-3.2	-5.4
Oskarshamn	-0.9	0.0	-2.4	-5.4
Vänersborg	0.3	-0.2	1.2	1.8
Mean	**-0.5**	**-0.1**	**-1.1**	**-0.6**
Std	**0.9**	**0.5**	**2.0**	**4.7**

The mast station results are significantly helped by both individual PCO and PCV values. The spread in The L3T results is still relatively large. This was also the case for the pillar results. The data from the visiting calibration data was noisier at low elevation than they were for the previous session about 5 years earlier. It is likely that the vegetation surrounding the relative low situated visiting antennas has larger influence in the recent data. Although it is tried to remove observations in directions where it is obvious that vegetation or other obstacles has had an influenced, there are certainly regions where data are slightly corrupted remaining at low elevations.

The L1 and L2 residuals when using the general PCV (cases 1 and 2), are given in Figure 3.23, and when using individual PCV models are found in Figure 3.24.

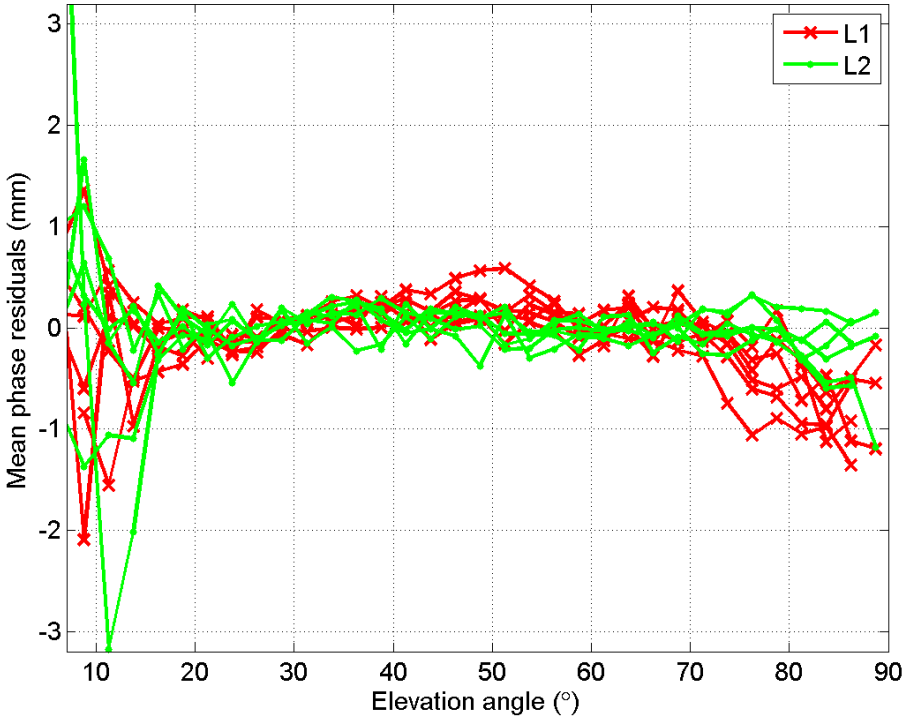

Figure 3.23. The L1 and L2 residuals when processing the steel-grid mast data with the model with updated general PCV.

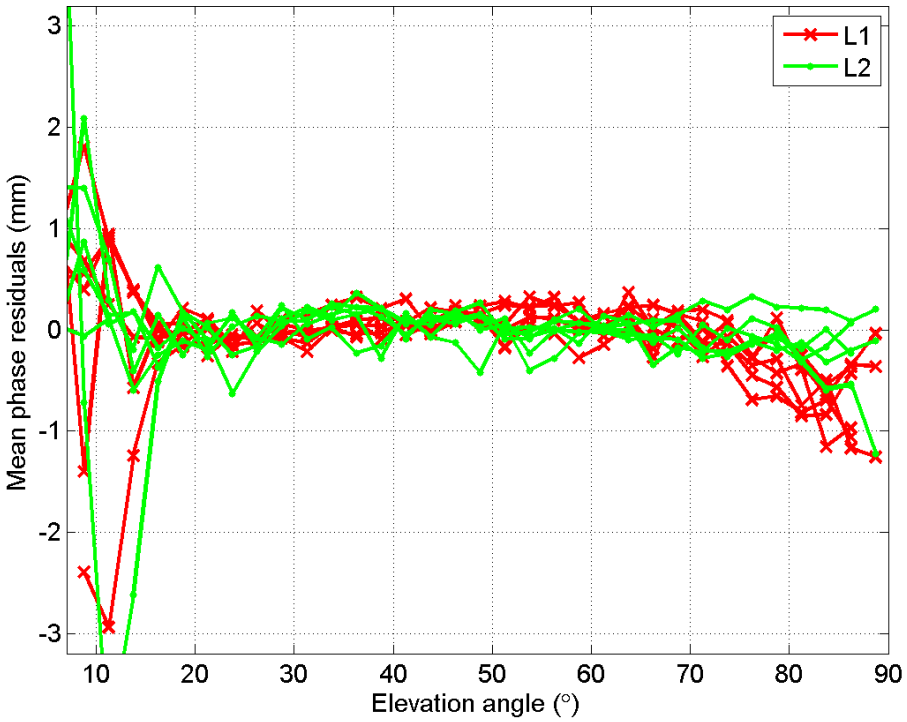

Figure 3.24. The L1 and L2 residuals when processing the steel-grid mast data with the model with updated individual PCV.

3.6 Discussion

In Sections 3.3 and 3.4, we investigated the possibility to generate general "antenna + monument" phase correction models for the antennas on concrete pillars, and steel grid mast antennas, respectively.

For the pillar stations the results in Section 3.3 shows that a general model seems to give consistent vertical coordinates typically on the level of a few mm, also for L3T solutions. A general model was constructed by using the original type-specific antenna model, and only adjusting the vertical part of the PCOs on L1 and L2 together with elevation-only dependent PCV corrections. In the processing, we did not investigate horizontal coordinates, partly because we were lacking good horizontal coordinates of the markers used for the visiting calibrations antennas at the time of processing, while we had good levelling data for vertical offset derivations. We think, however, that the east and north components of the antenna PCOs, as well as the azimuthal variations in the PCVs, are relatively unaffected by the monuments. The (mainly) circular symmetric structure around the vertical axis of the monuments used is believed to give rise to mainly elevation dependent phase deviations. For the Dorne/Margolin type antennas used on the pillar antennas, the individual variations in the east and north components of the L3 PCO from the type-specific PCO has been found to typically be 0-2 mm. We therefore think that also the east and north components resulting from using the derived general "antenna + monument" model in processing, is good to a few mm, as was the case for the vertical.

For the steel-grid masts with LEIAR25.R3 antennas using the derived general "antenna + monument" model performs worse than the pillar model. This was seen in both Sections 3.4 and 3.5. For the mast stations, individual antenna + monument models could be preferred. For such models, the original individual antenna models are probably better starting points, where the individual variations in east and north PCO, as well as individual azimuthal PCVs, could be inherited from the starting model.

In order to make a good antenna + monument model down to, say 10˚, clear visibility, e.g. without disturbing vegetation, down to 10˚ also for the visiting calibration antennas is vital. For the verification data in Section 3.5, this was not always the case. At lower elevation angles, when the phase observations normally get noisier, it is hard to distinguish between the more stochastic noise and the possibly systematic phase change caused by, e.g. vegetation. The generally increased scatter below 15˚ in many elevation angle graphs of this work package is likely to be caused by remaining disturbed data at lower elevation angles. These difficulties call for on-site removal of disturbing vegetation where this is possible and documentation of the directions where vegetation and other disturbances remain. The clear sky visibility is even more critical when a total updated antenna + monument model is constructed, i.e., 3D PCO and azimuth as well as elevation dependent corrections to the original PCV model are derived. In this case, we cannot afford to lose too big parts of the sky.

4 WP 3 – New Services

4.1 Introduction

The number of users of the national GNSS infrastructure SWEPOS is growing rapidly. The method currently used to achieve high accuracy is based on the concept of Virtual Reference Station (VRS) and requires two-way communication between the user and SWEPOS operational center. The need for two-way communication may in the future become a limitation, e.g. in terms of available communication lines, if the number of users continue to increase. As a consequence other real-time methods have been suggested which in principle is based on one-way communication and co-utilized or limited two-way communication (Master Auxiliary Concept, MAC, and Precise Point Positioning PPP).

The ongoing GNSS development results an increasing amount of GNSS satellites, each also broadcasting an increasing amount of different signals. SWEPOS service already comprises new GNSS and new signals which in turn increase the demand on the capacity of the communication lines. The VRS concept requires two-way communication between the operational center and rover and, in addition, the data is customized for the individual user. With an increase amount of satellites, signals and users we invision future limitations and the need for investigating alternative methods.

The idea of this work package is partly to study how a PPP service based on a dense network such as SWEPOS could be designed and investigate the level of performance that could be achieved. This study has included the simulation of the alternative methods VRS, MAC and PPP based on the current SWEPOS configuration.

The second part of this report deals with high-precision navigation at sea with the perspective that in the future keep track of boats with GNSS. The study has in particular investigated a possible high-precision service in the Baltic Sea with special focus on the vertical position.

4.2 Methods for supporting real time dynamic coordinate determination

Real Time Kinematic (RTK) is a system that utilizes Global Navigation Satellite Systems (GNSS) to provide accurate positioning in real time. The general idea in RTK is to receive GNSS-signals at a stationary reference station with known position coordinates and to use these to correct observation data at a roving receiver in another location. The ideal signal is perturbed by ionosphere, troposphere and imperfections related to ephemerides, clocks and multipath and thus the calculated position coordinates differ from the known coordinates. By calculating corrections that mathematically “moves” the reference to its known position and subsequently apply a similar set of corrections to the rover, the rover’s position can also be determined very accurately. As the reference and rover are at different locations, the signals have been perturbed differently and the correction data are therefore affected by uncertainties that compromise the reliability of the rover’s corrected position. An overview of the most significant error sources and their respective de-correlation characteristics are shown in Figure 4.1.

With RTK it is also implicit that, in addition to the broadcast code signals also the carrier phase of the signal is analyzed with a geodetic receiver. With this technique it is possible

to obtain position coordinates with accuracy of order 1 cm. The difference between RTK and Network RTK is that the latter combines data from several reference stations to provide the rover with corrections. With Network RTK the distance dependent errors are interpolated between the reference stations, which allows for increased distance between reference stations without losing position accuracy. There are currently several methods/concepts associate with the term Network RTK able to provide real-time services based on networks of permanent reference stations. In this report we address three of these i.e. VRS, MAC and PPP-RTK. Sometimes, and possibly more stringently, the VRS (Virtual Reference Station) and MAC (Master-Auxiliary Concept) are considered as Observation Space Representation (OSR-RTK), while for PPP-RTK (Precise Point Positioning) the term State Space Representation (SSR-RTK) are used (e.g. Choy et al 2016). Figure 4.2. gives a schematic picture of the data flow from the reference stations to a rover in the different methods.

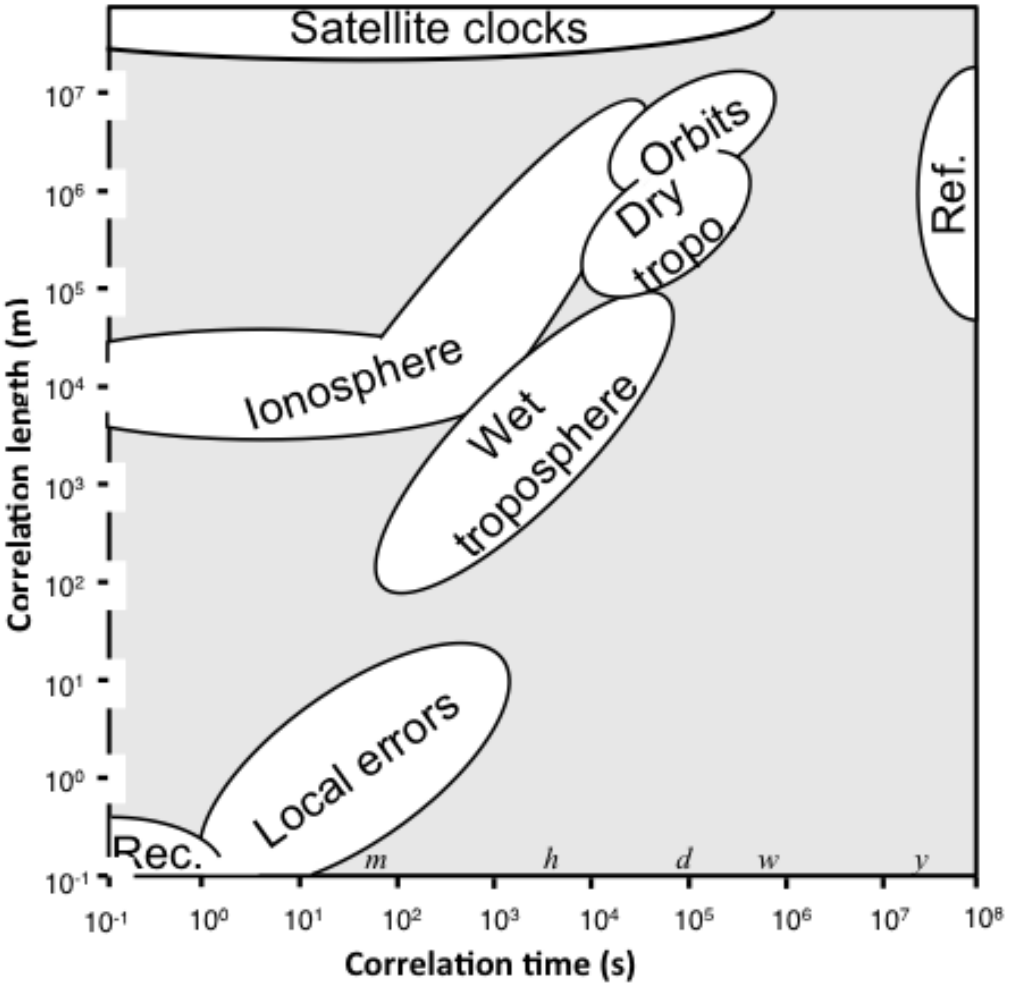

Figure 4.1. The correlation time versus correlation length for the most significant source of errors in GNSS.

4.2.1 Network RTK - VRS and MAC

In Virtual Reference Station, VRS, a rover calculates a position from uncorrected code data and uploads this navigated solution to the central unit (see Figure 4.2.). The central software then deploys a virtual reference station at the coordinates of the initial navigated solution on the common phase ambiguity level that is calculated from data from an

appropriate combination of the surrounding reference stations. From the synthetic data of the calculated surface, the VRS emulates a real reference receiver at the initial navigated coordinates. The rover receives the VRS data and calculates a relative positioning solution to the VRS from code and phase measurements of its own position on the relatively short baseline. In VRS one single stream of virtual reference station observations dedicated for the specific location, is sent to the rover. These observations are constructed from a combination of data from several surrounding reference stations.

Master-Auxiliary Concept, MAC, may be used as either a one-way or two-way communication system with minor modifications (see Figure 4.2.). Methodology in the case of two-way communication: As for the VRS, the rover uploads its navigated position to the central unit. The central software then appoints the closest reference station as Master and then transmits raw data from the Master and an appropriate set of Auxiliary stations to the rover. The rover receives raw data from the appointed stations and makes phase corrections to all of these. In MAC observational data from multiple reference stations are sent to the rover(s) in an area. For practical reasons data are sent as one (master) station stream, and the data from the other stations are sent in the form of deviations from the master station data. With MAC corrections the receiver performs some of the processing that the central software would do in the case of VRS, e.g. interpolation of station distance dependent effects.

The possible quality of coordinate determination achievable using VRS and MAC are basically equal, from our idealized theoretical perspective. The difference between the methods is merely a question of how to use distribution channels and calculation resources. In VRS the main correction calculations have been made centrally, and the rover can regard the data as coming from a single reference station and use standardized methods for RTK. A drawback with VRS, which is increasing in significance, is the necessity to form unique data streams for each rover. In MAC a greater demand on the rover ability to perform the calculation but the data streams could be designed for all rovers in an area.

4.2.2 PPP and PPP-RTK

The concept of (traditional) Precise Point Positioning (PPP) is based on dual-frequency code and phase observations with one single receiver. PPP requires precise satellite position and corresponding clock information. For post processing PPP applications this can be obtained, for example, from the International GNSS Service final (IGS) or rapid (IGR) products. For real-time applications the IGS provides an ultra-rapid product with predicted satellite positions (IGU).

This type of real-time service cannot, however, compete with VRS/MAC in real time since with PPP it is not possible to form double differences, thus, the ambiguities cannot be rounded to a nearest integer. Ambiguities in PPP processing remain real-valued. Using precise GPS satellite clock estimates, it has been shown that static PPP solutions can achieve solution precision comparable to differential processing. The main disadvantage of PPP with good clocks, compared to differential processing, is that the solutions generally take longer to converge than ambiguity-resolved differential solutions. It should be noted that some position dependent error remains in the PPP corrections due to residual satellite orbit errors.

PPP corrections of satellite positions and clock errors are in principle independent of the rover position and the same corrections can be applied to rovers over large areas.

Thus it has been suggested to try to combine the advantages of network RTK differential GPS and PPP to a concept sometimes referred to as PPP RTK (see Figure 4.2.). This concept implies that corrections can be determined from a regional network and broadcast to cover an area the size of a country or even a continent.

While the satellite positions can be predicted well, (10 cm level over several hours,) the corresponding satellite clock behavior cannot be predicted with equivalent accuracy and frequently have m-level errors. It is often assumed that IGU satellite positions to be correct and the dual frequency data from a ground-based reference network are used to estimate corresponding satellite clock corrections and atmospheric propagation path delays.

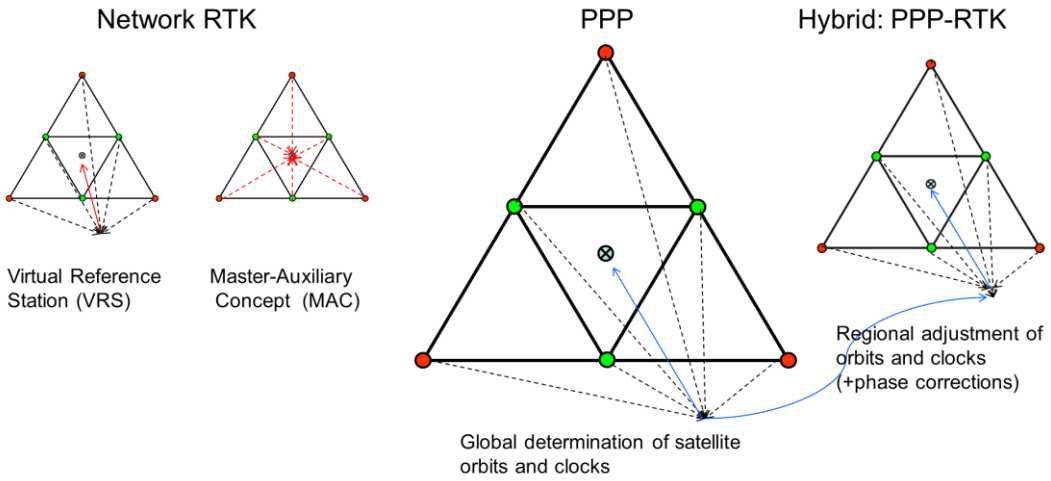

Figure 4.2. Real-time GNSS methods for high-precision positioning and navigation.

4.3 Network-RTK

In earlier studies (see CLOSE-RTK I) we have discussed the expected performance of network-RTK for typical baseline of 70 km and shorter. The CLOSE 1 report showed that it is possible to provide a network-RTK service better than 2 cm (3D) with a dense configuration of SWEPOS. This is also confirmed by the results in Figure 4.3.

However, for applications where such a dense infrastructure is difficult to establish, e.g. positioning service for the Baltic Sea, we need to investigate the effect of a sparser network of reference stations. We therefore performed simulations according to the same model as used in CLOSE-RTK I. The simulations are based on theoretical models of the main error sources propagating in to a virtual rover. In all simulations it has been assumed that the rover has been able to resolve integer phase ambiguities. Furthermore, we assume a dynamical (non-static) situation where coordinates, clock, and possibly other parameters such as ZTD, have to be estimated from observations lasting only a few seconds.

Figure 4.3 shows the result of the simulations for reference network with station separations up to 2000 km. It is obvious that the ionosphere-free linear combination, i.e. L3, should be used for baseline linger than 70 km. However, also the L3 linear combination has degradation with longer baselines due to increasing differences in the tropospheric propagation path delay between rover and reference stations. Based on such a conclusion it might be suggested to try to estimate the rover Zenith Tropospheric Delay (ZTD) along with the coordinate estimations. In Figure 4.3 we have included such

simulations and the result is somewhat disappointing. We find that including the estimation of ZTD on the rover side results in a RMS vertical error more or less independent of baseline length and becomes compatible with the normal L3 (without ZTD estimation) first at baselines around 1000 km. At that size of baseline lengths we may assume that phase ambiguity fixing is also extremely difficult which means that the entire concept of network-RTK breaks down anyway.

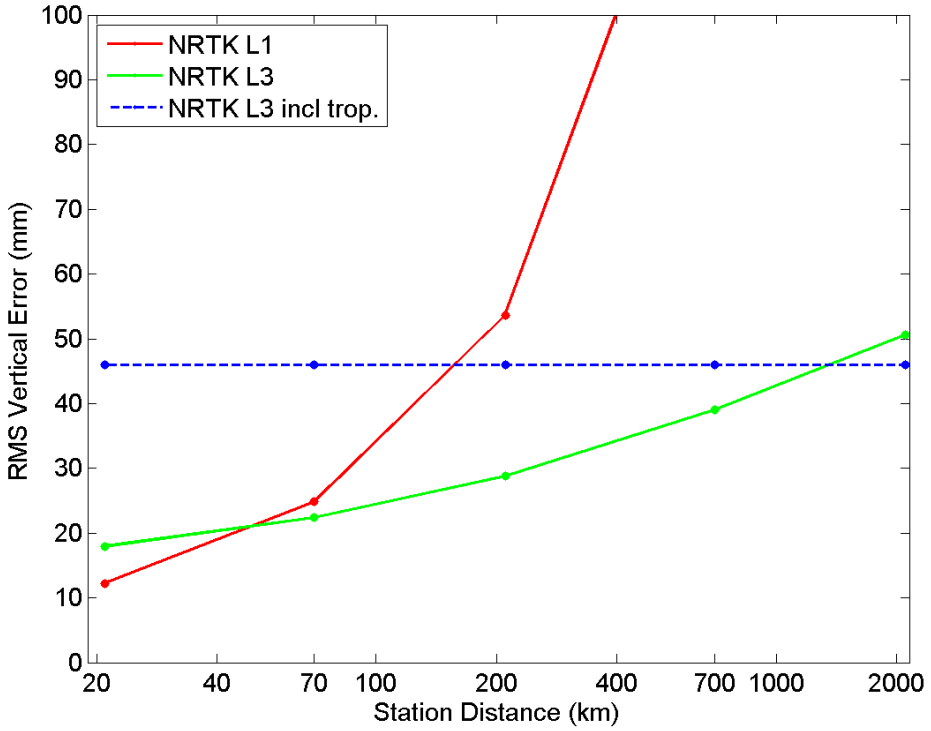

Figure 4.3 The vertical results of the simulations for reference network with station separations up to 2000 km for three different observing methods i.e. L1 and L3 with and without ZTD estimation.

Although estimating a local ZTD at first may seem favorable the drawback is that it opens up for interaction between estimated parameter leading to the absorption of small phase deviations in an incorrect way. With the inclusion of ZTD in the estimation process there are three parameters, which solely depend on elevation angle i.e. not azimuth. The partial derivative for the vertical component equals *–sin(el)*, the partial derivative for ZTD is close to *1/sin(el)*, and the clock partial derivative is a constant. The network-RTK software always tries to fit a set of phase deviations at different elevations to an optimal combination of these three functions. Such phase deviations are mainly real position and clock changes but a small fraction of the deviations may arise from unwanted effects. They will then also contribute to the estimates of the vertical, clock and ZTD. Obviously also the horizontal component may be affected but not at the level. Thus we here, for simplicity, focus on the vertical component. A simple illustration of how small and un-modeled phase deviations may cause incorrect estimates is provided in Figure 4.4.

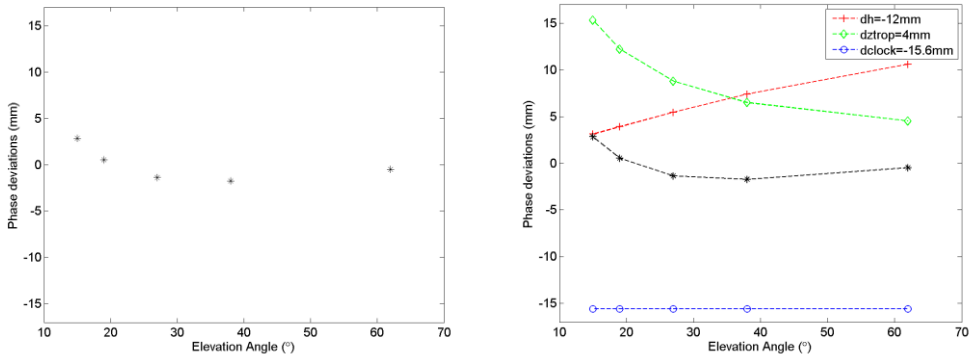

Figure 4.4. An illustration of the possible absorption of phase deviations when estimating ZTD. The left plot show a set of phase deviations as a function of satellite elevations; their sizes are such that they could originate from local reflections. The right plot show phase deviations originating from a) red curve: a vertical offset of -12 mm, i.e. the function 12*sin(el) mm, b) green curve: a ZTD offset of 4 mm, and c) blue curve: a receiver clock offset corresponding to -15.6 mm. The sum of these deviations gives the black curve, with phase deviations equal to those of the left plot. A least squares solution might therefore interpret the relatively small deviations of the left plot as originating from the combination of the bigger offsets of the right plot.

In the context of Network-RTK for longer baselines L3 has to be used. Including ZTD estimations do not improve the performance of network-RTK. It should however be noticed that we in our simulations the ZTD estimate has been regarded as a dynamic parameter. Thus, we have not made use of the fact that new estimates of ZTD can be based on knowledge of the past together with new observation as in Kalman-filtering. Kalman-filtering may be an alternative and this is handled in the next chapter.

4.4 Precise Point Positioning

The performance of PPP, or rather the regional method PPP-RTK, could in theory reach the same level as NRTK. The assumptions generally made when simulating PPP performance is that L3 is used in order to handle the ionospheric propagation path delay. As mentioned is chapter 4.2 the accuracy of the IGU orbits (predicted part) is at the level of 5-10 cm today which is sufficient for the real-time high-precision services. It is also unlikely that locally adding more stations will significantly improve the satellite orbit accuracy. On the other hand, prediction of clocks, in this case satellite clocks, are difficult or rather impossible. It has been demonstrated by the IGS and commercial services that satellite clock estimates can be calculated and provided to users in real time. It has also been demonstrated (Mervart et al, 2011) that adding local/regional reference stations can contribute to feed ZTD in real time to user in the vicinity.

In Figure 4.5. we show simulations of a possible scenario using NRTK and PPP RTK. The simulations assume dynamic conditions for first hour and then the software is demanded to treat the coordinates as static i.e. the data can be averaged after the first hour. Furthermore, we assume in the simulation that the PPP RTK solution requires 30 minutes to converge (dashed blue line). The dashed red line (NRTK simulations) indicates that there is a limitation due to the expected uncertainty in the reference station performance e.g. coordinates.

From Figure 4.5 we can also notice that PPP RTK in fact has the capability to beat dynamic NRTK if averaged over time scales of 30 minutes (Figure 4.5 where the blue

curve intercepts the straight red curve). On the other hand, if also NRTK is modeled as static i.e. averaged over longer time scales, it still performs better than PPP RTK

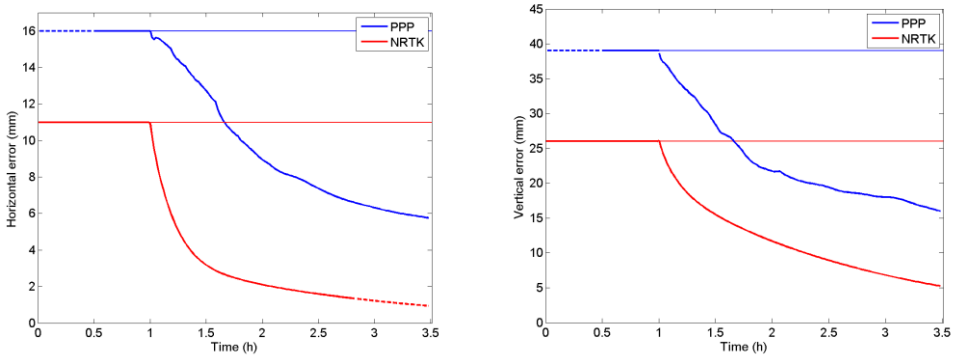

Figure 4.5. Simulations of a possible scenario using NRTK and PPP RTK. The simulations assume dynamic conditions for first hour and then the software is demanded to treat the coordinates as static i.e. the data can be averaged after the first hour. Furthermore, we assume in the simulation that the PPP RTK solution requires 30 minutes to converge (dashed blue line). The dashed red line (NRTK simulations) indicates that there is a limitation due to the expected uncertainty in the reference station performance e.g. coordinates.

In Figure 4.6 we show simulations of the PPP performance in terms of the horizontal (red) and vertical (blue) coordinate error as a function of the quality of the observables. For the simulations we have assumed that the ionospheric-free linear combination, L3, is used. Furthermore, we assume that the rover is required to estimate, besides receiver coordinates and clock, the zenith tropospheric propagation path delay (ZTD). The real problem is however to fix the phase ambiguities. Several scientific studies have shown that ambiguity resolution based on different PPP RTK techniques is possible. Unfortunately, it takes longer time then in NRTK. At least 10 minutes in rather perfect conditions are required. In comparison NRTK normally require less than a minute to achieve the same results and with a high likelihood of being correct. This was studied in detail in the project CLOSE-RTK I (Emardson et al, 2009). Similar results have been indicated in other more recent publications (e.g. Choy et al, 2016).

Another future option not shown in Figure 4.6 is that a future service based on PPP RTK is capable of providing, in addition to satellite orbits and clocks, accurate local ZTDs to a rover. In that case ZTD estimation at the rover is no longer required. In theory this gives a similar scenario as in the case of NRTK using L3 without estimating the ZTD. If ZTD is not estimated, we can assume a similar performance as in NRTK L3 (green) in Figure 4.3. However, again we have to remind ourselves that this performance is under the assumption that phase ambiguities are already resolved.

This means that there is, after initialization of phase ambiguities and under specific conditions, a possibility that PPP RTK can perform at the level stated by e.g. in FUGROs service Starfix.G2+. According to FUGRO the service is capable of, in ideal conditions, providing a service at the level of 30 mm. This is in accordance with the simulated results in Figure 4.6. In case of problems the service falls back to the decimeter-level stated by e.g. the NASA-Jet Propulsion Laboratory (JPL).

In the case of the FUGRO service, it is also likely that the rover system is a black box and cannot be replaced by other receiver systems. Thus, we are inclined to believe that the FUGRO rover estimates the ZTD together with receiver coordinates and clock. This is something that maybe a local reference network could assist with in a PPP-RTK solution. Our conclusion is however that the real key to getting an extended user group (outside the

decimeter-level applications) is to speed up the ambiguity resolution. Adding local information such ZTD in a PPP RTK service may be a step in the right direction but will not solve the whole problem.

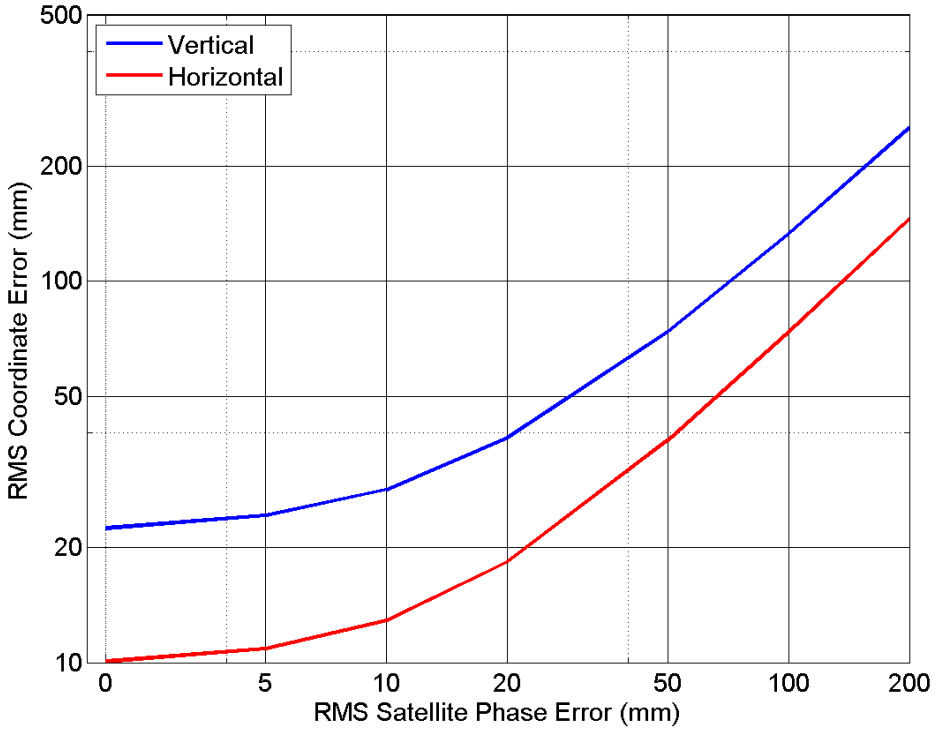

Figure 4.6. Simulations of the PPP performance in terms of the horizontal (red) and vertical (blue) coordinate error as a function of the quality of the observables. For the simulations we have assumed that L3 is to be used and that phase ambiguities are fixed. Furthermore, we assume that the rover is required to estimate, besides receiver coordinates and clock, the zenith tropospheric propagation path delay (ZTD). If ZTD is not estimated we can assume a similar performance as in NRTK L3 (green) in Figure 4.3.

Future PPP-RTK will be based on three-frequency observations and with the availability of many satellites and satellite systems. This will obviously increase the possibility to achieve robust and faster ambiguity fixing. However, in order to do so further research on inter-system and inter-satellite biases is required.

4.5 Future GNSS services for the Baltic Sea

4.5.1 Background

This work package is itended as a study of how a high performance GNSS service for the Baltic Sea can be designed. The intended application is a boat in motion. The work is of course strongly correlated with the insights obtained in chapter 4.4, but the study is not tied to a specific type of service. It may be Network RTK (VRS or MAC) or PPP, or variations of these. The performance of the proposed solution is analyzed to get an idea of how good it may be. Possible data communication aspects at sea is also considered as it may be regarded as an important factor. Furthermore, for some simulations, we have taken the liberty to add new permanent GNSS reference station where it seems appropriate and bring extra value in to a high-precision GNSS service in the Baltic Sea.

4.5.2 Possible use of NRTK

The dense SWEPOS network is likely to provide accurate virtual reference data to service the Baltic Sea areas near the Swedish shore. This has been tested and confirmed thorough investigations made by Lantmäteriet and SjöV (Norin et al 2012).

However, the width of the Baltic Sea is such that you can be located up to 100 km from the Swedish coast but still on Swedish waters and, thus, on borderline where the concept of NRTK fails to work. Even if the possibility to use the FinnRef stations is considered it still could be very difficult to achieve accurate positioning under dynamic conditions.

The map in of Figure 4.7 shows the locations of the SWEPOS stations along the Baltic Sea coast as well as the FinnRef stations. We have marked two locations within Swedish territorial waters with a cross in the map i.e.

1) A location with approximately 150 km to the closest reference station. However, a rover equipment in that area will be surrounded by reference stations provided that FinnRef stations can be included.

2) A location south of Gotland, far from the Swedish coast, and where it is likely that no new reference can be added in order to surround a possible rover equipment in the area. This situation, which implies access to reference stations only in one direction, is not beneficiary for accurately correcting for error sources such as atmospheric delay deviations and satellite orbit model errors.

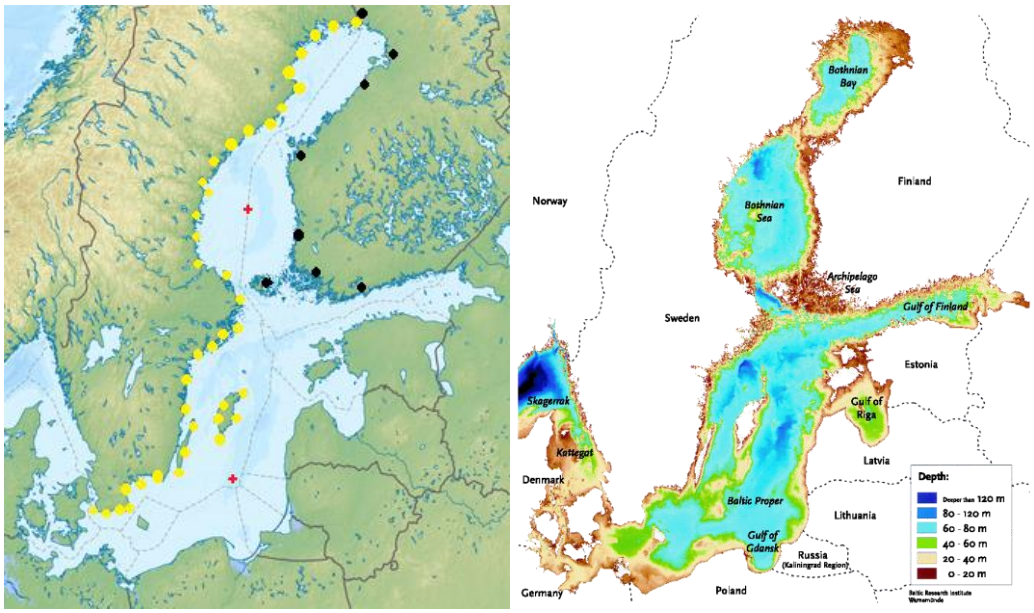

Figure 4.7. Left:The Baltic Sea area with the coastal SWEPOS stations marked in yellow, and coastal FinnRef stations marked in black. Red crosses mark locations far from existing reference station infrastructure. **Right**: Bathymetric map of the Baltic Sea (from Miljöstyrelsen, Denmark) where it shows relatively shallow waters in the neighborhood of the red crosses, indicating possibilities to add infrastructure also at sea.

The possibility to cover two locations marked with red crosses with an NRTK service is discussed in this section.

The expected coordinate accuracy for item 1, provided that the phase integer ambiguities are resolved, could be estimated from the previous chapter. Assuming access to data from the closest FinnRef stations we can say that the rover is surrounded by reference stations which form a network with baselines of the size 200 km. From Figure 4.3 it is seen that vertical RMS errors of the order of 30 mm can be expected.

The expected coordinate accuracy for item 2 is dependent on how well the Network RTK software has been able to distinguish the different error sources from each other. For instance, the influence of the satellite orbit modeling, is negligible for rover surrounded by a relatively dense network of reference receivers as discussed in the report CLOSE-RTK I (Emardson et al, 2009). However, in the present situation, where the models need to be extrapolated to a point outside the area of model construction, the influence of orbit model errors could be significant.

We have assumed that data from FinnRef stations along the coast could be included in the service. These stations are vital for providing an NRTK service in the Gulf of Botnia. The situation could be slightly improved if stations were established, e.g., in the archipelago of Luleå and on Holmöarna, but in the southern part of the Gulf of Botnia, in the area around the upper red mark in the map, there is a lack of island on which new installations can be made. In the southern part of the Baltic Sea the inclusion of an existing station on Bornholm, and a new installation on Gotska Sandön could give some improvements in their vicinities.

In Figure 4.7 right, some areas of relatively shallow waters, also far from the coast, is indicated. New infrastructure with additional GNSS reference stations also at these locations, would improve the possibility for a reliable high precision positioning service in the Baltic Sea significantly.

However, the main challenge for an NRTK service on the Baltic Sea is most likely not the degraded coordinate accuracy when integer ambiguities have been resolved, but merely the time it takes for this integer fixing and the probability that it will be resolved at all under turbulent atmospheric conditions. The questions about integer fixing is impractical to try to answer by any of our simulations, since they heavily depend on which algorithms that are used in the proprietary software code of the rovers. Instead, we suggest a set of experiments, involving real RTK rover equipment in conditions that emulate the expected conditions on the Baltic Sea.

4.5.3 Proposed experiments for better NRTK performance

A set of experiments could be conducted in order to give more qualified statements of the expected NRTK performance on the Baltic Sea. We could emulate the reference station configurations of interest using another set of stations on the Swedish mainland with similar configuration, and draw conclusions from that. There are a couple of options:

A) If it is possible to control the NRTK software in such a way that a predetermined set of reference stations are used we could select stations with a configuration that emulates 1) the sparse reference station configuration of the upper red mark, and 2) the “extrapolating” conditions associated with the lower red mark.
B) If it is impractical to deliberately select the reference station set in the NRTK software we could use stations outside of SWEPOS to conduct tests of the “extrapolation”. We could, for instance, use the coordinates of the FinnRef stations "FINS" on Åland and "VAA2" in Vaasa, which both are relatively close to the SWEPOS stations (about 100-150 km away). These coordinates could be

used in calls to the NRTK service and the resulting virtual reference station data be gathered for subsequent post-processing. In this processing the VRS data is compared to the actual data acquired at the two FinnRef stations, and error baselines could be determined.

C) The VRS from a sparse reference network, associated with the upper red mark, could also be simulated in software. Without involving the NRTK service at all, we could generate the expected VRS data stream by collecting the RTCM data from a receiver collocated with the rover (e.g. connected to the same antenna) and degrade the quality of the observation data by adding simulated errors according to models. See Figure 4.8.

For options A) and C) we can study the expected coordinate quality as well as the probability of and typical time to integer fixing. For option B) the expected quality can be evaluated in post-processing. For all three options we can also study the quality of a "fall back" DGPS service, using the VRS code data.

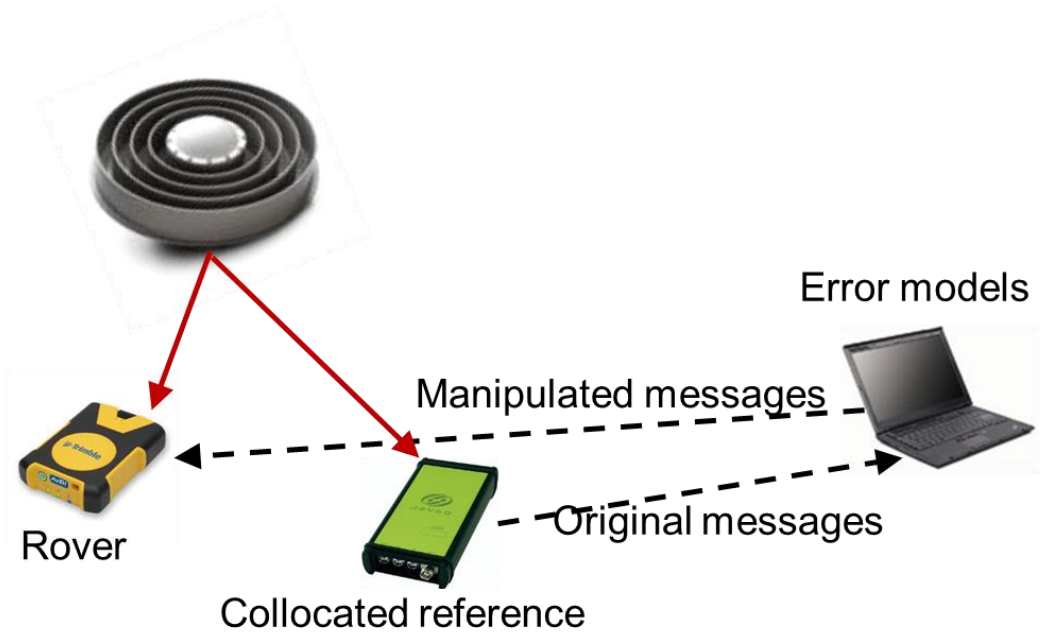

Figure 4.8. A possible experimental setup for analysing the preformance of an NRTK service in a sparse network of reference stations. The simulated VRS data stream is generated from the RTCM data produced by a receiver collocated with the rover receiver. The RTCM data are manipulated in real time by a PC based on models of the expected errors introduced by the large distance between the rover and the simulated reference stations. A similar experimental setup was used in the Close-RTK 2 project in order to simulate increased ionospheric activity see (Ref CLOSE-II).

4.6 Concept for a VRS-based mass market service

NRTK based on the VRS concept is described in chapter 4.2.1. Some limitations of this concept for the implementation as a mass-market service with connected units in the range of 100’ or millions may be identified:

- It requires two-way communication between each connected unit and the central service provider

- there are individually adapted data streams for each user which booth require large computer capacity at the service provider, as well as large data communication capacity.

Thus, the VRS concept is not primarily designed or optimized for a broad cast mass market service. On the other hand, it has shown to be a robust concept that has been implemented in most (European) countries and are used with good performance since more than a decade.

Some assumptions on the future cm-level GNSS mass market

A reasonable assumption may be that the units ("mobile phones" in the broad sense, or "vehicles" that may be autonomous or not to different degrees") that will consume the "cm-level GNSS mass market service" will be connected to the Internet. And this connection will most likely be through the mobile phone infrastructure like 3G, or rather 4G or the coming 5G. Since there are on-going development work within the 3GPP standardization activity regarding framework for precise GNSS in the mobile phone communication standards, we may assume that the providers for mobile communication will also provide the GNSS services to the end users. (But the services should preferably be based on the existing GNSS infrastructure like e.g. SWEPOS in Sweden.)

Possible design

Since the devices are connected to a base station in the mobile phone network, the service provider knows approximately where the user is located (to the extent that this information is needed). And in principle all users near a specific base station could share the same data stream from a VRS point close to that base station. And since the base station sometimes knows in which direction the users are, the VRS may even be located a bit away from a single base station, in order to have the VRS closer to the users. It can also be noted that the spatial density of mobile phone base stations is higher in 4G and 5G networks compared to the older 3G networks.

Taking this into account, the VRS-based mass-market service may utilize a number of "fixed" VRS-points close to radio base stations wherefrom RTK-data are broadcasted to all users connected to that base station. Since roaming is already taken care of in the mobile network, this information could also be beneficial for the RTK-service.

The number of needed VRS points and data streams for such a service is of interest. Sweden is about 450 000 km^2. An equilateral triangle with side length of 8.6 km have maximum distance to a node of 5 km and an area of approximate 32 km^2. A network of about 14 000 such triangles would cover Sweden and include 7000 nodes or VRS points.

Following these principles, it seems feasible to set up a NRTK service for a future mass market based on the VRS concept.

4.7 Discussion

The GNSS PPP concept has been used over several decades (Zumberge et al., 1997) but mainly in high-precision applications only requiring post-processing of GNSS data. Over the last decades several services based on the PPP technique have become available globally e.g. STARFIX by Fugro. These systems are provided on commercial basis and, thereby tied to use of manufacturer-dependent hard- and software. More services are

expected, perhaps directly from the GNSS systems (e.g. Galileo) themselves, in the near future.

The ongoing development of the PPP-RTK concept, besides using global satellite clock and orbit data, also investigate means to incorporate local or regional correction models for e.g. atmosphere and ionosphere. The results so far are promising however some obstacles have to be overcome. The means of distribution of these corrections are not yet fully implemented. In RTCM SSR, booth special messages for ionosphere and troposphere are included in the concept. Although not yet ready and accepted in the standard.

Future PPP-RTK will be based on three-frequency observations and with the availability of many satellites and satellite systems. Comparable to what is possible to achieve with PPP-RTK today, the adding of a third frequency will give an improvement in terms of time of convergence. This will obviously increase the possibility to achieve robust and faster ambiguity fixing. However, in order to do so further research on inter-system and inter-satellite biases is required.

Three-frequency PPP-RTK technique is very promising a will most likely be heavily used in many real-time applications in the future. New signal and system together with new innovation regarding algorithms and distribution will make possible more robust and faster solution. There will also be precision improvements and a 3-d position estimate at the level of 5 centimeters seems possible. Thus, PPP-RTK will be an important option for real time application not necessarily requiring the level provided by Network-RTK.

This page intentionally left blank.

5 References

Choy S, Bisnath S, Rizos C (2016) “Uncovering common misconceptions in GNSS Precise Point Positioning and its future prospect”. *GPS Solutions* (2017) 21: 13. https://doi.org/10.1007/s10291-016-0545-x

Emardson R, Jarlemark P, Bergstrand S, Nilsson T, Johansson J (2009) “Measurement accuracy in Network-RTK. SP Report 2009:23, SP Technical Research Institute of Sweden. https://www.lantmateriet.se/globalassets/kartor-och-geografisk-information/gps-och-matning/geodesi/rapporter_publikationer/publikationer/measurement-accuracy-in-network-rtk.pdf (sited 2017-08-21)

Emardson R, Jarlemark P, Johansson J, Bergstrand S (2011) “Ionospheric Effects on Network-RTK. SP Report 2011:80, SP Technical Research Institute of Sweden. https://www.lantmateriet.se/globalassets/kartor-och-geografisk-information/gps-och-matning/geodesi/rapporter_publikationer/publikationer/ionospheric-effects-on-network-rtk.pdf (sited 2017-08-21)

Görres, B., J. Campbell, M. Becker, and M. Siemes (2006), ”Absolute calibration of GPS antennas: laboratory results and comparison with field and robot techniques”, *GPS Solutions*, Vol. 10, 2, pp 136-145, May 2006.

Granström C (2006) “Site-Dependent Effects in High-Accuracy Applications of GNSS”, Licentiate Thesis, Chalmers University of Technology, Göteborg, Sweden.

Jarlemark P, Lidberg M, Kempe C, Jivall L, Johansson J M, Ning T (2012). ”Station calibration of the SWEPOS™ network” Report on the Symposium of the IAG Subcommission for EUROPE (EUREF), held in Saint-Mandé, France, 6-8 June 2012. http://www.euref.eu/symposia/2012Paris/P-02-p-Kempe.pdf (sited 2019-02-28)

Kempe, Tina, Lotti Jivall, and Martin Lidberg (2010), “Station Calibration of the SWEPOS™ Network”, In Proceedings of the 16th General Assembly of the Nordic Geodetic Commission, Edited by S O Henriksen and A Jörgensen, Sundvollen Norway, September 27-30, 2010.

Lehner W M (2011). “Evaluation of Environmental Stress on GNSS-monuments”. Master Thesis Vienna University of Technology and Chalmers University of Technology. http://publications.lib.chalmers.se/records/fulltext/165054.pdf (sited 2017-08-15)

Lidberg M, Jarlemark P, Ohlsson K, Johansson J (2016). ”Station calibration of the SWEPOS GNSS network”. Proceedings of the FIG WW in Christchurch, New Zeeland 2016. http://fig.net/resources/proceedings/fig_proceedings/fig2016/papers/ts02b/TS02B_lidberg_jarlemark_et_al_8293.pdf (sited 2017-08-24)

Mervart, Leos, Lukes, Zdenek, Rocken, Christian, Iwabuchi, Tetsuya (2008), "Precise Point Positioning with Ambiguity Resolution in Real-Time," *Proceedings of the 21st International Technical Meeting of the Satellite Division of The Institute of Navigation (ION GNSS 2008)*, Savannah, GA, pp. 397-405.

Norin D, Sunna J, Lundell R, Hedling G, Olsson U (2012) “Test of RTCM Version 3.1 Network RTK Correction Messages (MAC) in the Field and on Board a Ship for Uninterrupted Navigation”. http://www.lantmateriet.se/globalassets/kartor-och-

geografisk-information/gps-och-matning/geodesi/rapporter_publikationer/publikationer/norin_etal_iongnss2012.pdf

Schmitz, Martin, Gerhard Wübbena, and Michael Propp (2008), “Absolute Robot-Based GNSS Antenna Calibration – Features and Findings –“. Available from http://www.geopp.com/

STARFIX by Fugro, Available from https://www.fugro.com/our-services/marine-asset-integrity/satellite-positioning/starfix

Zumberge, J.F., M.B. Heflin, D.C. Jefferson, M.M. Watkins and F.H. Webb (1997). “Precise point positioning for the efficient and robust analysis of GPS data from large networks”. *Journal of Geophysical Research*, Vol. 102, No. B3, pp. 5005-5018.

Appendix A: Summary graphs from analysis of OTT2 and OTT4

Below follow summary graphs of the weekly analysis results for GPS and GLONASS using L1, L2, L3, and L3T (i.e. estimation including tropospheric parameters from L3). A total of 16 weeks, day of year 56 to 168, 2015 have been analyzed. The weekly hardware changes performed at stations OTT2 and OTT4 are presented in in the reports of Appendix B.

In each summary graph the three upper graphs show the excess 3-d coordinates of the present week, surrounded by the results for the previous and following week for clarity. The statistics shown to the right of the graphs are valid for the present week. It shows the mean values of the coordinates, as well as the standard deviation of the daily solutions. In the statistics the "change days" are counted as two half days. The bottom graph shows the mean values of the residuals when grouped into 2.5˚ elevation angle bins for the present week.

All coordinates of OTT2 are excess of the default baseline vector, ENV = [-22.02952, -40.39960, 1.25778] meter between OTT2 and OTT1, and OTT4 coordinates are excess of the default baseline, ENV = [6.85532, -84.85364, 1.77963] meter between OTT4 and OTT1. Occasional extra vertical offsets, either 70 mm or 90 mm, are written in the bottom right part of the summary graphs.

Identical antenna models were used for both ends of the baselines, except for some weeks. In the latter case the antenna models used are given in the bottom right part of the summary graphs.

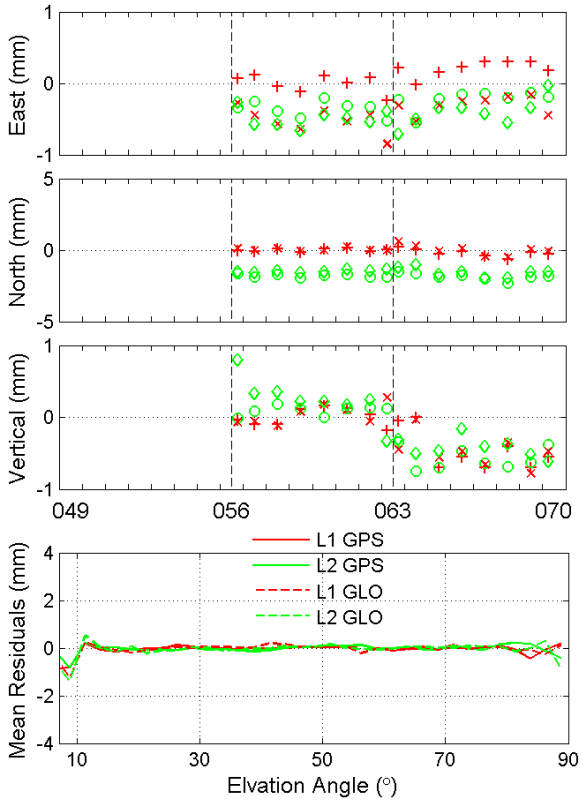

OTT2 Day number 056 - 063

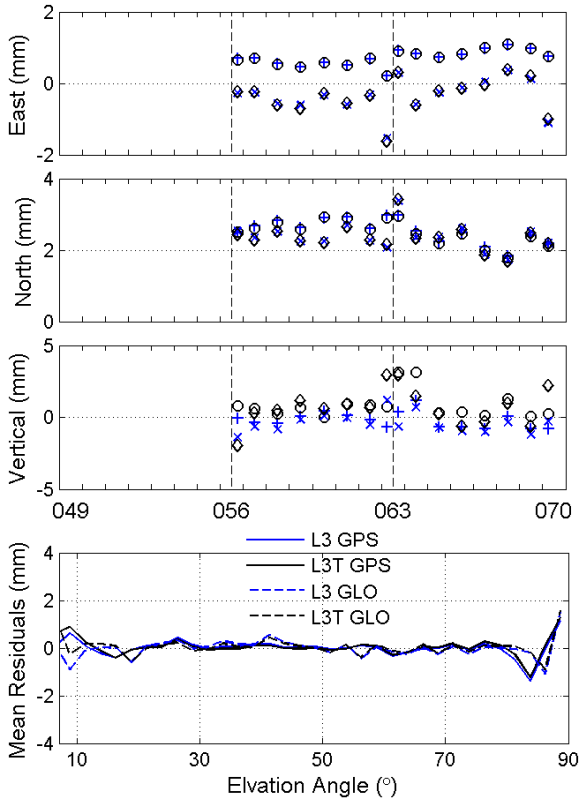

OTT2 Day number 056 - 063

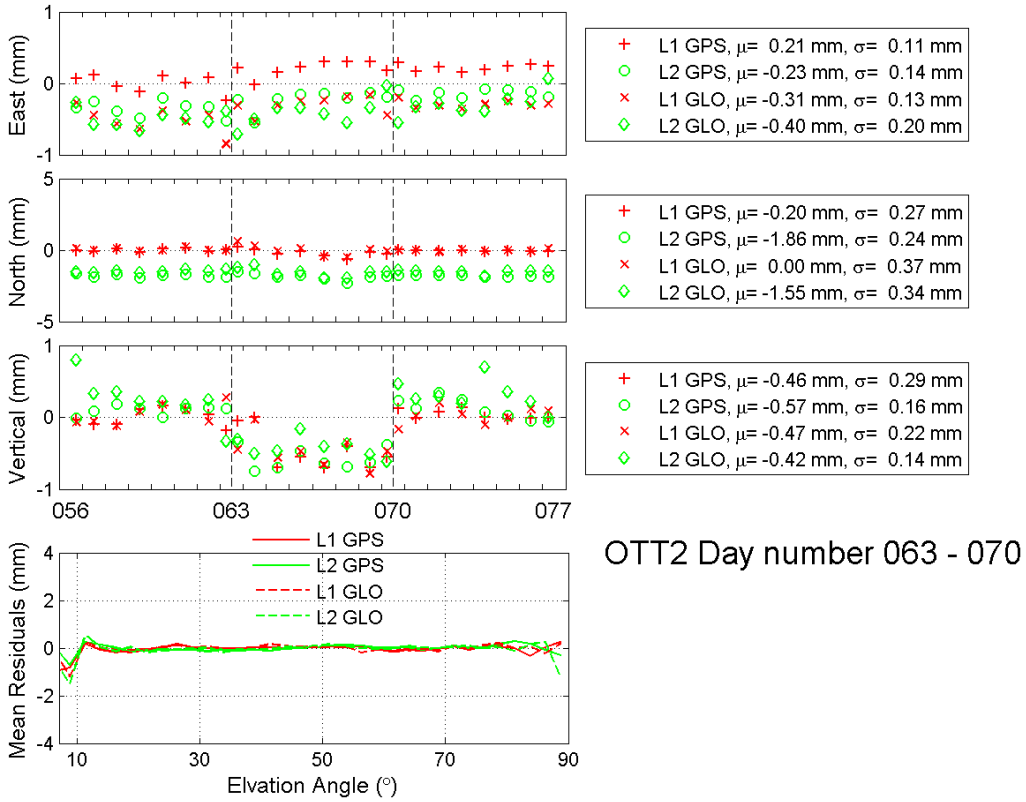

OTT2 Day number 063 - 070

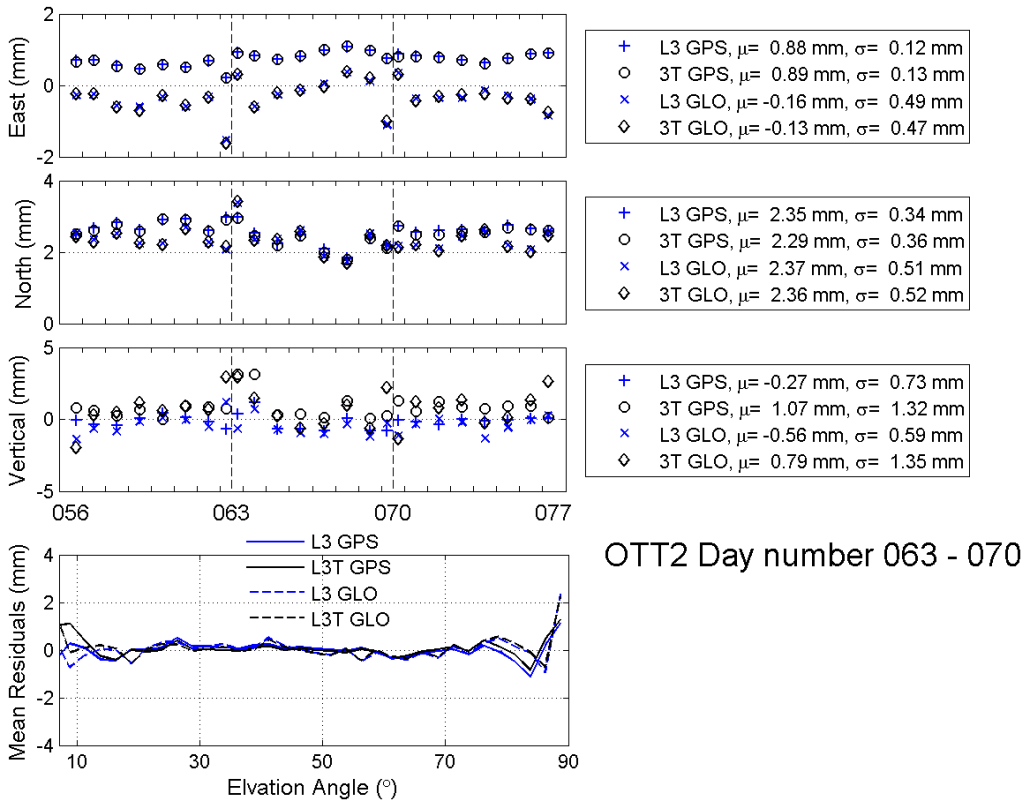

OTT2 Day number 063 - 070

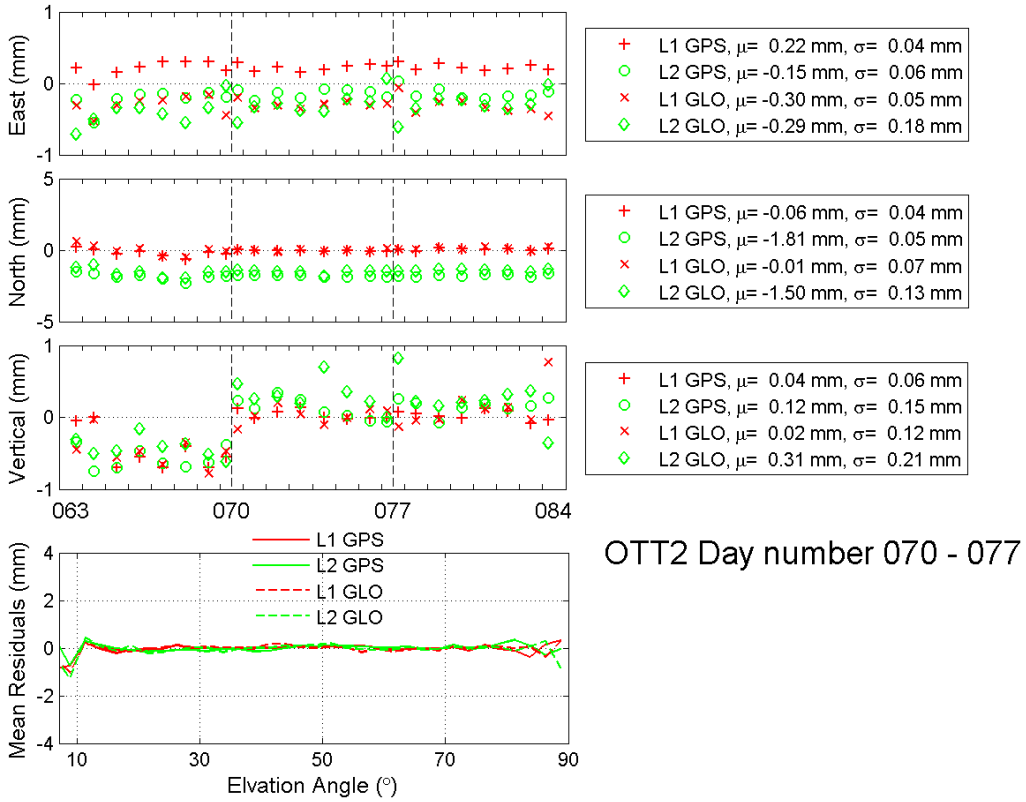

OTT2 Day number 070 - 077

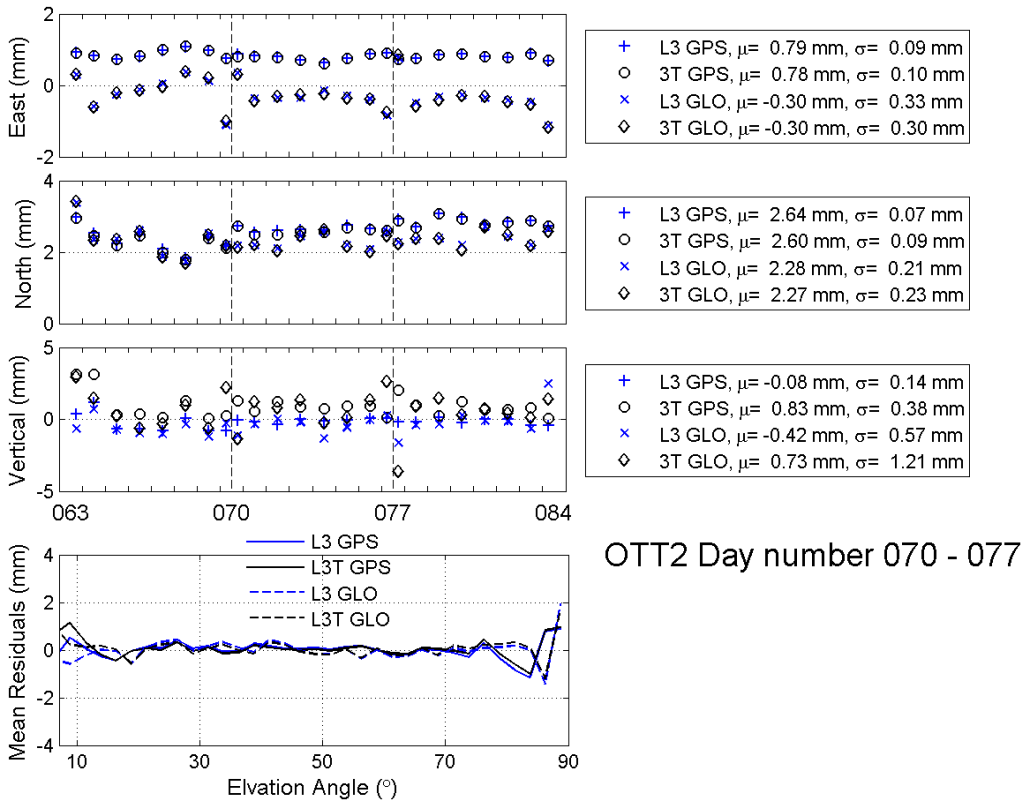

OTT2 Day number 070 - 077

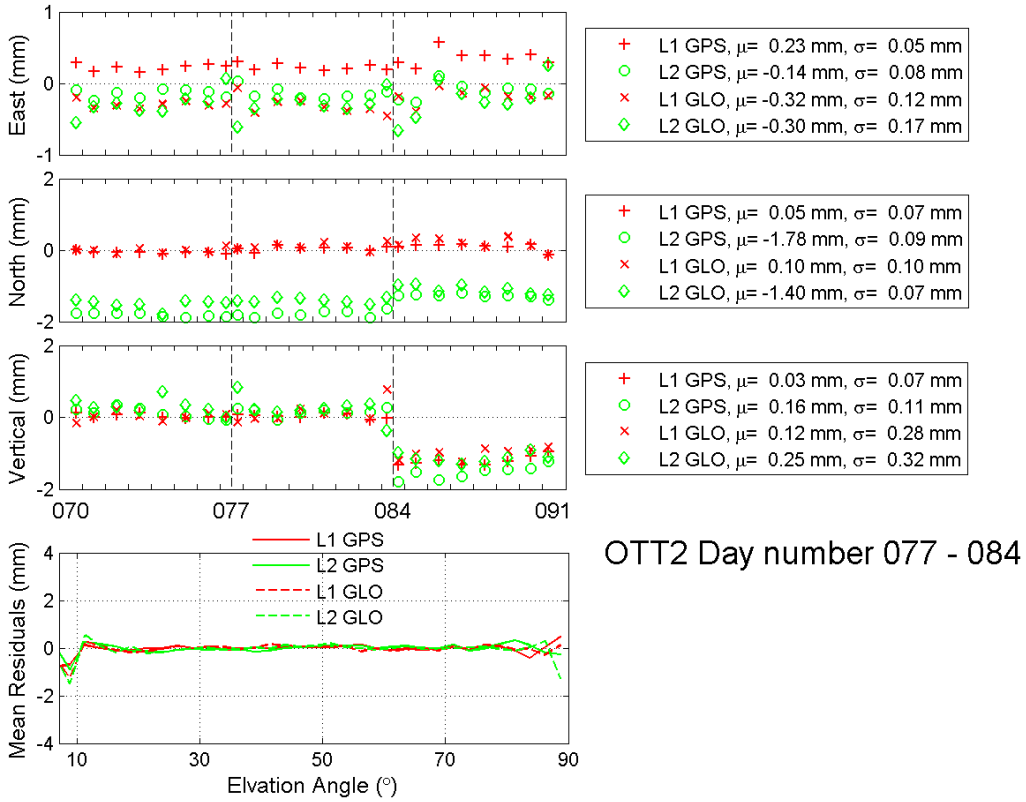

OTT2 Day number 077 - 084

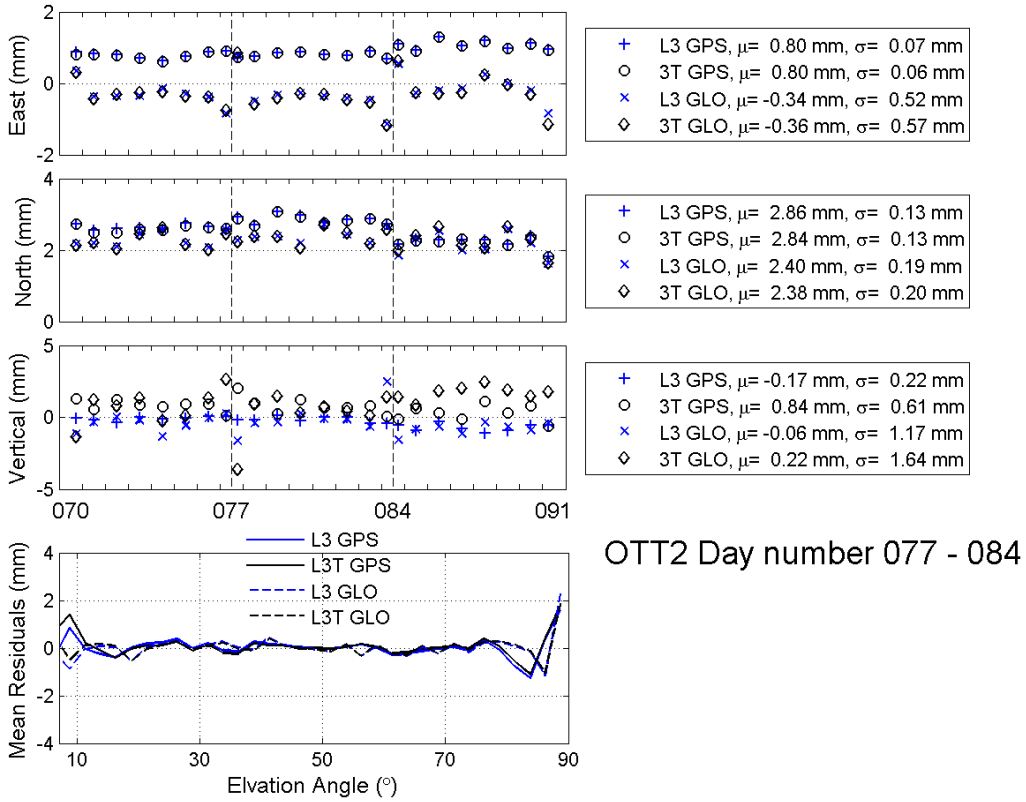

OTT2 Day number 077 - 084

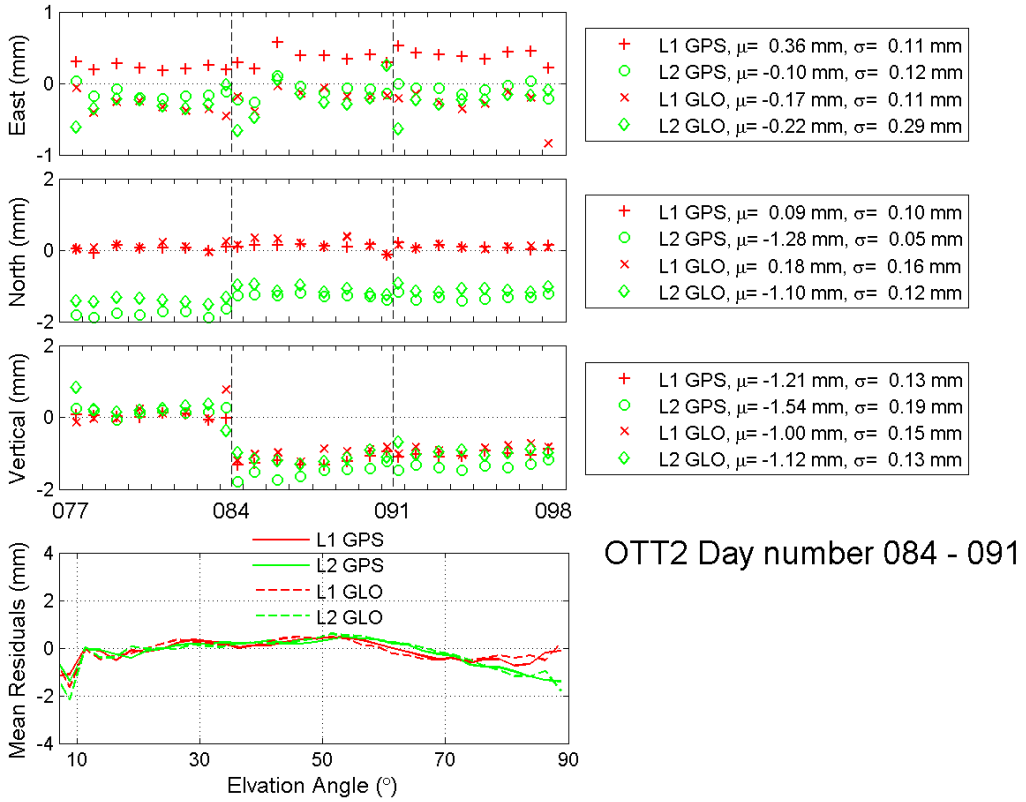

OTT2 Day number 084 - 091

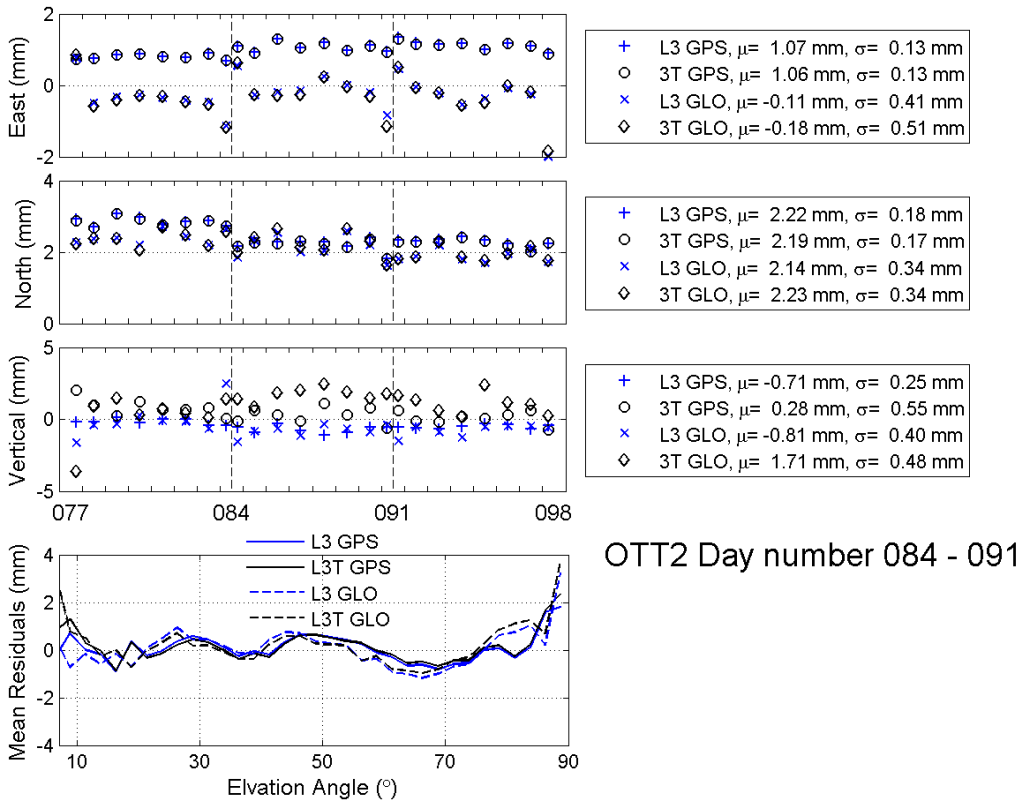

OTT2 Day number 084 - 091

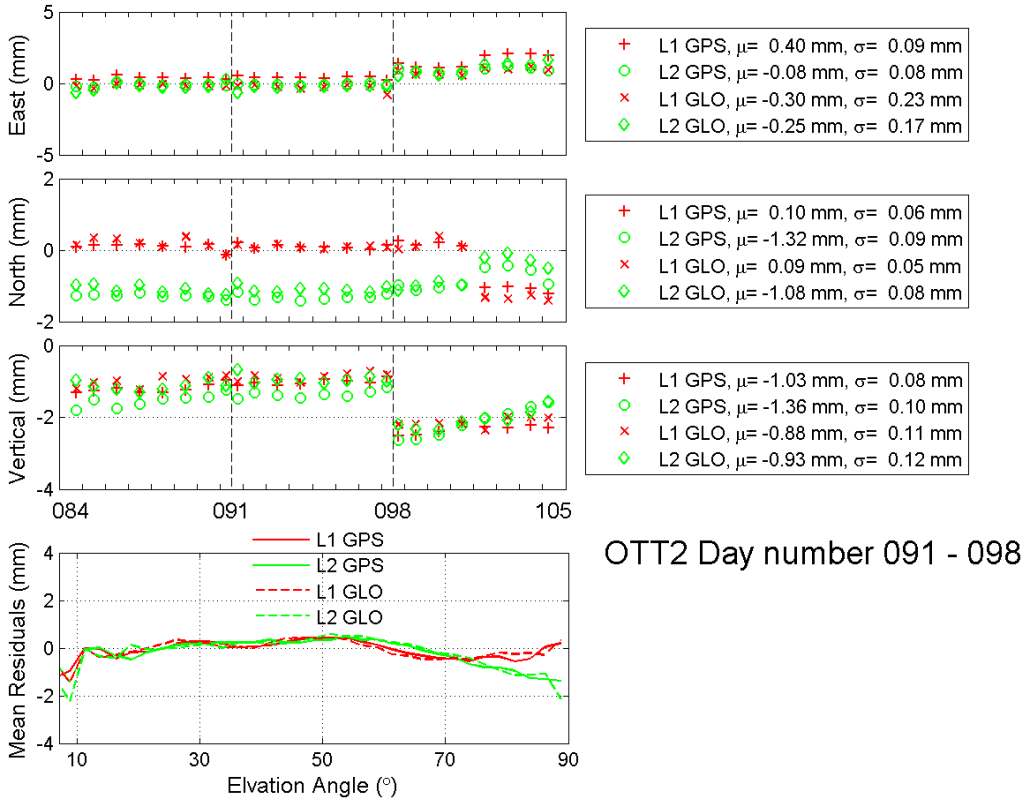

OTT2 Day number 091 - 098

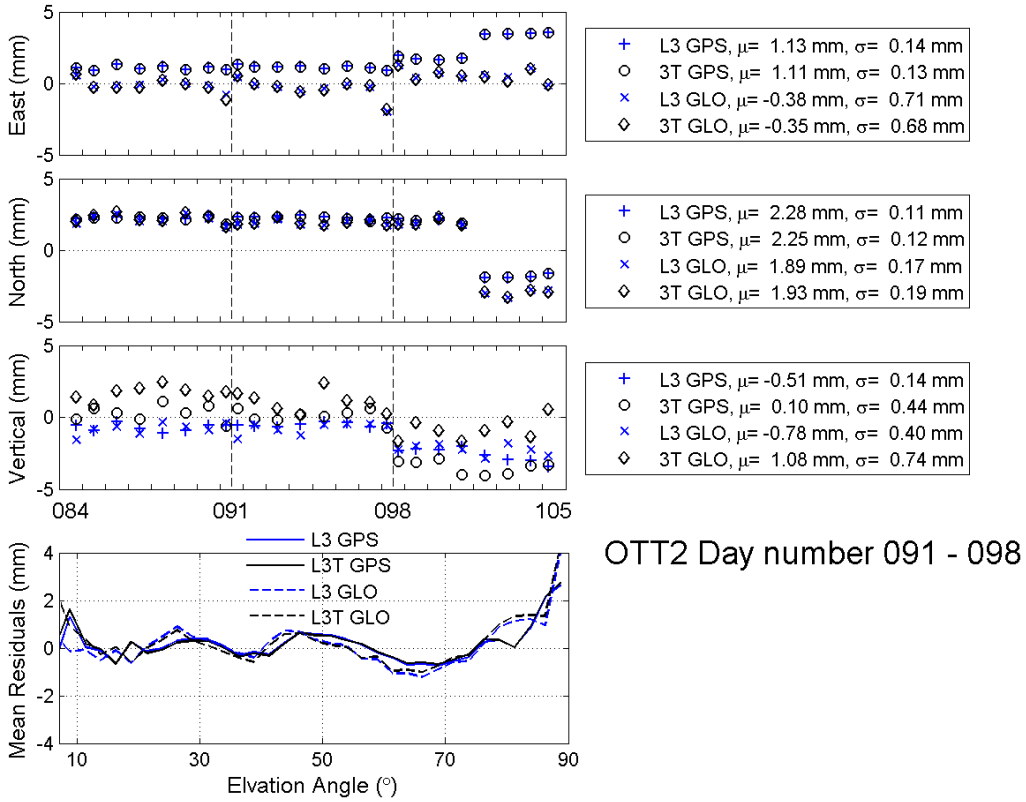

OTT2 Day number 091 - 098

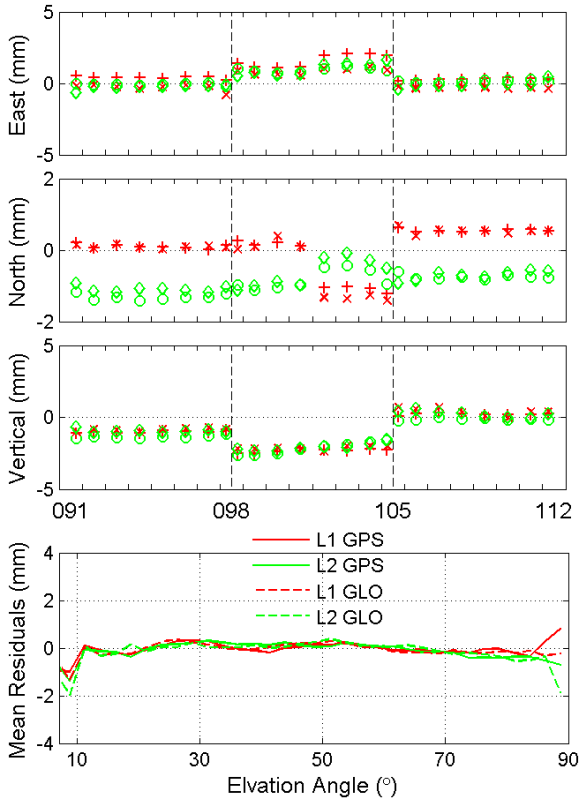

OTT2 Day number 098 - 105

Vertical offset: 90 mm

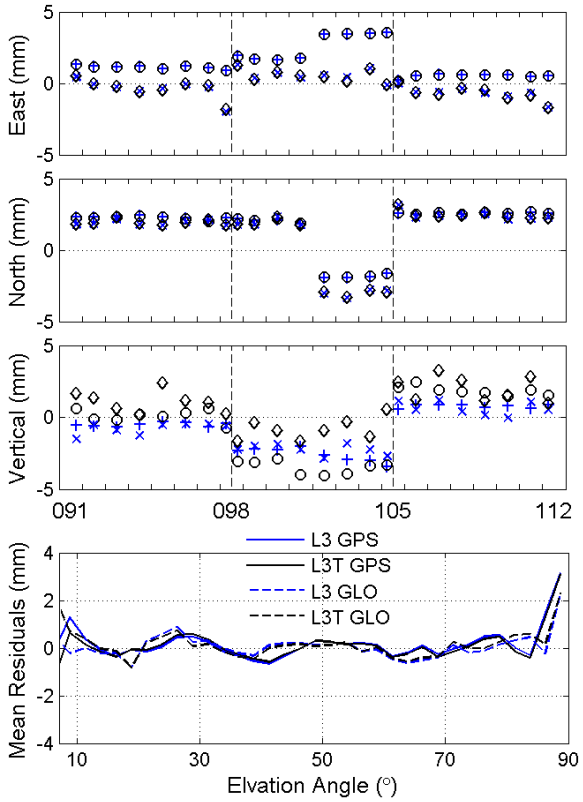

OTT2 Day number 098 - 105

Vertical offset: 90 mm

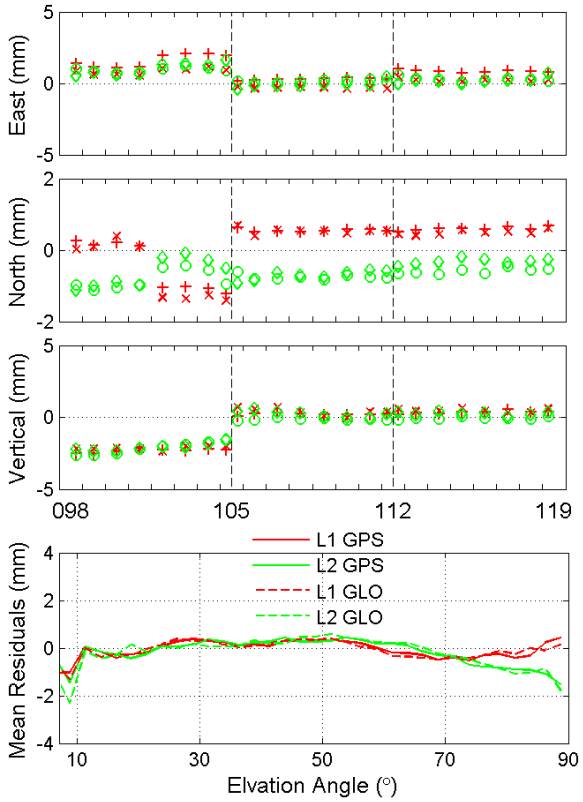

OTT2 Day number 105 - 112

Vertical offset: 90 mm

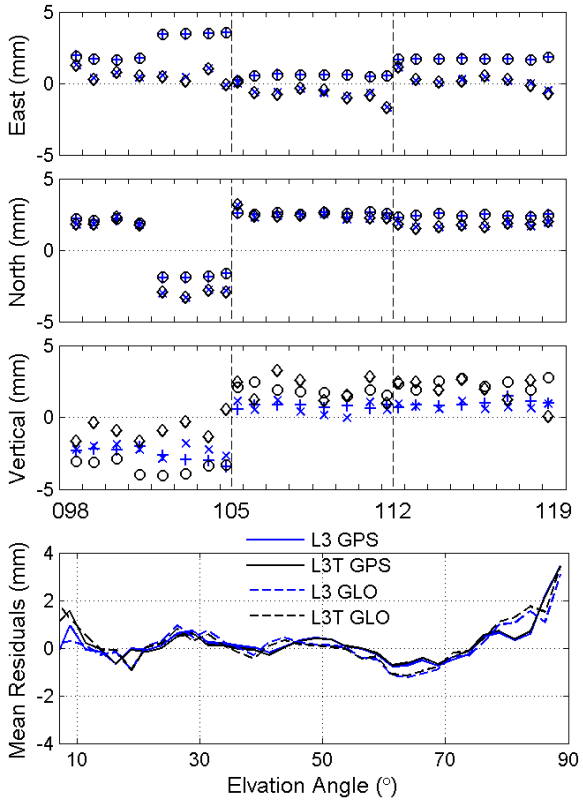

OTT2 Day number 105 - 112

Vertical offset: 90 mm

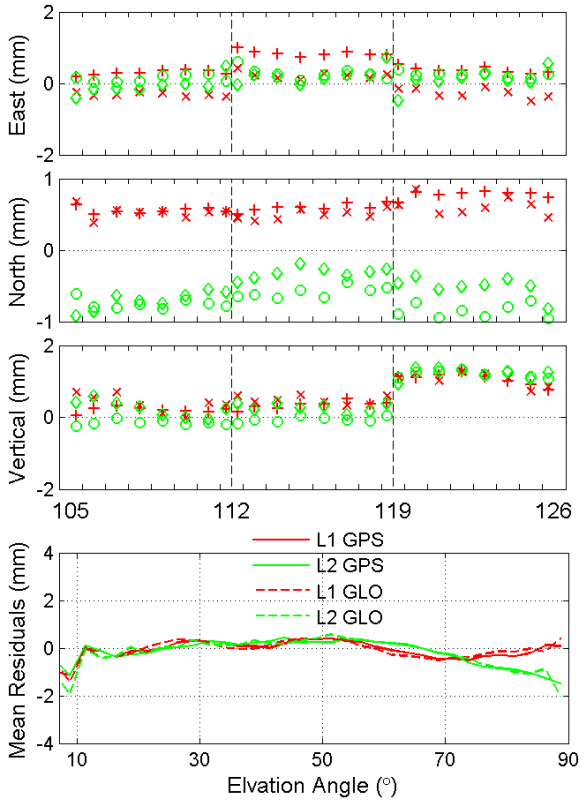

L1 GPS, μ= 0.84 mm, σ= 0.08 mm
L2 GPS, μ= 0.28 mm, σ= 0.16 mm
L1 GLO, μ= 0.21 mm, σ= 0.10 mm
L2 GLO, μ= 0.21 mm, σ= 0.24 mm

L1 GPS, μ= 0.59 mm, σ= 0.05 mm
L2 GPS, μ= -0.59 mm, σ= 0.08 mm
L1 GLO, μ= 0.49 mm, σ= 0.07 mm
L2 GLO, μ= -0.32 mm, σ= 0.08 mm

L1 GPS, μ= 0.34 mm, σ= 0.11 mm
L2 GPS, μ= -0.06 mm, σ= 0.07 mm
L1 GLO, μ= 0.47 mm, σ= 0.12 mm
L2 GLO, μ= 0.28 mm, σ= 0.12 mm

OTT2 Day number 112 - 119

Vertical offset: 90 mm

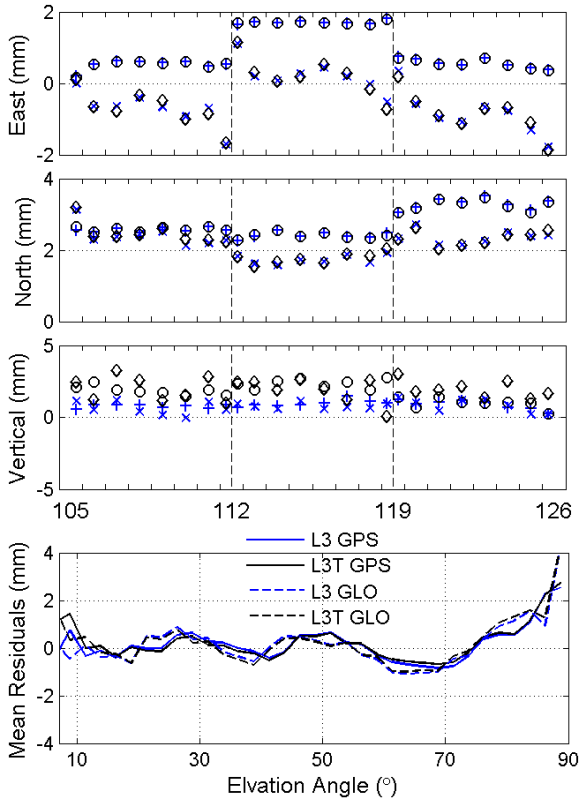

L3 GPS, μ= 1.71 mm, σ= 0.05 mm
3T GPS, μ= 1.70 mm, σ= 0.04 mm
L3 GLO, μ= 0.22 mm, σ= 0.46 mm
3T GLO, μ= 0.21 mm, σ= 0.54 mm

L3 GPS, μ= 2.41 mm, σ= 0.09 mm
3T GPS, μ= 2.41 mm, σ= 0.09 mm
L3 GLO, μ= 1.73 mm, σ= 0.13 mm
3T GLO, μ= 1.77 mm, σ= 0.16 mm

L3 GPS, μ= 0.97 mm, σ= 0.24 mm
3T GPS, μ= 2.34 mm, σ= 0.33 mm
L3 GLO, μ= 0.77 mm, σ= 0.20 mm
3T GLO, μ= 1.90 mm, σ= 0.88 mm

OTT2 Day number 112 - 119

Vertical offset: 90 mm

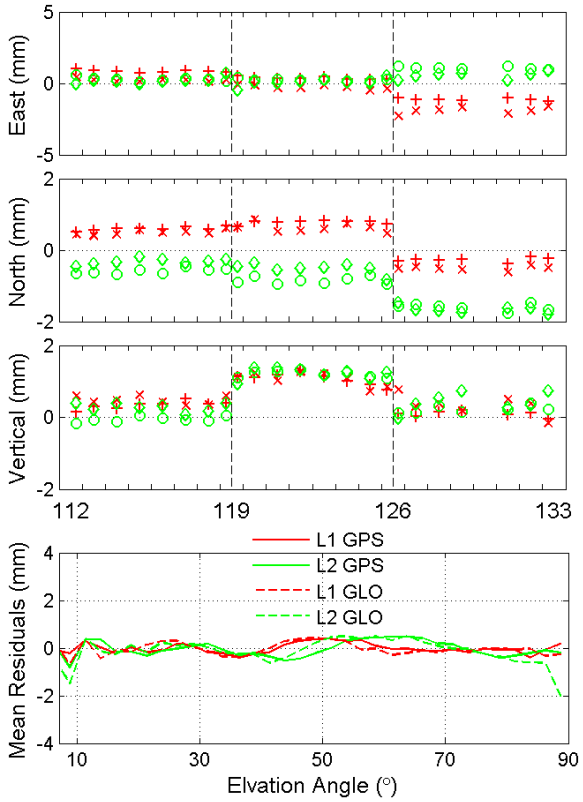

L1 GPS, μ= 0.37 mm, σ= 0.09 mm
L2 GPS, μ= 0.24 mm, σ= 0.08 mm
L1 GLO, μ= -0.28 mm, σ= 0.13 mm
L2 GLO, μ= 0.10 mm, σ= 0.28 mm

L1 GPS, μ= 0.77 mm, σ= 0.05 mm
L2 GPS, μ= -0.85 mm, σ= 0.10 mm
L1 GLO, μ= 0.62 mm, σ= 0.13 mm
L2 GLO, μ= -0.51 mm, σ= 0.14 mm

L1 GPS, μ= 1.07 mm, σ= 0.17 mm
L2 GPS, μ= 1.20 mm, σ= 0.09 mm
L1 GLO, μ= 1.06 mm, σ= 0.20 mm
L2 GLO, μ= 1.22 mm, σ= 0.16 mm

OTT2 Day number 119 - 126

Vertical offset: 90 mm

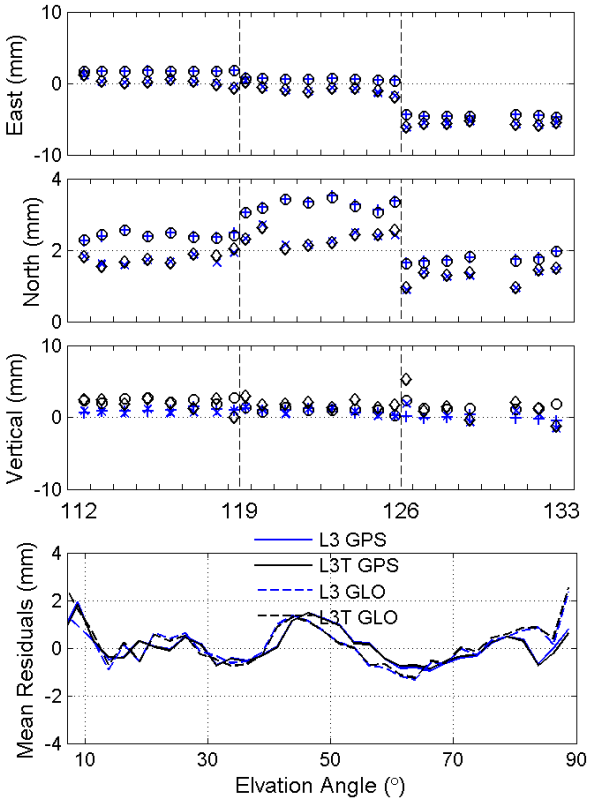

L3 GPS, μ= 0.56 mm, σ= 0.13 mm
3T GPS, μ= 0.55 mm, σ= 0.13 mm
L3 GLO, μ= -0.85 mm, σ= 0.62 mm
3T GLO, μ= -0.84 mm, σ= 0.59 mm

L3 GPS, μ= 3.29 mm, σ= 0.15 mm
3T GPS, μ= 3.26 mm, σ= 0.16 mm
L3 GLO, μ= 2.36 mm, σ= 0.19 mm
3T GLO, μ= 2.35 mm, σ= 0.21 mm

L3 GPS, μ= 0.87 mm, σ= 0.34 mm
3T GPS, μ= 0.96 mm, σ= 0.38 mm
L3 GLO, μ= 0.81 mm, σ= 0.49 mm
3T GLO, μ= 1.95 mm, σ= 0.58 mm

OTT2 Day number 119 - 126

Vertical offset: 90 mm

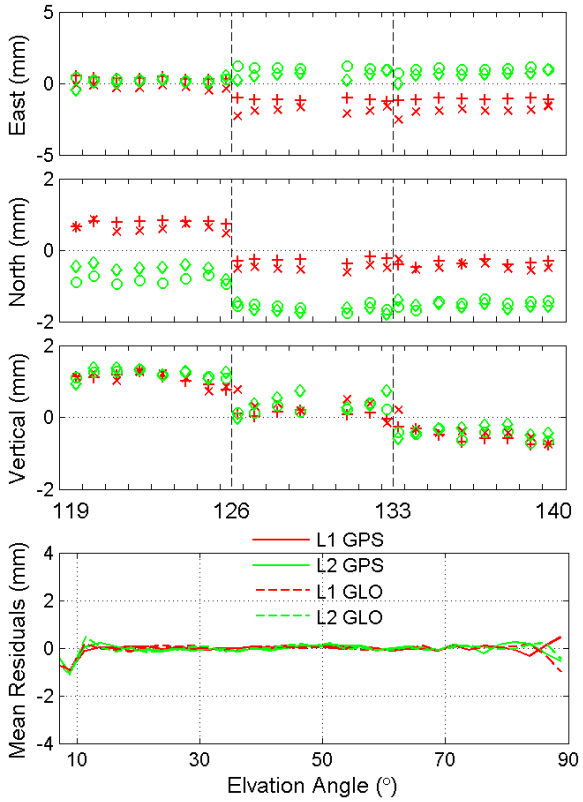

L1 GPS, μ= -1.13 mm, σ= 0.09 mm
L2 GPS, μ= 1.09 mm, σ= 0.09 mm
L1 GLO, μ= -1.91 mm, σ= 0.23 mm
L2 GLO, μ= 0.57 mm, σ= 0.25 mm

L1 GPS, μ= -0.27 mm, σ= 0.06 mm
L2 GPS, μ= -1.59 mm, σ= 0.10 mm
L1 GLO, μ= -0.51 mm, σ= 0.06 mm
L2 GLO, μ= -1.66 mm, σ= 0.10 mm

L1 GPS, μ= 0.09 mm, σ= 0.08 mm
L2 GPS, μ= 0.22 mm, σ= 0.10 mm
L1 GLO, μ= 0.33 mm, σ= 0.29 mm
L2 GLO, μ= 0.43 mm, σ= 0.27 mm

OTT2 Day number 126 - 133

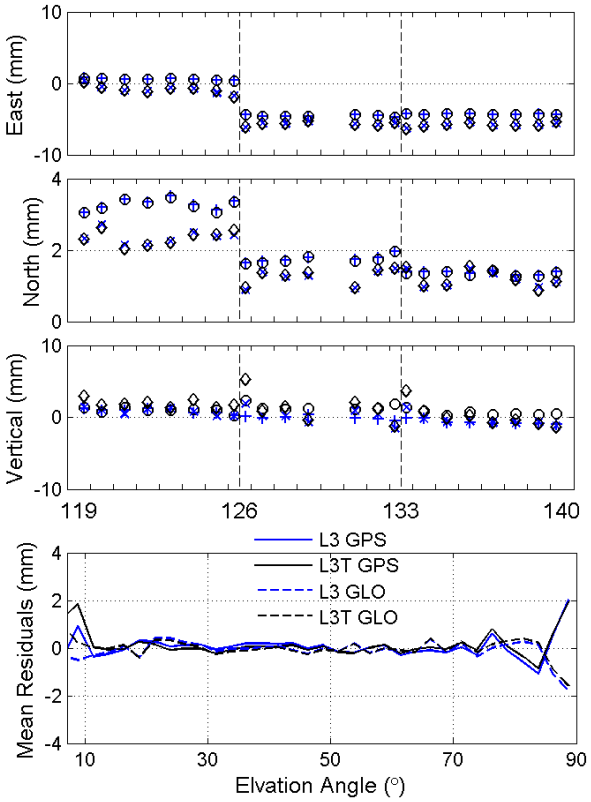

L3 GPS, μ= -4.56 mm, σ= 0.11 mm
3T GPS, μ= -4.57 mm, σ= 0.11 mm
L3 GLO, μ= -5.70 mm, σ= 0.26 mm
3T GLO, μ= -5.68 mm, σ= 0.26 mm

L3 GPS, μ= 1.76 mm, σ= 0.10 mm
3T GPS, μ= 1.74 mm, σ= 0.12 mm
L3 GLO, μ= 1.23 mm, σ= 0.23 mm
3T GLO, μ= 1.27 mm, σ= 0.23 mm

L3 GPS, μ= -0.10 mm, σ= 0.24 mm
3T GPS, μ= 1.43 mm, σ= 0.49 mm
L3 GLO, μ= 0.17 mm, σ= 1.10 mm
3T GLO, μ= 1.32 mm, σ= 2.06 mm

OTT2 Day number 126 - 133

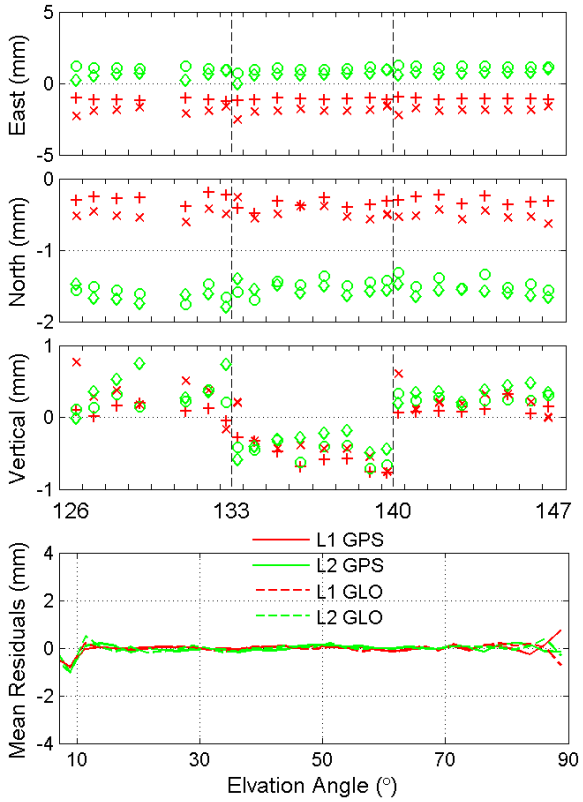

L1 GPS, μ= -1.10 mm, σ= 0.07 mm
L2 GPS, μ= 0.98 mm, σ= 0.12 mm
L1 GLO, μ= -1.94 mm, σ= 0.27 mm
L2 GLO, μ= 0.60 mm, σ= 0.29 mm

L1 GPS, μ= -0.37 mm, σ= 0.07 mm
L2 GPS, μ= -1.49 mm, σ= 0.10 mm
L1 GLO, μ= -0.46 mm, σ= 0.11 mm
L2 GLO, μ= -1.54 mm, σ= 0.08 mm

L1 GPS, μ= -0.56 mm, σ= 0.19 mm
L2 GPS, μ= -0.50 mm, σ= 0.14 mm
L1 GLO, μ= -0.39 mm, σ= 0.27 mm
L2 GLO, μ= -0.37 mm, σ= 0.14 mm

OTT2 Day number 133 - 140

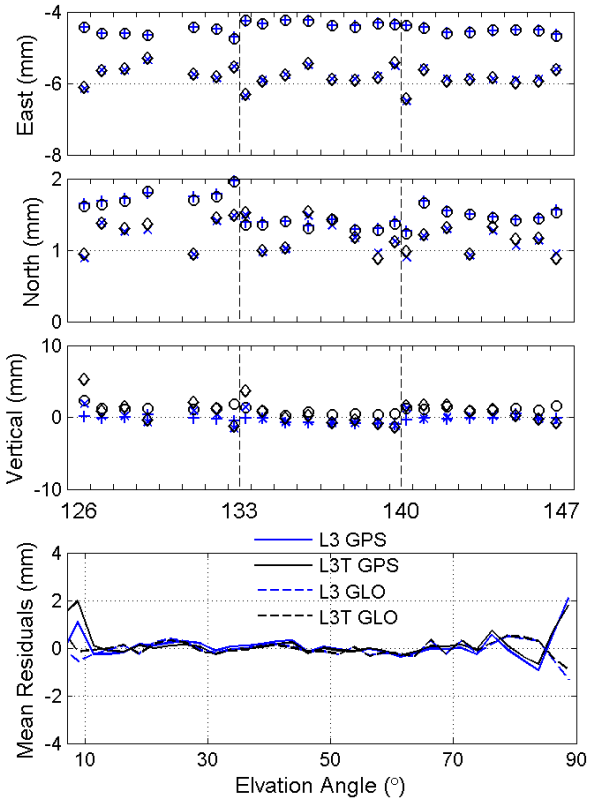

L3 GPS, μ= -4.31 mm, σ= 0.06 mm
3T GPS, μ= -4.32 mm, σ= 0.07 mm
L3 GLO, μ= -5.83 mm, σ= 0.27 mm
3T GLO, μ= -5.81 mm, σ= 0.28 mm

L3 GPS, μ= 1.37 mm, σ= 0.05 mm
3T GPS, μ= 1.35 mm, σ= 0.05 mm
L3 GLO, μ= 1.19 mm, σ= 0.22 mm
3T GLO, μ= 1.21 mm, σ= 0.25 mm

L3 GPS, μ= -0.66 mm, σ= 0.36 mm
3T GPS, μ= 0.62 mm, σ= 0.37 mm
L3 GLO, μ= -0.43 mm, σ= 0.80 mm
3T GLO, μ= 0.19 mm, σ= 1.56 mm

OTT2 Day number 133 - 140

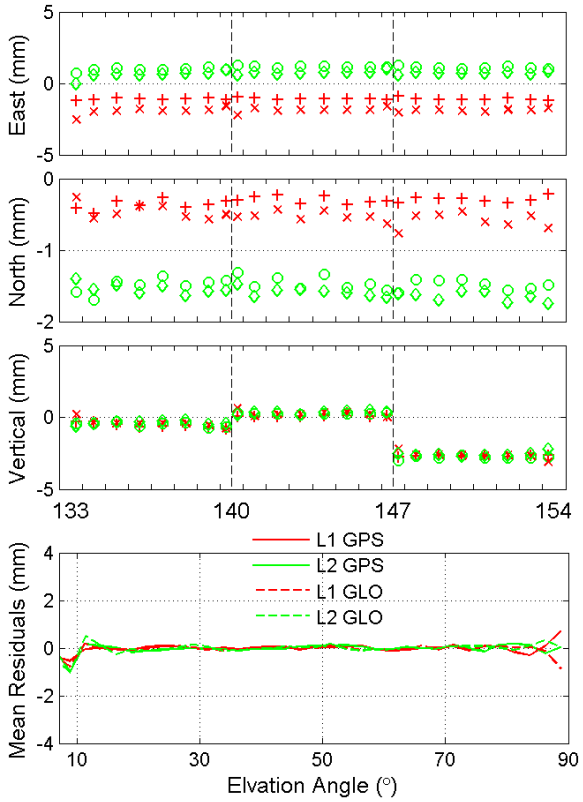

L1 GPS, μ= -1.07 mm, σ= 0.06 mm
L2 GPS, μ= 1.16 mm, σ= 0.06 mm
L1 GLO, μ= -1.87 mm, σ= 0.17 mm
L2 GLO, μ= 0.76 mm, σ= 0.12 mm

L1 GPS, μ= -0.30 mm, σ= 0.05 mm
L2 GPS, μ= -1.46 mm, σ= 0.10 mm
L1 GLO, μ= -0.53 mm, σ= 0.06 mm
L2 GLO, μ= -1.59 mm, σ= 0.06 mm

L1 GPS, μ= 0.12 mm, σ= 0.09 mm
L2 GPS, μ= 0.25 mm, σ= 0.05 mm
L1 GLO, μ= 0.25 mm, σ= 0.18 mm
L2 GLO, μ= 0.34 mm, σ= 0.10 mm

OTT2 Day number 140 - 147

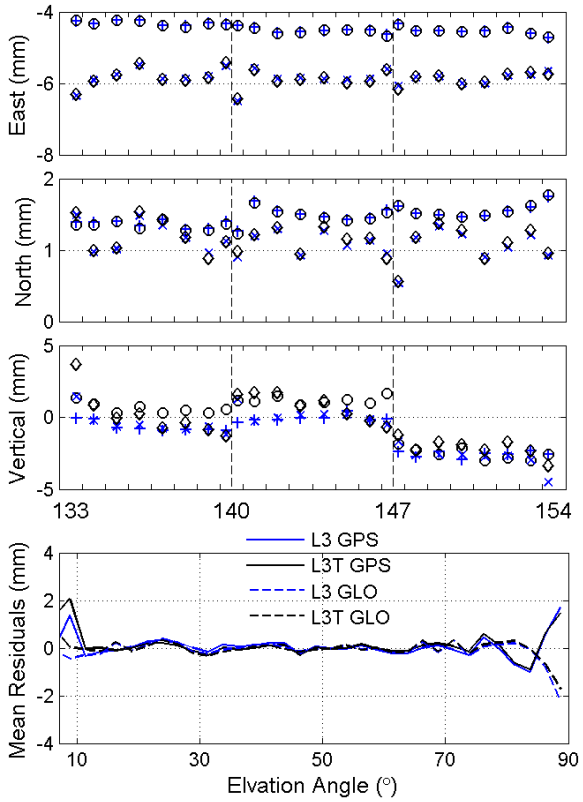

L3 GPS, μ= -4.51 mm, σ= 0.08 mm
3T GPS, μ= -4.53 mm, σ= 0.09 mm
L3 GLO, μ= -5.89 mm, σ= 0.28 mm
3T GLO, μ= -5.91 mm, σ= 0.25 mm

L3 GPS, μ= 1.49 mm, σ= 0.12 mm
3T GPS, μ= 1.47 mm, σ= 0.12 mm
L3 GLO, μ= 1.09 mm, σ= 0.16 mm
3T GLO, μ= 1.13 mm, σ= 0.17 mm

L3 GPS, μ= -0.10 mm, σ= 0.24 mm
3T GPS, μ= 1.19 mm, σ= 0.24 mm
L3 GLO, μ= 0.11 mm, σ= 0.52 mm
3T GLO, μ= 0.78 mm, σ= 0.93 mm

OTT2 Day number 140 - 147

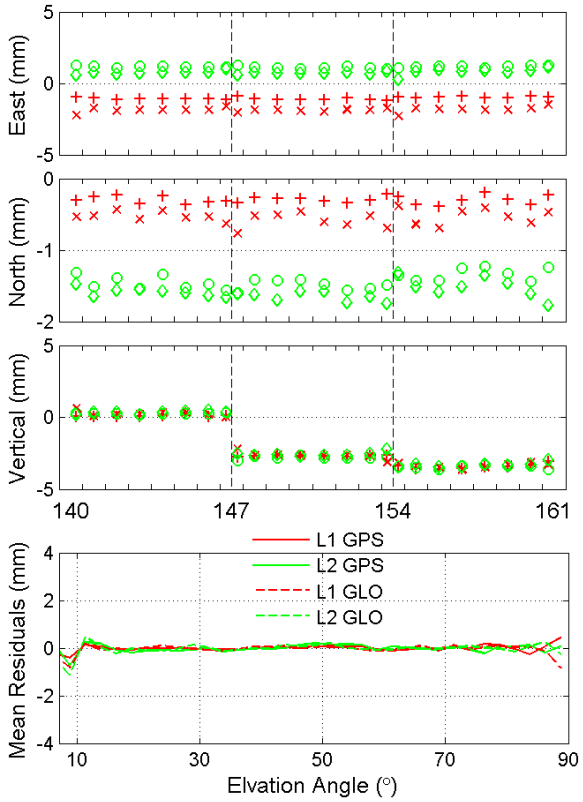

L1 GPS, μ= -1.10 mm, σ= 0.09 mm
L2 GPS, μ= 1.12 mm, σ= 0.08 mm
L1 GLO, μ= -1.89 mm, σ= 0.09 mm
L2 GLO, μ= 0.71 mm, σ= 0.07 mm

L1 GPS, μ= -0.29 mm, σ= 0.04 mm
L2 GPS, μ= -1.49 mm, σ= 0.07 mm
L1 GLO, μ= -0.59 mm, σ= 0.10 mm
L2 GLO, μ= -1.65 mm, σ= 0.07 mm

L1 GPS, μ= -2.70 mm, σ= 0.05 mm
L2 GPS, μ= -2.79 mm, σ= 0.11 mm
L1 GLO, μ= -2.66 mm, σ= 0.24 mm
L2 GLO, μ= -2.56 mm, σ= 0.15 mm

OTT2 Day number 147 - 154

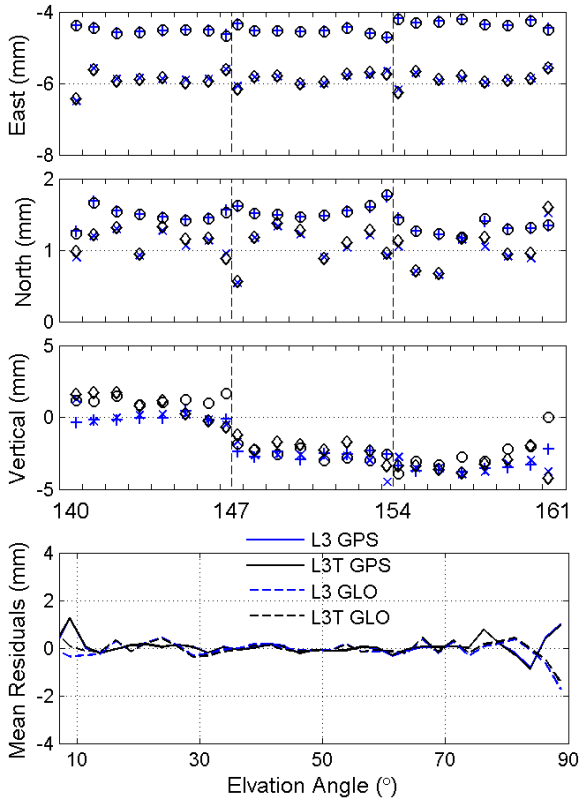

L3 GPS, μ= -4.54 mm, σ= 0.11 mm
3T GPS, μ= -4.54 mm, σ= 0.10 mm
L3 GLO, μ= -5.87 mm, σ= 0.14 mm
3T GLO, μ= -5.87 mm, σ= 0.17 mm

L3 GPS, μ= 1.56 mm, σ= 0.09 mm
3T GPS, μ= 1.56 mm, σ= 0.10 mm
L3 GLO, μ= 1.04 mm, σ= 0.25 mm
3T GLO, μ= 1.08 mm, σ= 0.27 mm

L3 GPS, μ= -2.56 mm, σ= 0.20 mm
3T GPS, μ= -2.53 mm, σ= 0.41 mm
L3 GLO, μ= -2.81 mm, σ= 0.78 mm
3T GLO, μ= -2.11 mm, σ= 0.63 mm

OTT2 Day number 147 - 154

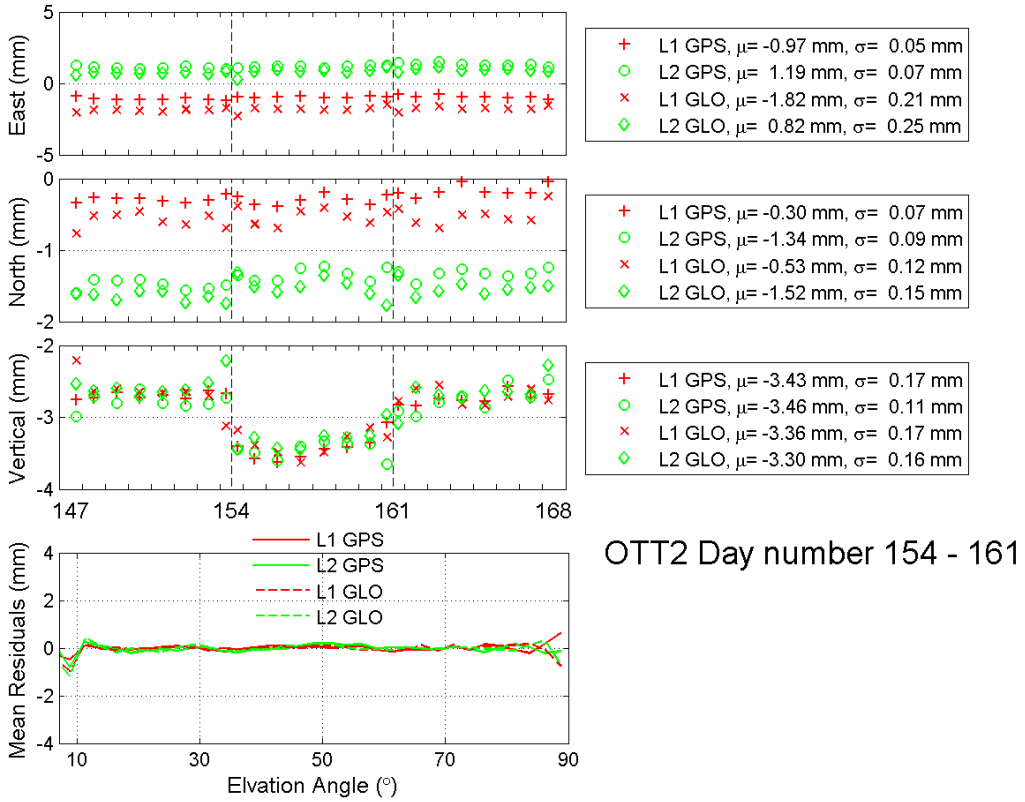

OTT2 Day number 154 - 161

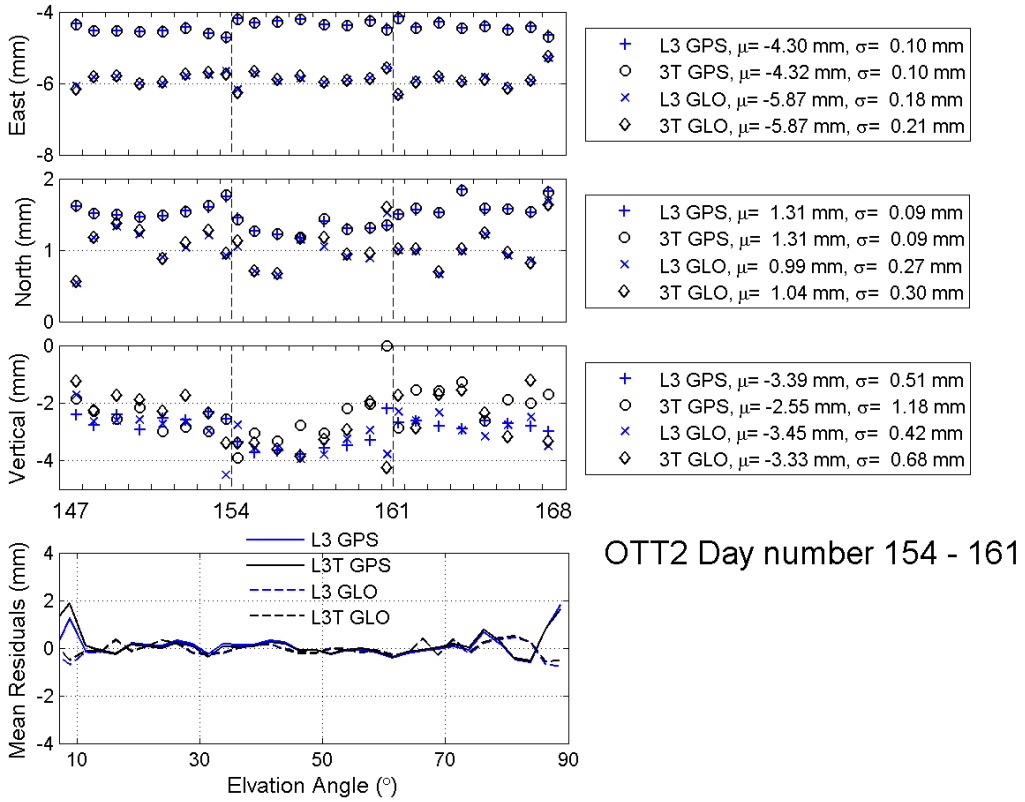

OTT2 Day number 154 - 161

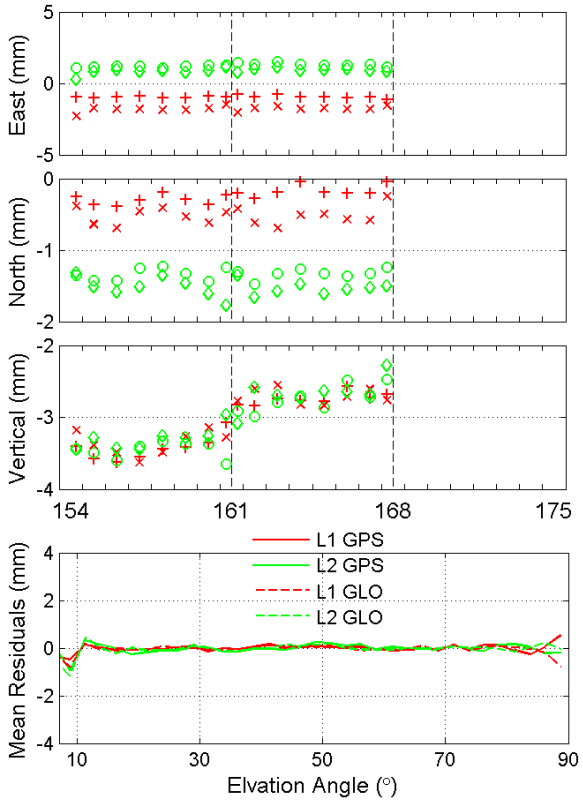

L1 GPS, μ= -0.92 mm, σ= 0.12 mm
L2 GPS, μ= 1.33 mm, σ= 0.11 mm
L1 GLO, μ= -1.76 mm, σ= 0.14 mm
L2 GLO, μ= 0.94 mm, σ= 0.12 mm

L1 GPS, μ= -0.17 mm, σ= 0.08 mm
L2 GPS, μ= -1.33 mm, σ= 0.07 mm
L1 GLO, μ= -0.52 mm, σ= 0.14 mm
L2 GLO, μ= -1.53 mm, σ= 0.09 mm

L1 GPS, μ= -2.74 mm, σ= 0.09 mm
L2 GPS, μ= -2.74 mm, σ= 0.19 mm
L1 GLO, μ= -2.71 mm, σ= 0.11 mm
L2 GLO, μ= -2.67 mm, σ= 0.22 mm

OTT2 Day number 161 - 168

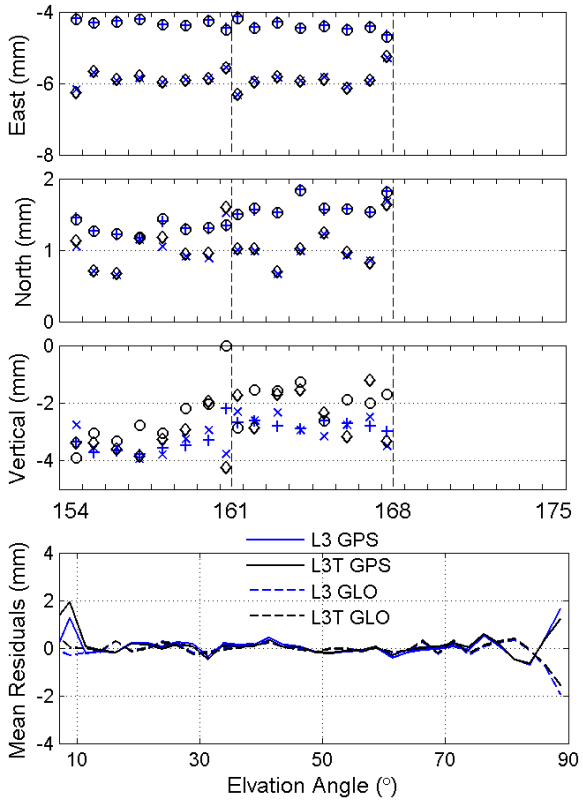

L3 GPS, μ= -4.41 mm, σ= 0.15 mm
3T GPS, μ= -4.43 mm, σ= 0.15 mm
L3 GLO, μ= -5.90 mm, σ= 0.29 mm
3T GLO, μ= -5.90 mm, σ= 0.30 mm

L3 GPS, μ= 1.61 mm, σ= 0.14 mm
3T GPS, μ= 1.62 mm, σ= 0.13 mm
L3 GLO, μ= 1.04 mm, σ= 0.30 mm
3T GLO, μ= 1.05 mm, σ= 0.29 mm

L3 GPS, μ= -2.77 mm, σ= 0.13 mm
3T GPS, μ= -1.93 mm, σ= 0.55 mm
L3 GLO, μ= -2.77 mm, σ= 0.41 mm
3T GLO, μ= -2.24 mm, σ= 0.80 mm

OTT2 Day number 161 - 168

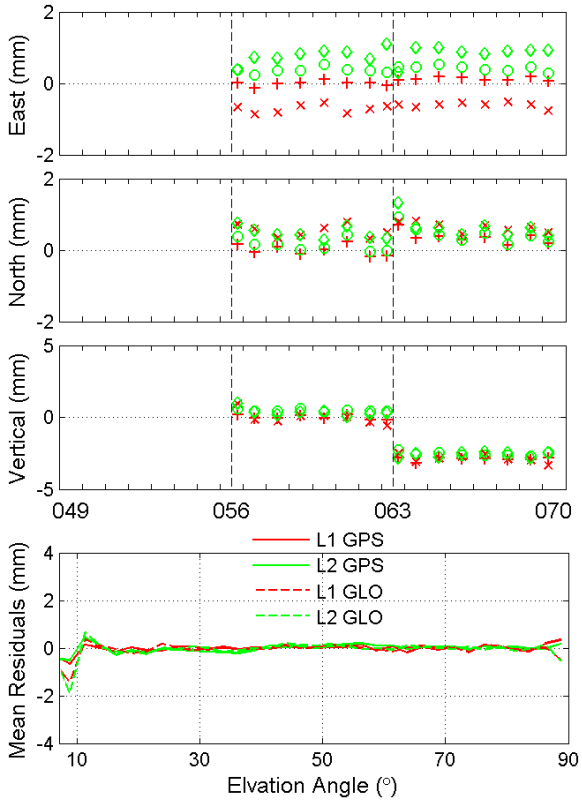

OTT4 Day number 056 - 063

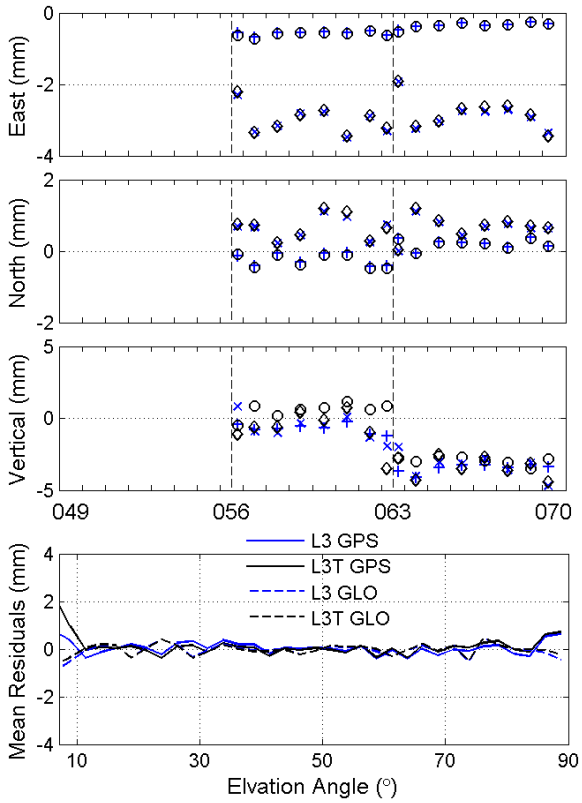

OTT4 Day number 056 - 063

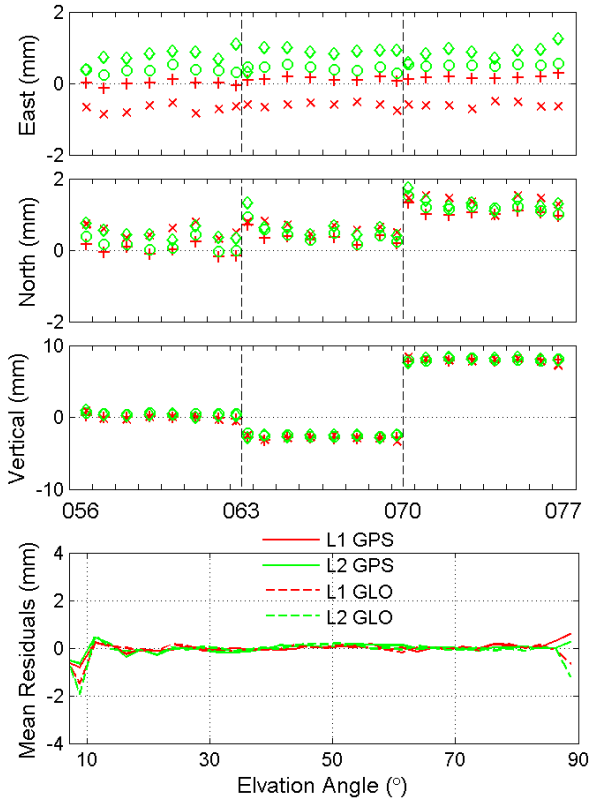

OTT4 Day number 063 - 070

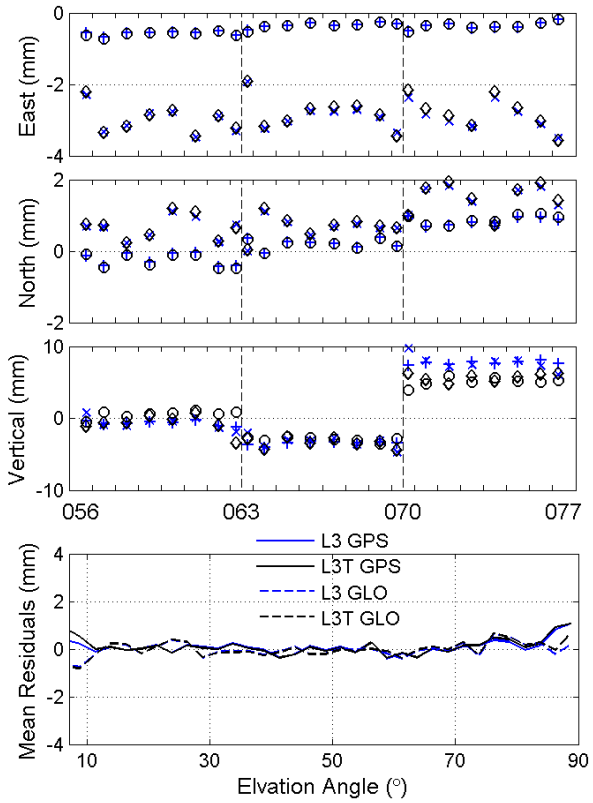

OTT4 Day number 063 - 070

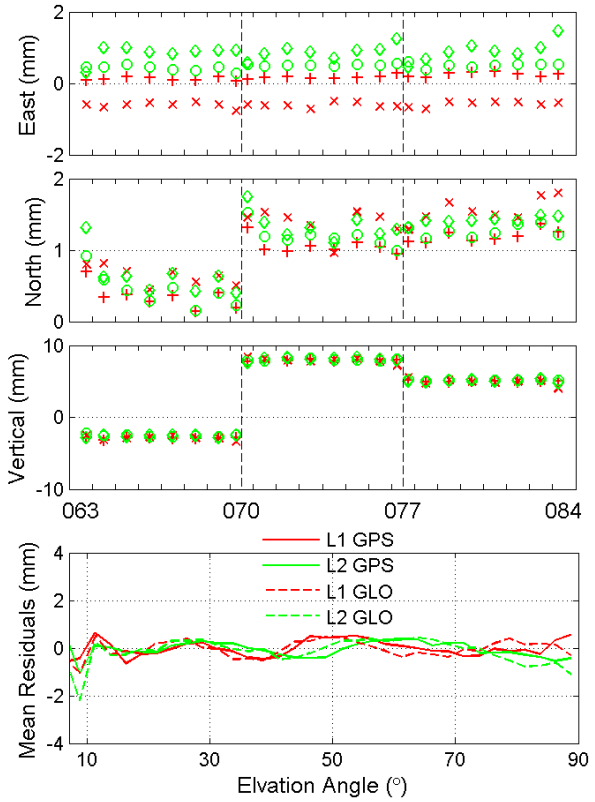

OTT4 Day number 070 - 077

Vertical offset: 70 mm

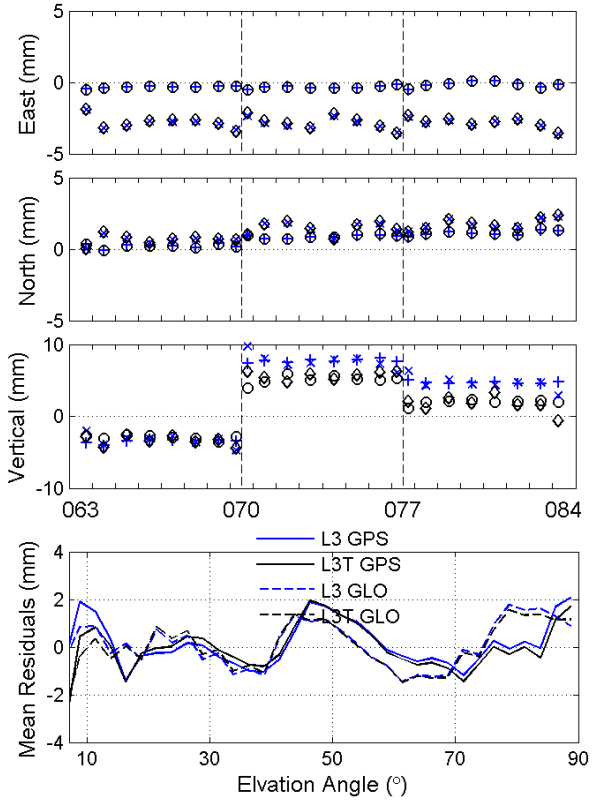

OTT4 Day number 070 - 077

Vertical offset: 70 mm

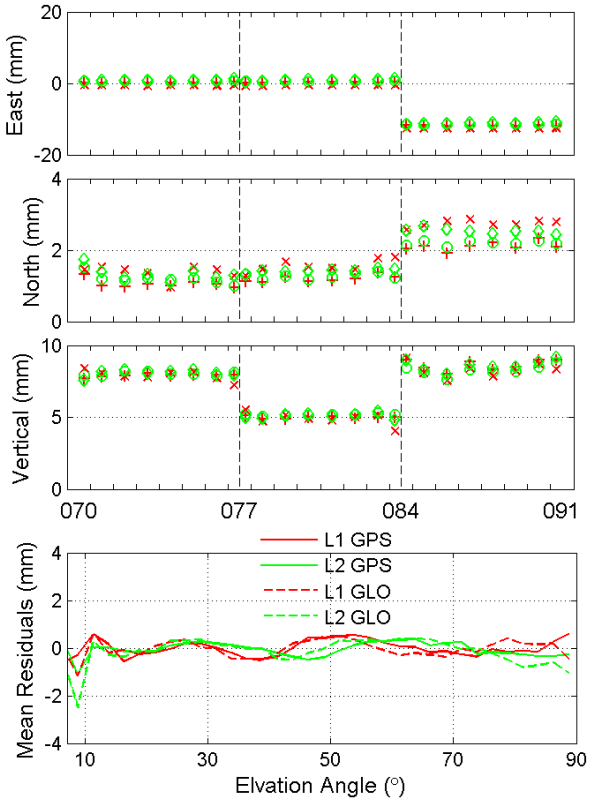

OTT4 Day number 077 - 084

Vertical offset: 70 mm

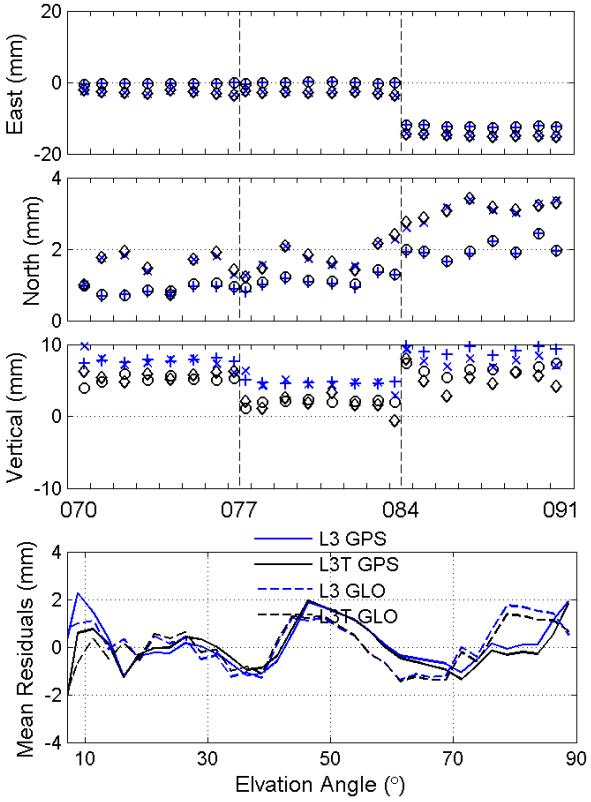

OTT4 Day number 077 - 084

Vertical offset: 70 mm

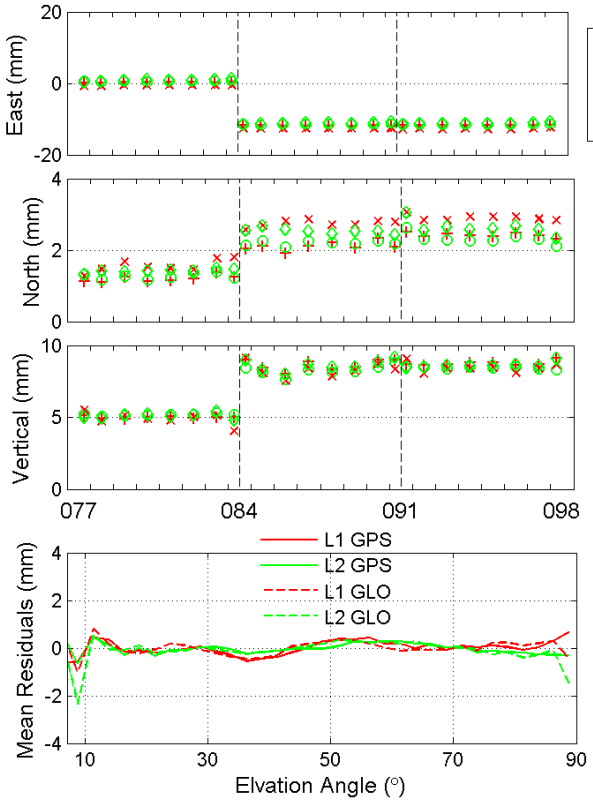

OTT4 Day number 084 - 091

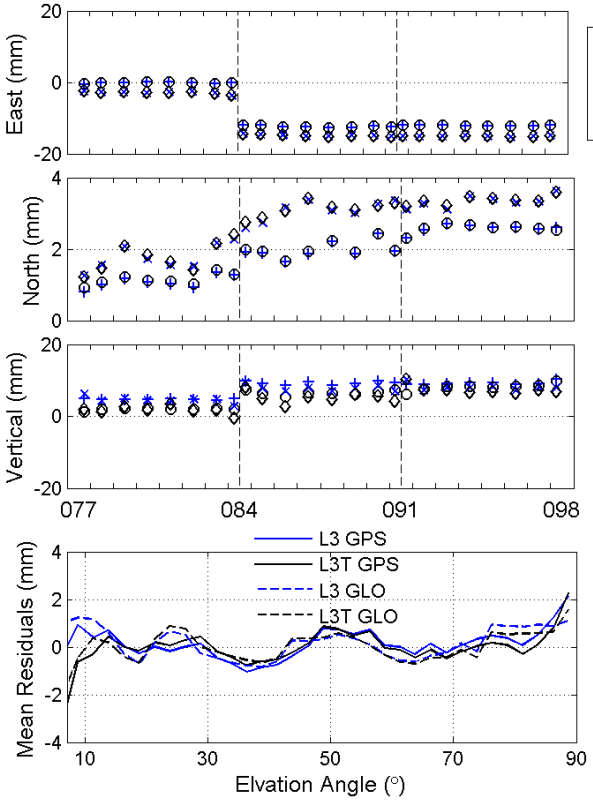

OTT4 Day number 084 - 091

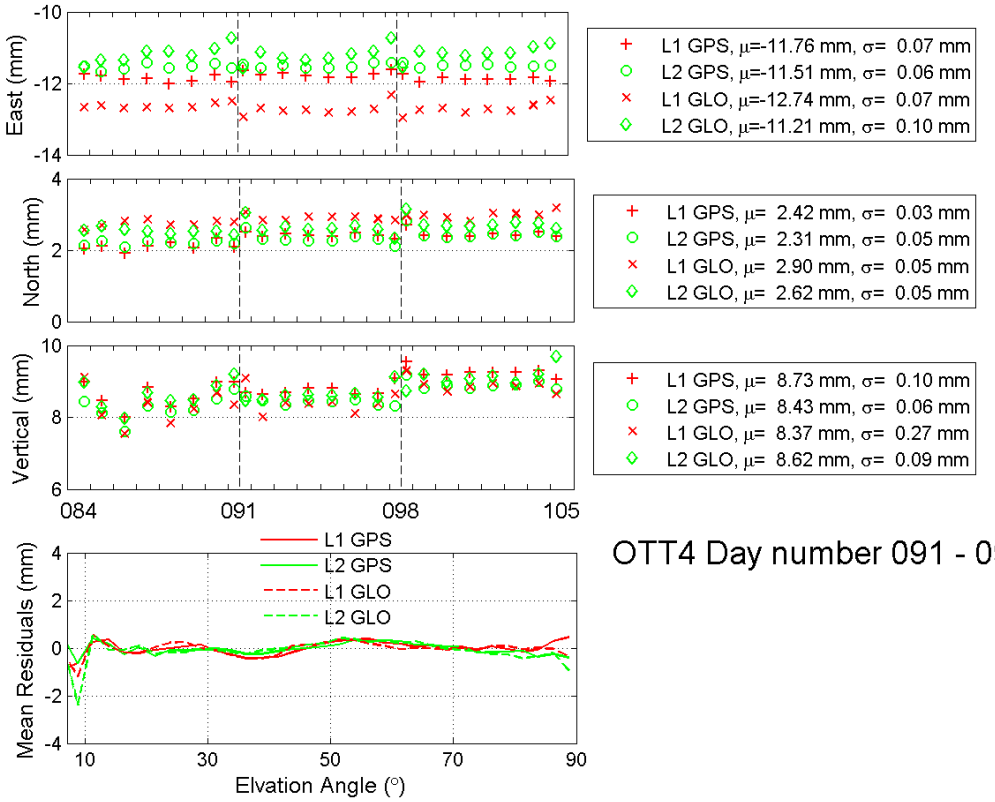

OTT4 Day number 091 - 098

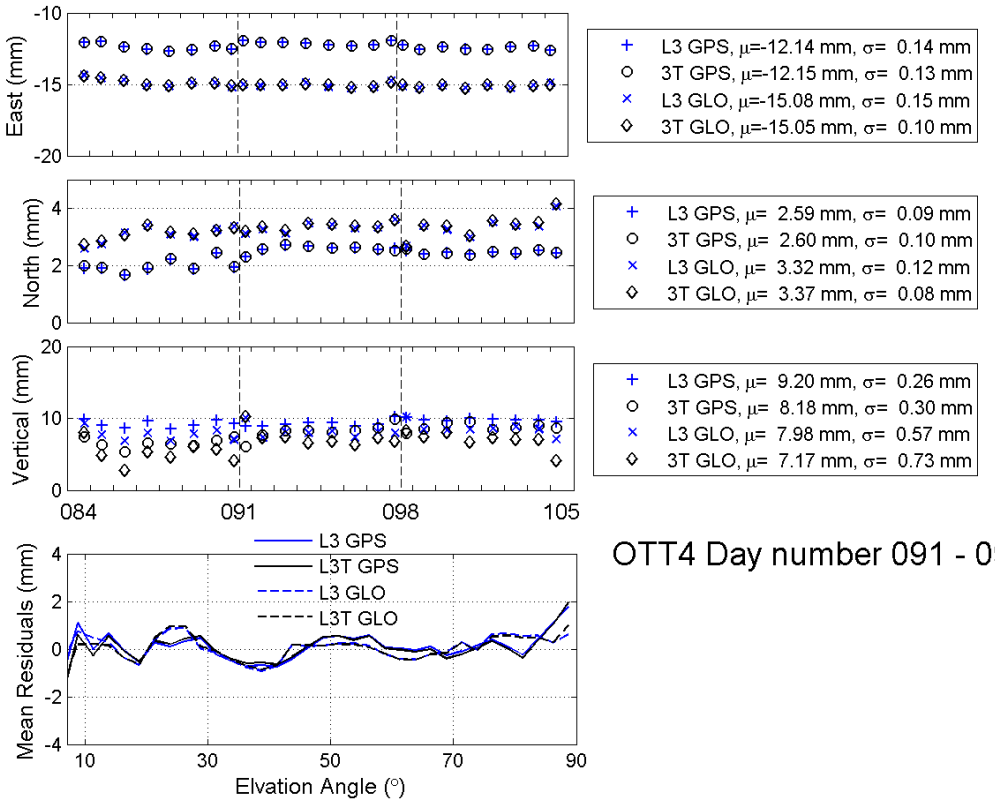

OTT4 Day number 091 - 098

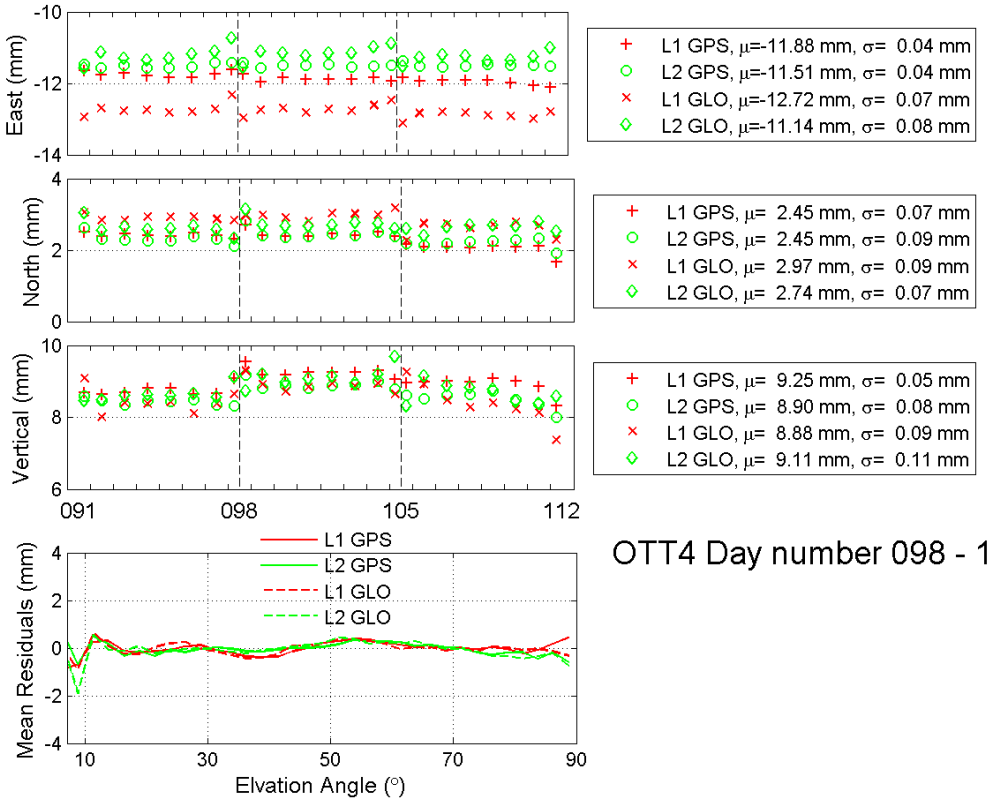

OTT4 Day number 098 - 105

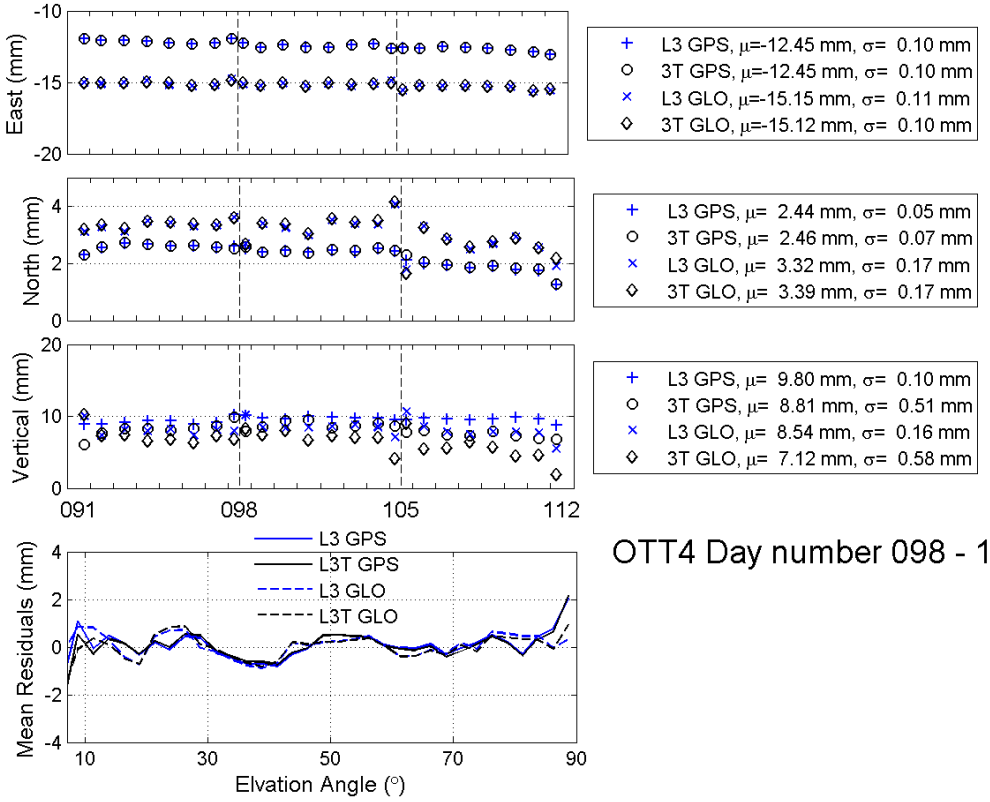

OTT4 Day number 098 - 105

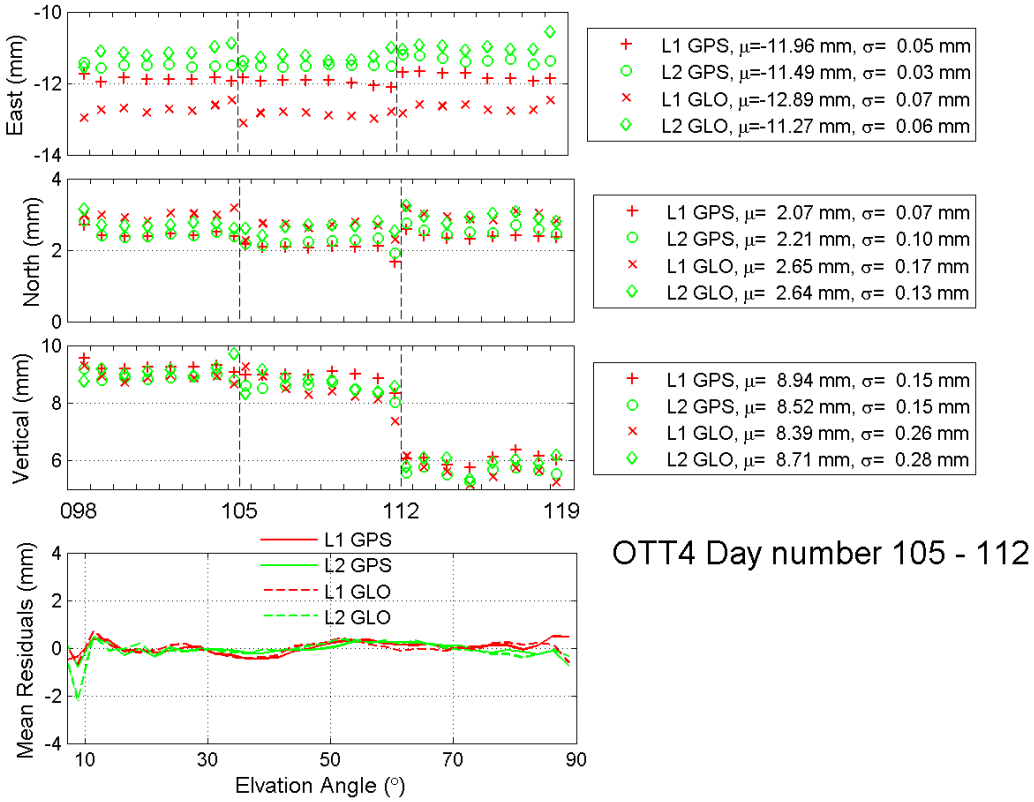
East (mm)
North (mm)
Vertical (mm)
L1 GPS, μ=-11.96 mm, σ= 0.05 mm
L2 GPS, μ=-11.49 mm, σ= 0.03 mm
L1 GLO, μ=-12.89 mm, σ= 0.07 mm
L2 GLO, μ=-11.27 mm, σ= 0.06 mm
L1 GPS, μ= 2.07 mm, σ= 0.07 mm
L2 GPS, μ= 2.21 mm, σ= 0.10 mm
L1 GLO, μ= 2.65 mm, σ= 0.17 mm
L2 GLO, μ= 2.64 mm, σ= 0.13 mm
L1 GPS, μ= 8.94 mm, σ= 0.15 mm
L2 GPS, μ= 8.52 mm, σ= 0.15 mm
L1 GLO, μ= 8.39 mm, σ= 0.26 mm
L2 GLO, μ= 8.71 mm, σ= 0.28 mm
098
105
112
119
L1 GPS
L2 GPS
L1 GLO
L2 GLO
Mean Residuals (mm)
Elvation Angle (°)
OTT4 Day number 105 - 112

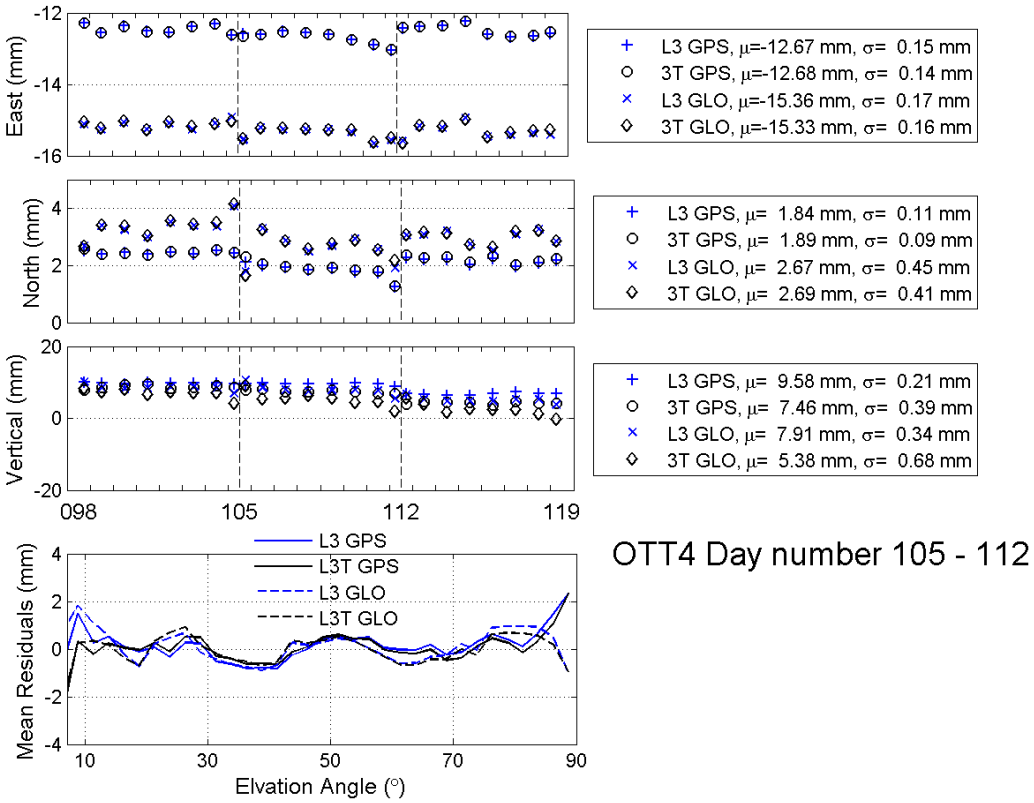
East (mm)
North (mm)
Vertical (mm)
L3 GPS, μ=-12.67 mm, σ= 0.15 mm
3T GPS, μ=-12.68 mm, σ= 0.14 mm
L3 GLO, μ=-15.36 mm, σ= 0.17 mm
3T GLO, μ=-15.33 mm, σ= 0.16 mm
L3 GPS, μ= 1.84 mm, σ= 0.11 mm
3T GPS, μ= 1.89 mm, σ= 0.09 mm
L3 GLO, μ= 2.67 mm, σ= 0.45 mm
3T GLO, μ= 2.69 mm, σ= 0.41 mm
L3 GPS, μ= 9.58 mm, σ= 0.21 mm
3T GPS, μ= 7.46 mm, σ= 0.39 mm
L3 GLO, μ= 7.91 mm, σ= 0.34 mm
3T GLO, μ= 5.38 mm, σ= 0.68 mm
098
105
112
119
L3 GPS
L3T GPS
L3 GLO
L3T GLO
Mean Residuals (mm)
Elvation Angle (°)
OTT4 Day number 105 - 112

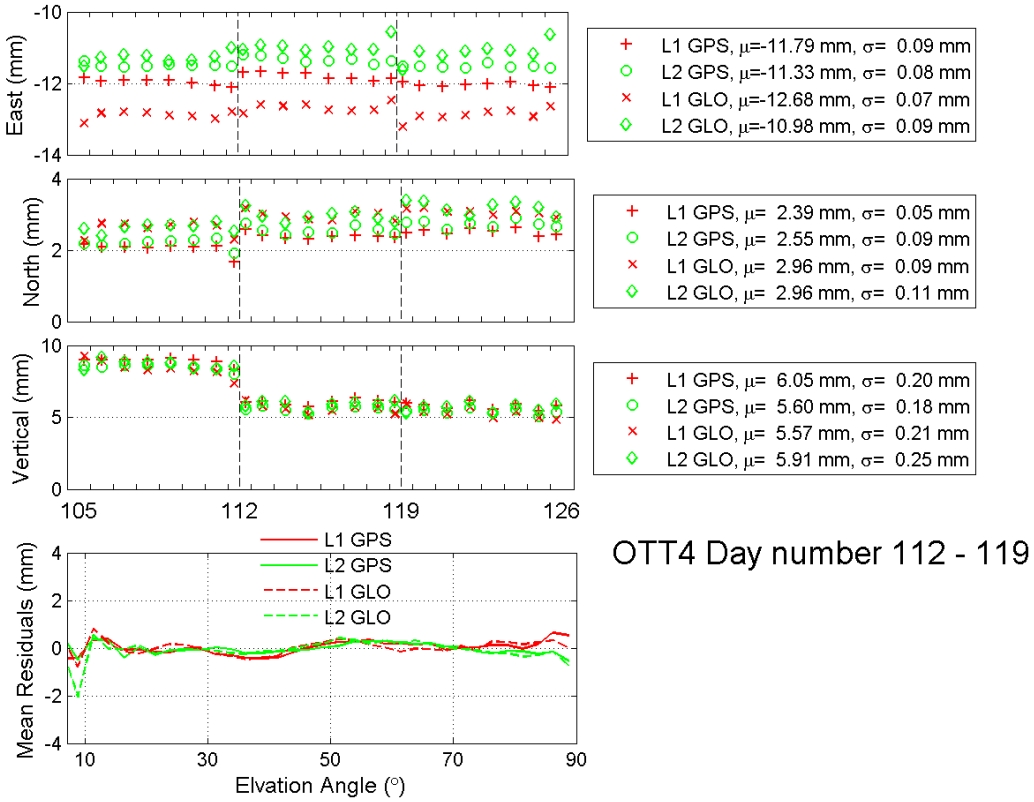

OTT4 Day number 112 - 119

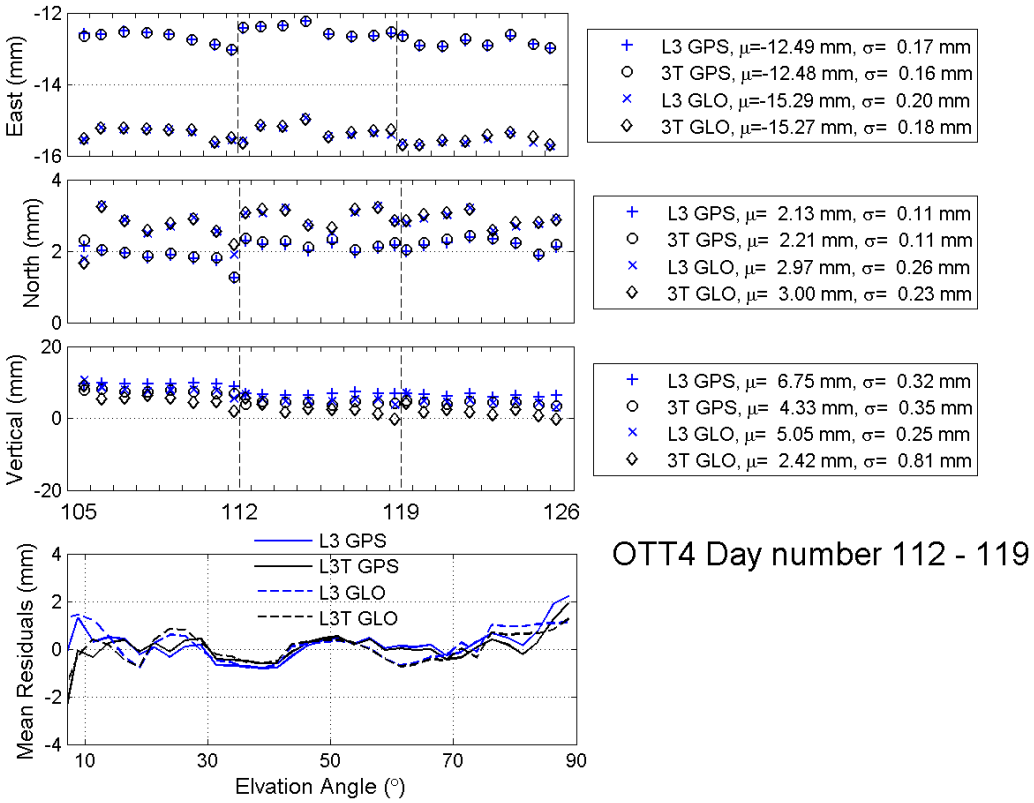

OTT4 Day number 112 - 119

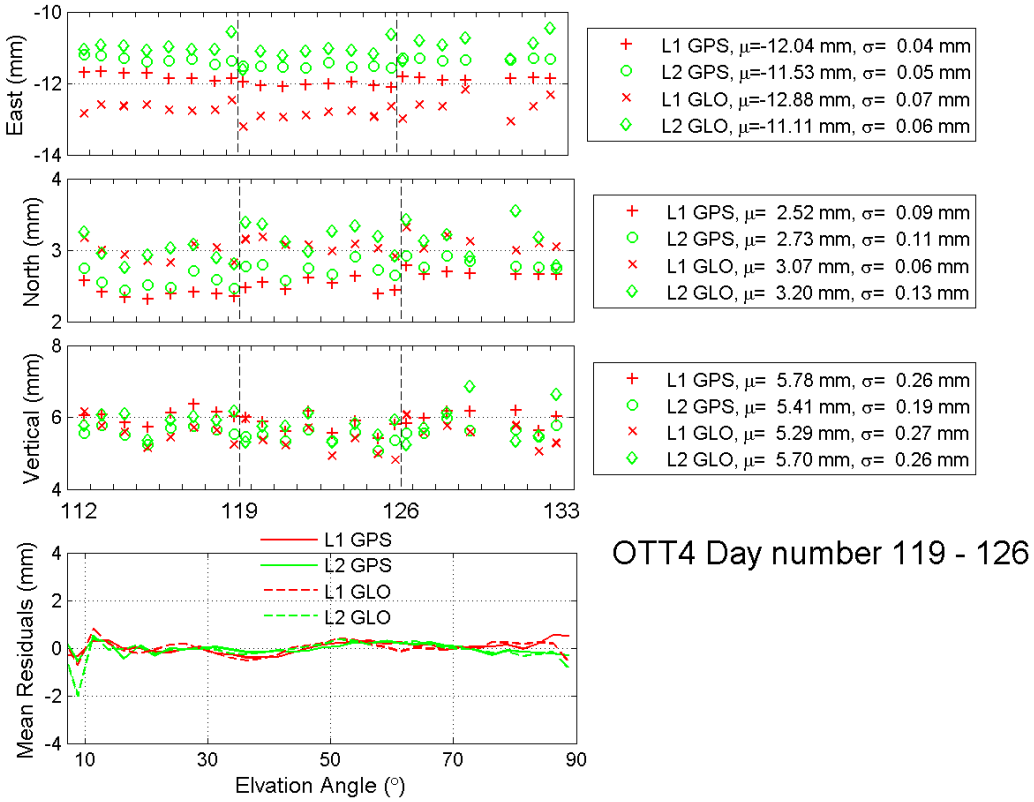

OTT4 Day number 119 - 126

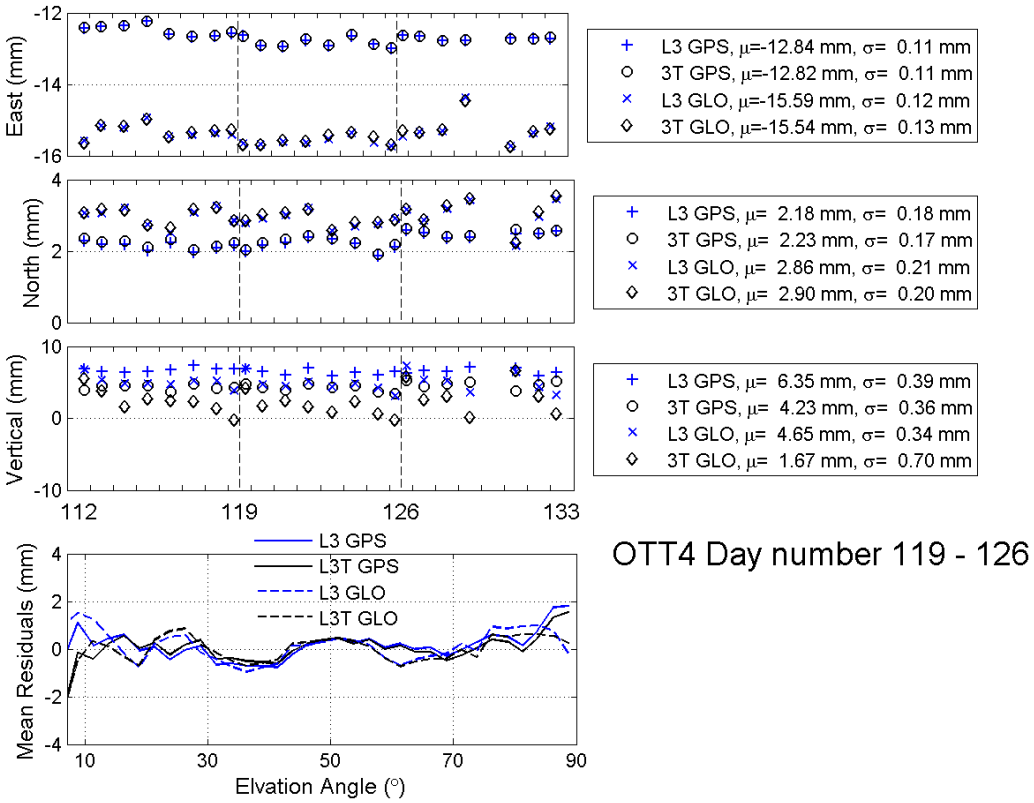

OTT4 Day number 119 - 126

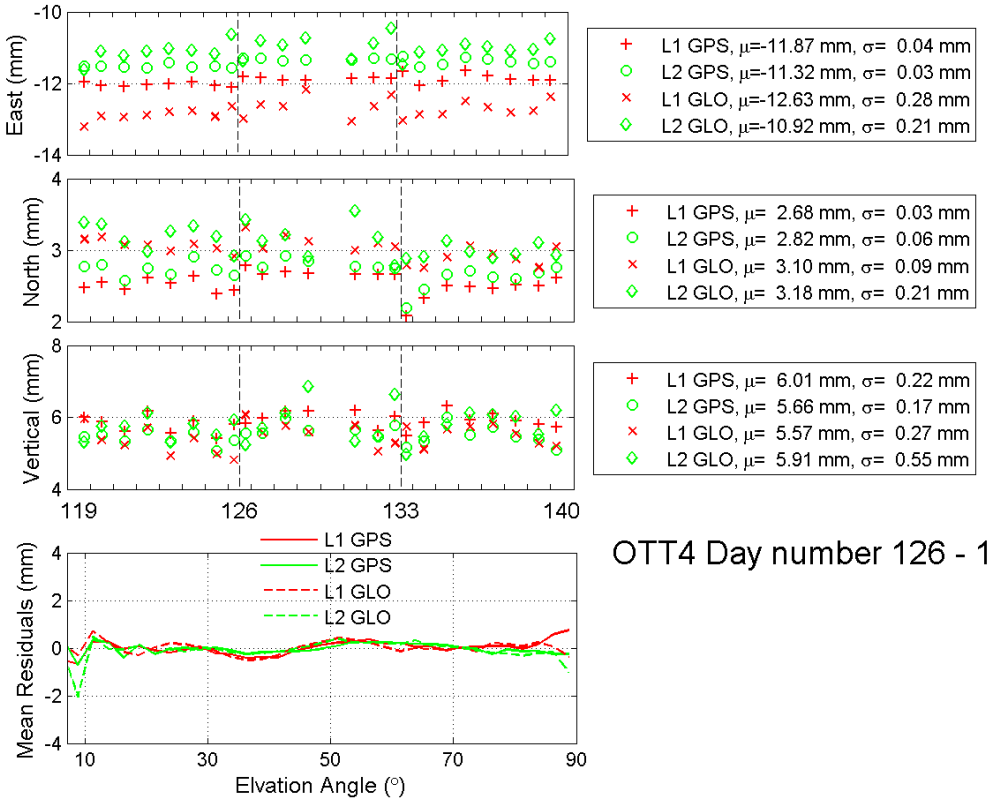

OTT4 Day number 126 - 133

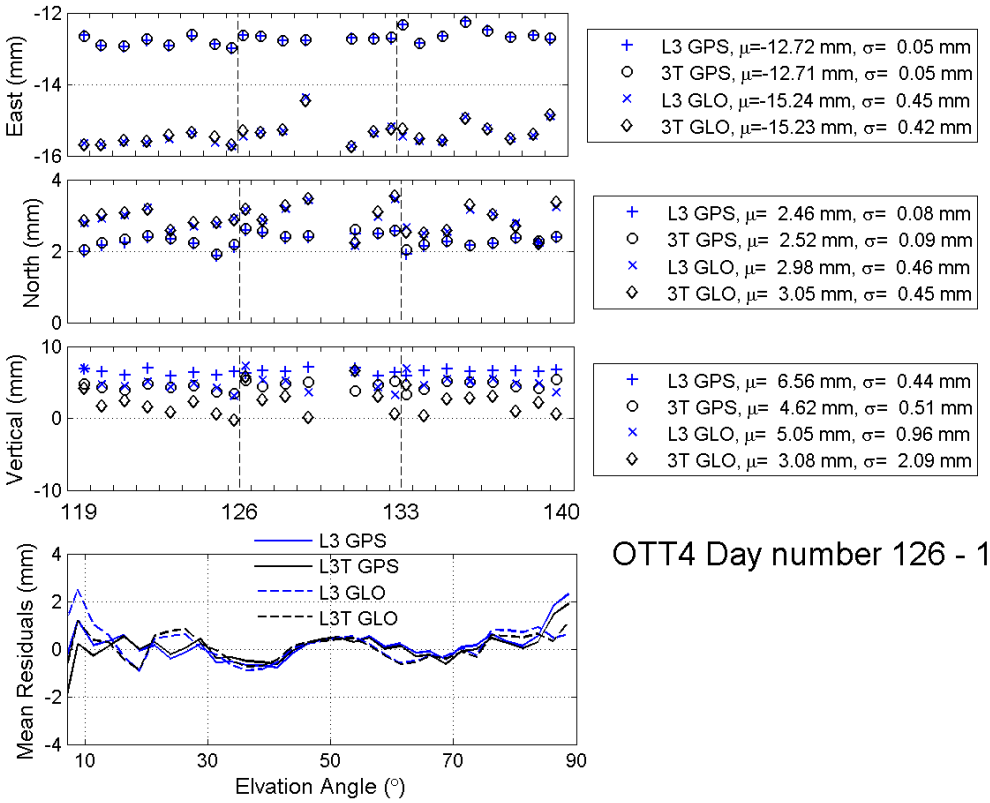

OTT4 Day number 126 - 133

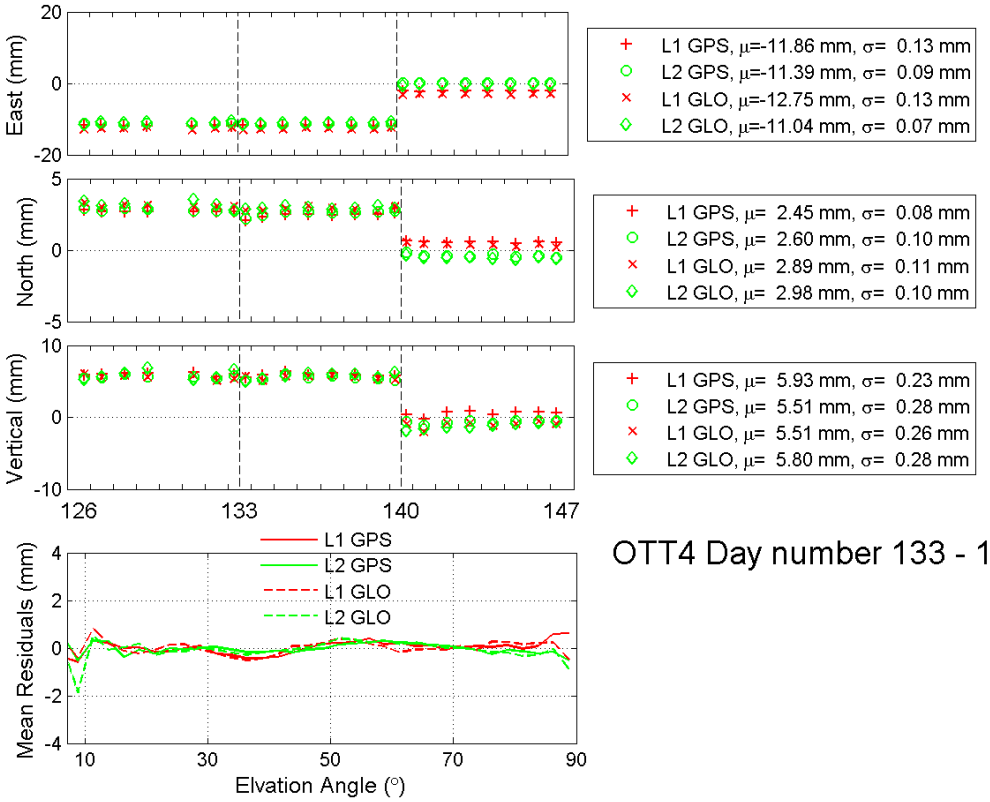

OTT4 Day number 133 - 140

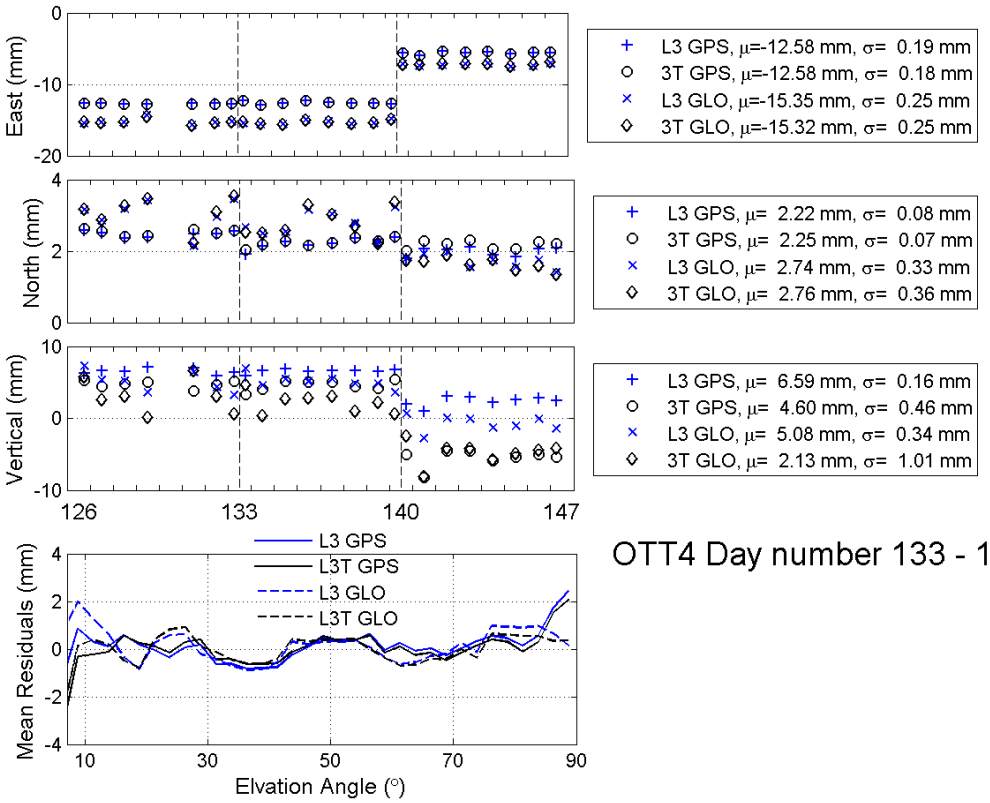

OTT4 Day number 133 - 140

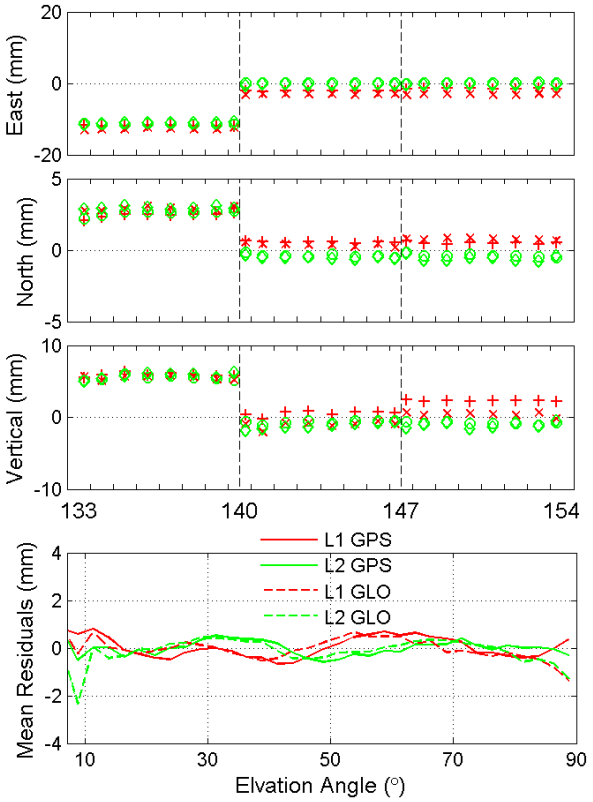

L1 GPS, μ= -2.15 mm, σ= 0.06 mm
L2 GPS, μ= 0.10 mm, σ= 0.07 mm
L1 GLO, μ= -3.06 mm, σ= 0.07 mm
L2 GLO, μ= -0.30 mm, σ= 0.12 mm

L1 GPS, μ= 0.55 mm, σ= 0.05 mm
L2 GPS, μ= -0.38 mm, σ= 0.07 mm
L1 GLO, μ= 0.37 mm, σ= 0.08 mm
L2 GLO, μ= -0.52 mm, σ= 0.08 mm

L1 GPS, μ= 0.52 mm, σ= 0.41 mm
L2 GPS, μ= -0.69 mm, σ= 0.24 mm
L1 GLO, μ= -1.03 mm, σ= 0.51 mm
L2 GLO, μ= -1.17 mm, σ= 0.30 mm

OTT4 Day number 140 - 147

OTT1: 00946.atx
OTT4: 10170020.atx

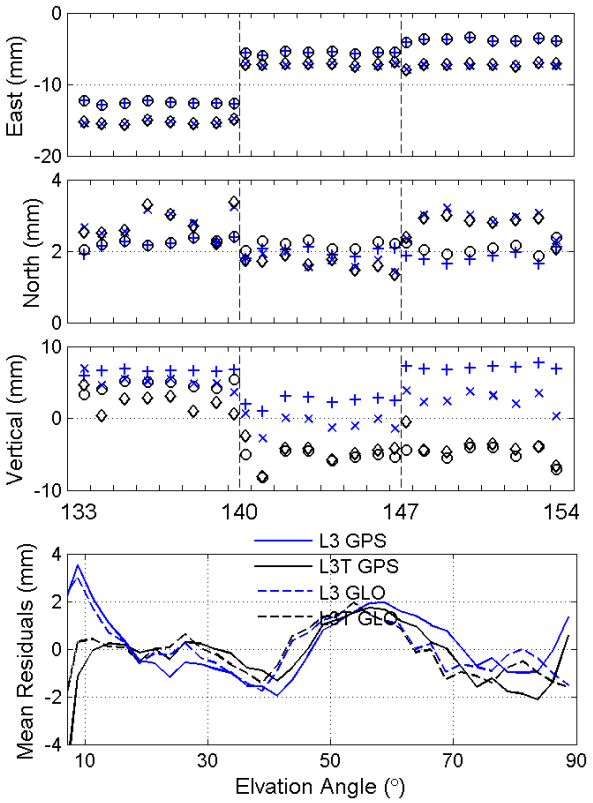

L3 GPS, μ= -5.62 mm, σ= 0.20 mm
3T GPS, μ= -5.58 mm, σ= 0.21 mm
L3 GLO, μ= -7.29 mm, σ= 0.16 mm
3T GLO, μ= -7.17 mm, σ= 0.15 mm

L3 GPS, μ= 1.99 mm, σ= 0.10 mm
3T GPS, μ= 2.18 mm, σ= 0.10 mm
L3 GLO, μ= 1.72 mm, σ= 0.17 mm
3T GLO, μ= 1.65 mm, σ= 0.15 mm

L3 GPS, μ= 2.39 mm, σ= 0.71 mm
3T GPS, μ= -5.55 mm, σ= 1.26 mm
L3 GLO, μ= -0.81 mm, σ= 1.02 mm
3T GLO, μ= -4.97 mm, σ= 1.57 mm

OTT4 Day number 140 - 147

OTT1: 00946.atx
OTT4: 10170020.atx

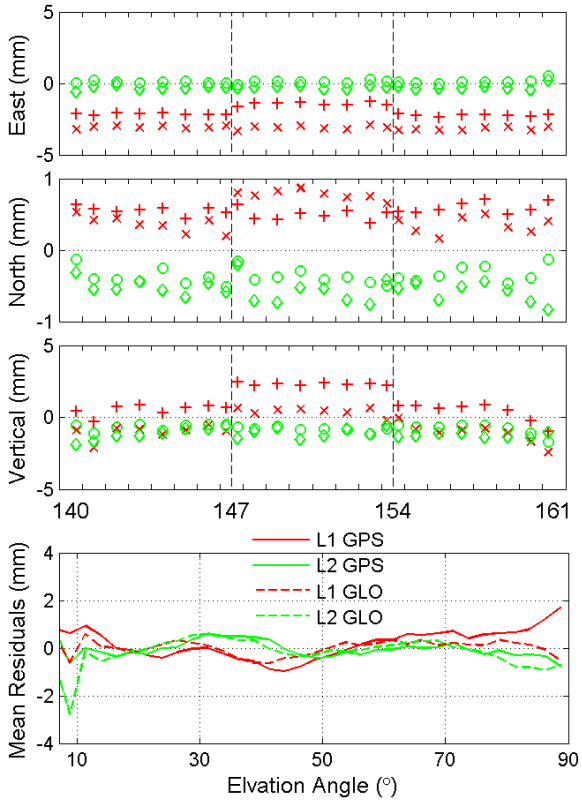

L1 GPS, μ= -1.43 mm, σ= 0.12 mm
L2 GPS, μ= 0.11 mm, σ= 0.08 mm
L1 GLO, μ= -3.09 mm, σ= 0.12 mm
L2 GLO, μ= -0.28 mm, σ= 0.12 mm

L1 GPS, μ= 0.48 mm, σ= 0.07 mm
L2 GPS, μ= -0.38 mm, σ= 0.05 mm
L1 GLO, μ= 0.78 mm, σ= 0.05 mm
L2 GLO, μ= -0.61 mm, σ= 0.16 mm

L1 GPS, μ= 2.29 mm, σ= 0.07 mm
L2 GPS, μ= -0.83 mm, σ= 0.17 mm
L1 GLO, μ= 0.42 mm, σ= 0.16 mm
L2 GLO, μ= -1.08 mm, σ= 0.29 mm

OTT4 Day number 147 - 154

OTT1: 00946.atx
OTT4: 10170020.atx

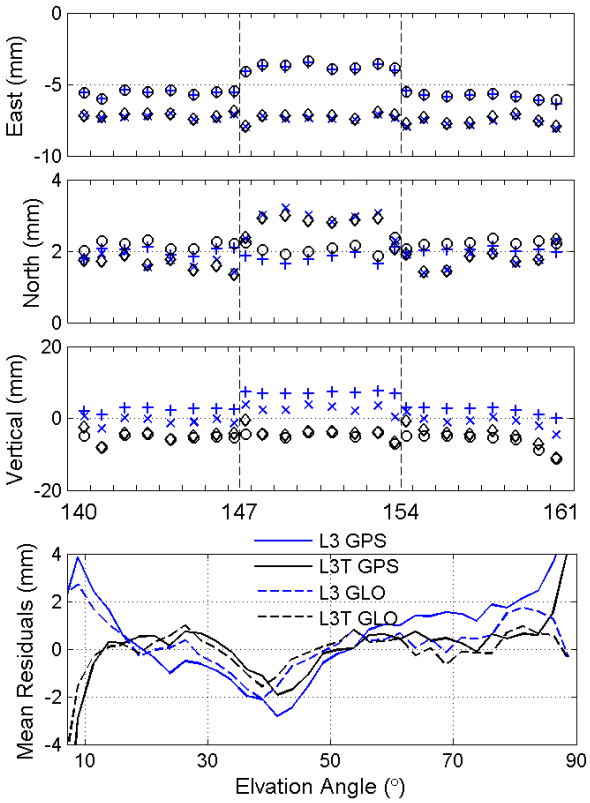

L3 GPS, μ= -3.80 mm, σ= 0.23 mm
3T GPS, μ= -3.72 mm, σ= 0.22 mm
L3 GLO, μ= -7.38 mm, σ= 0.18 mm
3T GLO, μ= -7.24 mm, σ= 0.19 mm

L3 GPS, μ= 1.81 mm, σ= 0.14 mm
3T GPS, μ= 2.06 mm, σ= 0.15 mm
L3 GLO, μ= 2.91 mm, σ= 0.29 mm
3T GLO, μ= 2.80 mm, σ= 0.27 mm

L3 GPS, μ= 7.11 mm, σ= 0.31 mm
3T GPS, μ= -4.70 mm, σ= 0.80 mm
L3 GLO, μ= 2.72 mm, σ= 0.72 mm
3T GLO, μ= -3.99 mm, σ= 0.47 mm

OTT4 Day number 147 - 154

OTT1: 00946.atx
OTT4: 10170020.atx

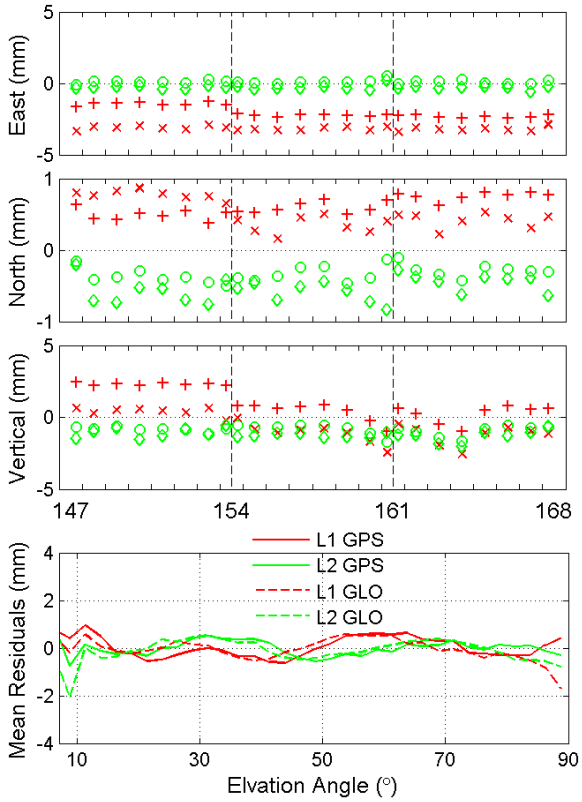

L1 GPS, μ= -2.26 mm, σ= 0.07 mm
L2 GPS, μ= 0.10 mm, σ= 0.10 mm
L1 GLO, μ= -3.20 mm, σ= 0.09 mm
L2 GLO, μ= -0.31 mm, σ= 0.16 mm

L1 GPS, μ= 0.59 mm, σ= 0.07 mm
L2 GPS, μ= -0.34 mm, σ= 0.09 mm
L1 GLO, μ= 0.34 mm, σ= 0.12 mm
L2 GLO, μ= -0.58 mm, σ= 0.12 mm

L1 GPS, μ= 0.44 mm, σ= 0.44 mm
L2 GPS, μ= -0.78 mm, σ= 0.25 mm
L1 GLO, μ= -1.09 mm, σ= 0.31 mm
L2 GLO, μ= -1.27 mm, σ= 0.14 mm

OTT4 Day number 154 - 161

OTT1: 00946.atx
OTT4: 10170020.atx

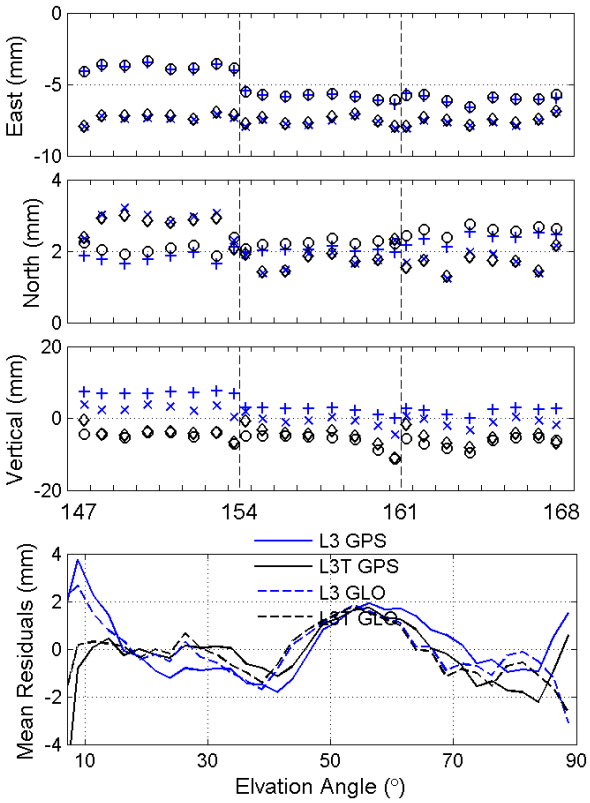

L3 GPS, μ= -5.89 mm, σ= 0.15 mm
3T GPS, μ= -5.81 mm, σ= 0.15 mm
L3 GLO, μ= -7.63 mm, σ= 0.28 mm
3T GLO, μ= -7.50 mm, σ= 0.28 mm

L3 GPS, μ= 2.03 mm, σ= 0.06 mm
3T GPS, μ= 2.23 mm, σ= 0.07 mm
L3 GLO, μ= 1.75 mm, σ= 0.26 mm
3T GLO, μ= 1.75 mm, σ= 0.26 mm

L3 GPS, μ= 2.33 mm, σ= 0.75 mm
3T GPS, μ= -6.19 mm, σ= 1.60 mm
L3 GLO, μ= -0.81 mm, σ= 0.79 mm
3T GLO, μ= -4.71 mm, σ= 1.40 mm

OTT4 Day number 154 - 161

OTT1: 00946.atx
OTT4: 10170020.atx

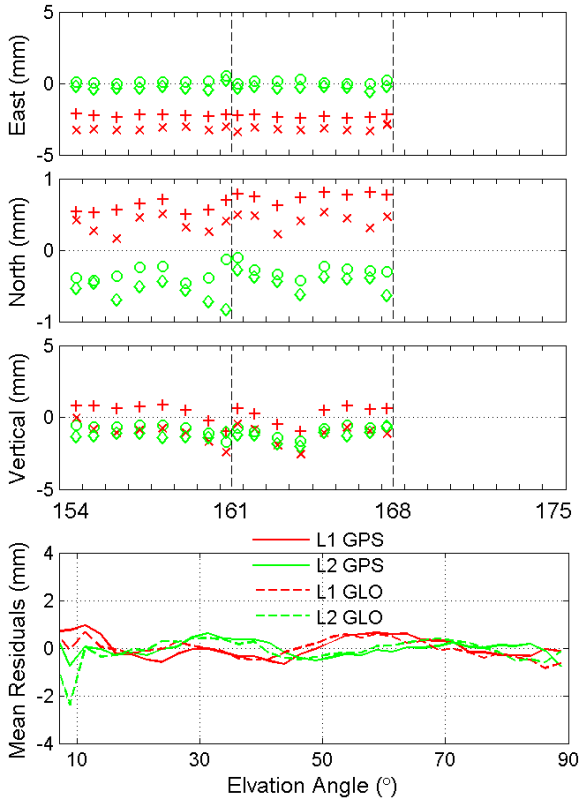

L1 GPS, μ= -2.33 mm, σ= 0.10 mm
L2 GPS, μ= 0.10 mm, σ= 0.12 mm
L1 GLO, μ= -3.22 mm, σ= 0.10 mm
L2 GLO, μ= -0.31 mm, σ= 0.14 mm

L1 GPS, μ= 0.75 mm, σ= 0.06 mm
L2 GPS, μ= -0.29 mm, σ= 0.07 mm
L1 GLO, μ= 0.41 mm, σ= 0.11 mm
L2 GLO, μ= -0.44 mm, σ= 0.09 mm

L1 GPS, μ= 0.18 mm, σ= 0.66 mm
L2 GPS, μ= -0.97 mm, σ= 0.42 mm
L1 GLO, μ= -1.27 mm, σ= 0.72 mm
L2 GLO, μ= -1.35 mm, σ= 0.43 mm

OTT4 Day number 161 - 168

OTT1: 00946.atx
OTT4: 10170020.atx

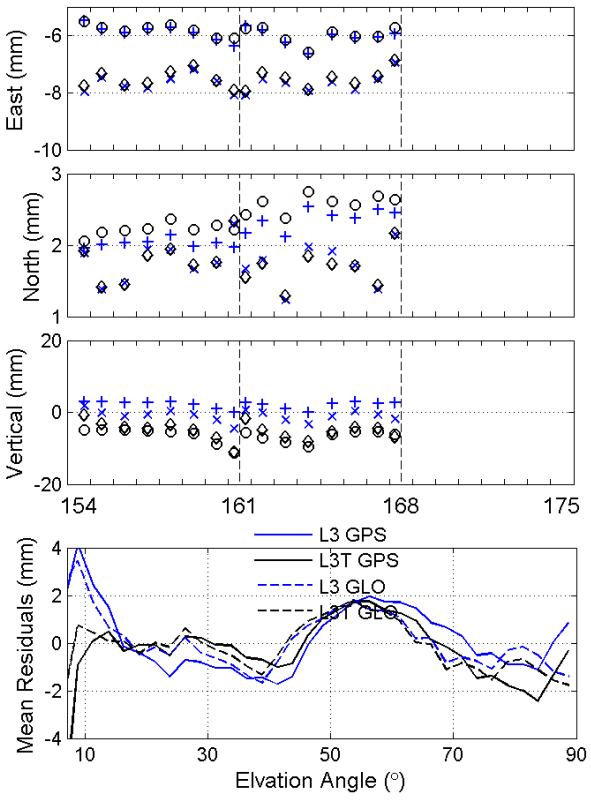

L3 GPS, μ= -6.09 mm, σ= 0.29 mm
3T GPS, μ= -6.02 mm, σ= 0.30 mm
L3 GLO, μ= -7.67 mm, σ= 0.18 mm
3T GLO, μ= -7.52 mm, σ= 0.19 mm

L3 GPS, μ= 2.37 mm, σ= 0.14 mm
3T GPS, μ= 2.59 mm, σ= 0.12 mm
L3 GLO, μ= 1.70 mm, σ= 0.29 mm
3T GLO, μ= 1.66 mm, σ= 0.21 mm

L3 GPS, μ= 1.96 mm, σ= 1.05 mm
3T GPS, μ= -6.87 mm, σ= 1.62 mm
L3 GLO, μ= -1.13 mm, σ= 1.26 mm
3T GLO, μ= -5.43 mm, σ= 1.51 mm

OTT4 Day number 161 - 168

OTT1: 00946.atx
OTT4: 10170020.atx

This page intentionally left blank.

Appendix B: Diary of installation and changes at the OTT test field

In this Appendix are described the initial installation at the OTT test sites in December 2014, as well as the weekly hardware changes performed at stations OTT2 and OTT4 during spring 2015.

Text are in Swedish.

This page intentionally left blank.

Ungefärliga positioner för de nya GNSS-stationerna

2014-12-18

Installation av antenner+radom och inkoppling till mottagare för station OTT1, OTT2, OTT4 och OTT6. Data loggas tillsvidare lokalt.

OTT1:

- Installation av okalibrerad antenn, Javadringant-DM 00868 (A0090868) med OSOS-radom (ej installerad enligt anvisning från Lantmäteriet).
- Antenn är installerad på 3m-mast med antennfot, isolerande skikt (plastskiva 3mm) och Onsala-tillverkad antennbult.
- Antennen är riktad mot norr med hjälp av handhållen kompass (0/360 grader +-2 grader).
- Inkoppling av Javad Sigma mottagare (JAVAD TRE_G3T SIGMA) 01585, ip: 192.168.229.199.
- Antenn och mottagare är inkopplad med 45m antennkabel: Rosenberger LDF4-50.
- Start av mottagare och lokal loggning klockan 15:01 (lokal tid; 14:01 UTC).

OTT1 fotograferad mot norr.

OTT2:

- Installation av okalibrerad antenn, Javadringant-DM 00823 (A0090823) med OSOS-radom (ej installerad enligt anvisning från Lantmäteriet).
- Antenn är installerad på 3m-mast med antennfot, isolerande skikt (plastskiva 3mm) och Onsala-tillverkad antennbult.
- Antennen är riktad mot norr med hjälp av handhållen kompass (0/360 grader +-2 grader).
- Inkoppling av Javad Sigma mottagare (JAVAD TRE_G3T SIGMA) 01588, ip: 192.168.229.200.
- Antenn och mottagare är inkopplad med 55m antennkabel: Rosenberger LDF4-50.
- Start av mottagare och lokal loggning klockan 15:15 (lokal tid; 14:15 UTC).

OTT2 fotograferad mot syd-ost (OTT4 i bakgrunden).

OTT4:

- Installation av okalibrerad antenn, Javadringant-DM 00821 (A0090821) med OSOS-radom (ej installerad enligt anvisning från Lantmäteriet).
- Antenn är installerad på 3m-mast med antennfot, isolerande skikt (plastskiva 3mm) och Onsala-tillverkad antennbult.
- Antennen är riktad mot norr med hjälp av handhållen kompass (0/360 grader +-2 grader).
- Inkoppling av Javad Sigma mottagare (JAVAD TRE_G3T SIGMA) 01595, ip: 192.168.229.203.
- Antenn och mottagare är inkopplad med 35m antennkabel: Rosenberger LDF4-50.
- Start av mottagare och lokal loggning klockan 13:58 (lokal tid; 12:58 UTC).

OTT4 fotograferad mot syd (OTT6 i bakgrunden).

OTT6:

- Installation av okalibrerad antenn, Javadringant-DM 00816 (A0090816) med OSOS-radom (ej installerad enligt anvisning från Lantmäteriet).
- Antenn är installerad på 2m-mast med antennfot, isolerande skikt (plastskiva 3mm) och Onsala-tillverkad antennbult.
- Antennen är riktad mot norr med hjälp av handhållen kompass (0/360 grader +-2 grader).
- Inkoppling av Javad Sigma mottagare (JAVAD TRE_G3T SIGMA) 01594, ip: 192.168.229.205.
- Antenn och mottagare är inkopplad med 70m antennkabel: Rosenberger LDF4-50.
- Start av mottagare och lokal loggning klockan 14:31 (lokal tid; 13:31 UTC).

OTT6 fotograferad mot syd.

2015-02-25 (dag 56)

Installation av absolutkalibrerade antenner och installation av ytterligare referensdubbar runt OTT3 och OTT5. RTK-mätningar av de nya referensdubbarna.

OTT1:

Klockan 09:30 (lokal tid; 08:30 UTC) börjar arbete runt OTT1.

- Befintlig okalibrerad antenn, Javadringant-DM 00868 (A0090868) med spontanpåskruvad OSOS-radom, tas ned.
- Kalibrerad antenn (absolutkalibrerad antenn+radom), Javadringant-DM 00957 (A0090957) med OSOS-radom, installeras med isolerande skikt (plastskiva 3mm) och Onsala-tillverkad antennbult på antennfoten på 3m-masten.
- Antennen är riktad mot norr med specialvertyg+kompass (som hålls mot hålen i choke-ringen) tillverkat av Lars Wennerbäck. Tyvärr har det visat sig senare att antennen blir något felriktad i azimut (antagligen pga närhet till antennsladd). Detta är uppmätt med handhållen kompass till 7 grader väst (353 grader +- 2 grader).

Installationen är färdig och stationen är igång klockan 10:30 (lokal tid; 09:30 UTC).

OTT1: borttagen okalibrerad antenn (vänster) och installerad absolutkalibrerad antenn (höger).

OTT2:

Klockan 10:30 (lokal tid; 09:30 UTC) börjar arbete runt OTT2.

- Befintlig okalibrerad antenn, Javadringant-DM 00823 (A0090823) med spontanpåskruvad OSOS-radom, tas ned.
- Kalibrerad antenn (absolutkalibrerad antenn+radom), Javadringant-DM 00951 (A0090951) med OSOS-radom, installeras med isolerande skikt (plastskiva 3mm) och Onsala-tillverkad antennbult på antennfoten på 3m-masten.
- Antennen är riktad mot norr med specialvertyg+kompass (som hålls mot hålen i choke-ringen) tillverkat av Lars Wennerbäck. Tyvärr har det visat sig senare att antennen blir något felriktad i azimut (antagligen pga närhet till antennsladd). Detta är uppmätt med handhållen kompass till 6 grader väst (354 grader +- 2 grader).

Installationen är färdig och stationen är igång klockan 10:50 (lokal tid; 09:50 UTC).

OTT2: installerad absolutkalibrerad antenn.

OTT6:

Klockan 10:50 (lokal tid; 09:50 UTC) börjar arbete runt OTT6.

- Befintlig okalibrerad antenn, Javadringant-DM 00816 (A0090816) med spontanpåskruvad OSOS-radom, tas ned.
- Kalibrerad antenn (absolutkalibrerad antenn+radom), Javadringant-DM 00956 (A0090956) med OSOS-radom, installeras med isolerande skikt (plastskiva 3mm) och Onsala-tillverkad antennbult på antennfoten på 2m-masten.
- Antennen är riktad mot norr med specialvertyg+kompass (som hålls mot hålen i choke-ringen) tillverkat av Lars Wennerbäck. Tyvärr har det visat sig senare att antennen blir något felriktad i azimut (antagligen pga närhet till antennsladd). Detta är uppmätt med handhållen kompass till 8 grader väst (352 grader +- 2 grader).

Installationen är färdig och stationen är igång klockan 11:10 (lokal tid; 10:10 UTC).

OTT6: borttagen okalibrerad antenn (vänster) och installerad absolutkalibrerad antenn (höger).

OTT4:

Klockan 14:50 (lokal tid; 13:50 UTC) börjar arbete runt OTT4.

- Befintlig okalibrerad antenn, Javadringant-DM 00821 (A0090821) med spontanpåskruvad OSOS-radom, tas ned.
- OSOS-radomen skruvas av och därefter skruvas OSOS-radomen på igen på samma antenn, Javadringant-DM 00821 (A0090821), enligt anvisning från Lantmäteriet.
- Den okalibrerade antenn med korrekt påskruvad OSOS-radom installeras igen med isolerande skikt (plastskiva 3mm) och Onsala-tillverkad antennbult på antennfoten på 3m-masten.
- Antennen är riktad mot norr med specialvertyg+kompass (som hålls mot hålen i choke-ringen) tillverkat av Lars Wennerbäck. Tyvärr har det visat sig senare att antennen blir något felriktad i azimut (antagligen pga närhet till antennsladd). Detta är uppskattat från mätningar vid de andra stationerna till 7 grader väst (353 grader +-2 grader).

Installationen är färdig och stationen är igång klockan 15:35 (lokal tid; 14:35 UTC).

OTT4: okalibrerad antenn med OSOS-radom påskruvad enligt Lantmäteriets anvisning.

ÖVRIGT:

För att rikta in antennerna på samma sätt vecka efter vecka mot norr tillverkades ett specialvertyg i verkstaden av Lars Wennerbäck. Verktyget hålls mot hålen i choke-ringen och kompassen som sitter på kommer då bort en bit ifrån själva antennen.

Tyvärr visade sig det senare att antennen blir något felriktad i azimut (antagligen pga närhet till antennsladden). Detta är uppmätt vid de 4 stationerna till 6-8 grader väst; azimut vinkel 352-354 grader. Mätosäkerheten uppskattas till ±2 grader.

För att inte introducera ytterliggaare ändringar under tiden då vi gör experimenten på OTT-GNSS-stationerna, så behålls denna azimutriktning om inget annat noteras. När experimenten är färdiga kommer vi att rikta in dem mot norr med handhållen kompass.

Verktyg med kompass för inriktning mot norr.

2015-03-04 (dag 63)

Stationsändringar för OTT2 och OTT4.

OTT2:

Klockan 13:00 (lokal tid; 12:00 UTC) börjar arbete runt OTT2.

- Befintlig OSOS-radom tas bort klockan ca 14:00 (lokal tid; ca 13:00 UTC).
- Borttagningen görs utan att antennen kopplas bort och utan att orienteringen av antennen ändras.

Arbetet är färdigt klockan 15:00 (lokal tid; 14:00 UTC).

OTT2 med absolutkalibrerad antenn och utan radom.

OTT4:

Klockan 13:00 (lokal tid; 12:00 UTC) börjar arbete runt OTT4.

- Antennen lossas och det befintliga isolerande skiktet (plastskiva 3mm) tas bort.
- Antennen skruvas tillbaka utan isolerande skikt.
- Ändringarna skedde i huvudsak 14:00-14:30 (lokal tid; 13.00-13.30 UTC).
- Antennen är riktas mot norr med kompass och ej med specialverktyg (det senare verkade visa några grader fel vid användandet). Detta medför att antennen har vridits något i azimut (ca 7 grader +-2 grader) efter installationen/borttagandet av det isolerande skiktet. Nuvarande orientering är 0/360 grader +-2 grader.

Arbetet är färdigt klockan 15:00 (lokal tid; 14:00 UTC).

OTT4 med borttaget isolerande skikt (plastskiva 3mm) mellan antenn och antennfot.

2015-03-11 (dag 70)

Stationsändringar för OTT2 (montering av OSOS-radom) och OTT4 (installation av trefot med adapter).

OTT2:

Klockan 13:50 (lokal tid; 12:50 UTC) börjar arbete runt OTT2.

- (Befintlig azimutriktning på antennen, ~nord: 6 grader väst; 354 grader +-2 grader, markeras med färg på antennfoten.)
- OSOS-radom (samma som tidigare har suttit på) monteras på antennen enligt anvisning från Lantmäteriet.
- Orienteringen av antennen ändras ej under installationen av radomen.

Arbetet är färdigt klockan 14:35 (lokal tid; 13:35 UTC).

- Notera att antennen är absolutkalibrerad med och utan radom. Vid kalibreringen med OSOS-radom följdes ej Lantmäteriets anvisningar vid radominstallationen.

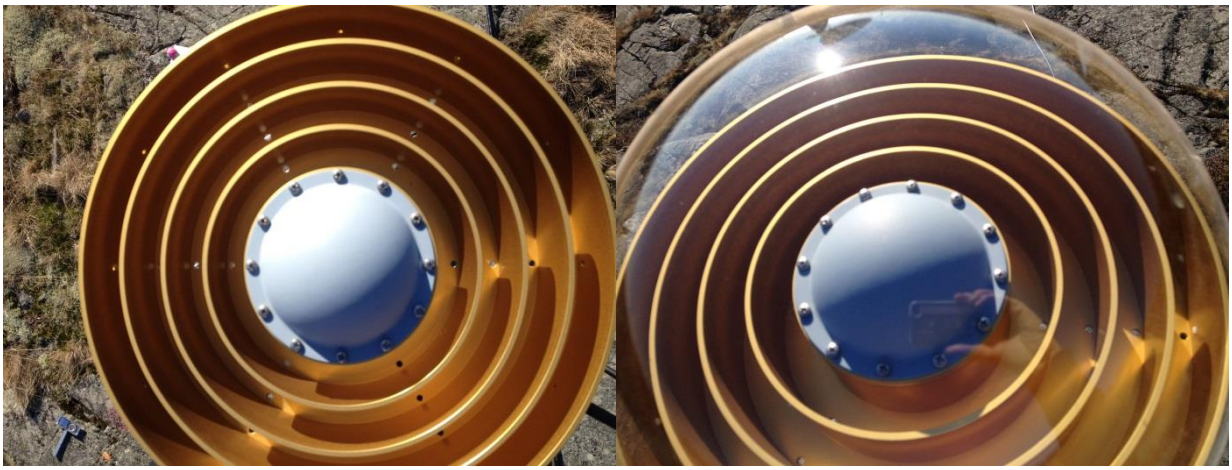

OTT2: absolutkalibrerad antenn utan radom (vänster) och med OSOS-radom (höger).

OTT4:

Klockan 14:35 (lokal tid; 13:35 UTC) börjar arbete runt OTT4.

- (Befintlig azimutriktning på antennen, nord: 0/360 grader +-2 grader, markeras med färg på antennfoten.)
- Antennensladden lossas från antennen och antennen lossas och lyfts av masten.
- Isolerande skikt (plastskiva 3mm) installeras på antennfoten.
- Trefot (Leica Tribrach PRO w/o optical plummet GDF321, 777508) och adapter (Leica Adapter tribrach rotating rev D, 2070-00) installeras med Onsala-tillverkad antennbult.
- Antennen installeras på adaptern och antennsladden kopplas in.
- Mätning med skjutmått av höjden på trefoten (Tribrach) med adapter (efter att den är inställd i våg): 77mm. Mätningen görs från botten av trefoten (grön del) till toppen av adaptern (svart del; ej toppen av skruven på adaptern).
- Mätning med skjutmått av avståndet från botten av trefoten (grön del) till BCR (Bottom of Choke-Ring): 112mm.
- Från IGS är avståndet från BPA (Bottom of PreAmplifier) till BCR: 34,5mm (för JAVRINGANT_DM). Med tidigare mätningar blir det alltså 77mm+34,5mm=111,5mm (~112mm).
- Antennen är riktad mot norr enligt tidigare markering på antennfoten (0/360 grader +-2 grader).

Arbetet är färdigt klockan 15:15 (lokal tid; 14:15 UTC).

- Notera att det som har kallats botten av trefoten (grön del) egentligen inte är det nedersta på trefoten utan det finns ytterligare en botten (svart del) med extra material vid trefotens hörn. Det gör att trefoten är upphöjd från underlaget/antennfoten ca 1-2mm. Detta har dock ej någon påverkan på skjutmåttsmätningarna.

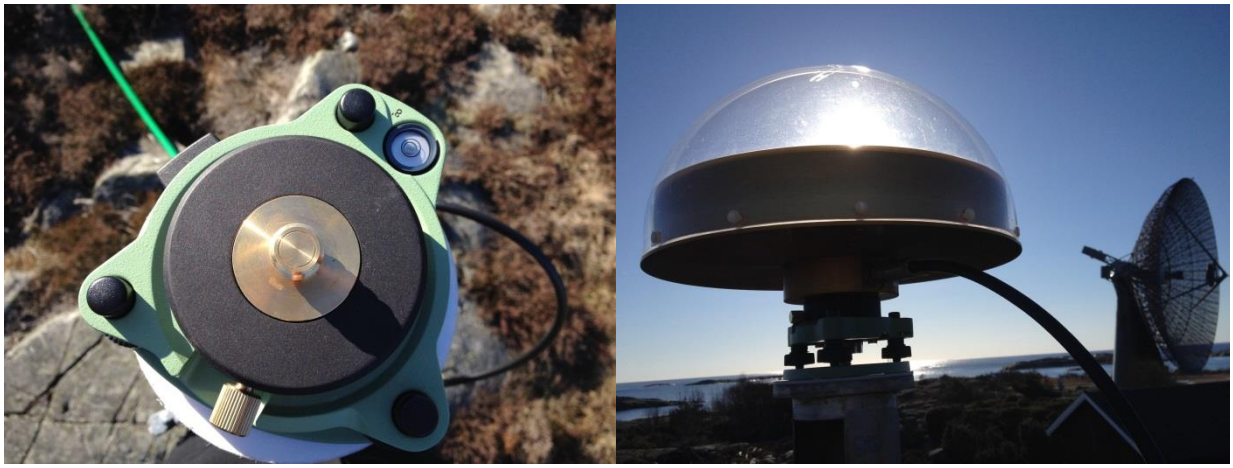

OTT4: Trefot i våg installerad på antennfoten tillsammans med ett isolerande skikt (vänster) och samma installation med antenn och radom (höger).

2015-03-18 (dag 77)

Stationsändringar för OTT2 (OSOS-radom skuvas av, lyfts och skruvas på igen på samma sätt) och OTT4 (isolerande skikt under trefot tas bort).

OTT2:

Klockan 13:55 (lokal tid; 12:55 UTC) börjar arbete runt OTT2.

- Befintlig OSOS-radom skruvas loss och lyfts av antennen.
- Samma OSOS-radom lyfts återigen på antennen och monteras (på samma sätt) enligt anvisning från Lantmäteriet.
- Borttagningen av radomen och återinstallationen görs utan att antennen kopplas bort och utan att orienteringen av antennen ändras.

Arbetet är färdigt klockan 14:45 (lokal tid; 13:45 UTC).

- Notera att antennen är absolutkalibrerad med och utan radom. Vid kalibreringen med OSOS-radom följdes ej Lantmäteriets anvisningar vid radominstallationen.

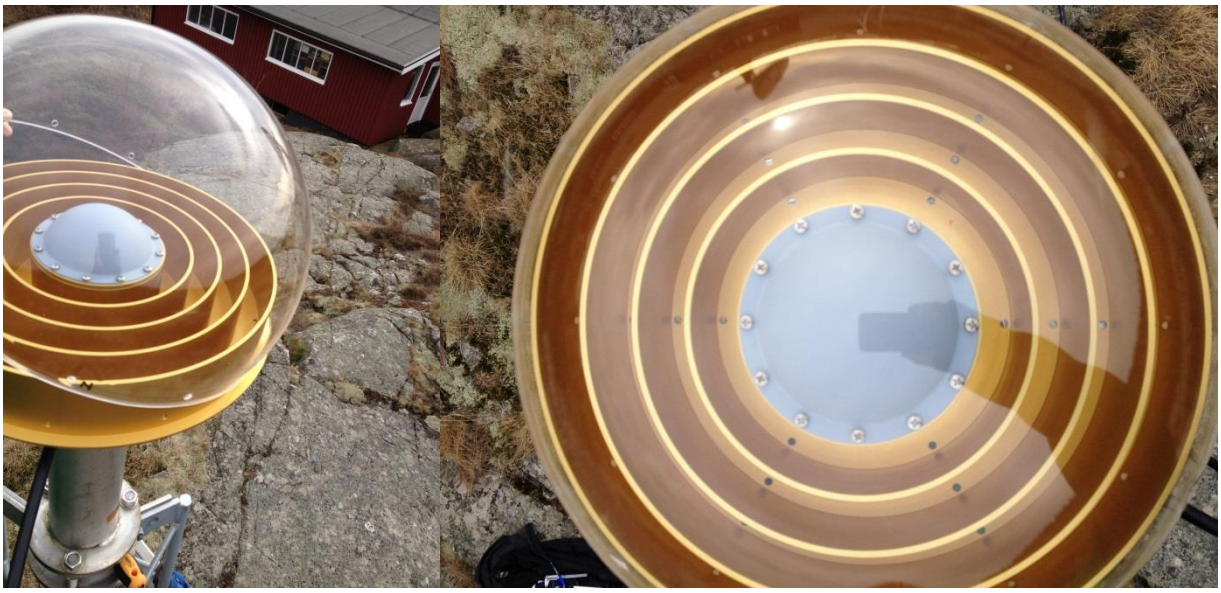

Radomen plockas av antennen (vänster) för att därefter direkt sättas tillbaka på antennen och återmonteras enligt Lantmäteriets anvisningar (höger).

OTT4:

Klockan 14:45 (lokal tid; 13:45 UTC) börjar arbete runt OTT4.

- (Positionen för trefotens, Leica Tribrach PRO w/o optical plummet GDF321 777508, "hörn" markeras på antennfoten.)
- Antennensladden lossas från antennen och antennbulten lossas (antennen fastsatt med trefot och adapter, Leica Adapter tribrach rotating rev D 2070-00, står löst på antennfoten).
- Antennen (ihop med trefot och adapter) lyfts och det isolerande skiktet (plastskiva 3mm) tas bort.
- Trefoten (fortfarande med antenn och adapter fastsatt) positioneras på antennfoten enligt tidigare markering och antennbulten fäster trefoten i antennfoten.
- Antennsladden kopplas in.
- Borttagningen av det isolerande skiktet görs utan att orienteringen av antennen ändras (höjden minskar med höjden på plastskivan 3mm) och utan ändring av trefoten. Avstånden från mätningarna 2015-03-11 är alltså fortfarande detsamma. Från botten av trefoten (grön del) till toppen av adaptern (svart del; ej toppen av skruven på adaptern): 77mm. Från botten av trefoten (grön del) till BCR (Bottom of Choke-Ring): 112mm.

Arbetet är färdigt klockan 15:10 (lokal tid; 14:10 UTC).

- Notera att det som har kallats botten av trefoten (grön del) är egentligen inte det nedersta på trefoten utan det finns ytterligare en botten (svart del) med extra material vid trefotens hörn. Det gör att trefoten är upphöjd från underlaget/antennfoten ca 1-2mm. Detta har dock ej någon påverkan på skjutmåttsmätningarna.

Före borttagandet av det isolerande skiktet (vänster) och efter borttagandet (höger).

2015-03-25 (dag 84)

Stationsändringar för OTT2 (eccosorbskiva fästs under antennen) och OTT4 (antennfot med OSOD-radom installeras).

OTT2:

Klockan 11:00 (lokal tid; 10:00 UTC) börjar arbete runt OTT2.

- Antennsladden lossas från antennen.
- Befintlig antenn (absolutkalibrerad Javadringant-DM 00951, A0090951) med OSOS-radom skruvas loss och lyfts av antennen.
- En kvadratisk eccosorbskiva (nr 10-09, vikt 1582g) sätts fast under antennens choke-ring. Eccosorbskivan sitter fast på antennen genom att sidorna i hålet (i mitten av skivan) klämmer fast i antennens för-förstärkare och så hålls skivan upp av antennsladdingången (tejp eller lim har ej använts).
- En vinkel-adapter (90-grader) fästs på antennens antennsladdutgång för att underlätta infästningen av antennsladden då eccosorb-skivan är i vägen för tidigare antennsladdinfästning.
- Antennen (med OSOS-radom och eccosorb) återinstalleras på masten, tillsammans med isolerande skikt (plastskiva 3mm), och riktas efter tidigare markering på antennfoten (azimutriktning ~nord: 6 grader väst; 354 grader +-2 grader).
- Antennsladden kopplas in.

Arbetet är färdigt klockan 13:00 (lokal tid; 12:00 UTC).

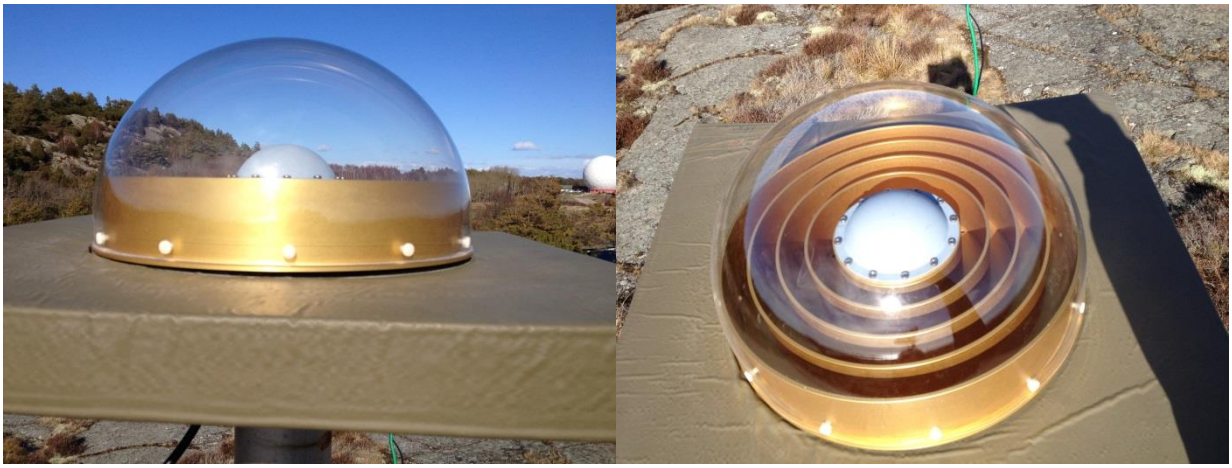

Absolutkalibrerad antenn med OSOS-radom och kvadratisk eccosorbskiva under choke-ringen.

OTT2-masten med kvadratisk eccosorbskiva under antennen (vänster) och bild på antennsladdsinfästningen (adapter med 90-graders vinkel) vid undersidan av eccosorbskivan (höger).

OTT4:

Klockan 11:00 (lokal tid; 10:00 UTC) börjar arbete runt OTT4.

- Antennsladden lossas från antennen och antennen (med OSOS-radom), trefot och adapter och isolerande skikt tas bort.
- Antennfoten (cirkulärt tvärsnitt) lossas från masten och lyfts bort.
- En ny antennfot (rektangulärt tvärsnitt) med 3st armar för en OSOD-radom installeras på masten. Antennfoten (med 3st armar) har höjden 41.8cm från toppen till botten av bottenplattan (ej benen som fästs i masten). Den tidigare installerade antennfoten har höjden 41.9cm från toppen till botten av toppdelen (notera att denna del är fäst med 3 bultar på den del som fästs i masten, fungerar som en trefot, och därför kan den totala höjden variera).
- På den nya antennfoten installeras samma isolerande skikt (plastskiva 3mm), trefot (Leica Tribrach PRO w/o optical plummet GDF321, 777508) och adapter (Leica Adapter tribrach rotating rev D 2070-00).
- Trefoten justeras till att vara i våg och höjden mäts med skjutmått. Från botten av trefoten (grön del) till BCR (Bottom of Choke-Ring) är avståndet 106.5mm/105.1mm (mätning på olika sidor av trefoten). Från IGS är avståndet från BPA (Bottom of PreAmplifier) till BCR: 34.5mm (för JAVRINGANT_DM). Detta ger trefot med adapter en höjd på: 106.5mm-34.5mm=72.0mm/70.6mm.
- Antennen (okalibrerad Javadringant-DM 00821, A0090821) utan radom skruvas på installationen och riktas mot nord med kompass (azimut 0/360 grader +-2 grader). Detta skall vara samma riktning som tidigare.
- En OSOD-radom lyfts över antennen och sätts fast på antennfotens tre armar.

Arbetet är färdigt klockan 13:00 (lokal tid; 12:00 UTC).

Den borttagna antennfoten med cirkulärt tvärsnitt (vänster) och den installerade antennfoten med rektangulärt tvärsnitt och 3st armar för att hålla fast en OSOD-radom (höger).

Antenninfästningen med trefot och isolerande skikt ovanpå den nyinstallerade antennfoten (vänster) och antennfoten på OTT4-masten med installerad OSOD-radom (höger).

2015-04-01 (dag 91)

Stationsändringar för OTT2 (ytterligare eccosorbbitar fästs under befintlig eccosorbskiva) och OTT4 (OSOD-radom tas av).

OTT2:

Klockan 15:15 (lokal tid; 13:15 UTC) börjar arbete runt OTT2.

- Diverse mindre eccosorbbitar tejpas med dubbelhäftande tejp fast under den befintliga kvadratiska eccosorbskivan.
- Installationen av ytterligare eccosorbbitar görs utan att riktningen av antennen eller av den befintliga eccosorbskivan ändras. Möjligen trycks den befintliga eccosorbskivan till något under installationen då de mindre bitarna appliceras underifrån.

Arbetet är färdigt klockan 16:30 (lokal tid; 14:30 UTC).

- De påtejpade eccosorbbitarna satt kvar vid inspektion under förmiddagen 2014-04-02.
- Vid inspektion under eftermiddagen 2014-04-07 hade de två långsmala eccosorbbitarna (fastsatta närmast antenninfästningen) lossat och fallit av. Det är oklart när under långhelgen som bitarna har lossat. De tre hörnbitarna satt dock kvar under den stora kvadratiska eccosorbskivan.

OTT2-antennen med en kvadratisk eccosorbskiva under choke-ringen samt ytterligare mindre eccosorbbitar fasttejpade under den stora skivan sedd från sidan (vänster) och snett underifrån (höger).

OTT2-masten med extra eccosorbbitar fastsatt under den befintliga eccosorbskivan direkt efter installation (vänster) och 5 dagar senare då två av de extra eccosorbbitarna har ramlat av (höger).

OTT4:

Klockan 16:25 (lokal tid; 14:25 UTC) börjar arbete runt OTT4.

- OSOD-radomen lossas från antennfotens tre armar och tas av masten.
- Arbetet utförs utan att riktningen av antennen ändras.

Arbetet är färdigt klockan 16:40 (lokal tid; 14:40 UTC).

OSOD-radomen monteras av från antennfoten på OTT4 utan att riktningen av antennen ändras.

2015-04-08 (dag 98)

Stationsändringar för OTT2 (tjockt isolerande skikt, trefot med adapter och antenn med eccosorbskiva installeras) och OTT4 (OSOS-radom installeras på befintlig antenn).

OTT2:

Klockan 13:40 (lokal tid; 11:40 UTC) börjar arbete runt OTT2.

- Antennsladd kopplas ur, befintlig antenn (absolutkalibrerad Javadringant-DM 00951, A0090951) med OSOS-radom och eccosorbskiva med extra eccosorbbitar (de som sitter kvar) lyfts av masten tillsammans med det isolerande skiktet (plastskiva 3mm).
- Ett tjockt isolerande skikt (plastskiva 20mm) läggs på toppen av antennfoten och en trefot (Leica Tribrach PRO w/o optical plummet GDF321, 777508) med adapter (Leica Adapter tribrach rotating rev D 2070-00) installeras ovanpå skiktet med hjälp av en lång OSO-tillverkad bult med längd 80.5mm (den korta/vanliga OSO-tillverkade bulten har längd 52.9mm och Lantmäteriets bult har längden 43.1mm). Denna installation är till för att nästa vecka kunna fungera med 2st kvadratiska eccosorbskivor under antennen.
- Trefoten justeras till att vara i våg och höjden mäts med skjutmått. Från botten av trefoten (grön del) till BCR (Bottom of Choke-Ring) är avståndet 106.0mm/105.4mm (mätning på olika sidor av trefoten). Från IGS är avståndet från BPA (Bottom of PreAmplifier) till BCR: 34.5mm (för JAVRINGANT_DM). Detta ger trefot med adapter en höjd på: 106mm-34.5mm=71.5mm/70.9mm. Ytterligare trefotsmått: från botten av trefoten (grön del) till toppen av trefoten (grön del, ej adaptern) är avståndet 48.15mm/48.20mm (mätning på olika sidor av trefoten).
- Samma antenn (absolutkalibrerad Javadringant-DM 00951, A0090951) med OSOS-radom och en kvadratisk eccosorbskiva under choke-ringen (nr 10-09, vikt 1582g; samma eccosorbskiva som använts under tidigare experiment) sätts fast på trefoten. Eccosorbskivan sitter fast på antennen genom att sidorna i hålet (i mitten av skivan) klämmer fast i antennens för-förstärkare och så hålls skivan upp av antennsladdingången (tejp eller lim har ej använts). De extra eccosorbbitarna som satt fast under den kvadratiska eccosorbskivan är borttagna.
- En vinkel-adapter (90-grader) fästs på antennens antennsladdutgång för att underlätta infästningen av antennsladden då eccosorb-skivan är i vägen för tidigare antennsladdinfästning.
- I vinkeladaptern fästs en extra antennslad, längd ca 514mm, som därefter fästs med en ytterligare adapter i antennsladden från mottagaren. Detta görs för att kunna använda installationen tillsammans med ytterligare en kvadratiska eccosorbskiva.
- Antennen riktas mot norr enligt tidigare markering på antennfoten (azimutriktning ~nord: 6 grader väst; 354 grader +-2 grader).

Arbetet är färdigt klockan 14:35 (lokal tid; 12:35 UTC).

- Anmärkning angående trefoten: det som har kallats botten av trefoten (grön del) är egentligen inte det nedersta på trefoten utan det finns ytterligare en botten (svart del) med extra material vid trefotens hörn. Det gör att trefoten är upphöjd från underlaget/antennfoten ca 1-2mm. Detta har dock ej någon påverkan på skjutmåttsmätningarna.

Toppen av antennfoten på OTT2 med ett tjockt isolerande skikt och en trefot installerad med en längre bult (vänster) och med antennen tillsammans med OSOS-radom, eccosorbskiva och extra antennkabel (höger).

Infästningen av den extra antennsladden (vänster) och antennen med OSOS-radom och eccosorbskiva (höger).

OTT4:

Klockan 14:40 (lokal tid; 12:40 UTC) börjar arbete runt OTT4.

- Den tidigare använda OSOS-radomen (ej OSOD!) lyfts på antennen och monteras enligt anvisning från Lantmäteriet.
- Arbetet utförs utan att riktningen av antennen ändras (azimut 0/360 grader +-2 grader).

Arbetet är färdigt klockan 15:20 (lokal tid; 13:20 UTC).

OTT4-antennen innan installation av OSOS-radom (vänster) och efter att OSOS-radom har installerats (höger).

OTT4 med antenn och OSOS-radom installerad på en antennfot med tre armar fotat åt öster (vänster) och åt söder (höger).

2015-04-15 (dag 105)

Stationsändringar för OTT2 (korrigeringar av förra veckans installation) och OTT4 (OSOS-radom tas av och OSOD-radom installeras).

OTT2:

Innan ändringen av OTT2 upptäcks att antennen med eccosorbskiva har ändrat läge under veckan:

- antennen har ändrat azimutriktning.
- eccosorbskivan sitter snett: västra delen av skivan har delvis åkt ner över trefoten.

De ofrivilliga ändringarna kommer troligtvis av starka vindar sedan konfigurationen installerades under förra veckan.

Klockan 14:05 (lokal tid; 12:05 UTC) börjar arbete runt OTT2.

- Antennsladden kopplas ur och befintlig antenn (absolutkalibrerad Javadringant-DM 00951, A0090951) med OSOS-radom, eccosorbskiva (nr 10-09, vikt 1582g) och trefot (Leica Tribrach PRO w/o optical plummet GDF321, 777508) med adapter (Leica Adapter tribrach rotating rev D 2070-00) lossas och tas ned från masten.
- Ett tunt isolerande skikt (plastskiva 3mm) placeras mellan adapter och antenn för att hålla fast eccosorbskivan på ett bättre sätt. Utöver detta sitter eccosorbskivan fast på antennen genom att sidorna i hålet (i mitten av skivan) klämmer fast i antennens för-förstärkare och så hålls skivan upp av vinkeladaptern (90-grader) på antennsladdingången (tejp eller lim har ej använts).
- Installationen av antennen med eccosorbskiva på masten görs därefter på samma sätt som förra veckan och med samma utrustning. Ett tjockt isolerande skikt (plastskiva 20mm) läggs på toppen av antennfoten. Trefoten med adapter och tunt isolerande skikt (plastskiva 3mm) ihop med antennen och eccosorbskivan installeras ovanpå det tjocka skiktet med hjälp av en lång OSO-tillverkad bult med längd 80.5mm. Denna installation är till för att nästa vecka kunna fungera med ytterligare en kvadratisk eccosorbskiva (totalt 2st) under antennen.
- För att se till att antennen verkligen sitter fast ordentligt har antenn, eccosorbskiva, trefot, adapter, isolerande skikt (tunt) monterats på marken och därefter har hela paketet installerats med den långa bulten (och det tjocka isolerande skiktet) på masten. Väl installerad är det svårt justera och att vara säker på att trefoten är helt i våg. Det kommer dock att ses till att trefoten under kommande installationer kommer att monteras på samma sätt och med samma riktning.
- Höjden på trefoten mäts med skjutmått vid 2 av trefotens ben. Från botten av trefoten (grön del) till det tunna isolerande skiktet mellan adaptern och BPA (Bottom of PreAmplifier) är avståndet 70.7mm och 70.0mm (mätning på olika sidor av trefoten).
- Efter installationen på masten fästs den extra antennsladden, längd ca 514mm, med ytterligare en adapter i antennsladden från mottagaren (på samma sätt som förra veckan). Den extra sladdbiten är till för att kunna använda installationen tillsammans med ytterligare en kvadratiska eccosorbskiva under nästa vecka.
- Antennen riktas mot norr enligt tidigare markering på antennfoten (azimutriktning ~nord: 6 grader väst; 354 grader +-2 grader).

Arbetet är färdigt klockan 15:00 (lokal tid; 13:00 UTC).

- Anmärkning angående trefoten: det som har kallats botten av trefoten (grön del) är egentligen inte det nedersta på trefoten utan det finns ytterligare en botten (svart del) med extra material vid trefotens hörn. Det gör att trefoten är upphöjd från underlaget/antennfoten ca 1-2mm. Detta har dock ej någon påverkan på skjutmåttsmätningarna.


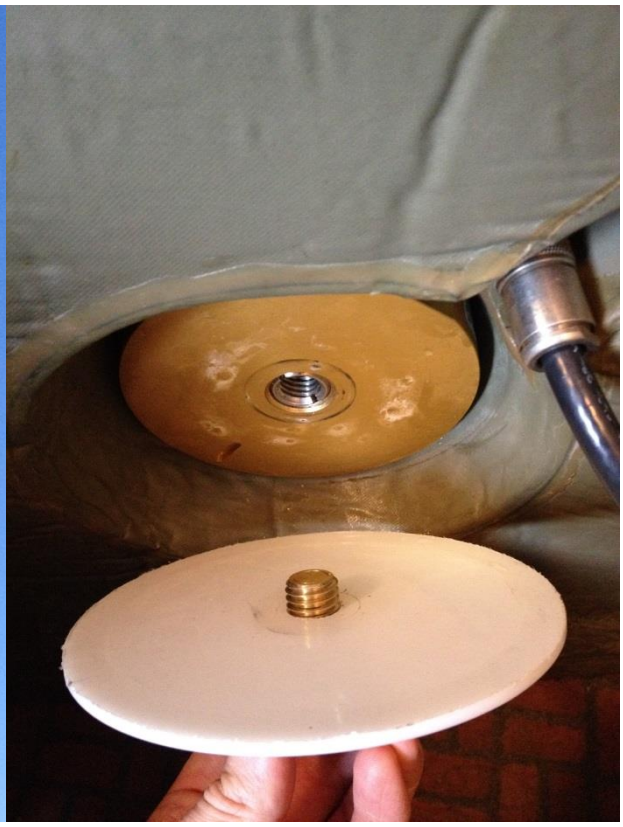

OTT2-masten innan ändringen (vänster), då eccosorbskivan sitter snett och antennen har ändrat azimutriktning, och installation av ett tunt isolerande skikt direkt under antennen (höger) för att hålla fast eccosorbskivan på ett bättre sätt.


Den nya installationen med tjockt isolerande skikt, trefot med adapter, tunt isolerande skikt och antenn med OSOS-radom och eccosorbskiva (vänster) och samma installation uppifrån (höger).

OTT4:

Klockan 15:00 (lokal tid; 13:00 UTC) börjar arbete runt OTT4.

- Den befintliga OSOS-radomen tas bort från antennen (okalibrerad Javadringant-DM 00821, A0090821).
- Samma OSOD-radom som tidigare har suttit fast på antennfoten (rektangulärt tvärsnitt) med 3st armar installeras igen på samma sätt (och åt samma håll) som vid tidigare installation.
- Arbetet utförs utan att riktningen av antennen ändras (azimut 0/360 grader +-2 grader).

Arbetet är färdigt klockan 15:40 (lokal tid; 13:40 UTC).

OTT4-masten innan ändringen då antennen har en OSOS-radom (vänster) och OTT4-masten efter ändringen då antennen har en OSOD-radom som sitter fast i antennfotens 3 armar (höger).

2015-04-22 (dag 112)

Stationsändringar för OTT2 (ytterligare en eccosorbskiva installeras under befintlig eccosorbskiva) och OTT4 (isolerande skikt mellan antennfot och trefot tas bort).

OTT2:

Klockan 14:05 (lokal tid; 12:05 UTC) börjar arbete runt OTT2.

- Antennsladden från mottagaren lossas från den extra antennsladden (längd ca 514mm) och dras på ett nytt sätt innan den fästs i den extra antennsladden igen. Antennsladden har tidigare dragits genom masten för att hindra den från att sticka ut för mycket från antennen, men nu behövs mer längd för att antennsladden skall klara att sticka ut mellan 2st eccosorbskivor. Den totala längden på antennsladden är samma som tidigare vecka.
- Den långa OSO-tillverkad antennbulten (längd 80.5mm) lossas från trefoten (Leica Tribrach PRO w/o optical plummet GDF321, 777508). Trefot ihop med adapter (Leica Adapter tribrach rotating rev D 2070-00), antenn (absolutkalibrerad Javadringant-DM 00951, A0090951) med OSOS-radom, tunt isolerande skikt (plastskiva 3mm) och befintlig kvadratisk eccosorbskiva (nr 10-09, vikt 1582g) lyfts upp. Därefter placeras ytterligare en kvadratisk eccosorbskiva (inget nr, 1495g) upp-och-ned på antennfoten över det tjocka isolerande skiktet (plastskiva 20mm). Trefot med antenn och eccosorbskiva lyfts tillbaka på det tjocka isolerande skiktet och allt skruvas fast med den långa antennbulten. Följande sitter nu på masten (nedifrån och upp): antennfot (cirkulär), tjockt isolerande skikt (20mm) med kvadratisk eccosorbskiva upp-och-ned utanpå (inget nr, 1495g), trefot med adapter, tunt isolerande skikt (3mm) och antenn med kvadratisk eccosorbskiva (nr 10-09, vikt 1582g) och OSOS-radom.
- Trefoten har ej ändrats i höjd och har satts fast så likt föregående veckas installation som möjligt, d.v.s. antennen är inriktad mot norr enligt tidigare markering på antennfoten (azimutriktning ~nord: 6 grader väst; 354 grader +-2 grader).
- Höjden på trefoten skall fortfarande vara enligt tidigare skjutmåttmätning gjord vid 2 av trefotens ben. Från botten av trefoten (grön del) till det tunna isolerande skiktet mellan adaptern och BPA (Bottom of PreAmplifier) är avståndet 70.7mm och 70.0mm (mätning på olika sidor av trefoten).
- Den extra antennsladden (fäst i antennen och nu utstickandes mellan de 2 eccosorbskivorna) kopplas ihop med antennsladden till mottagaren.

Arbetet är färdigt klockan 14:45 (lokal tid; 12:45 UTC).

- Anmärkning angående trefoten: det som har kallats botten av trefoten (grön del) är egentligen inte det nedersta på trefoten utan det finns ytterligare en botten (svart del) med extra material vid trefotens hörn. Det gör att trefoten är upphöjd från underlaget/antennfoten ca 1-2mm. Detta har dock ej någon påverkan på skjutmåttsmätningarna.

Installationen med en eccosorbskiva innan ändringen (vänster) och efter ändringen (höger) då två eccosorbskivor är installerade under antennen och antennsladden sticker ut mellan skivorna.

OTT2-antennen med 2st eccosorbskivor fotad uppifrån (vänster) och samma installation från sidan (höger).

OTT4:

Innan ändringen av OTT4 upptäcks att det finns fågelskit ovanpå OSOD-radomen och på masttoppen (de tre sidorna där antennfoten är fastsatt). Detta har ej synts tidigare på OTT2 eller OTT4. Vid undersökning av OTT1 och OTT6 syns även lite fågelskit ovanpå OSOS-radomen för OTT6, men ej på masttoppen.

Vid kontroll av antennriktningen verkar denna vara annorlunda än vad som tidigare noterats (azimut 0/360 grader +-2 grader). Den nya antennriktningen är mätt med handhållen kompass till azimutriktning ~nord: 10 grader väst (350 grader +-2 grader). Då antennen ej är lös och då den ej har lossats sedan installation misstänker jag att denna azimutriktning har varit densamma sedan installationen av den rektangulära trefoten utfördes 2015-03-25 (olika personer utförde installationen 2015-03-25 och 2015-04-22).

Klockan 14:45 (lokal tid; 12:45 UTC) börjar arbete runt OTT4.

- Trefotens (Leica Tribrach PRO w/o optical plummet GDF321, 777508) läge markeras på trefoten och antennfoten och antennbulten lossas.
- Trefot med adapter (Leica Adapter tribrach rotating rev D 2070-00) och antenn (okalibrerad Javadringant-DM 00821, A0090821) lyfts inuti OSOD-radomen och det isolerande skiktet (plastskiva 3mm) tas bort.
- Trefot med adapter och antenn ställs ned på antennfoten och skruvas fast med antennbulten.
- Antennen riktas mot norr enligt markeringar gjorda innan antennen lossades. Riktningen är då, enligt tidigare notering, azimutriktning ~nord: 10 grader väst (350 grader +-2 grader).

Arbetet är färdigt klockan 15:05 (lokal tid; 13:05 UTC).

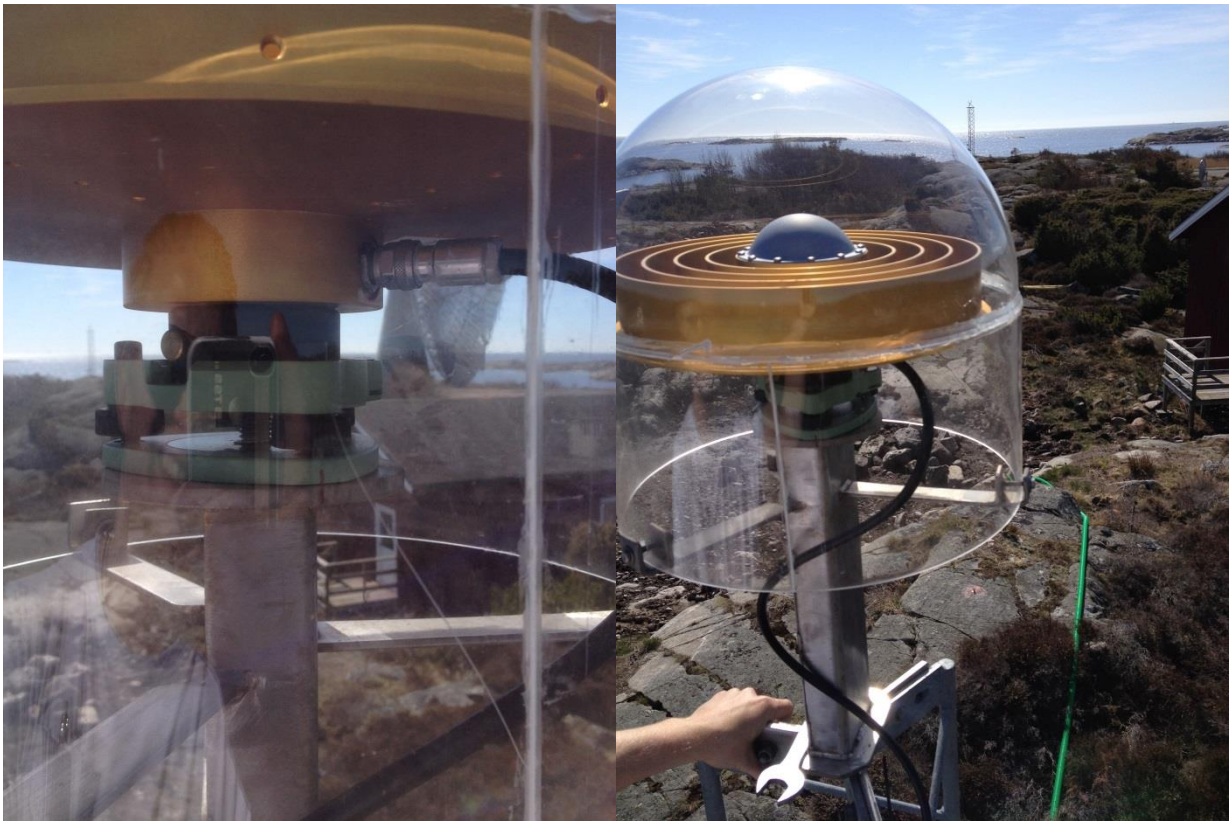

OTT4-antennen med en OSOD-radom efter att det tunna isolerande skiktet mellan trefoten och antennfoten är borttaget (vänster och höger).

ÖVRIGT:

- Mottagare för OTT1, OTT2 och OTT4 har låsts på extern oscillator (5MHz) under eftermiddagen 2015-04-22.
- Mottagaren för OTT6 har låsts på extern oscillator (5MHz) under förmiddagen 2015-04-23.

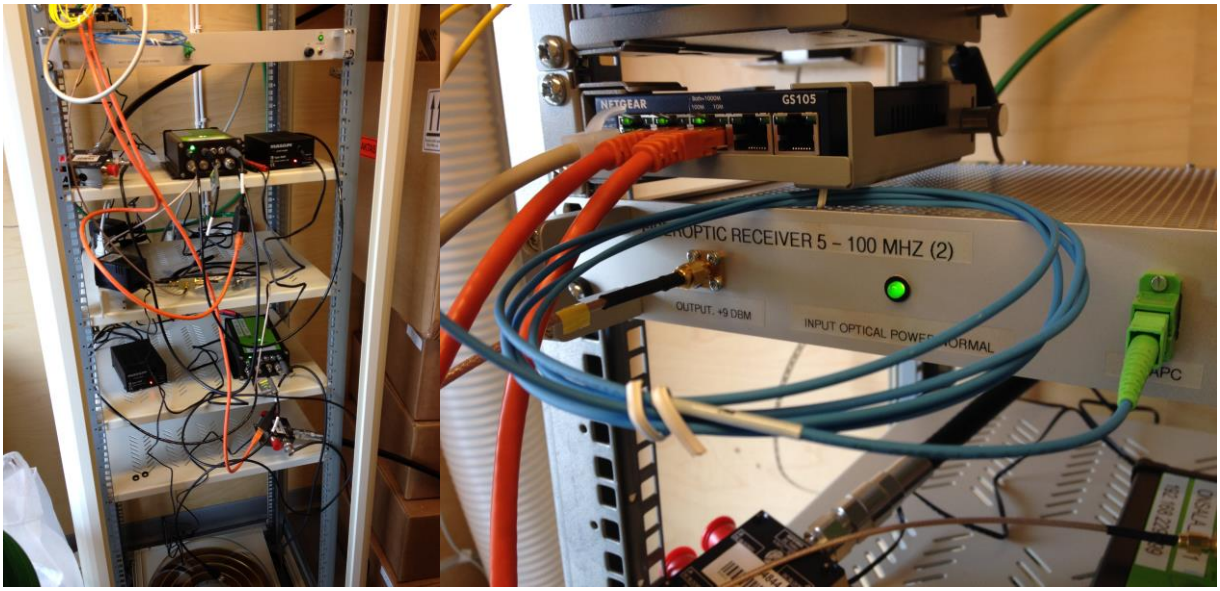

OTT1- och OTT2-mottagarna i racken (vänster) och utgången för 5MHz-signalen (höger).

2015-04-29 (dag 119)

Stationsändringar för OTT2 (båda eccosorbskivorna tas bort) och OTT4 (OSOD-radom roteras 1/3-varv).

OTT2:

Innan ändringen av OTT2 upptäcks att den undre eccosorbskivan har ändrat läge något, antagligen på grund av vind. Azimutriktningen för antennen är dock densamma som vid installation för en vecka sedan.

Klockan 14:20 (lokal tid; 12:20 UTC) börjar arbete runt OTT2.

- Den extra antennsladden (sitter fast i antennen), längd ca 514mm, lossas från adaptern och den långa antennsladden.
- Den långa OSO-tillverkad antennbulten (längd 80.5mm) lossas från trefoten (Leica Tribrach PRO w/o optical plummet GDF321, 777508). Trefoten ihop med adapter (Leica Adapter tribrach rotating rev D 2070-00), antenn (absolutkalibrerad Javadringant-DM 00951, A0090951) med OSOS-radom, tunt isolerande skikt (plastskiva 3mm) och fastsatt kvadratisk eccosorbskiva (nr 10-09, vikt 1582g) lyfts av antennen. Den andra kvadratiska eccosorbskivan (inget nr, vikt 1495g) som sitter på toppen av antennfoten över den tjocka isolerande skiktet (plastskiva 20mm) lyfts också av.
- På marken lossas trefoten från adaptern. Adaptern lossas från antennen och det tunna isolerande skiktet (plastskiva 3mm) tas bort. Därefter lossas eccosorbskivan (nr 10-09, vikt 1582g) från antennen.
- På antennfoten installeras (nedifrån och upp): tjockt isolerande skikt (plastskiva 20mm), trefot med adapter, tunt isolerande skikt (plastskiva 3mm) och antenn med OSOS-radom. Detta är samma installation som de två tidigare veckorna förutom att eccosorbskivorna är borttagna.
- Trefoten sätts fast med den långa OSO-tillverkade antennbulten. Trefoten ändras ej i höjd och sätts fast så likt föregående veckas installation som möjligt med hjälp av tidigare markeringar på antennfoten och trefoten. Det noteras även att trefoten är näst intill i våg. Höjden på trefoten skall fortfarande vara enligt tidigare skjutmått-mätning vid 2 av trefotens ben. Från botten av trefoten (grön del) till det tunna isolerande skiktet mellan adaptern och BPA (Bottom of PreAmplifier) är avståndet 70.7mm och 70.0mm (mätning på olika sidor av trefoten).
- Den extra antennsladden (fastsatt i antennen) kopplas ihop med antennsladden till mottagaren.
- Antennen riktas mot norr enligt tidigare markering på antennfoten (azimutriktning ~nord: 6 grader väst; 354 grader +-2 grader).

Arbetet är färdigt klockan 14:35 (lokal tid; 12:35 UTC).

- Anmärkning angående trefoten: det som har kallats botten av trefoten (grön del) är egentligen inte det nedersta på trefoten utan det finns ytterligare en botten (svart del) med extra material vid trefotens hörn. Det gör att trefoten är upphöjd från underlaget/antennfoten ca 1-2mm. Detta har dock ej någon påverkan på skjutmåttsmätningarna.

OTT2-masten med dubbla eccosorbskivor innan ändringen (vänster) och toppen av mastfoten för OTT2-masten efter ändringen (höger) då eccosorbskivorna har tagits bort och endast isolerande skikt och trefot är kvar.

OTT4:

Klockan 14:30 (lokal tid; 12:30 UTC) börjar arbete runt OTT4.

- De tre bultarna som håller fast OSOD-radomen lossas.
- OSOD-radomen roteras ett tredjedels varv i klockans riktning och bultarna sätts därefter fast igen för att fixera radomen.
- Inga övriga ändringar görs och antennriktningen är därför oförändrad, azimutriktning ~nord: 10 grader väst (350 grader +-2 grader).

Arbetet är färdigt klockan 14:50 (lokal tid; 12:50 UTC).

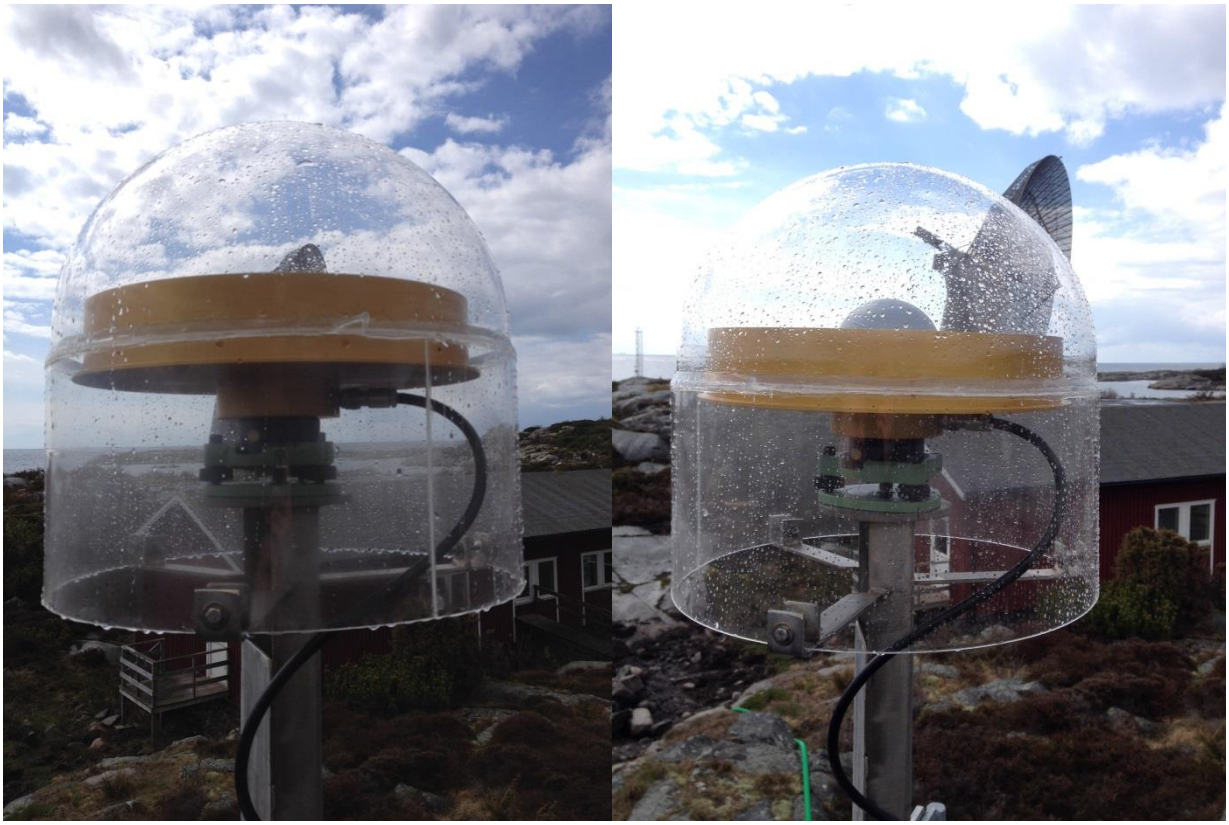

OTT4-masten innan ändringen (vänster) och OTT4-masten efter att OSOD-radomen har lossats, vridits ett tredjedels varv i klockans riktning och därefter sats fast (höger).

ÖVRIGT:

Två dubbelkalibrerade antenner (absolutkalibrerade i kammare och med robot) levererades till observatoriet:

- Javadringant-DM 00946, A0090946 med installerad OSOS-radom.
- LeiAR25.R3 (S. No.: 10170020, P/N: 01018079) med installerad Leica-radom (LEIT).

Tyvärr finns det en spricka i radomen till LeiAR25. Sprickan verkar komma ifrån ovarsamhet i transporten (antennen låg lite snett när jag öppnade förpackningen). Det är även så att endast 1 av skruvarna för att sätta fast/ta av radomen har huvudet kvar (de andra är söndriga), vilket gör att LEIT-radomen sitter lite löst. Detta har antagligen hänt när radomen installerades på antennen vid kalibreringstillfället.

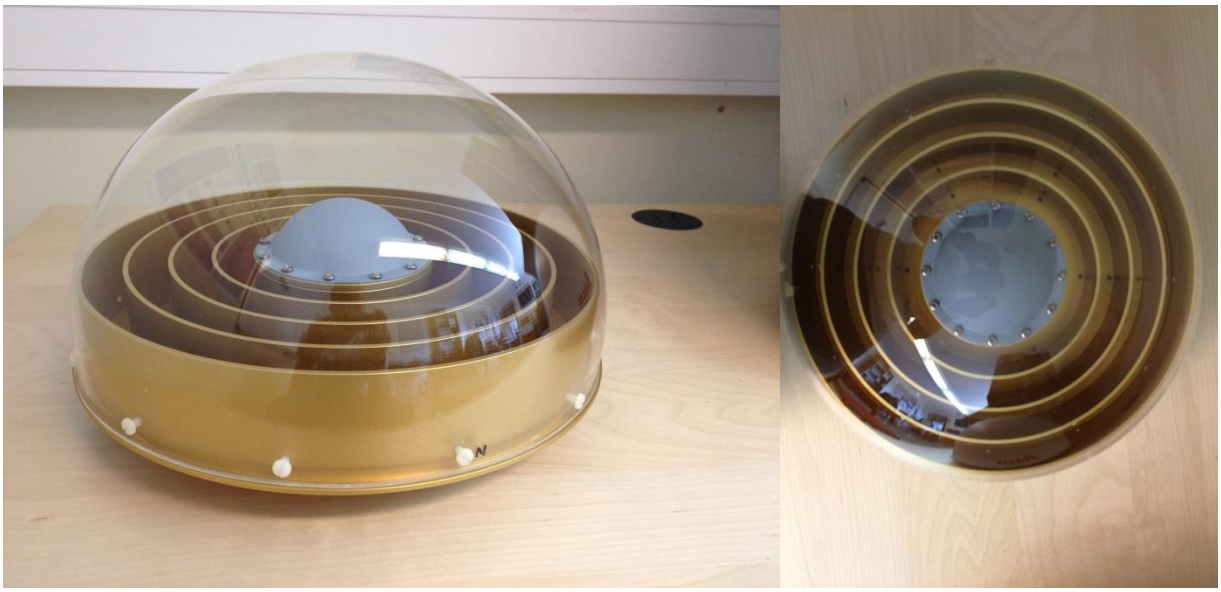

Den levererade dubbelkalibrerade antennen (absolutkalibrerad i kammare och med robot) Javadringant-DM med OSOS-radom från sidan (vänster) och uppifrån (höger).

Den levererade dubbelkalibrerade antennen (absolutkalibrerad i kammare och med robot) LeiAR25.R3 med LEIT-radom (vänster och höger). Tyvärr har det blivit en spricka i radomen (antagligen under transporten) och de flesta plastskruvarna för att hålla fast radomen är sönder (antagligen vid installation av radomen).

2015-05-06 (dag 126)

Stationsändringar för OTT2 (borttagning av befintlig antenn och installation av dubbelkalibrerad Javadringant-DM-antenn) och OTT4 (OSOD-radom roteras 1/3-varv).

OTT2:

Klockan 14:45 (lokal tid; 12:45 UTC) börjar arbete runt OTT2.

- Den extra antennsladden och adaptern (som kopplar ihop den extra biten med den vanliga antennsladden) lossas och tas av installationen.
- Den befintliga antennen (absolutkalibrerad Javadringant-DM 00951, A0090951) med OSOS-radom, tunt isolerande skikt och trefotsadapter lossas och tas av antennen.
- Den långa OSO-tillverkade antennbulten tillsammans med trefot och det tjocka isolerande skiktet lossas och tas av installationen.
- En ny dubbelkalibrerad antenn (absolutkalibrerad i kammare och med robot; Javadringant-DM 00946, A0090946) med OSOS-radom (installerad vid absolutkalibreringen) installeras på antennfoten med ett tunt isolerande skikt (plastskiva 3mm) mellan antenn och antennfot. Antennen installeras med en vanlig OSO-tillverkad antennbult.
- Antennsladden kopplas in i antennen.
- Antennen riktas mot norr (azimutriktning nord: 0/360 grader +-2 grader).

Arbetet är färdigt klockan 15:15 (lokal tid; 13:15 UTC).

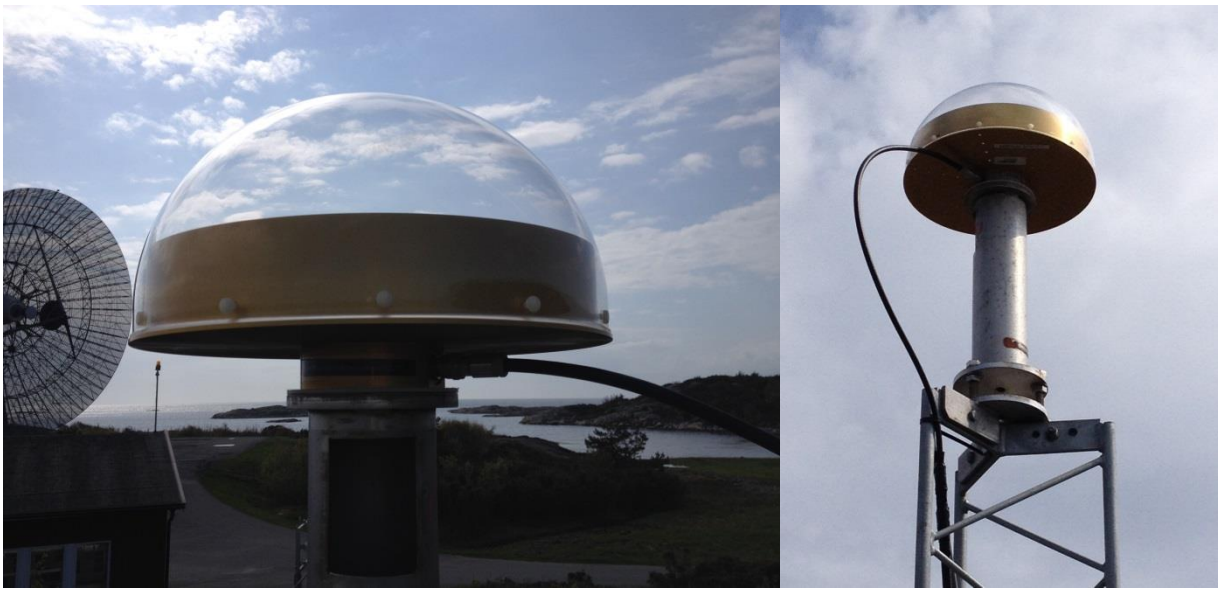

Installationen av den dubbelkalibrerade antennen (absolutkalibrerad i kammare och på robot) med OSOS-radom på OTT2-masten (vänster och höger).

OTT4:

Klockan 15:15 (lokal tid; 13:15 UTC) börjar arbete runt OTT4.

- De tre bultarna som håller fast OSOD-radomen lossas.
- OSOD-radomen roteras ett tredjedels varv i klockans riktning och bultarna sätts därefter fast igen för att fixera radomen.
- Inga övriga ändringar görs och antennriktningen är därför oförändrad, azimutriktning ~nord: 10 grader väst (350 grader +-2 grader).

Arbetet är färdigt klockan 15:30 (lokal tid; 13:30 UTC).

OTT4-masten innan ändringen (vänster) och OTT4-masten efter att OSOD-radomen har lossats, vridits ett tredjedels varv i klockans riktning och därefter sats fast (höger).

2015-05-13 (dag 133)

Stationsändringar för OTT2 (borttagning av OSOS-radom för den dubbelkalibrerade antennen) och OTT4 (OSOD-radom roteras 1/3-varv till utgångspositionen).

OTT2:

Klockan 13:50 (lokal tid; 11:50 UTC) börjar arbete runt OTT2.

- Befintlig OSOS-radom skruvas loss och lyfts av antennen (Javadringant-DM 00946, A0090946, dubbelkalibrerad: absolutkalibrerad i kammare och med robot).
- Borttagningen av radomen görs utan att antennen kopplas bort och utan att orienteringen av antennen ändras, vilket betyder att azimutriktningen är nord: 0/360 grader +-2 grader.

Arbetet är färdigt klockan 14:15 (lokal tid; 12:15 UTC).

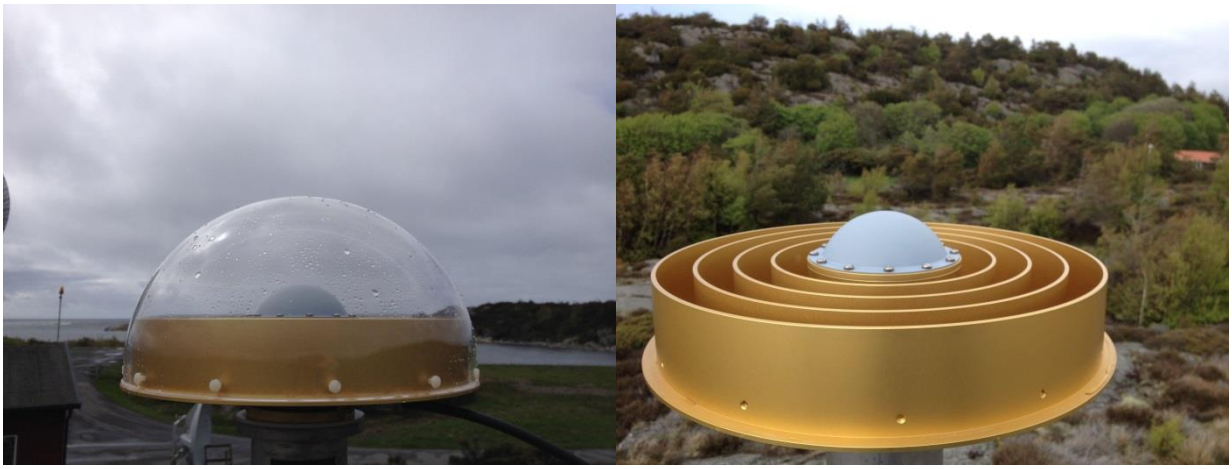

Den dubbelkalibrerade (absolutkalibrerad i kammare och med robot) Javadringant-DM-antennen med OSOD-radom innan ändring (vänster) och utan radom efter ändring (höger).

OTT4:

Klockan 14:15 (lokal tid; 12:15 UTC) börjar arbete runt OTT4.

- De tre bultarna som håller fast OSOD-radomen lossas.
- OSOD-radomen roteras ett tredjedels varv i klockans riktning till utgångspositionen, d.v.s. den position som radomen hade 2015-04-22 (efter ändring; radomen rördes ej detta datum, men antennbulten lossades) alternativt 2015-04-29 (innan ändring). Bultarna sätts därefter fast igen för att fixera radomen.
- Inga övriga ändringar görs och orienteringen av antennen ändras ej, vilket gör att antennriktningen är oförändrad med azimutriktning ~nord: 10 grader väst (350 grader +-2 grader).

Arbetet är färdigt klockan 15:30 (lokal tid; 13:30 UTC).

OTT4-masten innan ändringen (vänster) och OTT4-masten efter att OSOD-radomen har lossats, vridits ett tredjedels varv i klockans riktning till ursprungspositionen och därefter sats fast (höger).

ÖVRIGT

Det har varit visst arbete i närheten av OTT4 (söder om, mellan OTT4 och OTT6) med att anlägga en väg för tvillingteleskopen. Arbetet har utförts under dagtid på tisdag (2015-05-19) och onsdag (2015-05-20). Antagligen kommer påverkan på signalerna och omgivningen att vara liten, men det kan vara bra att notera.

Vi har även satt upp 3st stationskalibreringsstationer runt OTT1 under måndag (2015-05-18) och tisdag (2015-05-19). De 3 stationerna är antingen utrustade med 1, 2 eller ingen eccosorbskiva under antennen.

Arbetet med vägen söder om OTT4, mellan OTT4 och OTT6, som påbörjades under tisdag (vänster) och stationskalibreringsstationer med olika mycket eccosorb runt OTT1 (höger).

2015-05-20 (dag 140)

Stationsändringar för OTT2 (återinstallation av OSOS-radom för den dubbelkalibrerade antennen) och OTT4 (antennfot byts ut och dubbelkalibrerad LEIAR25.R3 installeras med LEIT-radom).

OTT2:

Klockan 14:45 (lokal tid; 12:45 UTC) börjar arbete runt OTT2.

- OSOS-radom (samma som tidigare har suttit på antennen) monteras på antennen (Javadringant-DM 00946, A0090946, dubbelkalibrerad: absolutkalibrerad i kammare och med robot) enligt anvisning från Lantmäteriet.
- Orienteringen av antennen ändras ej under installationen av radomen, vilket betyder att azimutriktningen är nord: 0/360 grader +-2 grader.

Arbetet är färdigt klockan 15:15 (lokal tid; 13:15 UTC).

- Notera att antennen (Javadringant-DM) är absolutkalibrerad (2 gånger: dubbelkalibrerad) med och utan radom. Vid kalibreringen med OSOS-radom är det oklart om Lantmäteriets monteringsanvisningar följdes.

Den dubbelkalibrerade Javadringant-DM utan radom innan ändringen (vänster) och samma antenn med en OSOS-radom efter ändringen (höger).

OTT4:

Klockan 15:15 (lokal tid; 13:15 UTC) börjar arbete runt OTT4.

- De tre bultarna som håller fast OSOD-radomen lossas och OSOD-radomen lyfts av.
- Antennsladden lossas från antennen och antennskruven lossas. Antennen (okalibrerad Javadringant-DM 00821, A0090821) tillsammans med trefot (Leica Tribrach PRO w/o optical plummet GDF321, 777508) och adapter (Leica Adapter tribrach rotating rev D 2070-00) tas ned.
- De 3st stora bultarna som håller fast antennfoten i masten lossas och den befintliga antennfoten (rektangulärt tvärsnitt med 3st armar för en OSOD-radom) och tas ned från masten.
- En ny antennfot med cirkulärt tvärsnitt (detta är samma antennfot som togs av installationen 2015-03-25) installeras på masten med de 3st stora bultarna. Antennfoten installeras åt samma håll som den tidigare har suttit och det kontrolleras att toppen på antennfoten är i våg. Antennfoten är i våg utan att några ändringar görs. Den borde därför sitta på precis samma plats som den gjorde innan den togs av installationen 2015-03-25 (antennfoten installerades under slutet av 2014).
- En ny dubbelkalibrerad antenn LEIAR25.R3 (absolutkalibrerad i kammare och med robot; LEIAR25.R3, S. No.: 10170020, P/N: 01018079) installeras med LEIT-radom (Art. No.: 765734) och ett tunt isolerande skikt (plastskiva 3mm) mellan antenn och antennfot. Antennen installeras med en OSO-tillverkad antennbult. Notera att radomen har en spricka på norra sidan (från transporten) och att nya OSO-tillverkade plastskruvar (de gamla drogs antagligen sönder under kalibreringen) används.
- Antennsladden kopplas in och antennen riktas mot norr med hjälp av en handhållen kompass. Azimutriktningen är nord: 0/360 grader +-2 grader.

Arbetet är färdigt klockan 16:05 (lokal tid; 14:05 UTC).

Den befintliga antennen med OSOD-radom tas ned (vänster). Därefter byts den rektangulära antennfoten, ses i bakgrunden, ut mot den tidigare använda cirkulära antennfoten, ses i förgrunden, (höger).

Den circulära antennfoten installeras åt samma håll som tidigare med toppen i våg (vänster). På antennfoten installeras därefter antennen LEIAR25.R3 (höger).

Den dubbelkalibrerade LEIAR25.R3 installeras med en LEIT-radom på OTT4-masten (höger och vänster).

ÖVRIGT:

Det har varit visst arbete i närheten av OTT4 (söder om, mellan OTT4 och OTT6) med att anlägga en väg för tvillingteleskopen. Arbetet har utförts under dagtid och startade på tisdag (2015-05-19). Arbetet har fortsatt under onsdag (2015-05-20), torsdag (2015-05-21) och fredag (2015-05-22). Antagligen kommer påverkan på signalerna och omgivningen att vara liten, men det kan vara bra att notera.

Vi satte även upp 3st stationskalibreringsstationer runt OTT1 under måndag (2015-05-18) och tisdag (2015-05-19). De 3 stationerna är antingen utrustade med 1, 2 eller ingen eccosorbskiva under antennen. Antennerna togs ned under fredag (2015-05-22), men stativen står tillsvidare kvar. Vädret har varit ostadigt och trefoten över ON01 hade flyttats några mm antagligen pga hård vind.

Arbetet med vägen mellan OTT4 och OTT6, har pågått under tisdag till fredag (vänster) och stations-kalibreringsstationer med olika mycket eccosorb som installerades runt OTT1 i början av veckan (höger).

2015-05-27 (dag 147)

Stationsändringar för OTT2 (det isolerande skiktet mellan antennfot och antenn tas bort) och OTT4 (LEIT-radomen tas av från den dubbelkalibrerade LEIAR25.R3-antennen).

OTT2:

Klockan 14:30 (lokal tid; 12:30 UTC) börjar arbete runt OTT2.

- Antennens azimutriktning markeras på antennfoten och antennskruven lossas.
- Befintlig antenn (Javadringant-DM 00946, A0090946, dubbelkalibrerad: absolutkalibrerad i kammare och med robot) med OSOS-radom lyfts något och det tunna isolerande skiktet (plastskiva 3mm) tas bort.
- Antennen med radom ställs därefter tillbaka på antennfoten och den OSO-tillverkade antennskruven sätts återigen fast.
- Azimutriktningen på antennen ställs in med tidigare nämnd markering på antennfoten till azimutriktning nord: 0/360 grader +-2 grader.

Arbetet är färdigt klockan 14:50 (lokal tid; 12:50 UTC).

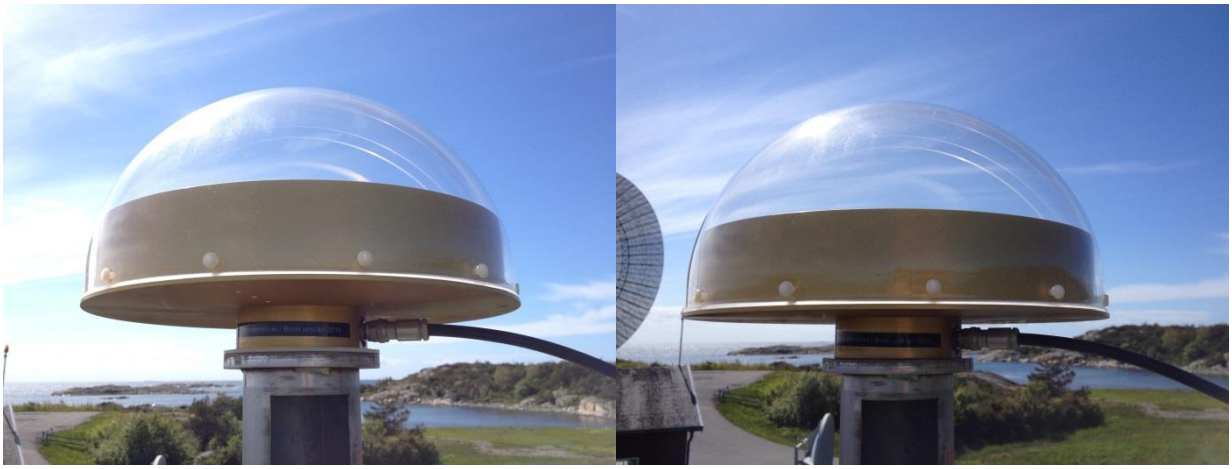

Den dubbelkalibrerade Javadringant-DM med OSOS-radom på OTT2-masten med ett isolerande skikt mellan antenn och antennfot innan ändringen (vänster) och utan isolerande skikt efter ändringen (höger).

OTT4:

Klockan 14:50 (lokal tid; 12:50 UTC) börjar arbete runt OTT4.

- De 6st plastskruvarna som håller fast LEIT-radomen (Art. No.: 765734) på antennen lossas och radomen tas av den dubbelkalibrerade antennen LEIAR25.R3 (absolutkalibrerad i kammare och med robot; LEIAR25.R3, S. No.: 10170020, P/N: 01018079).
- Borttagningen av radomen görs utan att antennen kopplas bort och utan att orienteringen av antennen ändras, vilket betyder att azimutriktningen är nord: 0/360 grader +-2 grader.

Arbetet är färdigt klockan 15:05 (lokal tid; 13:05 UTC).

Antennen LEIAR25.R3 installerad på OTT4-masten med LEIT-radom innan ändringen (vänster) och samma antenn utan radom efter ändringen (höger).

LEIAR25.R3-antennen utan radom visad uppifrån (vänster) och hela OTT4-masten mot söder (höger).

ÖVRIGT:

Arbetet med vägen för tvillingteleskopen, mellan OTT4 och OTT6, är för tillfället avslutat. Det sista arbetet gjordes 2015-05-22, men några maskiner finns fortfarande kvar på platsen.

OTT4-masten fotat mot söder med OTT6-masten till vänster i bakgrunden (vänster) och den nya vägen fotad mot norr med OTT4-masten i bakgrunden (höger).

2015-06-03 (dag 154)

Stationsändringar för OTT2 (OSOS-radomen tas av den dubbelkalibrerade Javadringant-DM-antennen) och OTT4 (LEIT-radomen återinstalleras på den dubbelkalibrerade LEIAR25.R3-antennen).

OTT2:

Klockan 15:05 (lokal tid; 13:05 UTC) börjar arbete runt OTT2.

- Plastskruvarna som håller fast OSOS-radomen på antennen (Javadringant-DM 00946, A0090946, dubbelkalibrerad: absolutkalibrerad i kammare och med robot) lossas och OSOS-radomen tas av antennen. Notera att antennen fortfarande står direkt på antennfoten (ej isolerande skikt).
- Borttagningen av radomen görs utan att antennen kopplas bort och utan att orienteringen av antennen ändras, vilket betyder att azimutriktningen är nord: 0/360 grader +-2 grader.

Arbetet är färdigt klockan 15:20 (lokal tid; 13:20 UTC).

Antennen (Javadringant-DM) på OTT2-masten med OSOS-radom innan ändring (vänster och höger).

Antennen (Javadringant-DM) på OTT2-masten utan radom efter ändring (vänster och höger).

OTT4:

Klockan 15:15 (lokal tid; 13:15 UTC) börjar arbete runt OTT4.

- LEIT-radomen (Art. No.: 765734) lyfts på antennen (LEIAR25.R3, S. No.: 10170020, P/N: 01018079, dubbelkalibrerad: absolutkalibrerad i kammare och med robot) och de 6st plastskruvarna fäster radomen i antennen. Notera att det finns ett tunt isolerande skikt (plastskiva 3mm) mellan antennen och antennfoten.
- Återinstallationen av radomen görs utan att antennen kopplas bort och utan att orienteringen av antennen ändras, vilket betyder att azimutriktningen är nord: 0/360 grader +-2 grader.

Arbetet är färdigt klockan 15:30 (lokal tid; 13:30 UTC).

Antennen (LEIAR25) på OTT4-masten utan radom innan ändring (vänster och höger).

Antennen (LEIAR25) med LEIT-radom efter ändring (vänster och höger).

ÖVRIGT:

Arbetet med vägen för tvillingteleskopen i närheten av OTT4 och OTT6 har fortsatt under veckan. Det mesta av arbetet görs längre västerut än tidigare och borde därför störa signalerna något mindre än tidigare.

Bild på OTT4-antennen mot söder med vägarbetet och OTT6-masten i bakgrunden.

2015-06-10 (dag 161)

Stationsändringar för OTT2 (OSOS-radomen installeras på den dubbelkalibrerade Javadringant-DM-antennen) och OTT4 (inga ändringar görs på masten, men 3st ytterligare mottagare kopplas in).

OTT2:

Klockan 13:50 (lokal tid; 11:50 UTC) börjar arbete runt OTT2.

- OSOS-radom (samma som tidigare har suttit på) monteras på antennen (Javadringant-DM 00946, A0090946, dubbelkalibrerad: absolutkalibrerad i kammare och med robot) enligt anvisning från Lantmäteriet. Notera att isolerande skikt mellan antenn och antennfot ej är installerat.
- Orienteringen av antennen ändras ej under installationen av radomen, vilket betyder att azimutriktningen är nord: 0/360 grader +-2 grader.

Arbetet är färdigt klockan 14:15 (lokal tid; 12:15 UTC).

OTT2-antennen (Javadringant-DM) utan radom innan ändring (vänster) och samma antenn med OSOS-radom efter ändring (höger).

OTT4:

Inga ändringar görs under dagen på masten OTT4. Det betyder att på OTT4-masten finns ett tunt isolerande skikt (plastskiva 3mm), en antenn (LEIAR25.R3, S. No.: 10170020, P/N: 01018079, dubbelkalibrerad: absolutkalibrerad i kammare och med robot) och en radom (LEIT-radom, Art. No.: 765734).

Under förmiddagen kopplas 3st ytterligare mottagare in på masten genom den befintliga splittern (GPS Networking Inc., 84843). Mottagarna är följande:

- Leica GNSS 1200+ (s/n: 495522, art.nr.: 766733)
- Javad Delta (s/n: 00369, p/n: 01-580300-01)
- Trimble NetR9 (s/n: 5114K74696, 67668-10)

Inkopplingen av varje mottagare i splittern görs med en 1.5m-lång antennkabel (Rosenberger 550870, CNT-400-500M, flexible cable 50 Ohm). Leica- och Trimble-mottagaren kopplas därefter till en dator (laptop) med nätverkskabel genom en router och Javad Delta-mottagaren kopplas till datorn med en USB-kabel. Den befintliga Javad Sigma-mottagaren (JAVAD TRE_G3T SIGMA, 01595) är fortfarande kopplad med nätverkskabel till Lantmäteriets nät.

Observationsdata loggas varje sekund (1Hz sampling) av alla 3 mottagare och skicka/sparas lokalt på datorn. För Leica- och Trimble-mottagaren sparas data genom FTP-push och en FTP-server på datorn (FileZilla). För Javad Delta-mottagaren sparas data genom programmet NetView och optionen Real-Time Logging.

– Loggningen av data startade för Leica GNSS 1200+ klockan 10:40 (lokal tid; 08:40 UTC), för Javad Delta klockan 10:45 (lokal tid; 08:45 UTC) och för Trimble NetR9 klockan 10:50 (lokal tid; 08:50 UTC).

Klockan 14:25 (lokal tid; 12:25 UTC) kopplas den korta antennkabeln mellan splittern och den befintliga mottagaren Javad Sigma ur. Därefter kopplas istället en 1.5m-lång antennkabel (Rosenberger 550870, CNT-400-500M, flexible cable 50 Ohm; samma som för de övriga 3 mottagarna) in mellan splittern och mottagaren. Inkopplingen är färdig klockan 14:30 (lokal tid; 12:30 UTC).

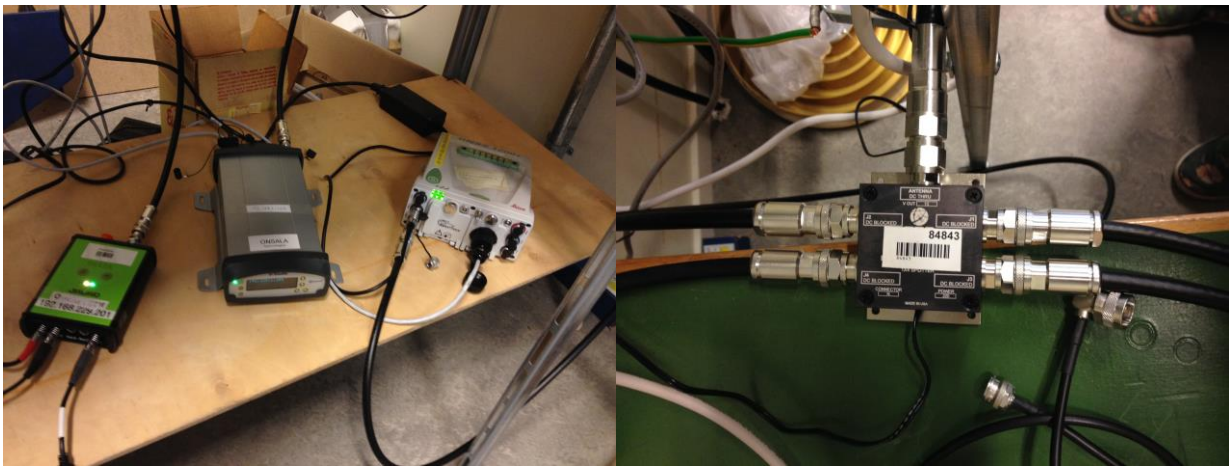

De tre nya mottagarna (Javad Delta, Trimble NetR9 och Leica GNSS 1200+) som kopplas in parallellt med den befintliga Javad Sigma (vänster) och splittern som delar upp antennsignalen (höger).

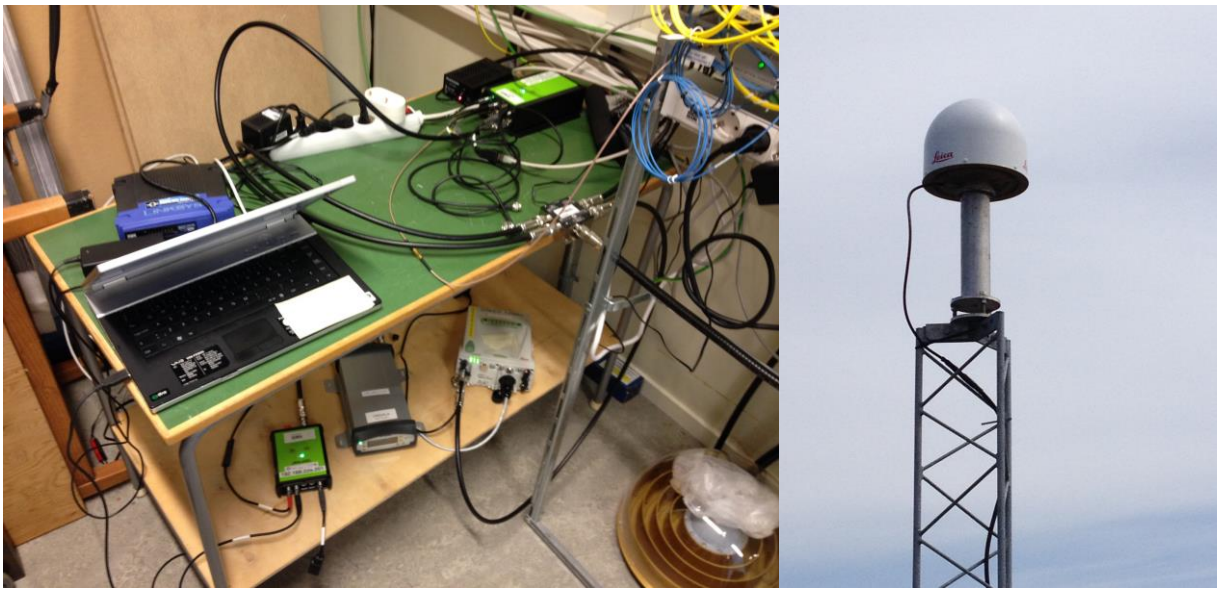

Hela uppställningen med 4 mottagare, en splitter och laptop (vänster) och OTT4-masten med antennen LEIAR25.R3 med LEIT-radom (höger).

ÖVRIGT:

Gunnar Elgered med sällskap observerade en mås på antennen/OSOS-radomen på OTT6 den 5 juni (doy 156) vid 11-tiden (lokal tid; 09-tiden UTC). Måsen i fråga verkade stå där under flera minuter.

Arbetet i närheten av OTT4 har slutat för tillfället. Det står ej några maskiner där nu (2015-06-10).

Mås observerad på OTT6 vid 11-tiden (lokal tid; 9-tiden UTC) den 5:e juni.

OTT4-masten och den nya vägen mellan OTT4 och OTT6 (vänster) och den nya vägen och OTT4-masten fotograferad från platsen för OTT5 (höger).

2015-06-17 (dag 168)

Stationsändringar för OTT2 (ett tunt isolerande skikt installeras under den dubbelkalibrerade Javadringant-DM-antennen) och OTT4 (det tunna isolerande skiktet mellan antennfoten och den dubbelkalibrerade LEIAR25.R3 tas bort).

OTT2:

Klockan 13:55 (lokal tid; 11:55 UTC) börjar arbete runt OTT2.

- Den OSO-tillverkade antennbulten lossas och antennen (Javadringant-DM 00946, A0090946, dubbelkalibrerad: absolutkalibrerad i kammare och med robot) lyfts något, så att ett tunt isolerande skikt (plastskiva 3mm) kan stickas in mellan antenn och antennfot.
- Antennbulten skruvas åter fast och antennen riktas mot norr enligt en tidigare gjord märkning på antennfoten.
- Orienteringen kontrolleras med handhållen kompass och skall vara densamma som tidigare, vilket betyder att azimutriktningen är nord: 0/360 grader +-2 grader.

Arbetet är färdigt klockan 14:15 (lokal tid; 12:15 UTC).

- Notera att ändringen med att återigen installera det isolerande skiktet görs för att förbereda inför nästa ändring då antennbulten skall bytas ut mot en plastbult för att ta bort metall-kontakten mellan antenn och mast.

Toppen av OTT2-masten utan isolerande skikt mellan antenn och antennfot innan ändringen (vänster) och med isolerande skikt (höger).

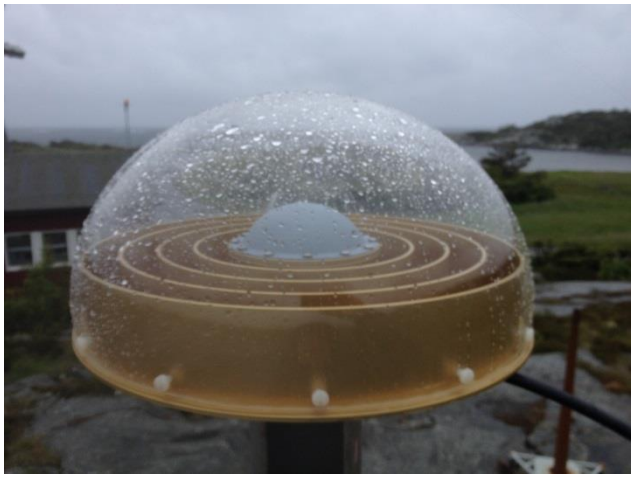

OTT2-antennen (dubbelkalibrerad Javadringant-DM) med OSOS-radom.

OTT4:

Klockan 14:10 (lokal tid; 12:10 UTC) börjar arbete runt OTT4.

- Antennens azimutriktning markeras på antennfoten och den OSO-tillverkade antennbulten lossas.
- Antennen (LEIAR25.R3, S. No.: 10170020, P/N: 01018079, dubbelkalibrerad: absolutkalibrerad i kammare och med robot) med radom (LEIT-radom, Art. No.: 765734) lyfts något och det tunna isolerande skiktet (plastskiva 3mm) mellan antenn och antennfot tas bort.
- Antennbulten skruvas åter fast och antennen riktas mot norr enligt tidigare gjord markering.
- Orienteringen kontrolleras med handhållen kompass och skall vara densamma som tidigare, vilket betyder att azimutriktningen är nord: 0/360 grader +-2 grader.

Arbetet är färdigt klockan 14:25 (lokal tid; 12:25 UTC).

- Notera att de 3 mottagarna Leica GNSS 1200+ (s/n: 495522, art.nr.: 766733), Javad Delta (s/n: 00369, p/n: 01-580300-01) och Trimble NetR9 (s/n: 5114K74696, 67668-10) som kopplades in parallellt med Javad Sigma-mottagaren (JAVAD TRE_G3T SIGMA, 01595) genom en splitter fortfarande är inkopplade och sparar data lokalt på en laptop (det är möjligt att Trimble-mottagaren endast sparar data externt). Datan från veckan från de 3 mottagarna spara för tillfället i lokalt arkiv.

Toppen av OTT4-masten med isolerande skikt mellan antenn och antennfot innan ändringen (vänster) och utan isolerande skikt (höger).

OTT4-antennen (dubbelkalibrerad LEIAR25) med LEIT-radom.

ÖVRIGT:

En mås observerades på OTT6 torsdagen den 11 juni vid 12-tiden. Måsen flög iväg under minuten 12:02 (lokal tid; 10:02 UTC).

Några flak med sten dumpas vid vägbygget mellan OTT4 och OTT6 under 2015-06-17.

Mås på OTT6 den 11 juni vid 12-tiden.

This page intentionally left blank.

Appendix C: Article “Station Calibration of the SWEPOS™ Network”

Station Calibration of the SWEPOS™ Network, Revised 2013-09-25

Jarlemark P, Lidberg M, Kempe C, Jivall L, Johansson J M, Ning T.
Proceedings of the EUREF symposia in Saint-Mandé, France, 6-8 June 2012.
http://www.euref.eu/symposia/2012Paris/P-02-p-Kempe.pdf (Sited 2017-03-20)

This page intentionally left blank.

STATION CALIBRATION OF THE SWEPOS™ NETWORK

Per Jarlemark[1], Martin Lidberg[2], Christina Kempe[2], Lotti Jivall[2], Jan M Johansson[1,3], and Tong Ning[3]

[1] SP Technical Research Institute of Sweden, Borås, Sweden
[2] Lantmäteriet, Gävle, Sweden
[3] Chalmers University of Technology, Gothenburg, Sweden

Revised 2013-09-25

Abstract – Twelve GNSS stations in the SWEPOS network have been surveyed in order to quantify the effect of the antenna near-field on the GNSS height determinations. Height components ~ 10 mm too low were found. An updated antenna-monument model can, to a large extent, correct the height errors.

1. INTRODUCTION

Site-dependent effects are important and limiting factors in high-accuracy GNSS positioning. Electrical coupling between the antenna and its near-field environment could change the characteristics of the antenna from what has been determined for the isolated antenna [1]. The average position of apparent signal reception, the phase center offset (PCO) and the directional dependent phase center variations (PCV) [2] derived for the antenna in e.g. absolute calibration may not be valid when it is mounted for permanent use.

Lantmäteriet has started in-situ station calibration of its permanent reference stations, SWEPOS™, with focus on the 21 concrete pillar stations that serve as the backbone for SWEREF99 (the national reference frame). The pillar design is presented in Figure 1.

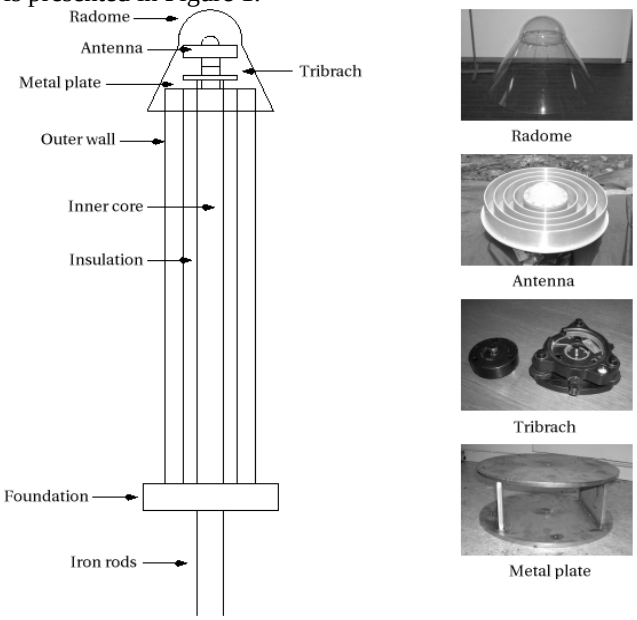

Figure 1. Structure of a concrete pillar foundation in SWEPOS, designed in 1992. The pillar height is ~ 3 m, and is anchored onto crystalline rock. Note the relatively large metal plate used as foundation for the tribrach.

One purpose of the calibration is to examine the site-dependent effects on the height determination in SWEREF 99 when the presently available antenna PCO/PCV models are used. Another purpose is to establish corrected PCO/PCV descriptions for antennas mounted at SWEPOS stations as alternatives or complement to those resulting from absolute calibrations of the isolated antenna.

The station calibration campaigns started in 2009 and continued in 2010, so far at twelve stations. Here we present results of the site-dependent effects on height determinations as well as an estimation of PCO/PCV corrections.

2. SURVEYING

We used three well calibrated antennas on tripods as references. Microwave absorbing material (Eccosorb®) was installed in order to reduce multipath from the ground (see Figure 2). The reference antennas were placed on markers in a local network surrounding the concrete pillar where the SWEPOS antenna is installed. The configuration is illustrated in Figure 3. The distances between reference antennas and the pillar are of the order of 10 m. The height differences were determined to sub-mm using terrestrial methods. Each campaign lasted five full 24 h sessions.

Figure 2. One of the benchmark setups at Hässleholm, 2010. An Eccosorb plate is mounted directly below the choke-ring antenna.

Figure 3. SWEPOS antenna at Vänersborg together with two reference antennas.

3. HEIGHT DETERMINATION

The data from the campaigns were processed with daily solutions for each single antenna, and the resulting height differences between the SWEPOS antennas and their associated reference antennas were compared to the height differences derived in the terrestrial survey. The L3 (ionosphere-free) linear combination of the observables was used, and troposphere parameters were estimated together with coordinates and receiver clock errors.

Different processing strategies have been applied, e.g. regarding elevation cut off angle, and the use of relative and absolute antenna models [3][4]. In Figure 4 results from 10° for both relative and absolute antenna models are presented. Typically height differences of ~ 10 mm were found. The

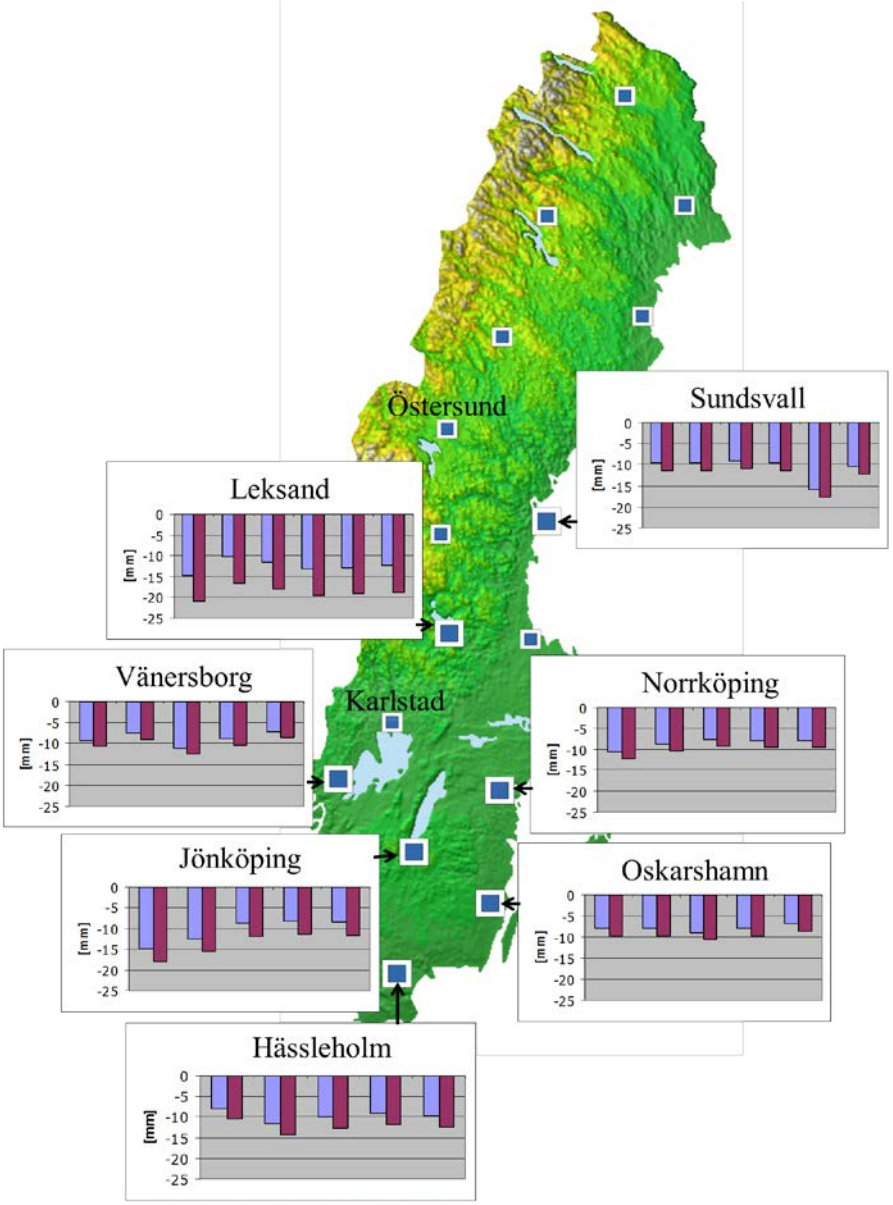

Figure 4. Diagrams showing daily repeatability of the estimated height bias for seven SWEPOS stations. Blue color denotes processing with relative antenna models and red denotes processing with absolute antenna models.

GNSS determined heights of the SWEPOS antennas were significantly lower than expected from the terrestrial survey. There was, however, a significant variation in the results depending on which processing strategy was used. Using absolute antenna models gave lower estimated heights than using relative models.

4. PCO AND PCV ESTIMATIONS

We aim to quantify the influence of the SWEPOS pillars on the phase observables. In order to accomplish this we estimated the baselines between the reference and SWEPOS antennas from phase differences (see, e.g. [5]). For each baseline processed, the recorded phase data from the two antennas involved were subtracted, and the resulting phase differences were used as observables.

For all antennas we first compensated the phase data by their PCO and PCV values as determined from absolute calibrations. By assuming that the PCO and PCV descriptions of the surrounding reference antennas give a "correct", bias free, representation of the observed phase we can associate deviations in the estimated baselines, as well as systematic signatures in the post-fit residuals, as originating from imperfections in the PCO and PCV of the SWEPOS antenna when mounted on the pillar. The baseline estimation scheme was performed for GPS observation on L1 and L2 separately.

The post-fit residuals had no significant variation with azimuth angle. They had, on the other hand, significant elevation angle dependence, with different structure on L1 and L2. We sorted the residuals into 2.5° elevation angle bins. The mean values for the data in each bin were taken to represent the PCV error introduced by the pillar mounting. Also the vertical components of the baselines were slightly different from what was expected from the terrestrial survey; a few mm discrepancies were typically found. These differences were regarded as measures of the errors in the vertical PCO for the SWEPOS antennas. Unfortunately, the horizontal components of the baseline are not as accurately determined by terrestrial methods, but from the circular symmetry of the antenna setup we do not expect any large horizontal biases.

The baseline estimation scheme also contains a parameter taking care of clock and hardware delay differences between the two receivers in the baseline. This "clock parameter" will, however, absorb a fraction of the phase deviation that we would like to detect as PCO or PCV errors. In order to minimize this effect we iterated the baseline estimation. After the first iteration we made a preliminary updated version of the PCO and PCV descriptions for the SWEPOS antennas. We added the approximate values of the PCV errors found from the elevation bins to the corresponding PCV components in the original PCO/PCV description of the SWEPOS antennas. We then used this updated preliminary PCO/PCV description file for correcting the SWEPOS antenna observations in a second iteration of baseline estimation. Again we sorted the residuals into 2.5° bins and derived PCV error values from the mean values in each bin. This time the sizes of the PCV errors were only about 1/10 of the error sizes found in the first iteration.

The total resulting PCV errors, the sum of the results from the two iterations, are presented in Figure 5 for the nine SWEPOS antennas we analyzed. Each curve is formed from the mean values of the (very similar) contributions from the three baselines associated with the three reference antennas around the SWEPOS antenna. The elevation structure of the curves (~ 1 oscillation over the elevation range 0-90°) is typical for electromagnetic interaction with a surface located ~ ½ wavelength below the antenna [6]. It could therefore be associated with the metal plate (in combination with the top of the concrete pillar) ~0.1 m below the SWEPOS antennas (see Figure 1).

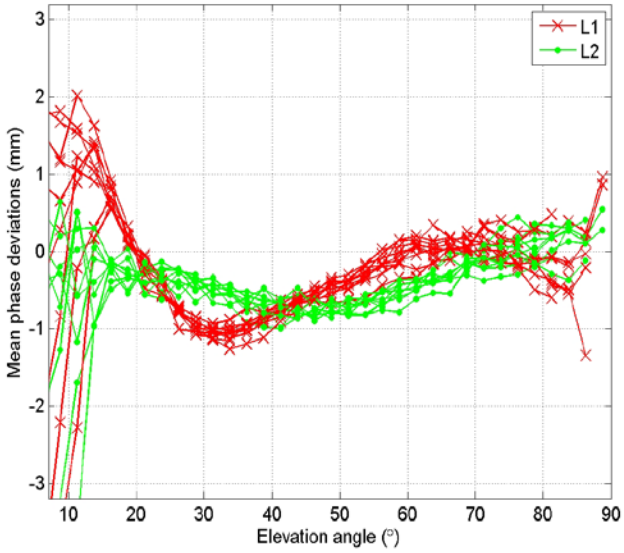

Figure 5. Phase deviations of the nine SWEPOS stations investigated. The deviations are formed by sorting the residuals into 2.5° bins and calculate the mean value for each bin.

The total resulting vertical PCO errors, sum of the results from the two iterations, are presented in Table 1. Again, the values for each SWEPOS station are the mean value of the results from the three surrounding baselines.

It should be pointed out that the baseline estimation scheme contained estimation of neither atmospheric delay nor phase biases. The ambiguous phase biases were adjusted prior to the baseline estimation (cycle fixing), so was the small correction for the expected atmospheric delay difference due to height differences between the two antennas in the baseline. For these short baselines we expect that the remaining atmospheric delay differences typically are smaller than 0.1 mm. The baseline estimation scheme only contains parameters for three coordinates per day and one clock difference per epoch. In the results presented here 15 s epochs were used.

Table 1. Estimated vertical PCO offsets

Station	L1 vertical offset (mm)	L2 vertical offset (mm)
Östersund	2.6	3.2
Sundsvall	-0.3	0.4
Leksand	1.5	3.3
Karlstad	1.1	1.0
Vänersborg	-0.3	0.9
Norrköping	-0.3	1.6
Jönköping	-0.6	0.6
Oskarshamn	0.8	1.8
Hässleholm	-0.7	0.4
Mean	**0.4**	**1.5**

4.1. A common antenna description file

The similarities between different stations vertical PCO and PCV errors suggest that a common "monument specific" PCO/PCV description file could be made. The original PCO/PCV descriptions for all stations, except Leksand, were identical. The Leksand descriptions differed only slightly from the others. We therefore formed mean PCV errors for both L1 and L2 (see Figure 6) and corrected the most common original PCV description with these values. The vertical components of the L1 and L2 PCO were also corrected using the mean values, 0.4 mm and 1.5 mm, found in Table 1.

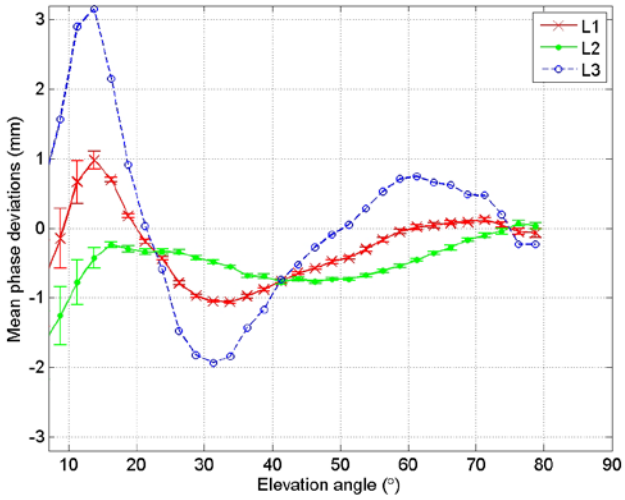

Figure 6. Mean of the phase deviations for the nine SWEPOS stations for L1 and L2 based on the data of Figure 5. An L3 curve is also included, generated as a "ionosphere free" linear combination of the L1 and L2 curves. Notice the significantly larger amplitude of the L3 curve.

In order to test the applicability of this updated PCO/PCV we repeated the baseline estimation, but this time with the original PCO/PCV descriptions replaced by the updated version. Again we looked at the vertical component estimates compared to those derived from terrestrial surveying. The agreement is presented in Table 2. We also sorted the post-fit residuals by elevation angle. The result is shown in Figure 7. In the elevation angle range 15°- 75° the mean residuals are significantly smaller than was the case when using the original PCO/PCV description file. For the lower elevation angles the surroundings around each reference antenna can have an influence on the observed phase. At elevations >75° there are typically a reduced number of observations, so the measurement noise on the individual observations have larger influence. The mean values of the curves of Figure 7 are presented in Figure 8. No great systematic errors can be seen for L1 and L2. However, for the L3 combination some structure remains, especially at very low and very high elevation angles.

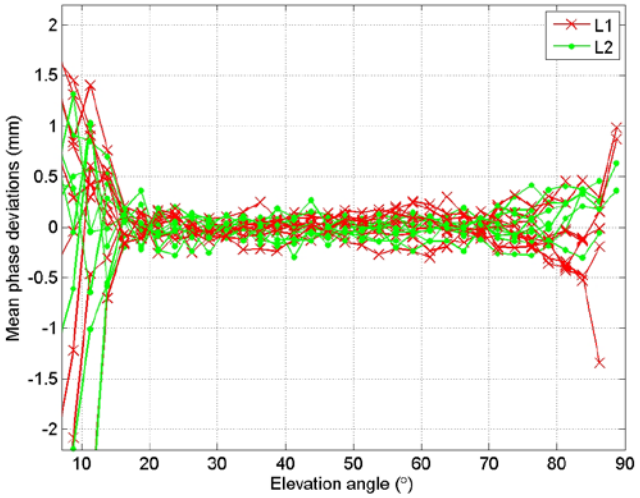

Figure 7. Phase deviations of the nine SWEPOS stations investigated when using the updated PCO/PCV description file for SWEPOS antennas. The signature in the region 15° to 75° is significantly smaller than in Figure 5.

Table 2. Estimated vertical PCO offsets using the updated PCO/PCV description file

Station	L1 vertical offset (mm)	L2 vertical offset (mm)
Östersund	2.2	1.9
Sundsvall	-0.8	-0.9
Leksand	0.2	1.4
Karlstad	0.7	-0.3
Vänersborg	-0.7	-0.3
Norrköping	-0.7	0.4
Jönköping	-1.0	-0.6
Oskarshamn	0.5	0.6
Hässleholm	-1.0	-0.8
Mean	**-0.1**	**0.2**

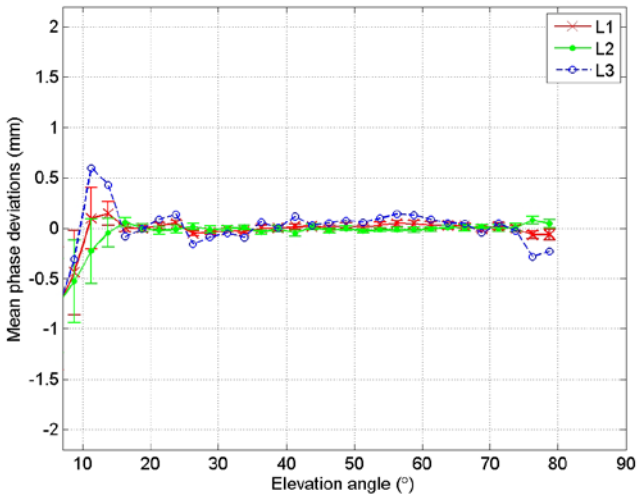

Figure 8. Mean of the phase deviations for the nine SWEPOS stations for L1 and L2 when using the updated PCO/PCV description file for SWEPOS antennas. An L3 curve is also included, generated as a "ionosphere free" linear combination of the L1 and L2 curves.

4.2. Consequences of unmodelled phase deviations

When estimating atmospheric delay together with coordinates and clock parameters in a least squares sense the estimation process has at least three parameters that potentially can absorb an elevation dependent source of error. In the case of our height determination from L3 we think that the unmodelled part of the L3 PCV signature (which we depicted in Figure 6) has partly been absorbed as a (negative) extra height component. In order to understand this model misfit we made numerical experiments with the unmodelled L3 PCV found in Figure 6. We found that a combination of excess atmospheric delay, height, and clock difference could produce a change in the observed L3 that had a resemblance with the L3 PCV, at least below ~70°elevation angle, where most of the observations occur. The numeric experiment is presented in Figure 9. This suggests that an excess height of -9 mm originate from the L3 PCV. From the mean L1 and L2 PCO offsets of 0.4 mm and 1.5 mm (see Table 1) a mean L3 PCO offsets of about -1 mm results. The combined expected height error due to the unmodelled PCO/PCV is then expected to be approximately -1 mm – 9 mm = - 10 mm.

A more thorough analysis is required in order to quantify the consequences of estimating coordinates and atmospheric delay from L3 data using the original PCO/PCV descriptions. We again used the baseline estimation scheme. This time we added a parameter representing atmospheric delay difference to the scheme. For each baseline to process we made L3 phase differences that were fed to the estimation scheme. An elevation cut off angle of 12° was used, in order to avoid too much disturbances from the surroundings of the reference antennas. The resulting height differences between these L3 estimates and the terrestrial survey as well as the estimated atmospheric delay differences are presented in Table 3. The mean values suggest slightly larger deviations than those predicted by the numerical experiment. However, significant variations between the stations are found.

We repeated the baseline estimation scheme with atmospheric delay estimation using L3 data, but this time using the updated PCO/PCV description file for the SWEPOS antennas. The results are presented in Table 4. There is still a noticeable variation from station to station, but the mean values for the height error and atmospheric delay difference is now significantly reduced.

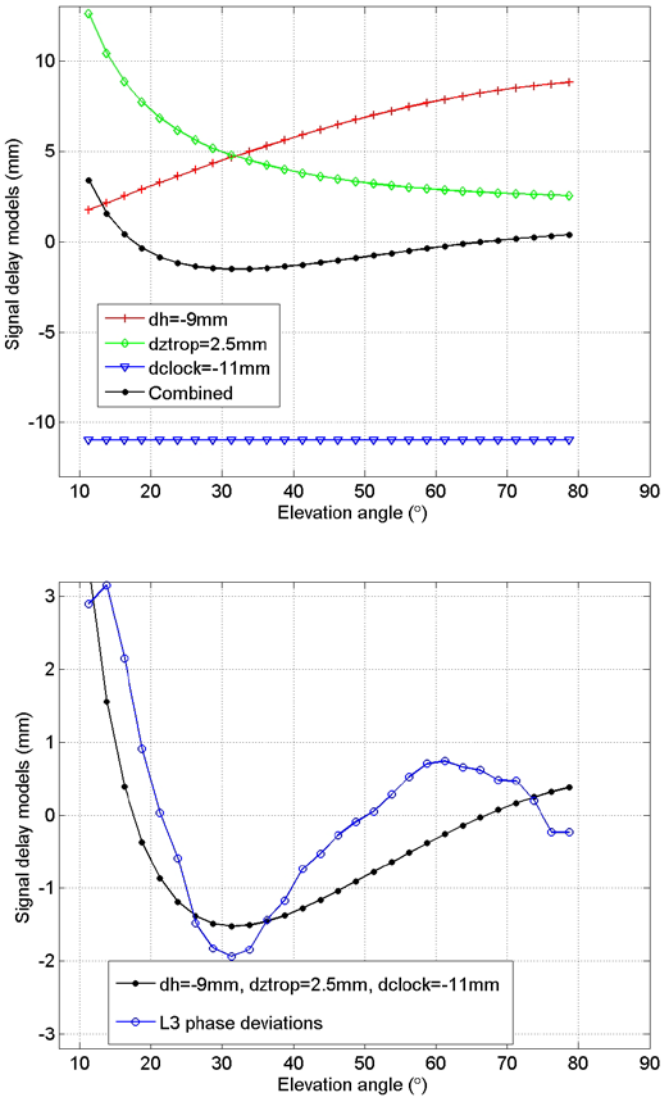

Figure 9. Upper part: graphs depicting the phase changes due to separate changes in height, atmospheric delay, and clock difference, and the sum of the changes (black curve). Lower part: the sum of the phase changes (from upper part) together with the unmodelled L3 PCV.

Table 3. Estimated vertical offsets and atmospheric delay difference when using L3 observables

Station	Vertical offset (mm)	Atmospheric delay offset (mm)
Östersund	-10.4	3.6
Sundsvall	-13.6	3.5
Leksand	-9.2	2.4
Karlstad	-7.0	2.4
Vänersborg	-13.6	3.5
Norrköping	-14.1	3.1
Jönköping	-15.7	4.0
Oskarshamn	-12.3	3.5
Hässleholm	-13.0	3.2
Mean	**-12.1**	**3.2**

Table 4. Estimated vertical offsets and atmospheric delay difference when using L3 observables and the updated PCO/PCV description file

Station	Vertical offset (mm)	Atmospheric delay offset (mm)
Östersund	2.4	0.1
Sundsvall	-1.4	0.2
Leksand	-1.4	-0.1
Karlstad	4.7	-0.8
Vänersborg	-2.1	0.4
Norrköping	-2.6	0.0
Jönköping	-4.2	0.8
Oskarshamn	-0.8	0.3
Hässleholm	-1.5	0.1
Mean	**-0.8**	**0.1**

5. SUMMARY AND DISCUSSION

When using the presently available antenna models GNSS determination of the height difference between the SWEPOS pillar antennas and the surrounding reference antennas gave ~ 10 mm too low heights for the SWEPOS antennas. This error was derived from a comparison with conventional terrestrial surveys. The result varied significantly between days, and also between different processing strategies. PCO/PCV errors derived from GNSS phase differences showed elevation angle signatures that can explain the low estimated height components, in combination with too high atmospheric delay estimates. Electromagnetic coupling between the antenna and a metal plate below the antenna is probably contributing to the systematic PCO/PCV errors found.

Simulations using the derived PCO/PCV errors suggest 7-16 mm lower heights due to these errors, i.e. approximately of the same sizes as was found in the "real" GNSS height determination. In the simulations the PCO/PCV descriptions of the reference antennas were considered to be known after being calibrated. During calibration they were mounted on a "robot arm" that might have introduced systematic errors. The possible size of this effect is, at present, unknown to us. It has been suggested that in-situ calibration could be done with antennas mounted on something that mimic the top of the robot arm during local calibrations in order to reduce the possible effect [1].

In this paper we have excluded three stations (Kiruna, Skellefteå, and Visby). For these stations features in the surroundings of the pillars made the recorded phase variations to differ from what was found for the other nine stations. However, for the nine remaining stations the common "monument specific" PCO/PCV model derived describes fairly well the phase data, and this model can serve as a first guess for the behavior at other, not yet calibrated, stations.

REFERENCES

[1] Wübbena, G., and M. Schmitz, "On GNSS Station Calibration of Antenna Near-Field Effects in RTK-Networks", International Symposium on GNSS, Space-based and Ground-based Augmentation Systems and Applications, October 10-11, 2011, Berlin, 2011.

[2] Rothacher, M., G. Mader, "Receiver and satellite antenna phase center offsets and variations" In: Tétreault, P., Neilan, R., Gowey, K. (eds.) Proceedings of the Network, Data and Analysis Centre 2002 Workshop, pp. 141-152, Ottawa, 2003. (http://igs.org/igscb/resource/pubs/02_ott/session_8.pdf)

[3] Schmid, R., G. Mader, and T. Herring, "From relative to absolute antenna phase center corrections" In: Meindl, M. (ed.) Proceedings of the IGS Workshop and Symposium 2004, Bern, 2005. (http://igs.org/igscb/resource/pubs/04_rtberne/Session10_1.pdf)

[4] Jivall, L. "Hur antenn-modeller påverkar GNSSmätning", GNSS/SWEPOS- seminariet 2011, Gävle Sweden, 2011. (In Swedish)

[5] Hoffman-Wellenhof, B., H. Lichtenegger, and J. Collins, *GPS: Theory and practice*, Springer Verlag, New York, 1994.

[6] Elósegui P., J. L. Davis, R. T. K. Jaldehag, J. M. Johansson, A. E. Niell, and I. I. Shapiro, "Geodesy using the Global Positioning System: The effects of signal scattering on estimates of site position" J. Geophys. Res., Vol. 100, No. B6, pp 9921-9934, 1995.

This page intentionally left blank.

Through our international collaboration programmes with academia, industry, and the public sector, we ensure the competitiveness of the Swedish business community on an international level and contribute to a sustainable society. Our 2,200 employees support and promote all manner of innovative processes, and our roughly 100 testbeds and demonstration facilities are instrumental in developing the future-proofing of products, technologies, and services. RISE Research Institutes of Sweden is fully owned by the Swedish state.

I internationell samverkan med akademi, näringsliv och offentlig sektor bidrar vi till ett konkurrenskraftigt näringsliv och ett hållbart samhälle. RISE 2 200 medarbetare driver och stöder alla typer av innovationsprocesser. Vi erbjuder ett 100-tal test- och demonstrationsmiljöer för framtidssäkra produkter, tekniker och tjänster. RISE Research Institutes of Sweden ägs av svenska staten.

RISE Research Institutes of Sweden AB
Box 857, SE-501 15 BORÅS, Sweden
Telephone: +46 10 516 50 00
E-mail: info@ri.se, Internet: www.ri.se

MEASUREMENT SCIENCE
AND TECHNOLOGY
RISE Report 2019:101
ISBN:978-91-89049-32-1

© RISE Research Institutes of Sweden